Développement, validation et applications d'un système de mesure des propriétés hygroscopiques des particules atmosphériques type VH-TDMA

Paolo Villani

UNIVERSITE BLAISE PASCAL
U.F.R. de Recherche Scientifique et Technique

ECOLE DOCTORALE DES SCIENCES FONDAMENTALES N° 519

THESE

Présentée pour obtenir le grade de

DOCTEUR D'UNIVERSITE

Par **Paolo VILLANI**

Diplomé d'Etudes Approfondies en Climat et Physico-Chimie de l'Atmospère (CPCA)

Développement, validation et applications d'un système de mesure des propriétés hygroscopiques des particules atmosphériques type VH-TDMA

Soutenue publiquement le 14 décembre 2006, devant la commission d'examen :

Présidente	Nadine Chaumerliac
Rapporteur	Ernest Weingartner
Rapporteur	Denis Boulaud
Examinateur	Laurent Gomes
Examinateur	Alfred Wiedensohler
Directeur de thèse	Paolo Laj
Co-directrice de thèse	Karine Sellegri

Table des matières

Introduction générale

Les aérosols et les nuages jouent un rôle important sur le bilan radiatif de la terre mais les mécanismes par lesquels ils influencent le climat sont complexes. L'interaction aérosols/nuages est souvent abordée au travers de l'effet Twomey (Twomey, 1974). Cet effet décrit l'augmentation du nombre de gouttelettes et la diminution de leur rayon moyen en réponse à une augmentation du nombre de noyaux de condensation (CCN). Cet effet est potentiellement accompagné d'une rétroaction des aérosols sur les nuages (effet semi-direct) via la modification de leur dynamique, en raison de la modification du bilan énergétique du nuage. Ce problème est complexe et explique pourquoi l'évaluation quantitative des effets Twomey et semi-direct reste, parmi les différents forçages anthropiques connus, la plus incertaine. Elle est estimée entre 0 et –1.5 W m^{-2} (IPCC, 2001). La difficulté principale pour réduire cette incertitude provient de la complexité de tenir compte à la fois de l'action des aérosols sur les nuages et des rétroactions.

A la base de ces interactions aérosols/nuages, la prévision du comportement des particules en présence de la vapeur d'eau atmosphérique est complexe. Les conditions dans l'atmosphère ne permettent pas la formation homogène de gouttelettes d'eau liquide. Cette nucléation homogène demanderait en effet des sursaturations (pression partielle de vapeur d'eau en excès de la pression de vapeur saturante) de l'ordre de 200%. La condensation de la vapeur d'eau se fait donc principalement sur des noyaux de condensation et l'interaction entre la particule et l'eau est généralement décrite au travers de la loi empirique de Köhler (1936). Cette théorie montre que la quantité de vapeur d'eau condensée en surface des particules dépend de la taille des particules et de leur composition chimique ainsi que des conditions ambiantes d'humidité relative. Même en l'absence de nuage, une fraction des particules présentes dans l'atmosphère contient donc une proportion importante d'eau.

La loi de Köhler est décrite de la manière suivante :

$$\frac{e_a}{e_{sat,w}} = \exp\left(\frac{2M_w \sigma_{s,a}}{RT\rho_w a} - \frac{\upsilon \phi_s \varepsilon_v M_w \rho_s r_N^3}{M_s \rho_w (a^3 - r_N^3)} \right)$$

Où e_a: actual water vapour pressure; $e_{sat,w}$: saturation vapor pressure; M_w: molecular weight of water; M_s: molecular weight of salt; υ: total number of ions into which the salt dissociates; φ_s:

osmotic coefficient of salt in solution; ε_v: volume fraction of soluble material in the aerosol nucleus; r_N: radius of dry aerosol nucleus; a: radius of humid aerosol particle; ρ_w: density of water; $\sigma_{s,a}$: surface tension.

Lorsqu'une particule d'aérosol est en équilibre avec la vapeur d'eau atmosphérique, l'activité de l'eau condensée est égale à l'humidité de l'air corrigée par la courbure de la particule. Une particule atteindra donc une taille à l'équilibre qui dépendra de son diamètre "sec" (diamètre à humidité relative faible) et de sa composition chimique. Pour une taille donnée, une particule contenant une quantité plus importante de matériel soluble contiendra donc une quantité plus importante d'eau condensée. Ceci s'accompagne bien évidemment par un changement de taille et de masse des particules. La fraction massique de l'eau varie de quelques % à plusieurs dizaines de % voire beaucoup plus en présence de gouttelettes de nuages (Putaud et al., 2003). Les propriétés hygroscopiques des particules peuvent être caractérisées par l'augmentation de la taille de particules en fonction de l'humidité relative. Cette augmentation du diamètre est appelée le facteur de croissance hygroscopique (Hygroscopic Growth Factor, HGF) et correspond simplement au rapport des diamètres sec et humide. Pour des sels inorganiques purs, l'augmentation du diamètre est décrite par les courbes de Hanël (Hanël, 1976). La Figure 1 montre, à titre d'exemple, la croissance hygroscopique des particules de diamètre initial de 100 nm, constituées de NaCl pur, en fonction de l'humidité relative (RH%).
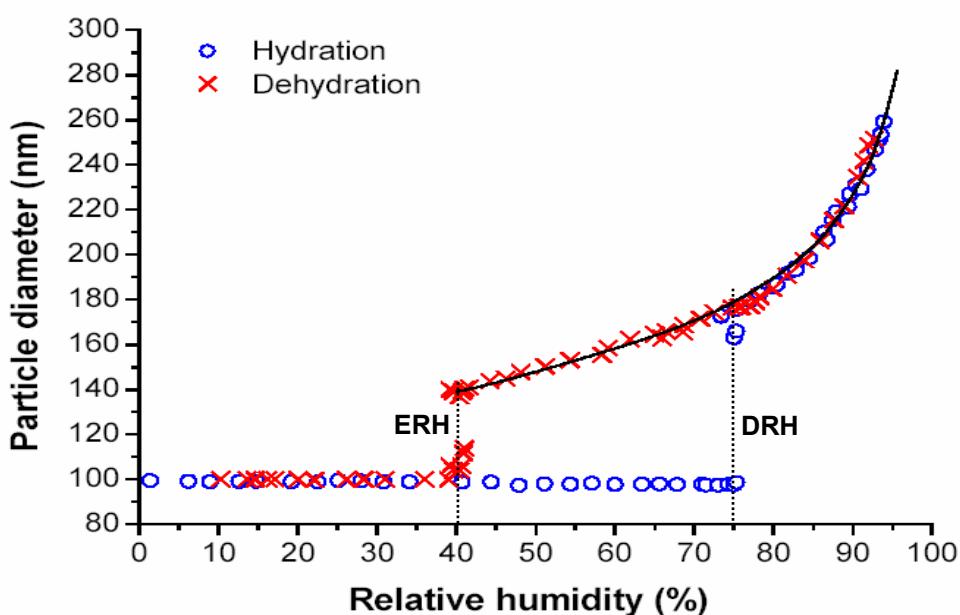

Figure 1 : Changement du diamètre des particules de NaCl en fonction de l'humidité relative observé durant un cycle d'hydratation (cercle bleu) et de déshydratation (croix rouge) pour un diamètre initial de 100 nm. La courbe en noir représente la loi de Köhler théorique.

Grâce à cette représentation de croissance hygroscopique, on peut attribuer pour chaque composé chimique un couple (Deliquescence Relative Humidity, DRH; Efflorescence Relative Humidity, ERH). Le DRH est l'humidité à laquelle le composé solide se transforme en gouttelette (pendant l'hydratation) et l'ERH est l'humidité à laquelle la gouttelette redevient un cristal de sel (pendant la déshydratation). La principale caractéristique de ce couple est que l'ERH est toujours inférieure au DRH à cause du phénomène d'hystérésis. On peut noter que la théorie de Köhler dans le cas d'une humidité relative inférieure à 100% (courbe noire, Figure 1) ne prévoit pas ce phénomène d'hystérésis ni les transitions cristal↔gouttelette.

La mesure expérimentale des facteurs de croissance hygroscopique montre une grande variabilité suivant l'origine des particules d'aérosols. La croissance hygroscopique mesurée en milieu marin montre généralement des valeurs correspondantes aux sels de mer classiques (HGF = 2.0-2.4) (Covert and Heintzenberg, 1989 ; Svenningsson et al., 1992 ; McMurry and Stolzenbourg, 1989 ; Zhang et al., 1993 ; Pitchford and McMurry, 1994 ; Kerminem, 1996 ; Swietlicki et al., 2000). En milieu urbain, les facteurs de croissance sont généralement beaucoup plus faibles (Massling et al., 2005 ; Rissler et al., 2005 ; Vestin et al., 2005). Ces mesures ont amené à formuler l'hypothèse que l'aérosol était composé d'une fraction active (sels inorganiques) régissant le comportement hygroscopique des particules. Cette hypothèse apparaît néanmoins trop simpliste.

Les aérosols atmosphériques ont en effet des compositions chimiques variées incluant à la fois des composés inorganiques et organiques, en mélange interne (mélange de composés chimiques mélangés dans une même particule) ou en mélange externe (mélange de particules de composition chimique différente). La fraction organique des particules est elle-même mal définie, notamment pour ses propriétés de solubilité. En théorie, la connaissance des propriétés physiques et chimiques des particules permet de prévoir leur croissance hygroscopique. Si ceci est avéré pour des particules inorganiques, ce n'est pas le cas pour des particules plus complexes contenant soit exclusivement des substances organiques de solubilité variables (Saxena et al., 1996), soit un mélange de substances organiques et inorganiques.

Puisqu'une fraction non négligeable de substances organiques se retrouve dans les systèmes nuageux (Fuzzi and Zappoli, 1996 ; Facchini et al., 1999 ; Raymond et Pandis, 2002,2003), on ne peut exclure que même des substances organiques peu solubles puissent servir de noyau de condensation de nuage et donc, en conditions de sous-saturation, montrer des facteurs de croissance significatifs (Saxena et al., 1995 ; Choi et Chan, 2002 ; Speer et al., 2003).

Facchini et al. (1999) ont montré, à partir d'échantillons de brouillard, qu'une décroissance de la tension de surface des aérosols, causée par la présence de composés organiques actifs à la surface, entraînerait une augmentation du nombre de gouttelettes formées associée à un forçage radiatif négatif de l'ordre de -1 W m-2. Nenes et al. (2002) ont montré que les "effets chimiques" (c'est-à-dire la dissolution de gaz solubles et de solutés partiellement solubles, la diminution de la tension de surface due à la présence de composés organiques dissous, et la modification du coefficient d'accommodation due à la formation d'un film organique à la surface des aérosols) sur le nombre de gouttelettes formées peuvent être du même ordre de grandeur que l'effet Twomey dû uniquement à l'augmentation du nombre d'aérosols. Plusieurs études en laboratoire, utilisant des chambres CCN seules ou associées à des DMA, ont cherché, récemment, à déterminer la capacité des aérosols organiques à former des gouttelettes (Broekhuizen et al., 2004 ; Hori et al., 2003 ; Shanz et al., 2003). Récemment, Sellegri et al., (2003) ont montré que la capacité des aérosols organiques à servir de noyau de condensation était lié à leur propriétés thermiques (et donc indirectement à leur complexité structurelle). Rojas et al., (soumis) ont également mis en évidence qu'une simple thermo-désorption de l'aérosol, sans modification mesurable de la taille des particules, était susceptible, dans certaines conditions, de modifier de manière significative le spectre d'activation des CCNs. Les études effectuées sur différents sites montrent que les variations de l'hygroscopicité peuvent être, soit positives (augmentation du ratio CCN/CN) soit négatives suivant l'origine des masses d'air. Ces études concluent que la présence d'une espèce soluble en trace (sulfate d'ammonium par exemple) ou d'une espèce organique en trace active à la surface des aérosols étudiés, augmente la capacité à former des gouttelettes. La structure du mélange interne entre substances organiques et inorganiques, et notamment les propriétés de surface, pourraient donc jouer un rôle important dans la croissance hygroscopique des particules.

Cette complexité, que la loi de Köhler ne permet pas d'appréhender complètement, pourrait être à l'origine des désaccords dans les études de fermeture entre les mesures expérimentales et la théorie. A l'heure actuelle, les modèles de simulation de la formation des nuages ne permettent pas de prévoir la fraction des particules d'aérosols pouvant agir comme CCN (Snider et Brenguier, 2000). Celle-ci varie de 20 à 90% suivant la dynamique du nuage et les propriétés de la population d'aérosols (taille et composition chimique). En règle générale, la fraction CCN est plus importante pour des masses d'air propres que pour des masses d'air polluées alors que le spectre en taille des CCNs varie considérablement suivant les types de nuages (Hallberg et al., 1997 ; Hallberg et al., 1998 ; Bower et al., 2000 ; Geremy et al.,

2000). Les études in-situ montrent généralement la présence d'une population de particules "actives" (CCN) et d'une population de particules "non actives" restant dans la phase interstitielle du nuage mais aucune classification chimique claire de ces deux populations n'a pu être proposée jusqu'à présent. Il apparaît que, si la majorité des particules (en particulier celles d'origine anthropique) est, en théorie, susceptible de jouer le rôle de CCN, seule une fraction d'entre elles le sont effectivement dans les conditions naturelles. L'objectif principal de ce travail de thèse est donc de contribuer à mieux comprendre le lien entre la nature de l'aérosol et ses propriétés hygroscopiques et notamment, à mieux évaluer le rôle des propriétés de surface des aérosols.

La réalisation de cet objectif nécessite en premier lieu de travailler sur les méthodes instrumentales pour la mesure à la fois de la croissance hygroscopique et de certaines propriétés de surface des aérosols fins. La mesure du HGF est généralement obtenue par méthode d'analyse différentielle de mobilité en tandem (Tandem Differential Mobility Analysers , TDMA). Cette technique a été décrite à l'origine par Rader and McMurry en 1986 et le principe général de mesure est présenté sur la Figure 2.
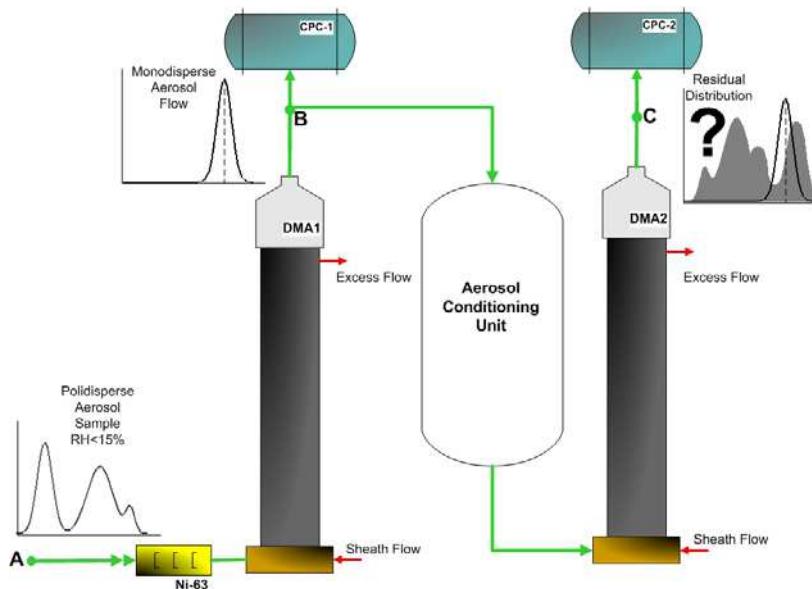
Figure 2 : Schéma du Tandem-DMA

Les TDMA sont classiquement constitués de trois parties principales qui permettent la sélection des particules, le conditionnement de l'aérosol et la mesure de la distribution granulométrique des particules conditionnées. Notre travail est organisé au travers du développement et de l'utilisation de systèmes TDMA.

Ces développements sont décrits en détail dans le chapitre relatif au développement instrumental (Chapitre I). La sélection des particules polydispersées se fait via un système DMPS (Differential Mobility Particle Sizer) dont le fonctionnement est décrit dans l'Appendix A.1. Les particules sont chargées à l'équilibre dans un neutraliseur (généralement une source radioactive) et sélectionnées en taille via un analyseur de mobilité différentielle DMA-1 (cf. Appendix A.2). Les particules chargées sont classées en fonction de leur mobilité

électrique. En sortie du DMA-1, le flux de particules quasi-monodispersées est dirigé en partie vers le premier compteur de particule CPC-1 (cf. Appendix A.3) pour connaître la concentration des particules classées initialement, et en partie vers l'unité de conditionnement de l'aérosol. Les DMAs sont la base essentielle des mesures granulométriques des particules fines. Dans la première section du chapitre I (chapitre I.1 : « Design, optimisation and evaluation of a Differential Mobility Analyser (DMA) » et Appendix A.4) de ce travail, nous décrirons comment les améliorations apportées aux DMAs commerciaux permettent d'augmenter de manière significative l'efficacité de transfert des colonnes DMA mais également d'améliorer la précision avec laquelle la colonne produit un flux monodimensionnel de particules.

L'unité de conditionnement est variable suivant le type d'étude entrepris. Elle permet de modifier la nature des particules en les plaçant par exemple en contact avec de l'air humide (H-TDMA) ou dans une enceinte chauffée à une certaine température (V-TDMA). La réponse de l'aérosol monodispersé à ce conditionnement permet d'en déterminer certaines propriétés. Les particules qui sortent de l'unité de conditionnement vont passer dans la troisième partie du système pour qu'on puisse mesurer la distribution en taille de l'aérosol modifié. Cette granulométrie résultante est déterminée avec un deuxième DMA (DMA-2) qui balaye une plage de diamètres des particules en combinaison avec un deuxième CPC (CPC-2) qui mesure la concentration des particules pour chaque canal. Les différents types de conditionnement utilisés dans cette étude sont donc le conditionnement thermique et le conditionnement humide. Les Figures 3 et 4 illustrent le comportement des particules lorsqu'on les conditionne en température et humidité, respectivement.
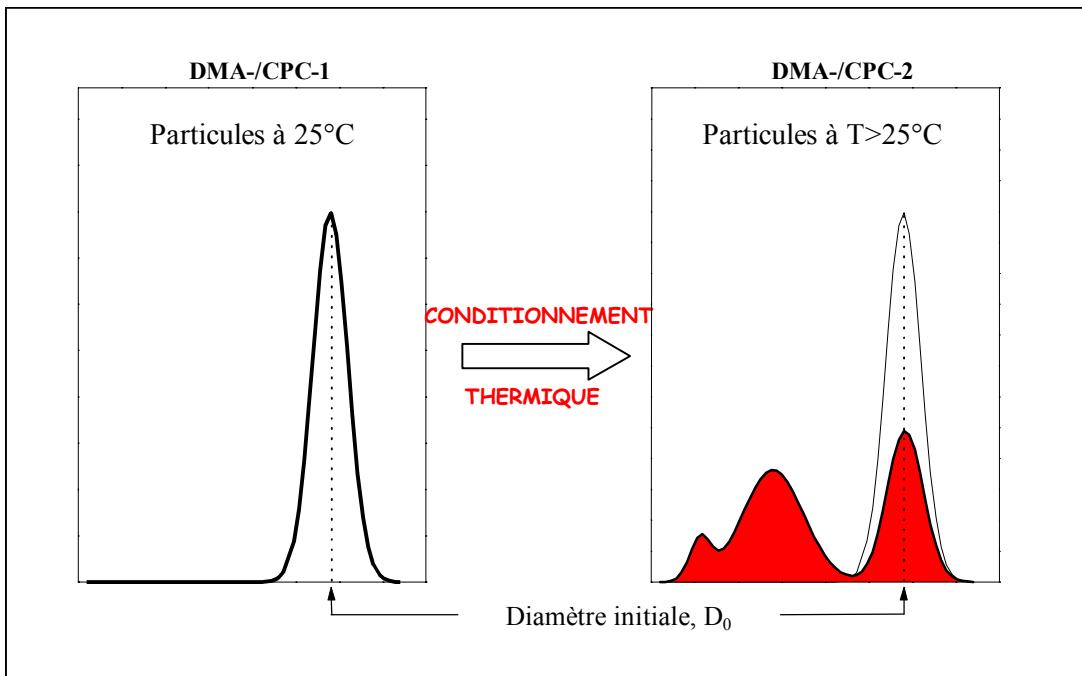
Figure 3 : Illustration de distributions granulométriques après conditionnement des particules exposées à des températures élevées.
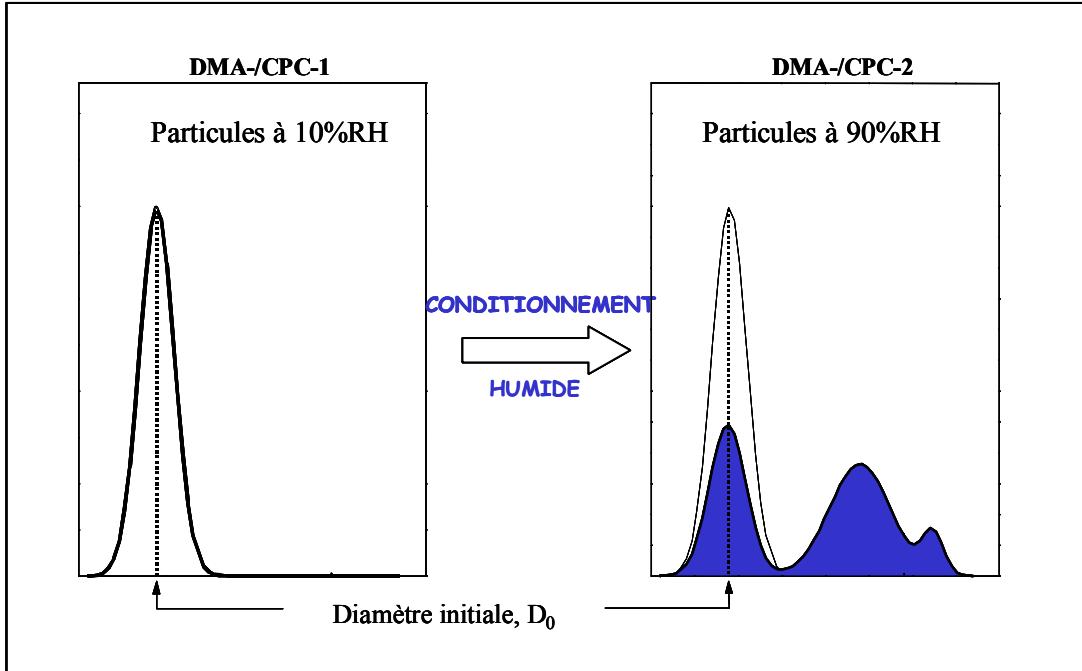

Figure 4 : Illustration de distributions granulométriques après conditionnement des particules exposées à des humidités élevées.

Le conditionnement thermique utilisé dans ce travail (i.e. Volatility-TDMA) utilise une unité de conditionnement où l'aérosol quasi-monodispersé est conditionné à une température fixée (Chapitre I.2.1 et Appendix A.5). Le conditionnement humide a été développé dans le cadre d'une version combinée du conditionnement thermique et humide de l'aérosol (VH-TDMA), et qui permet d'humidifier les particules à une humidité fixée après thermo-désorption à une température fixée. A notre connaissance, ce couplage VH-TDMA n'a été mis en place que par l'équipe de Johnson à l'International Laboratory for Air Quality and Health, Queensland University of Technology, Brisbane, Australia (Johnson et al., 2003). Des développements similaires sont en cours au PSI (Paul Scherrer Institute) en Suisse.

Ces deux types de conditionnement ont été développés au laboratoire et sont décrits en détails dans les sections 2 (Chapitre I.2.1 : « Design and validation of a 6-Volatility Tandem Differential Mobility Analyser (V-TDMA)» et Appendix A.5) et 3 (Chapitre I.3.1 : « A Multi-TDMA to characterise relationship between thermal and hygroscopic properties of atmospheric aerosol particles » et Appendix A.5, A.6) où sont présentés en détails le principe de fonctionnement, les dessins techniques, les tests de validation et les mesures en laboratoire. En particulier, le H-TDMA du VH-TDMA a été inter-comparé aux autres systèmes existants en Europe dans le cadre du Réseau d'Excellence ACCENT.

La réponse de l'aérosol au conditionnement thermique et humide offre des perspectives intéressantes pour mieux comprendre le rôle de la nature complexe de l'aérosol sur leurs propriétés hygroscopiques. Les V-TDMAs ont été généralement utilisés pour déterminer la nature chimique des particules. Cette utilisation s'est néanmoins révélée problématique compte tenu de la complexité des propriétés thermiques. Nous avons, dans ce travail, utilisé la thermo-désorption comme élément de modification des propriétés de surface des particules en ne travaillant qu'avec des températures ne modifiant pas le spectre dimensionnel des particules.

Les résultats des campagnes de mesure effectuées avec le VH-TDMA sont présentés dans le chapitre II. Ces résultats sont présentés sous la forme de deux manuscrits, l'un concernant les mesures de croissance hygroscopique effectuées lors de diverses campagnes dans des milieux urbains, côtiers, et sur un site de troposphère libre (Chapitre II.1 : « Hygroscopic behaviour of aerosol particles in diverse environments »), l'autre concernant l'impact du conditionnement thermique des particules (et donc de l'évaporation de sa composante la plus volatile) sur les propriétés hygroscopiques (Chapitre II.2 : « The role of surface layers on particle

hygroscopic properties » et   Chapitre II.3 : « Effect of surface modification on the hygroscopic properties of natural aerosol particles »).

Dans la conclusion de ce travail, le lecteur trouvera des éléments de prospectives à la fois concernant une version améliorée du système VH-TDMA mais également des propositions pour mieux contraindre les études effectuées lors de cette thèse.

CHAPITRE I.1

Differential Mobility Analyser

L'analyseur différentiel de Mobilité (DMA) est un élément fondamental pour la granulométrie des particules fines. Associé à un compteur de particules et à un neutraliseur, il permet très schématiquement de procéder à la mesure de la dimension des particules entre quelques nm et quelques centaines de nm. Il est bien sûr un élément essentiel de nos mesures de granulométrie tandem (V-TDMA et de H-TDMA).

Comme leur nom l'indique, chacun de ces analyseurs tandem est constitué d'une série de 2 DMA. Associé comme nous le faisons lors de campagnes expérimentales avec un simple granulomètre type DMPS / SMPS, et / où avec un granulomètre pour la fraction volatile (V-DMPS / V-SMPS), le nombre de colonnes DMA nécessaires à une caractérisation complète de l'aérosol lors d'une campagne de mesure est de l'ordre de 4 à 6. L'équipe instrumentale du LaMP participe parfois de manière simultanée à plusieurs campagnes expérimentales nécessitant par là même un nombre important de colonne.

Cet état de fait ainsi que le coût important d'une colonne DMA (15 k€) nous a poussé, comme la plupart des groupes Européens travaillant sur l'aérosol atmosphérique à procéder à la construction de nos propres colonnes DMA que nous avons entrepris sur la base du DMA TSI (Modèle 3081). Plus qu'une simple anode / cathode, les colonnes DMA sont complexes (Voir Figure I.1.1) car elles nécessitent un contrôle extrêmement précis des flux d'air et d'aérosols et de leur mélange. Plutôt que de procéder à la copie du système TSI, nous avons, suivant les indications fournies par Chen, Pui et al., 1998, cherché à procéder à une amélioration du DMA TSI en redessinant en partie le système de mélange des flux d'air sec et d'aérosols, et le système de sortie d'air échantillonné.
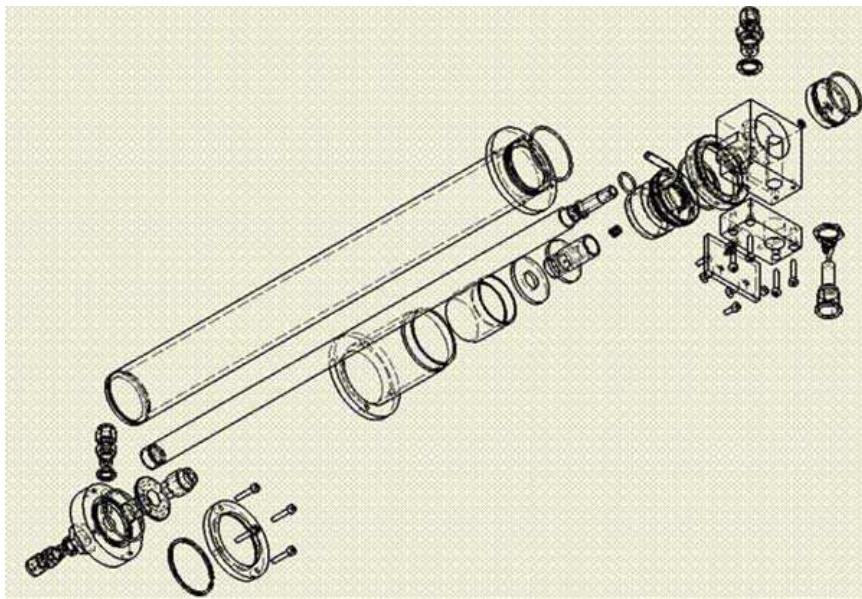
Figure I.1.1 : Schéma du DMA construi au LaMP.

Ceci a demandé la modification d'un grand nombre de pièces par rapport au système original TSI. Nous avons également procédé à la construction de DMAs courts (non présenté dans ce chapitre) permettant une amélioration de la sélection de particules dans la gamme de taille < 50 nm.

Les modifications apportées au DMA font l'objet du Chapitre 1.1. Une description précise de ces modifications est rapportée ici ainsi que les procédures de validation à la fois via le logiciel Fluent et expérimentale. Les résultats montrent que les DMAs modifiés permettent à la fois un meilleur transfert de particules, notamment pour les particules fines en raison d'une diffusion turbulente limitée, et une meilleure précision dans la sélection d'un diamètre de mobilité donné à la fois par rapport au DMA TSI mais aussi par rapport au DMA type Vienna construit par nos collègues de l'université de Lund (Suède) et qui équipaient les premières versions de nos DMPSs. Ce chapitre fera l'objet d'un rapport OPGC.

Les DMAs sont désormais réalisés soit entièrement au laboratoire, soit, pour certaines pièces, auprès d'une entreprise de constructions mécaniques. Grâce à ces développements, le LaMP dispose désormais d'un savoir-faire fondamental pour l'étude de la granulométrie de l'aérosol. L'utilisation de nos DMAs nous permet de procéder simultanément à l'ensemble des mesures nécessaires à la caractérisation physique de l'aérosol. Nous maîtrisons l'ensemble de la construction de systèmes DMPS, SMPS et TDMA. Les récentes intercomparaisons de granulomètres montrent qu'il est en effet tout à fait nécessaire de comprendre, modifier et valider l'ensemble d'un système DMPS / SMPS pour obtenir une granulométrie fiable de l'aérosol, ce qui n'est pas le cas des systèmes commerciaux.

DESIGN, OPTIMISATON AND EVALUATION OF A DIFFERENTIAL MOBILITY ANALYSER (DMA)

Villani, P., Picard, D. and Laj, P.

Abstract

Several features of a Differential Mobility Analyser (DMA) have been improved for measuring the size distribution of nanometer aerosol particles. The design is based on a cylindrical symmetry configuration (Knutson and Whitby, 1975) and is optimised by means on field fluid flow model calculation using the Computational Fluid Dynamics (CFD) Flow Modelling Software, FLUENT 6.1. Two important design features were included: a modified aerosol/sheath inlet (as suggested by Chen, Pui et al., 1998) and a modified aerosol exit. For reducing particle loss at the DMA base all bends were eliminated and to avoid flow and particles recirculation the inlet slit width is reduced and aerodynamically shaped. Numerical results are presented comparing the fluid flow and particles trajectories of the old and new inlet for different flow ratios. After numerical evaluation and construction, the performance of the DMA is evaluated using the Tandem DMA technique following the procedure suggested by Stolzenburg (1988). The transfer functions of the optimised DMA are determined experimentally for particle size range of 10-100 nm by using two identical DMAs with an analyser length of 44 cm. By comparing the experimental results obtained using the Tandem containing the new DMAs with the same experimental setup containing two identical "(Non Genuine) Vienna Type" DMAs, it is concluded that the re-designed features increase the performances of a DMA.

Keywords: Aerosol particles, DMA, Transfer Function

1. INTRODUCTION

Size classification of aerosol particles according to their electrical mobility using differential mobility analysers (DMAs) has become a standard technique for characterising aerosol physical properties. The accuracy of this thechnique concerning its resolution in time on particle size is superior related to most of the other technniques wich are typically used for aerosol studies of this particle size range (e.g. diffusion batteries, cascade impactors). Previously, DMAs often have been used in the field of aerosol analysis. Examples related to this work are the Differential Mobility Particle Sizer (i.e. DMPS) and the Tandem Differential Mobility Analyser (i.e. TDMA) (Rader and McMurry, 1986). The differential mobility method, first described by Hewitt (1957), is a powerful tool for the classification of submicrometer aerosol particles. Work performed by Liu and Pui (1974), Knutson and Whitby (1975), Stolzenburg and McMurry (1988) established this method for the generation of monodisperse particles and for the size selection for polydisperse aerosol particles. Recently their capabilities have been extended down to the so called ultra fine range (2 - 20 nm) and even approaching the size of molecular clusters (Reischl, 1991).

As a further development of the old designs there are at least four modern types of DMAs available: TSI type (Knutson and Whitby, 1975), Vienna type (Reischl, 1991) and two of the "radial" types, described by Mesbah et al., (1993) and Zhang and Flagan (1996). The term DMA is almost exclusively used for the ones having a cylindrical symmetry. Additional versions of the instrument exist fabricated elsewhere according to more or less similar design and often made for specific purposes (Whang and Flagan, 1990; Wiedensohler et al., 1998; Collins et al., 1999).

The aim of this paper is to evaluate the performances of a modified TSI DMA type. The paper provides detailed designs of the new DMA features as well as simulations of the flows inside the modified DMA. Performances of the modified DMA column are then compared with conventional Vienna type DMA from built by Lund University (Sweden).

2. DMA OPERATION PRINCIPLES

The operation principle of a DMA has been extensively described in literature (Hewitt,1957; Pui, 1974; Knutson and Whitby, 1975; Stolzenburg and McMurry, 1988) and is shown in Figure A.1.1.

The DMA consists of a center electrode surrounded by a grounded outer concentric cylinder. A particle free "Sheath air" flow Qsh and an aerosol "Sample flow" Qs flow downward and axially between the two cylinders. Before entering the DMA, the aerosol particles are charged by passing through a bipolar diffusion charger (neutraliser), where a well-defined charge distribution is established. With a voltage applied to the center electrode, a narrow electrical mobility bandwidth of particles can be selected from the charged aerosol sample and drawn through a small exit slit at the base of the DMA. In the electrostatic field of the classifier, particles experience an electrostatic force and accelerate perpendicularly to their trajectories, until this force is balanced by the Stokes drag force.
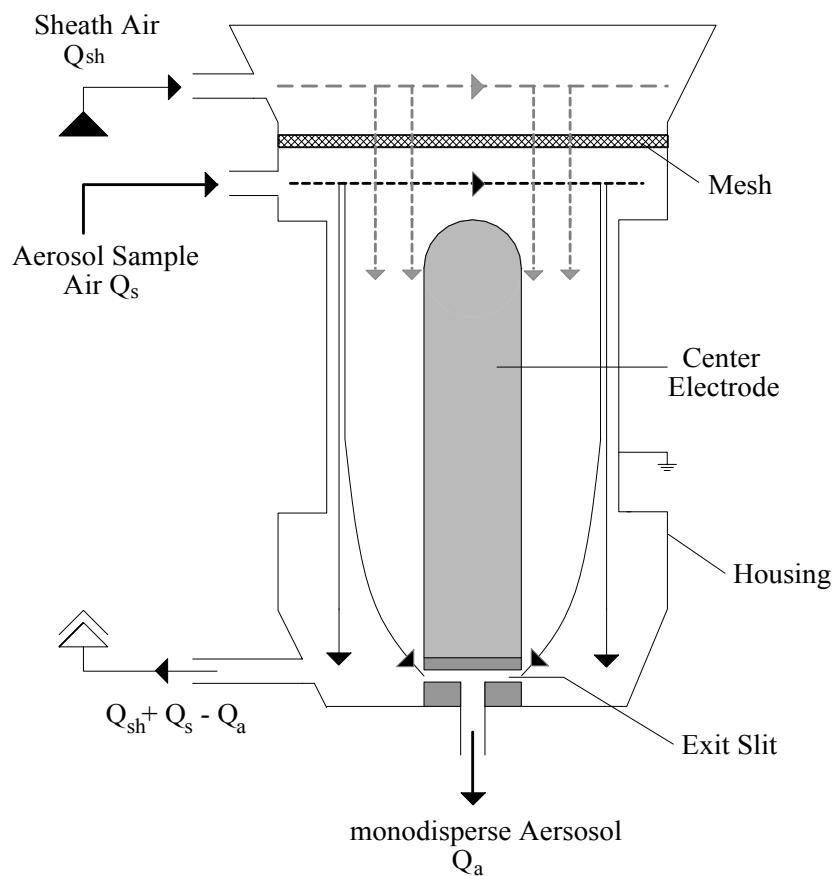

Figure A.1.1: Schematic of the "Lund-Vienna Type" differential mobility analyser.

The magnitude of electrical mobility Zp is a measure for the ability of a particle to move in an electric field. It is expressed as (Knutson and Whitby, 1975):

$$Z_p = \frac{i \cdot e_0 \cdot C_c(D_p)}{3\pi \cdot \mu \cdot D_p} \qquad (1)$$

where D_p = Mobility equivalent diameter

i   = number of elementar charge (e_0)

$\mu(T)$ = Air Viscosity

$C_c(D_p, \lambda)$ = Cunningham Slip Correction Factor

Throughout this paper, when the diameter of the particles is mentioned, we refer to the concept of "*mobility equivalent diameter*". Equation 1 is generally known to apply successfully to particle sizes down to at least D_p=5 nm. Particles with high electric mobility deposit on the center rod upstream of the sampling slit. Those with low mobility are carried out with the main outlet flow. In between, there exists a narrow range of mobility for which the particles reach into the sampling slit and are carried out with the sampling flow. Only those particles whose electric mobility lies within a certain narrow range will reach the sampling flow. This range may be altered by adjusting the operating conditions of the mobility analyser.

An efficient formalism to describe the performance of a DMA is the concept of the DMA transfer function. Knutson and Whitby (1975) introduced the transfer function Ω as the probability that an aerosol particle which enters the mobility analyser via the aerosol inlet to leave via the sampling flow, for a given mobility Zp. Due to its nature as a "probability" function, the transfer function indicates how many particles of any distinct mobility entering the DMA will successfully go across the analyser column. For cylindrical DMAs, Knutson and Whitby (1975) derived a transfer function of triangular shape in the mobility space, illustrated in Figure A.1.2.

This simple model ignores particle diffusion inside the DMA. The centroid of the mobility band Z_p^* is given by:

$$Z_p^* = \frac{2 \cdot Q_{sh} + Q_a - Q_s}{\pi \cdot V \cdot L} \cdot \ln\left(\frac{R_{est}}{R_{int}}\right) \qquad (2)$$
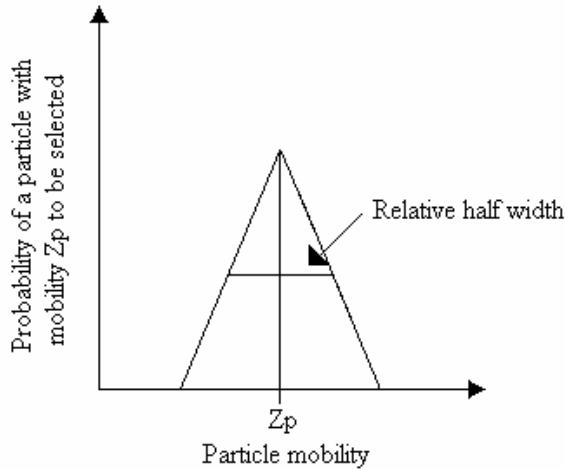
Figure A.1.2: Ideal DMA transfer function.

And the half-width of the mobility band, ΔZ_p, is given by:

$$\Delta Z_p = \frac{(Q_s + Q_a)}{2 \cdot \pi \cdot V \cdot L} \cdot \ln\left(\frac{R_{est}}{R_{int}}\right) \quad (3)$$

The relative half-width is obtained by normalising ΔZ_p with the midpoint mobility Z_p^*:

$$\frac{\Delta Z_p}{Z_p^*} = \frac{(Q_a + Q_s)}{(Q_{sh} + Q_{ex})} = \beta \qquad (4)$$

Equation (4) shows that the relative half-width of the mobility band is controlled by the flow raytes. In normal use, the flows are selected such that $\beta = 0.1$.

The ratio of half-width at half-height (HWHH) to the mean particle size is used to characterise the operation of a DMA in terms of performances of the classifier resolution measurements (Chen and Pui, 1998; Karlsson and Martinsson, 2003). However, a number of experiments revealed that in the ultrafine size range (Dp<20 nm) the DMA transfer function deviate significantly from his ideal triangular shape (Kousaka et al, 1995; Zhang et al., 1995; Fissan et al., 1996; Reischl et al., 1997). Two principle effects of Brownian diffusion were identified to be responsible for this behaviour of the DMA. First, particles losses in connecting tubing, canalisations,

bends and inlets of the DMA decrease the overall area of the transfer function. Second, the broadening of particle trajectories inside the analyser column increases the half-width band of the transfer function. The latter effect was incorporated into the transfer function formalism by Stolzenburg (1988).

3. DESIGN MODIFICATIONS OF TSI DMA

As shown originally by Knutson and Whitby (1975), the size resolution of the DMA is proportional to the aerosol/sheath flow ratio in the classifying region. Therefore, DMAs have a good potential for high resolution measurement by operating at a small flow ratio. The resolution of the current TSI DMA is less than predicted for an aerosol/sheath flow ratio of 0.05 (i.e. β=1:20). As revealed by Chen and Pui (1997), there is a mismatch between the aerosol and sheath flow velocities at the wide inlet entrance slit of the DMA classifying region. This flow mismatch causes a flow recirculation pattern to develop in the immediate region of the entrance slit.

The mismatch condition worsens when the DMA is operated at low aerosol/sheath flow ratio for high sizing resolution measurements. It restricts the usable flow ratio range and limits the DMA resolution. Several causes contribute to this non-ideal performance of DMAs:

(a) Due to the wide opening of the aerosol entrance slit, it allows the electric field to penetrate into the aerosol passage upstream of the entrance slit (Chen et al., 1997). It is undesirable because this penetration results in inaccurate measurement of electrical mobility and, when combined with the flow recirculation pattern, it cause more aerosol deposition prior to entering the classifying region. The electric field distortion therefore makes accurate mobility determination very difficult. The wide slit width also makes it difficult to define the DMA characteristic length of the classifying region, L. The length is defined as the distance between the mid-plane of the mobility analyser entrance slit and sampling exit slit: the current TSI DMA length is close to 444 mm.

(b) The TSI-standard design has a high voltage Teflon insulator below the aerosol exit slit on the collector tube. The insulator charges up during voltage cycling and causes electrostatic deposition of classified, charged aerosol particles on the inside surface of the insulator tube.

(c) For particle size below 20 nm the effect of bends and elbows on particle diffusion loss is significant (Wang et al., 2001): the bend placed after the mono-dispersed aerosol exit slit in the current TSI DMA base increase this phenomenon.

The aim of this work was to re-design and optimise a DMA in terms of transmission efficiency and size resolution in particular in the small particle range (<20nm). In order to limit flow recirculation at the aerosol inlet slit and to minimize particle losses in the DMA, our work focussed in new designs to reduce the slit width, to aerodynamically shape the inlet and to reduce aerosol passage transport length and eliminate bends.

3.1 Modification of the aerosol flow entrance slit

In order to reduce the slit width of the existing TSI DMAs, the inlet cone length is increased from 41.3 mm to 50.7 mm, detailed dimension are given in Figure A.1.3 and A.1.4.
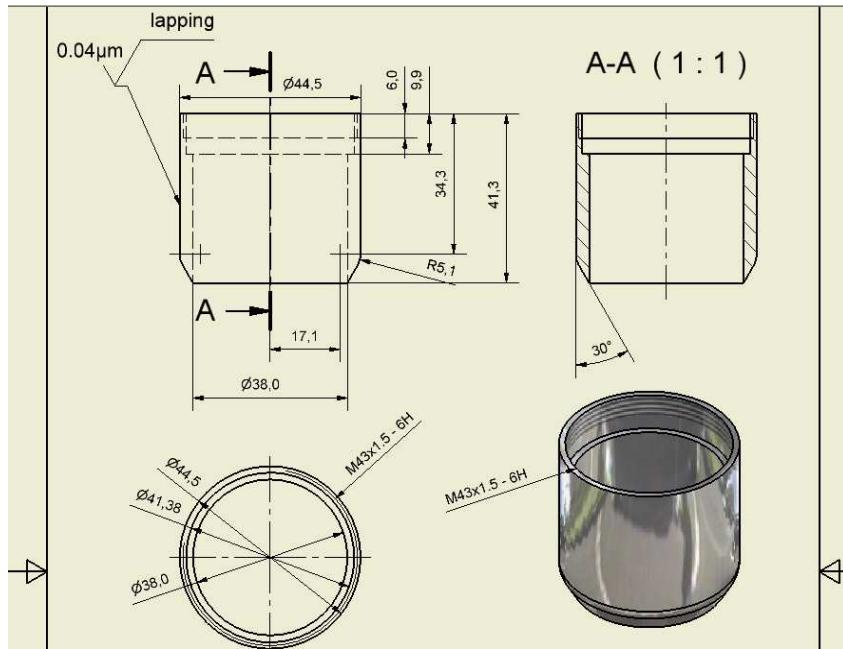

**Figure A.1.3**: Drawing of the original aerosol inlet cone.
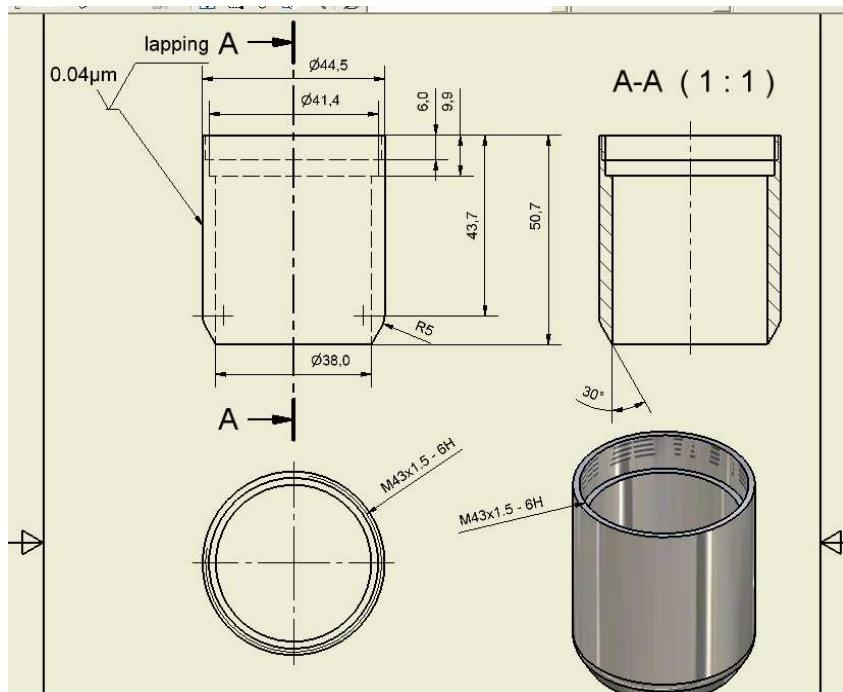
Figure A.1.4: Drawing of the modified aerosol inlet cone.

The increase of cone length to 9.4 mm allows to confine the flow by filling the open zone and to avoid electric field penetration into the upstream side of the entrance slit.

The original gap spacing between the entrance of the classifying region and the existing conical inlet is 10,5 mm. To aerodynamically shape the inlet the outer cylinder were modified: a 45° sloped wall is used to guide the aerosol gradually into the classifying region. A consequence of the cone length modification, the overall length of the column is reduced to 440 mm. Figure A.1.5 and A.1.6 shows the design of the aerosol entrance slit before and after the modification.
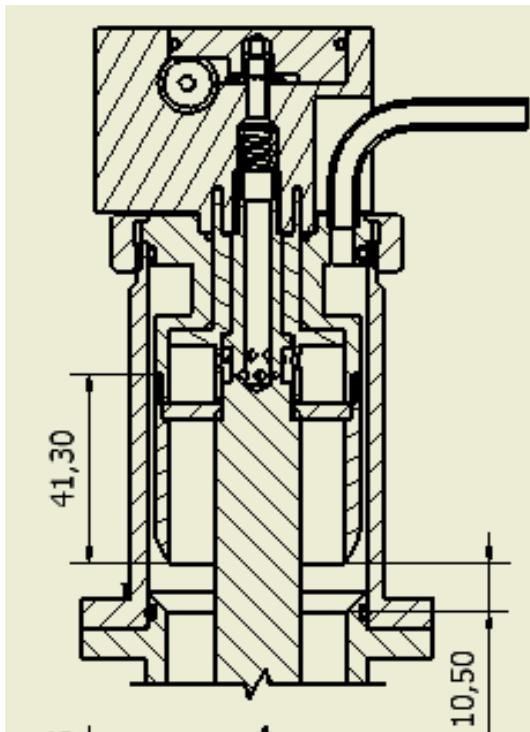
**Figure A.1.5**: Drawing of the original aerosol/sheath DMA inlet. (gap=10.5 mm)
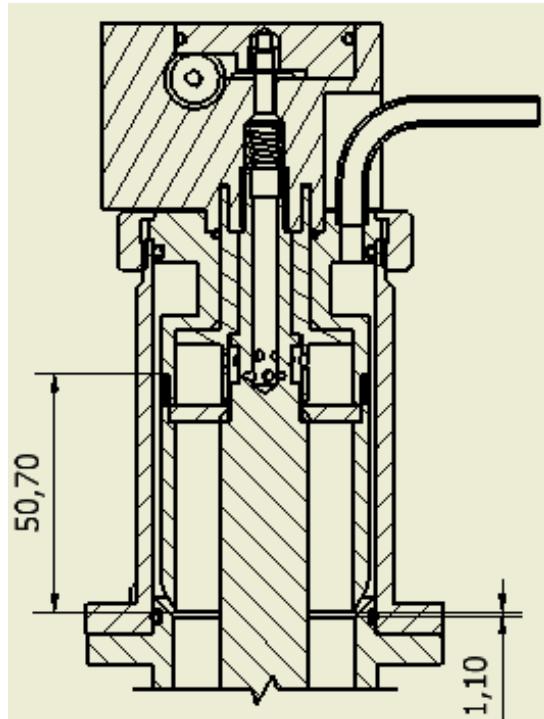
Figure A.1.6: Drawing of the modified aerosol/sheath DMA inlet. (gap=1.1 mm)

3.2 Modification of the DMA base

To reduce particle losses at the exit slit, the length of the insulator is shortened to a minimum for reducing charged particle deposition. The Teflon insulator is replaced with slightly conducting material (Kemetal®), which contributes to dissipate some of the electric charges built up on the insulator surface. In addition, the bend of the transport passage in the metal base is suppressed so that the mono-dispersed aerosol exits the column in a straight way. The design of the modified aerosol DMA base is shown in Figure A.1.7.


Insulator
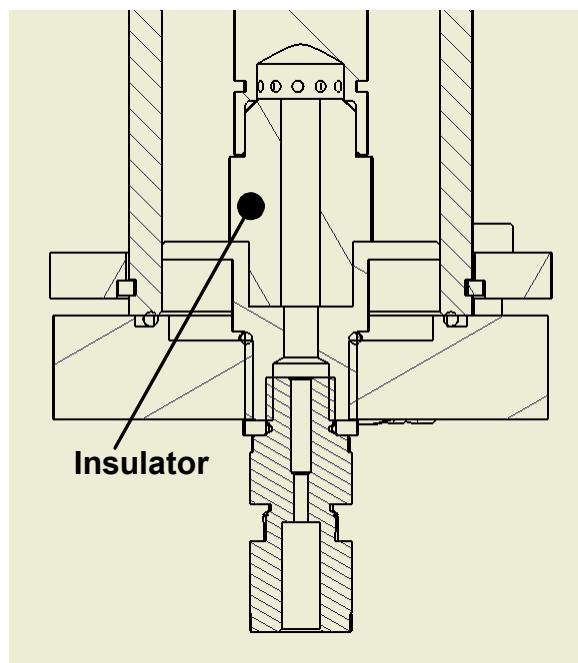
Figure A.1.7: Drawing of the modified DMA base.

4. VALIDATION OF THE MODIFIED TSI DMA USING NUMERICAL MODELING

Prior to the construction of the modified inlet, the performance of the original TSI DMA inlet and the modified one was evaluated using the Computational Fluid Dynamics (CFD) Flow Modelling Software, FLUENT 6.1. The computational domain consists of the aerosol transport passage starting from the exit of the aerosol plenum chamber and extending through the classifying region of the TSI DMA. The aerosol exit slit is not included.

Figure A.1.8a and A.1.8b shows the mesh distribution around the region where the aerosol flow and the sheath flow meet for the original and modified inlet.
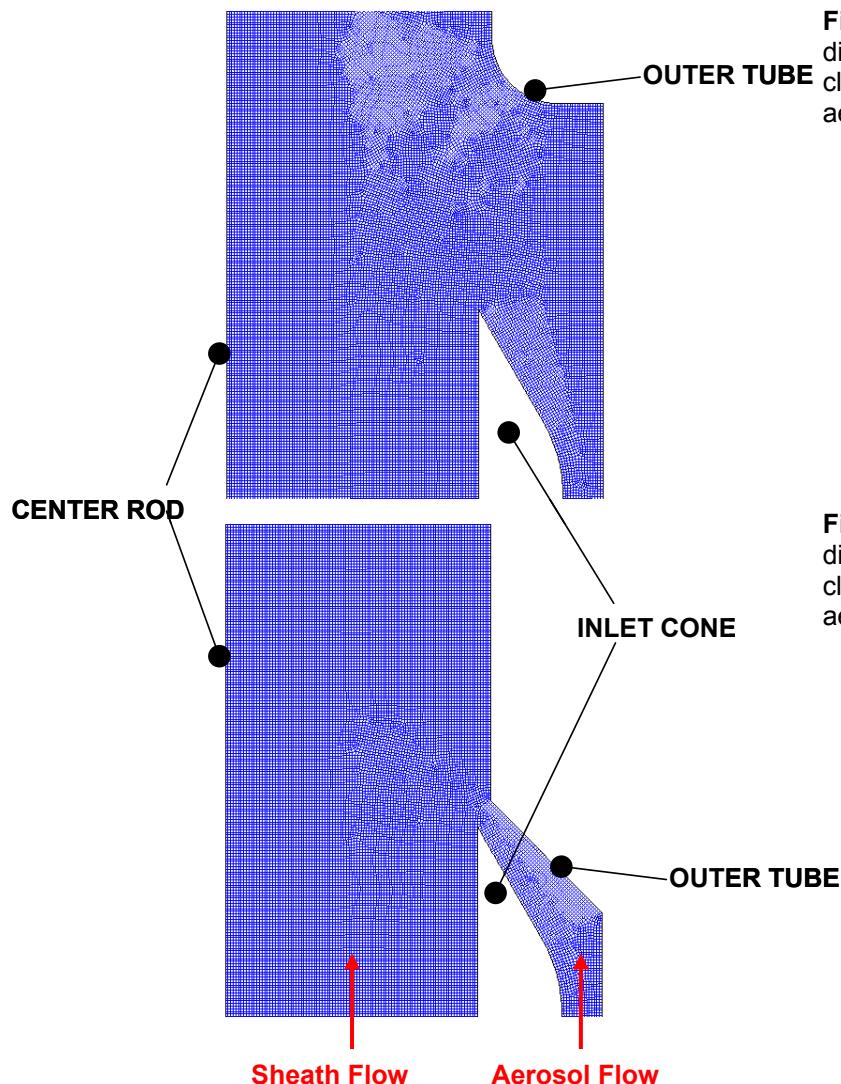

Figure A.1.8a: Mesh distribution around the region close to the original TSI DMA aerosol entrance slit.

Figure A.1.8b: Mesh distribution around the region close to the modified TSI DMA aerosol entrance slit.

Figure A.1.9a and A.1.9b shows the modelled velocity vector coloured by velocity magnitude (ms^{-1}) in the region close to the entrance slit for aerosol/sheath flow ratio β = 1.0/10.0 (lmin^{-1}) / (lmin^{-1}) both for original and modified inlet.
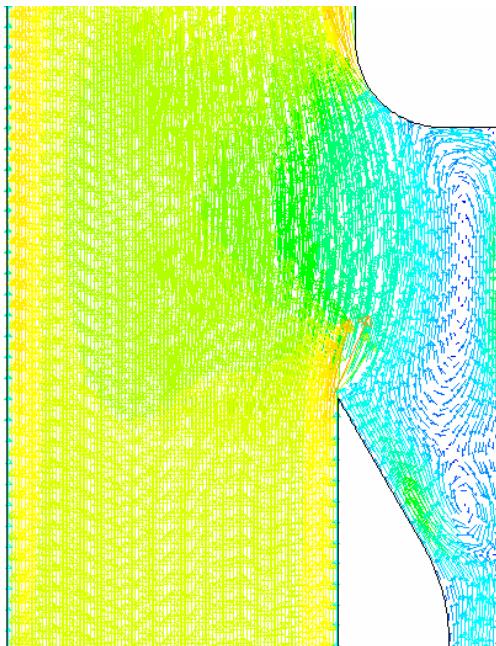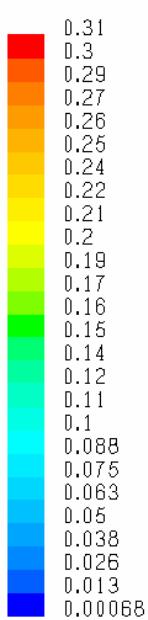
Figure A.1.9a: Flow pattern for the region close to the aerosol entrance slit of TSI DMA at β=1.0/10.0
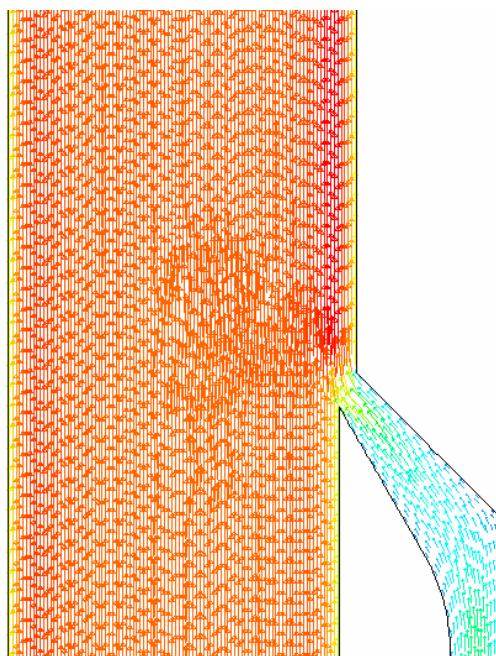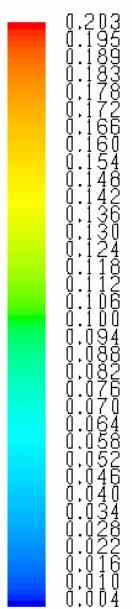
Figure A.1.9b: Flow pattern for the region close to the aerosol entrance slit of modified DMA at β=1.0/10.0

A flow recirculation zone is predicted only for the conventional TSI DMA inlet, as shown in Figure A.1.9a. The modified inlet shows a good flow matching between the aerosol and sheath streams for β = 1.0/10.0 (lmin^{-1}) / (lmin^{-1}) and lower (i.e. 1.0/20, 0.5/20 and 0.3/20, not in this document).

The particles trajectories inside the original TSI DMA inlet have been modelled. The re-circulating particle vortex increases with decreasing aerosol/sheath flow ratio but is

not present when the modified inlet cone is used, as is clearly shown in Figure A.1.10a and A.1.10b for the same particle diameter and flow ratio.
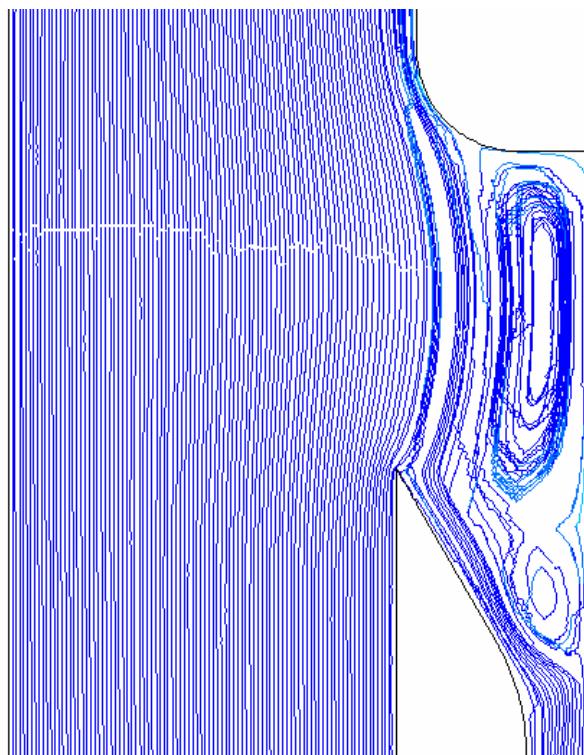
Figure A.1.10a: 100 nm particle traces close to the aerosol entrance slit of TSI DMA at β=1.0/10.0
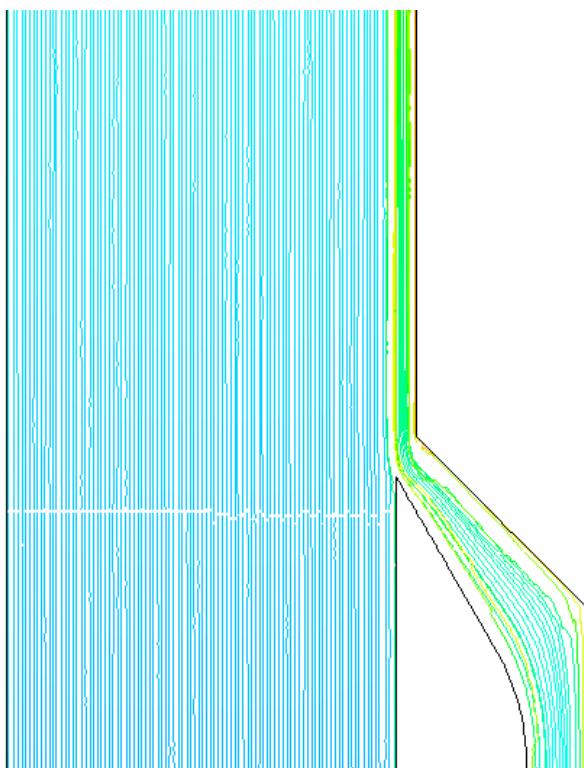
Figure A.1.10b: 100 nm particle traces close to the aerosol entrance slit of the modified inlet DMA at β=1.0/10.0

Clearly, recirculation will increase even more for the conventional TSI DMA inlet when using lower aerosol/sheath flow ratio as is illustrated in Figure A.1.11a and A.1.11b.
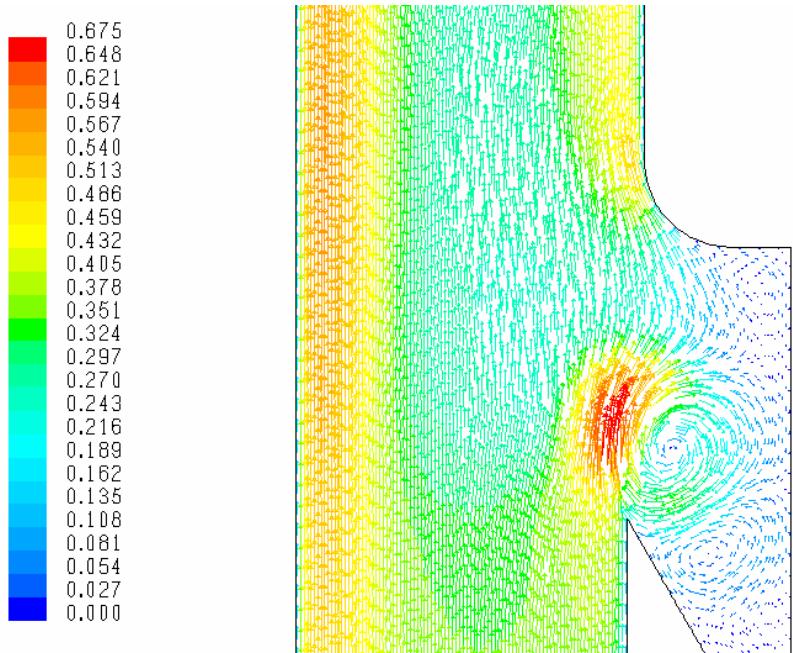

Figure A.1.11a: Flow pattern for the region close to the aerosol entrance slit of TSI DMA at β=0.3/20
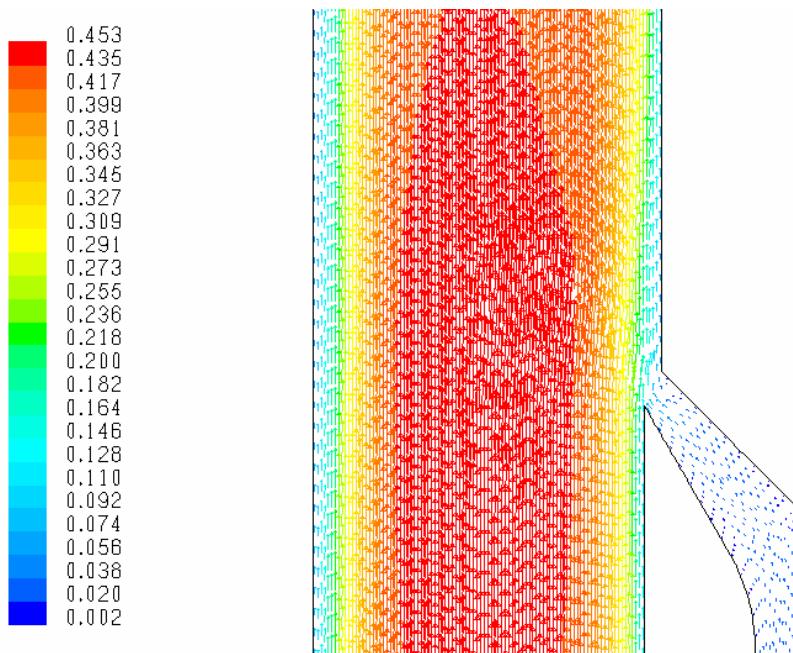
Figure A.1.11b: Flow pattern for the region close to the aerosol entrance slit of modified DMA at β=0.3/20

We can therefore conclude that the modifications of the aerosol entrance slit greatly enhance the coherence of the aerosol flow and limits turbulent diffusion. The transfer efficiency as well as the size resolution of the DMA column are therefore potentially improved by these modification.

5. EXPERIMENTAL VALIDATION OF THE MODIFIED DMA

5.1. Tandem DMA arrangements

The experimental determination of a DMA transfer function is often performed using a Tandem DMA (TDMA) arrangement, as suggested by e.g., Stolzenburg (1988) and Rader and McMurry (1986). The TDMA arrangement implies that similar DMAs are used in series. In this study, two different TDMA setups are operated with the specificities shown in Table A.1.1:

	DMA Type	Inner radius	Outer radius	Effective length	Qa DMA1	Qa DMA2	Qex=Qsh DMA1	Qex=Qsh DMA2
TDMA 1	Vienna type (Lund)	2.5 cm	3.3 cm	11.4 cm	2.0 lmin^{-1}	1.0 lmin^{-1}	13.5 lmin^{-1}	6.75 lmin^{-1}
TDMA 2	TSI type modified	0.9375 cm	1.95 cm	44.0 cm	2.0 lmin^{-1}	1.0 lmin^{-1}	13.5 lmin^{-1}	6.75 lmin^{-1}
Table A.1.1: TDMA specificities used in this work.								

TDMA1 and TDMA2 setups were used to compare the real transfer function of the DMA built at Lund University (i.e. medium Vienna Type DMA) and the modified DMA in the size range 10 -150 nm. A schematic of this setup is shown in Figure A.1.12.
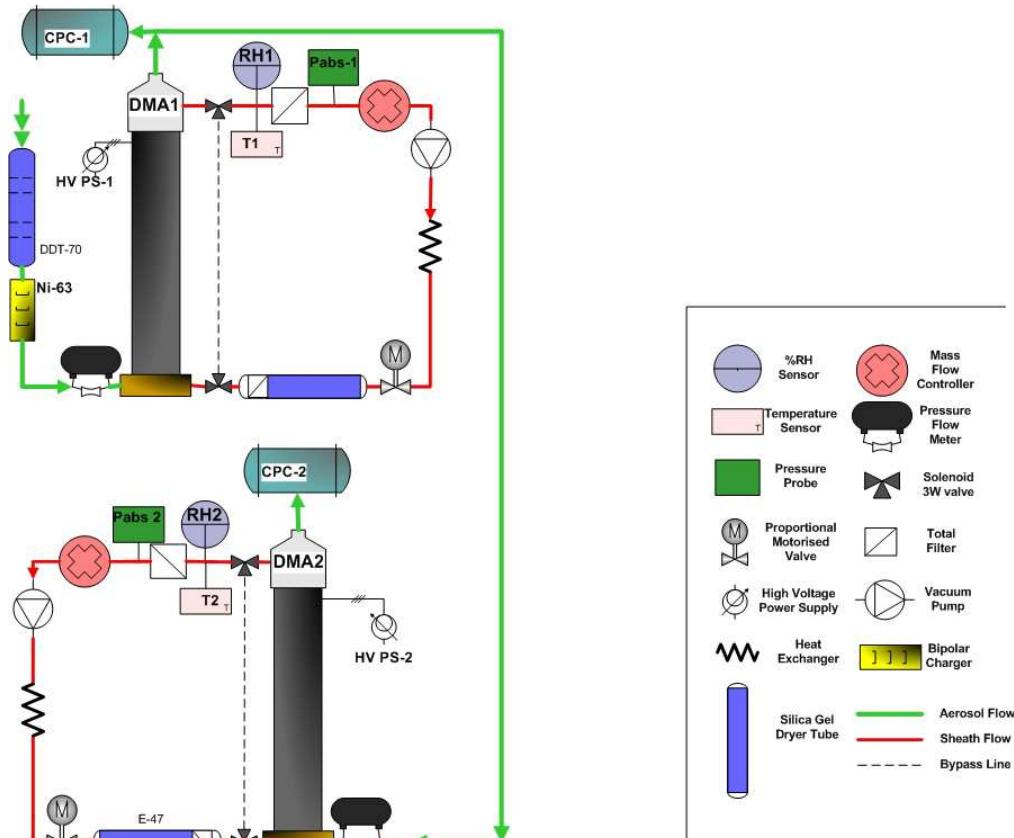
Figure A.1.12: The experimental setup used in this work for TDMA1 and TDMA2.

5.2. Particles generation

Two different aerosols species were generated using two different setups. The first arrangement, illustrated in Figure A.1.13, was used to measure aerosol particles in the size range 20 -150 nm.
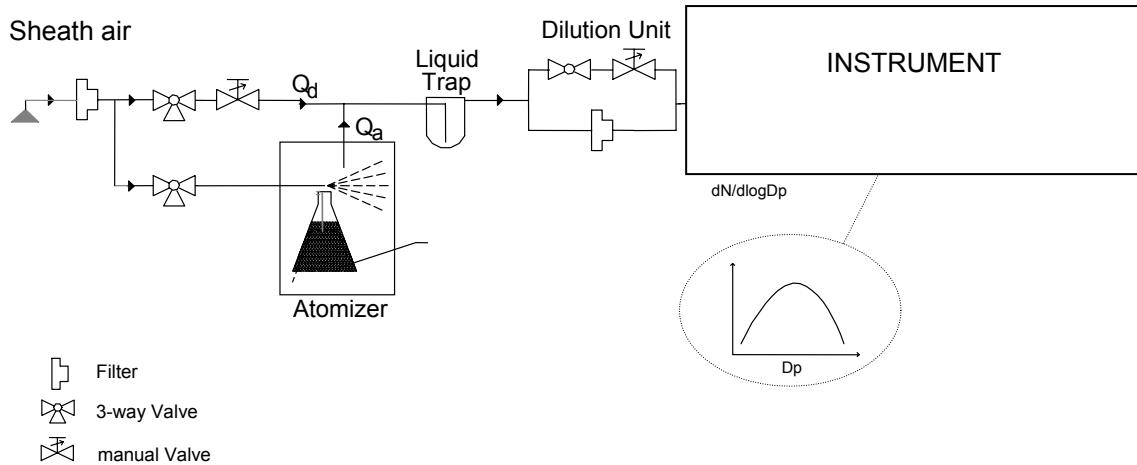
Figure A.1.13: Schematic of aerosol generation setup to produce NaCl particles. Q_a and Q_d refer to the gas flow of the atomizer and the additional dilution air flow, respectively.

A laboratory NaCl aerosol was produced by nebulising a 0.1 weight percent solution of NaCl and by clean water (18.2 MegaOhm Ultra Pure Water) with an atomiser (TSI Model 3670). After dispersion, the polydisperse NaCl aerosol is further mixed with sheath air for drying and dilution in a mixing chamber (100 l) to ensure a stable particle concentration during time. When approaching the sizes well below 20 nm another aerosols generation arrangement was necessary. We used a hot wire generator (custom made) shown in Figure A.1.14.
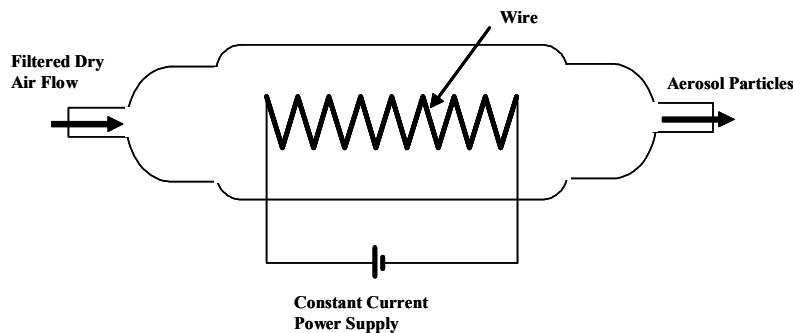
Figure A.1.14: Schematic of the hot wire generator. The cover is Pirex glass and the removable pure Cu-Zn wire have a spiral shape.

The primary output material of the heated pure Cu-Zn wire is assumed to consist of vapor phase oxides of Cu and Zn, presumably a mixture of CuO and ZnO, wich rapidly ends up in particulate phase due to high temperature gradients. However, for the matter of this study, the nature of the particles is irrilevant.

The total flow rate of clean air through the generator were varied in the range of 1-10 lmin^{-1} and the electric current through the wire was varied between 4 and 7 A, depending on the particle size range and concentration needed.

As exemple, a particle size distribution from the hot wire generator and the atomiser generator are presented in Figure A.1.15a and A.1.15b, respectively.
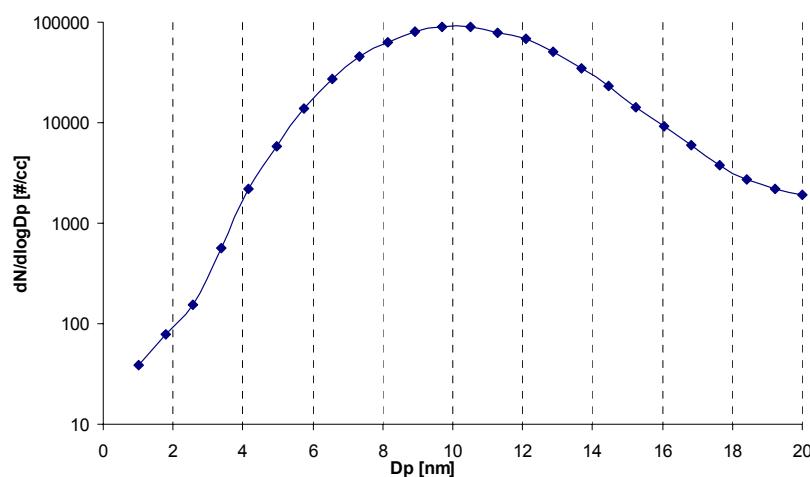
Figure A.1.15a: Size distribution from the wire generator (current 5 A, flow 3 lmin^{-1}) measured by DMA and TSI Electrometer.
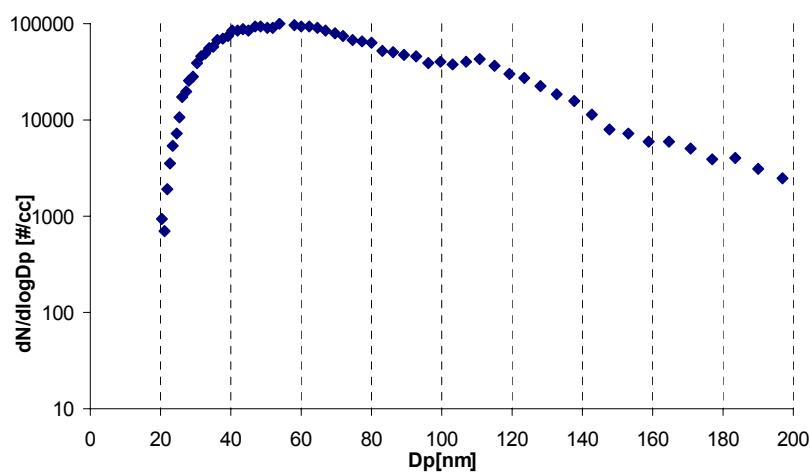
Figure A.1.15b: Size distribution from the atomiser generator measured by DMA and TSI CPC 3010.

5.3. DMA size calibration with latex spheres

As discussed above, the certainty of the size selection of a DMA depends on the stability of flow rates, the geometry and the voltage supply which consists of the computer device in connection with the high voltage supply. For characterization of the size selection of the DMA, latex spheres with diameters of 100 and 300 nm suspended in distilled water have been nebulized using an atomizer (TSI 3076) for production of submicrometer aerosol particles.

After leaving the atomizer the particles were dried using a diffusion dryer tube, although it has been assumed that the particles have not taken up any water. It has been found that all particles were selected at grater diameters than expected. In Table A.1.2, the expected and the experimentally derived diameters are listed.

Expected diameter of latex spheres (nm)	Experimentally derived diameter with the TSI Modified DMA (nm)	Deviation in %
100	107	7
300	304	4

Table A.1.2: Expected and experimentally derived diameters of latex spheres using a TSI modified DMA.

As comparaison with previous study (Massling, 2002), in Table A.1.3 are summarized the results of the same calibration test made with an Hauke Type DMA (i.e. similar geometry to the Lund Vienna Type DMA).

Expected diameter of latex spheres (nm)	Experimentally derived diameter with the TSI Modified DMA (nm)	Deviation in %
100	118	18
248	268	8

Table A.1.3: Expected and experimentally derived diameters of latex spheres using a Hauke Type DMA.

As shown in Table A.1.3 the deviation of sizing observed with the "Non genuine" Vienna Type DMA are nearly the double of the TSI DMA. A possible reason for the size discrepancy could be the different design and the poor coaxiality of central rod inside the column of the DMAs.

In Figure A.1.16, the number size distribution of the 100 nm latex spheres taken with a TSI Modified DMA is shown.
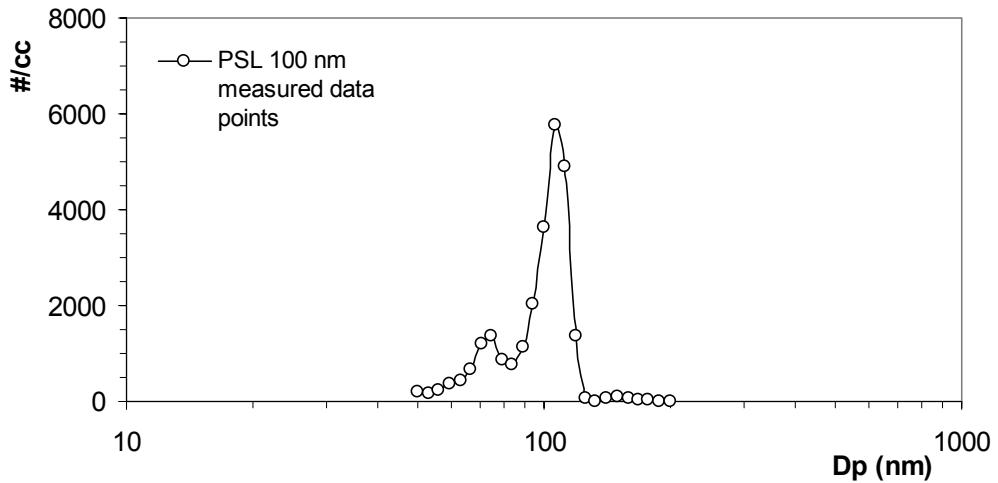
Figure A.1.16: Particle number size distribution taken with a TSI Modified DMA without the modified inlet cone of 100 nm latex spheres.

Obviously, the particles have been found at a value of 107 nm. All maxima found on the left side of the main maximum can be attributed to multiply charged particles (see Appendix A.1). The mean diameters of each peak show exactly the multiple value of electrical mobility of the main peak.

5.4. TDMA Comparison results

The comparison of the transfer functions for 15, 50 and 100 nm particle diameters for both the Vienna Type Lund TDMA arrangement and the TSI Type Modified TDMA arrangement are shown in Figure A.1.17. Identical flow ratio in the first DMA (2.0 / 13.5 lmin^{-1} / lmin^{-1}) and the second DMA (1.0 / 6.75 lmin^{-1} / lmin^{-1}) are used for both TDMAs. Y-axis represents the count ratio between CPC2 and CPC1 (i.e. relative counts).
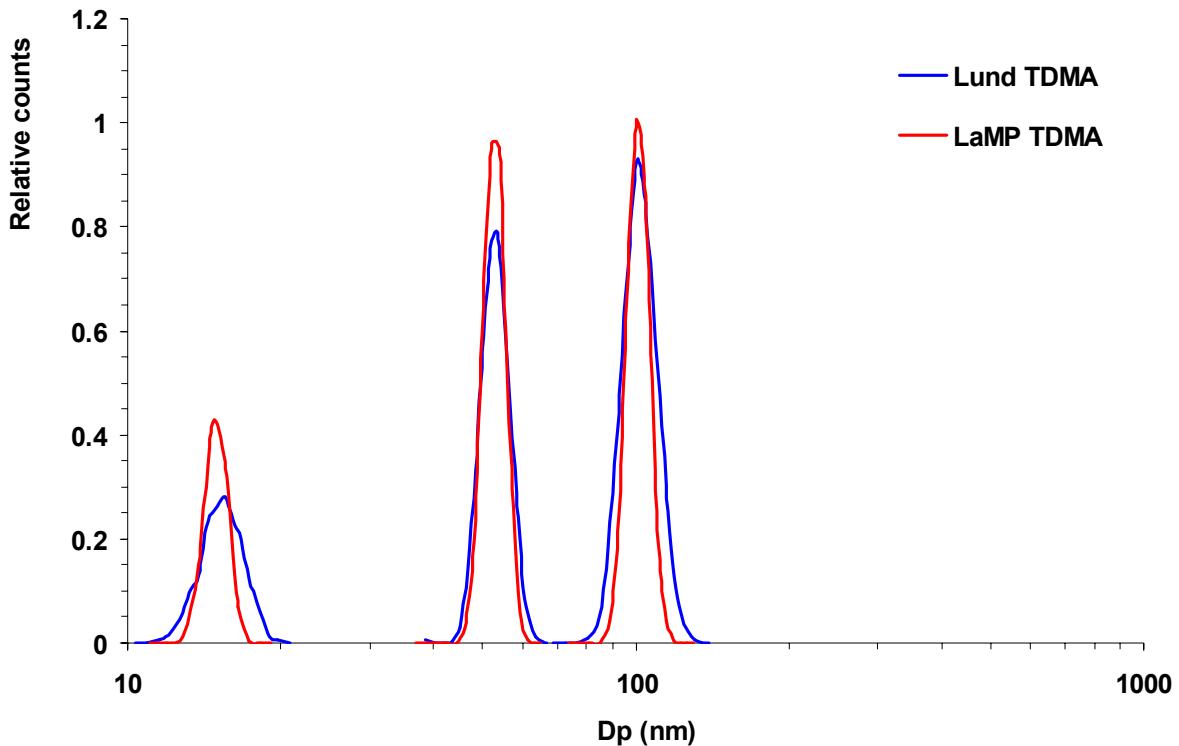
Figure A.1.17: Transfer function comparison for Lund DMA and LaMP-DMA for 15, 50 and 100 nm particle.

A significant improvement is clearly seen for the TSI Modified DMA as respect to Lund Vienna Type DMA. The improvement concerns both the detection sensitivity and transfer function width in particular for the 15 nm particles. It is seen that the resolution of the TSI Modified DMA is nearly ideal (with transfer function Half-Width of 0.15) down to 15 nm. The Lund Vienna Type DMA transfer function deviates significantly from the ideal condition. As it is seen in Figure A.1.17 the broadening of the transfer function width is higher than predicted by theory even for 100 nm diameter particle (with transfer function Half-Width of 0.2).

Because we do not have two original TSI DMAs for performing a comparison between modified TDMA and original TSI TDMA, an additional test was conducted to investigate the impact of the modified aerosol inlet cone in the DMA. Figure A.1.18 shows results from a comparison between the two DMAs with and without the modified inlet cone for 10 nm particles.
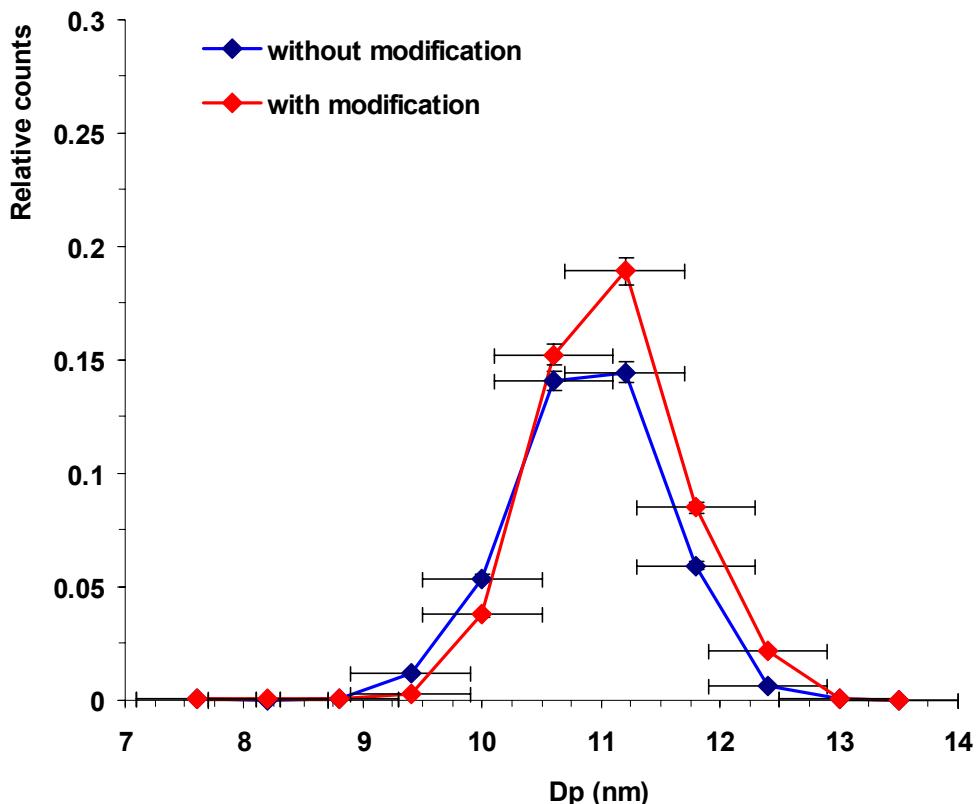
Figure A.1.18: Modified DMA transfer function comparison for 10 nm particle with the standard inlet cone ("without") and with the modified one ("with").

This test confirms results obtained previously showing that the new inlet design permits higher resolution measurement than conventional TSI- or Vienna-type DMAs. The modifications permit a significant reduction of diffusion losses and limit the broadening effect of the transfer function width in the ultra-fine size range. This improved ability to select a precise particle size is not obtained at the expense of the DMA transfer efficiency. This is confirmed by a direct comparison of a DMPS spectrum, with an integrated counting performed using a CPC, given for the two DMAs with and without the modified inlet cone.
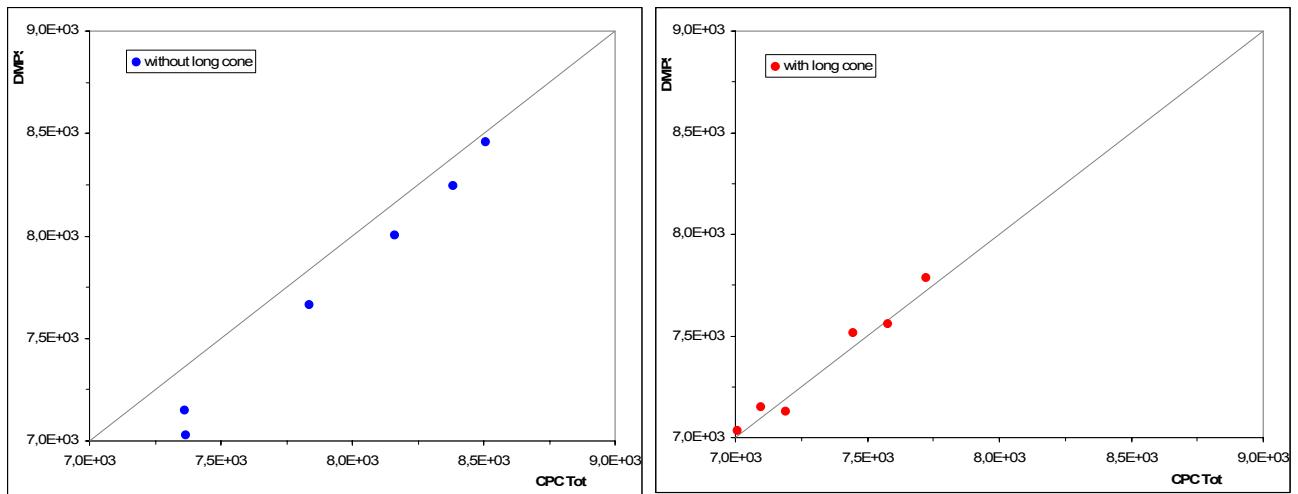
Figure A.1.19: Total CPC count vs integrated DMPS spectra with (red dot) and without (blue dot) the modified DMA.

The experiment was performed using generated aerosols of dimension lower than the maximum scanning diameter of the DMPS (i.e. range=5 - 250 nm). Results are shown in Figure A.1.19. Clearly, a very good agreement is found leading to the conclusion that the modified DMA is well-suited for atmospheric aerosol size characterization.

6. CONCLUSIONS

The particle classification using a DMA relies heavily on geometry and optimal designs of the DMA column as well as on the accurate control of all the air flows in the DMPS. In this context, the most important sources of error and, furthermore, deviations from the ideal transfer function shape for the "Non genuine" Vienna Type DMA (i.e. Lund DMA) could arise from:

(a) poor design and consequently mixing of the aerosol and sheath air flows inside the DMA analyser leading to irregularities (i.e. "humps" visible especially in Figure A.1.17 for 15 nm particles) in the transfer function.

(b) poor coaxiality of central rod inside the DMA column leading to irregularities in the electric field (the central rod is not fixed at two extremities).

(c) furthermore, some minor errors are generated due to inaccuracies in the definition and measurement of the DMA dimensions as well as in the measurement of the DMA voltage for each mobility class.

We have validated in our study a newly-built Differential Mobility Analyser. After numerical evaluation and construction we have shown that the aerosol/sheath flow inlet modification permit a significant reduction of diffusion losses and limit the broadening effect of the transfer function width in the ultra-fine size range. It is concluded that the re-designed features increase the performances of a DMA.

REFERENCES

Ankilov, A., Baklanov, A., Colhoun, M., Enderle, K. H., Gras, J., Julanov, Y., Kaller, D., Lindner, A., Lushnikov, A. A., Mavliev, R., McGovern, F., O'Connor, T. C., Podzimek, J., Preining, O., Reischl, R., Rudolf, R., Sem, G. J., Szymanski, W. W., Vrtala, A. E., Wagner, P. E., Winklmayr, W., Zagaynov, V. (2002). Particle size dependent response of aerosol counters. J. Atmos. Research. 62, 209-237.

Birmili, W., Stratmann, F., Wiedensohler, A., covert, D., Russell, L. M. (1997). Determination of Differential Mobility Analyser Transfer Functions using identical instruments in series. Aerosol Sci. and Techno. 27:215-223.

Chen, D. R., Pui, Y. H., Mulholland, W. and Fernandez, M. (1999). Design and testing of an aerosol/sheath inlet for high resolution measurements with a DMA. J. Aerosol Sci. 30 (8), 983-999.

Chen, D. R., Pui, Y. H., Hummes, D., Fissan, H., Quant, F. R. and Sem, G. J. (1998). Design and evaluation of a nanometer aerosol differential mobility analyser (Nano-DMA). J. Aerosol Sci. 29 (5/6), 497-509.

Collins, D. R., Nenes, A., Flagan, R. C. and Seinfeld, J. H. (2000). The scanning flow DMA. J. Aerosol Sci. 31 (10), 1129-1144.

Flagan, R. C. (1999). On differential mobility analyszer resolution. Aerosol Sci. and Technol. 30:556-570.

Flagan, R. C. (2004). Opposed migration aerosol classifier (OMAC). Aerosol Sci. and Technol. 38:890-899.

Jokinen, V. and Makela, M. (1997). Closed-loop arrangement with critical orifice for DMA sheath/excess flow system. J. Aerosol Sci. 28 (4), 643-648.

Karlsson, M. N. A., Frank, G. and Martinsson, B. G. (2000). Measurement of the differential mobility analyser transfer function. J. Aerosol Sci. 31 (S1), S23-S24.

Karlsson, M. N. A. and Martinsson, B. G. (2003). Method to measure and predict the transfer function size dependence of individual DMAs. J. Aerosol Sci. 34, 603-625.

Knutson, E. O. and Whitby, K. T. (1975). Aerosol classification by electric mobility: apparatus, theory, and applications. J. Aerosol Sci. 6, 443-451.

LaFranchi, B. W., Knight, M., Petrucci, G. A. (2003). Leaching as a source of residual particles from nebulization of deionized water. J. Aerosol Sci. 34, 1589-1594.

Le Bronec, E., Renoux, A., Boulaud, D. and Pourprix, M. (1998). Use of a radial flow mobility analyser to determine the mass and density of aerosol particles. J. Aerosol Sci. 29 (S1), S409-S410.

Maisels, A., Kruis, F. E., Fissan, H. (2004). Coagulation in bipolar chargers. J. Aerosol Sci. 35, 1333-1345.

Mertes, S., Schroder, F. and Wiedensohler, A. (1995). The particle detection efficiency curve of the TSI-3010 CPC as a function of the temperature difference between saturator and condenser. Aerosol Sci. and Technol. 23:257-261.

Reischl, G. P., Makela, J. M., Necid, J. (1997). Performance of Vienna type differential mobility analyser at 1.2-20 nanometer. Aerosol Sci. and Technol. 27:651-672.

Scheibel, H. G. and Porstendörfer, J. (1983). Generation of monodisperse Ag- and NaCl-aerosols with particle diameters between 2 and 300 nm. J. Aerosol Sci. 14, 113-126.

Stolzenburg, M. R. and McMurry, P. H. (1988). TDMAFIT Users' Manual. Minneapolis, Minnesota

Stratmann, F., Orsini, D. and Kauffeldt, T. (1997). Inversion algorithm for TDMA measurements. EAC 1997, Hamburg. J. Aerosol Sci. S701-S702.

Stratmann, F.,Kauffeldt, T., Hummes, D. and Fissan, H. (1997). Differential electrical mobility analysis: a theoretical study. J. Aerosol Sci. and technol. 26,368-383.

Wang, S. C. and Flagan, R. C. (1990). Scanning electrical mobility spectrometer. Aerosol Sci. and Technol. 13:230-240.

Wiedensohler, A. (1988). An approximation of the bipolar charge distribution for particles in the submicron size range. J. Aerosol Sci. 3, 387-389.

CHAPITRE I.2

Volatility Tandem Differential Mobility Analyser

La mesure des propriétés volatiles de l'aérosol a été initiée au LaMP à la suite des travaux de Sellegri et al. (2003) montrant que les composés organiques les moins volatiles étaient également les mieux lessivés par les gouttelettes de nuages. Ceci avait motivé la construction d'un analyseur différentiel de mobilité tandem pour la mesure de la volatilité des particules (V-TDMA) dont la première version a été achevée dans le cadre de la thèse de Régis Dupuy (Dupuy, 2003) et de mon DEA (Villani, 2003).

L'objectif du V-TDMA était de pouvoir procéder à une analyse des fractions volatiles en ligne, en particulier derrière un système d'impacteur virtuel à contre-flux (CVI : counter flow virtual impactor). Le principe du V-TDMA se base sur le fait que la température de volatilisation d'une particule d'aérosol dépend de sa composition chimique. Lorsqu'une population d'aérosols est chauffée, une partie de ses composants retourne à l'état gazeux. La volatilisation d'une fraction ou de la totalité de ses composants correspond à une perte en masse de la phase aérosol au profit de la phase gazeuse et affecte la granulométrie de l'aérosol, d'où l'intérêt du couplage volatilité / granulométrie. La température à laquelle se produit cette volatilisation donne donc une indication sur la nature chimique des particules. La nature chimique des particules pouvant évoluer en fonction de leur taille, l'information sur la température de volatilité doit être accessible sur toute la gamme de taille des aérosols. Cette technique a permis de montrer que la plupart des particules de taille inférieure à 1 µm sont dominées par le sulfate (Clarke, 1987 ; Pinnick, 1993 ; Rood, 1987). Le V-TDMA a été utilisé pour étudier les composés volatiles à base de sulfate à des températures de 250°C (Covert and Heintzenberg, 1993) et pour identifier la fraction d'acide sulfurique des aérosols avec une température de 120°C (Orsini et al., 1999). La première partie de ma thèse a donc consisté au développement d'une version améliorée du V-TDMA ainsi qu'à sa validation. C'est l'objet du chapitre I.2 de ce travail de thèse.

L'analyseur de volatilité / granulométrie se compose schématiquement de deux parties distinctes. La première partie concerne la mesure des particules et comprend les deux DMAs décrit dans le chapitre précédent, et leurs systèmes d'acquisition / contrôle, le neutraliseur de charge (Appendix A.1) ainsi que les deux compteurs de particules (Appendix A.2). La seconde partie est constituée par le système de thermo-désorption (Appendix A.5). Le V-TDMA est illustré sur la Figure I.2.1.
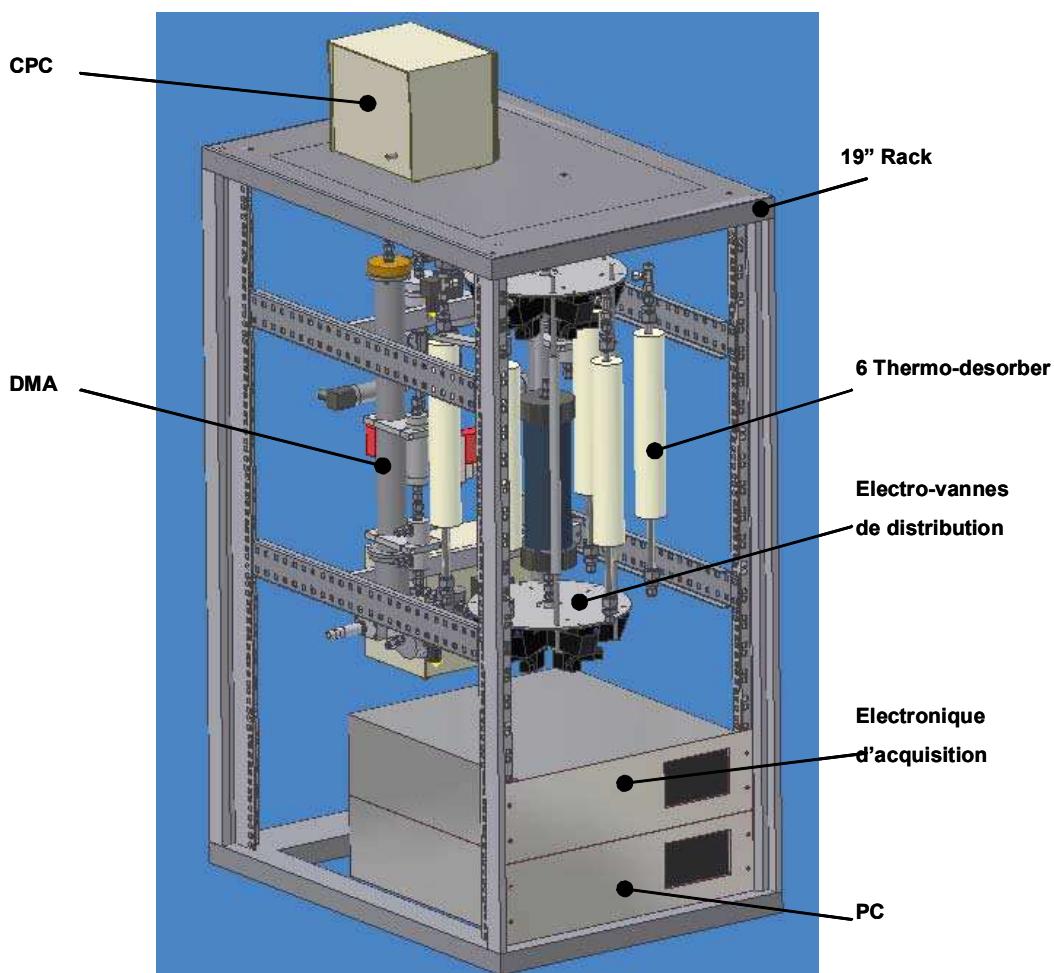
Figure I.1.2: V-TDMA

Le chapitre suivant décrit en détails le système V-TDMA, les procédures de contrôle et d'inversion des données, la détermination de la fonction de transfert des particules et les tests de validation de l'appareil. Ce chapitre fait l'objet d'une publication en révision à Aerosol Research and Technology.

DESIGN AND VALIDATION OF A 6-VOLATILITY TANDEM DIFFERENTIAL MOBILITY ANALYSER (V-TDMA)

P. Villani[1], D. Picard[1], N. Marchand[1, *], K. Sellegri[1], P.Laj[1]

[1]Laboratoire de Météorologie Physique ,CNRS, Université Blaise Pascal, Aubière, France

[*] now at: Laboratoire de Chimie et Environnement, Université de Provence, Marseille Cedex 3, France

ABSTRACT

A volatility tandem differential mobility analyzer (V-TDMA) was developed to allow fast field measurement of the volatile fraction of atmospheric aerosol particles in the particle size range 20-650 nm. In this V-TDMA the volatile compounds are evaporated by heating the aerosol to a temperature between 25°C and 300°C. The heating unit is equipped with six symmetric columns kept at different temperatures that allow the heating temperature to be rapidly changed so that a higher temporal resolution can be achieved compared to a regular V-TDMA. This work first focuses on the design and calibration of the heating units for the conditioning of a selected aerosol sample while minimizing sample losses due to thermophoresis and diffusion. The design was based on the modeling of the profiles of temperature and velocity and the behavior of a monodisperse aerosol in the heating units, using Computational Fluid Dynamics (CFD) Flow Modeling Software, FLUENT 6.1. This allowed for initial estimations of the heater dimensions and also calculation of the minimum length of heating tube needed to completely evaporate the aerosol particles at high temperature with sufficient residence time, as well as to cool the aerosol sample down to ambient temperature. Next, the aerosol heating rate and aerosol deposition losses within the flow tube were estimated, and re-condensation of volatilized compounds evaluated. Then the V-TDMA was calibrated and tested in the laboratory to determine the transfer efficiency, and finally, atmospheric aerosols were analyzed, with the first results presented here. This work emphasizes the need for better standardization of thermo-desorbing units for atmospheric aerosol studies.

1. Introduction

In recent years, much attention has been directed towards understanding the effect of aerosols on a variety of processes in the earth's atmosphere. Physical properties such as aerosol total number concentration, number size distribution and the chemical composition of submicron atmospheric aerosol particles are key parameters controlling the direct and indirect radiative forcing of the climate by aerosols (IPCC, 2001). These particles affect the radiation budget directly by scattering and absorbing incoming solar radiation, and indirectly through their ability to modify cloud microphysics and albedo (IPCC, 2001). There has been an increasing need for size-resolved measurement of the chemical behavior of fine atmospheric aerosols. Many techniques for the determination of aerosol chemical composition and structure are currently used for atmospheric studies.

Analyses of particle thermal properties are based on the fact that most components present in aerosols are volatile at a characteristic temperature. When temperature increases, a fraction of the chemical constituents of an aerosol particle volatilizes resulting in a change in both number concentration (when a particle is totally volatilised) and size. From the temperature at which complete or partial volatilization takes place, the chemical composition and the degree of mixing within the population can be estimated.

The most common airborne volatility methods to determine aerosol composition are based on the principle of passing the aerosol through a conditioning tube where the specific chemical components are evaporated at predefined temperatures (O'Dowd et al., 1992; Jennings et al., 1994 and 1997; Burtscher et al., 2001). To determine the corresponding refractory fraction, the residual size distribution is measured with either an optical particle counter or a scanning mobility particle sizer, and is then compared to the initial distribution. To separate the volatile from the non-volatile compounds (e.g., elemental carbon, crustal material, sea salt), most of these measurements are made at temperatures below 300°C. To infer the fraction of elemental carbon, measurements are made between 800°C–1000°C, however, they require complex instrumentation and an inert atmosphere (Jennings and O'Dowd, 1992; Jennings et al., 1994; Smith et al., 1996).

Tandem Differential Mobility Analyzer (TDMA) provides information on particle composition and size, in almost real time, and hence offers a powerful advantage over many other methods that require longer time-integration. Classically, TDMAs are used to characterise either hygroscopic properties (Humidity-TDMA) (Rader et al. (1986) or thermal properties of atmospheric particles (Volatility-TDMA) (Orsini et al. (1998)).

In this work, we present the development of a new Volatility-TDMA (V-TDMA) system constructed to measure the size-resolved volatile behavior of aerosols in the size range $20 < D_p < 550$ nm with fast time-integration at temperature up to 300°C. In this paper, a detailed technical description of this newly-built V-TDMA is presented together with an accurate evaluation of the different artifacts associated with V-TDMA operations. The first measurements performed are presented in addition to the potential application of V-TDMA techniques to study the role of particle coating.

2. Instrument design

2.1 TDMA system

2.1.1 Conception of the TDMA

The TDMA system, shown in Figure A.2.1, is based on two DMAs assembled in series (i.e. Vienna Type DMA, inner radius =2.5 cm, outer radius =3.3 cm, length =28 cm, Aerosol-Related Atmospheric Research Lund University, Swietlicki et al., 2002) in order to study aerosol properties as a function of the selected particle size. All aerosol tubes in the TDMA are of stainless steel with inner and outer diameters of 4 and 6.35 mm, respectively. In order to avoid particle losses, the tube lengths and number of bends were minimized. A laminar flow is maintained through all sampling lines (Re<2000).
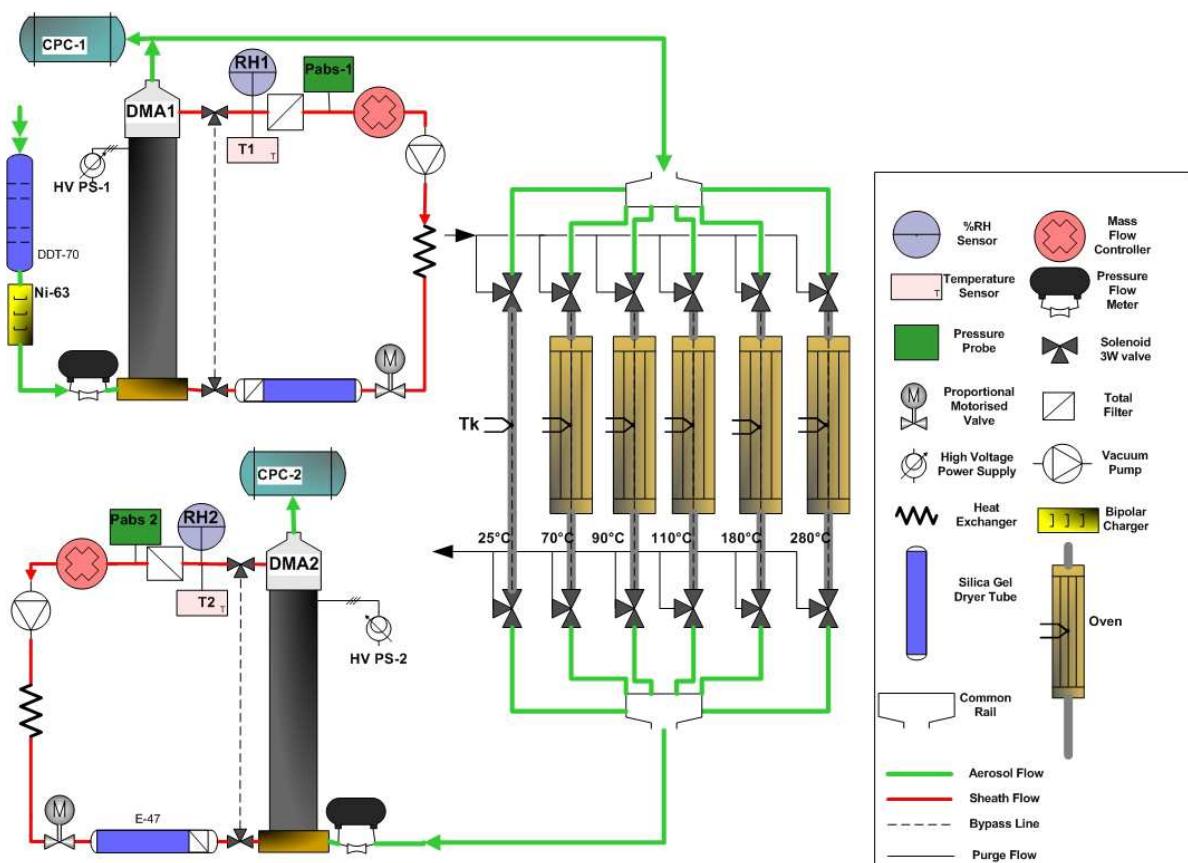

Figure A.2.1: Schematic view of the V-TDMA

The system can be broken down into three main steps:

- Step 1 consists of particle selection from the polydisperse aerosol sample source using the first differential mobility analyser (DMA 1). In this step the aerosol first enters a silica gel diffusion dryer to dry the particles down to RH<15%. The dry aerosol is then charged with a bipolar diffusion charger (^{63}Ni) and enters DMA1. A voltage V1 is set to select a narrow mobility bandwidth aerosol from the polydisperse aerosol source. The narrow size range is defined by the transfer function of the differential mobility analyser (DMA) (Knutson and Whitby (1975)). The monodisperse sample aerosol flow Qs exiting DMA1 is split into two paths: one half of the sample is directed to step 2 and the other to the first condensation particle counter (CPC1, TSI Model 3010). CPC1 is used to continuously monitor the concentration of the DMA1-selected aerosol (i.e. the concentration of the aerosol sent to step 2).

- In step 2, the aerosol is heated to predefined temperatures in one of the six parallel heating columns. If the aerosol sample is volatile at the given temperature, the conditioning process could alter the mobility distribution, so a measurement of residual particle number size distribution is required.

- In step 3 the second DMA (DMA2), in series with a second condensation particle counter (CPC2, TSI Model 3010), scans 24 channels in a stepping mode (i.e. DMPS) to determine the new conditioned mobility distribution. One measurement of one particle diameter for each conditioning temperature takes about 8 min.

2.1.2 Sheath Airflow System

The DMAs are operated at flow rates (sample flow/sheath air flow) of 2.0/13.5 lmin^{-1} (β=0.15, DMA1) and 1.0/6.75 lmin^{-1} (β=0.15, DMA2). Air flow is arranged in a closed re-circulating loop. The sheath air is treated with diffusion dryers and two total filters are placed in both sheath lines and excess-flow lines to remove particles and protect mass-flow meters and needle valves. Apart from the stability of the flows, operating the DMAs in a closed-loop arrangement also has the advantage of being relatively simple and robust for field campaign measurements. Another critical point is that the pump works at a temperature of approximately 50°C. Outgassing material from inside

the pump (e.g., from rubber membranes or O-rings) may condense at a lower temperature inside the V-TDMA and significantly change the aerosol and gas-phase composition. For the instrument presented in this paper, membrane pumps were used operating with Teflon membranes, thus avoiding any artifact by outgassing material. The sample flows in DMAs are monitored by measuring the pressure drop across flow restriction. The sheath air flows (13.5 and 6.75 lmin^{-1}) are controlled by mass-flow controllers/meters located in the excess air outlet of the DMAs and piloted by the aerosol flow measurement in a feed-back regulation system. This feature added to the program increases system reliability and stability with flow auto regulation. The volumetric flow is calculated by measuring the excess flow absolute pressure and temperature in each DMA loop just before the mass-flow controller/meter (see Figure A.2.1). These pressures and temperatures are used in the program to calculate particle mobility in each DMA. The pulsation in the air exiting the pump is removed by the buffer/cooler volume of the diffusion dryer tube (3,5 l). The sheath air is also fed into two heat exchangers to ensure sufficient air cooling.

The prescribed and conditioned aerosol size distributions after DMA1 and DMA2 respectively are retrieved using an inversion-fitting procedure that inverts measured aerosol mobility scans and accounts for losses in the measurement system (see following sections). The quantitative results, integral number and volatile volume are acquired for the distribution by fitting normal-gauss modes into the solution. It is important to note that most information relevant to the TDMA is acquired by comparison of prescribed and conditioned aerosol size distributions and does not necessarily require an absolute inversion to ambient aerosol distribution.

2.2 Conception of the Aerosol heating unit: design and performance

The design of the aerosol heater was considered to consist of three main tasks: modeling, construction and calibration. The goal was to construct an aerosol heater that would volatilize atmospheric particles up to 1000°C with minimum artefacts. Hence, the aerosol heater was designed to:

a)   Heat and hold the sample aerosol at a desired temperature long enough to evaporate completely particles in the diameter size range 20-550 nm.

b)   Minimize the losses by thermophoresis.

Moreover, for operational safety reasons the heating devices was to be built to avoid high surface temperatures (<100°C) even when operated at maximum heating capacity.

2.2.1 Aerosol heating in a laminar flow tube: design and construction

The objective was to keep the construction of the aerosol heater as simple as possible and at the same time satisfy the requirements of point a). The oven consists of a stainless-steel volatilization tube (i.d.=8.6 mm, o.d.=13.5 mm and length =60 cm) housed in a second concentric ceramic tube (i.d.=15 mm, length =30 cm). For additional insulation, the ceramic tube and heating wire are surrounded by refractory material. First, the thickness of the insulation (i.e., the outer radius of the refractory material) was calculated by an iterative process from the heat balance on the oven. For this purpose, the conduction heat power between the inner radius (r_i=0.0075 m) at the utilization temperature T_i and the outer radius (r_e) of the refractory material at temperature T_a (ambient temperature) was calculated as follow:

$$Q^{cond} = \frac{2\pi \cdot \lambda \cdot (T_i - T_a)}{\ln\left(r_e / r_i\right)} \cdot L, \quad [W] \qquad (1)$$

In a similar way, the convection heat power between the air at temperature T_a and the refractory surface (S) at temperature T_p was estimated as:

$$Q^{conv} = \alpha \cdot S \cdot (T_p - T_a), \quad [W] \qquad (2)$$

where λ [W/mK] is the thermal conductivity of the refractory material and α [W/m^{2}K] the convection coefficient, both of them being temperature dependent, L=0.3 m is the length of the ceramic heating tube (i.e. the length of the refractory material).

Hence, the heat balance can be written:

$$Q^{cond} = Q^{conv} \qquad (3)$$

In order to derive the insulation thickness (r_e) from these equations, we fixed the desired wall temperature and the utilization temperature (e.g. T_p=80°C at T_i=1000°C). The insulation thickness calculations for 6 different temperatures are listed in Table A.2.1.

	Ti (°C)	Tp (°C)	r_e (cm)	S (m^2)	V (m^3)	W (Kg)
Oven 1	100	40	3	0.062	8.5x10^{-4}	0.8
Oven 2	200	50	4	0.085	1.5x10^{-3}	1.35
Oven 3	400	60	4	0.085	1.5x10^{-3}	1.35
Oven 4	600	65	5	0.11	2.3 x10^{-3}	2.1
Oven 5	800	70	6	0.135	3.4 x10^{-3}	3
Oven 6	1000	80	6	0.135	3.4 x10^{-3}	3

Table A.2.1: Results of iterative calculations: Ti=oven utilization temperature, Tp=desired oven wall temperature, re=calculated oven outer radius, S=oven outer surface, V=oven volume, W=oven refractory weight.

We can see that, given the properties of the refractory material, the required thickness of insulation remains limited, even for elevated operating temperatures. This is confirmed by modeling of the heating system.

2.2.2 Modeling of the temperature profiles in the heating unit

The purpose of modeling is to have access to the temperature profiles inside the heating unit, including in the sample flow, in order to assess the performances of the unit, both in terms of heating efficiency and particle behavior. The predictions of thermal heating profiles in the oven and particle dynamics of an aerosol in a laminar flow tube were performed using FLUENT 6.1 (Computational Fluid Dynamic 3D modeling code) in a 7 equations model (K-ε). The CFD code predicts a) the temperature profiles in the volatilization tube and in the refractory insulation, b) the aerosol concentration profiles and the total aerosol losses through the heating unit due to thermophoresis and diffusion. A series of simulations were performed under the conditions listed in Table A.2.1. In Figure A.2.2, we present modeled predictions of the oven 2D temperature profile, corresponding to condition Oven 6 of Table A.2.1, with a ceramic tube wall at constant temperature of Ti=1000°C surrounded by refractory material with a diameter of 12 cm.
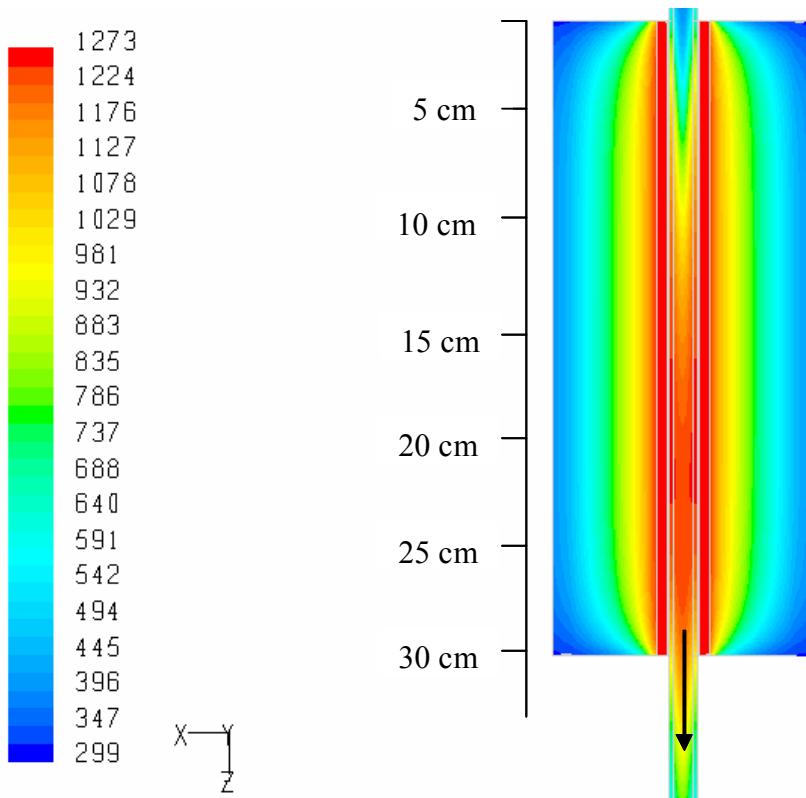
Figure A.2.2: Modeled 2D temperature profile for T_{amb}=25°C and T_i=1000°C (oven heating path).

During the simulation, the aerosol sample flow rate was 1 l min^{-1}, with an initial temperature of 25°C. The flow enters the stainless-steel tube from the top and flows downstream. After entering the heater, the aerosol flow is heated radially from the wall boundary to the centerline. At a distance of 13 cm from the entrance, the flow is uniformly heated and reaches a temperature slightly lower (20°C) than the ceramic tube wall temperature of 1000°C. After the heating path (30 cm) the flow is cooled down to ambient temperature over a distance of 25 cm.

In the model, air density and material conductive coefficients were tested for temperatures ranging from 25° to 1000°C. As a result, the predicted maximum temperature path length in the stainless-steel tube was about 10-12 cm (from 13 cm to 25 cm). This path was located at center-bottom of the oven due to thermal inertia and downstream flows. The modeled temperature profiles along the heating path were then compared to observations. The temperature measurements were performed by passing a thin thermocouple through the tube for different heating temperatures with a resolution of 5 cm along the tube. These results, shown in Figure A.2.3, confirm that the maximum temperature is reached approximately in the center

of the heating path and a uniform temperature is measured over 10-12 cm for each set temperature T_i (i.e. the thermal entry length is more or less constant with oven set temperature) .
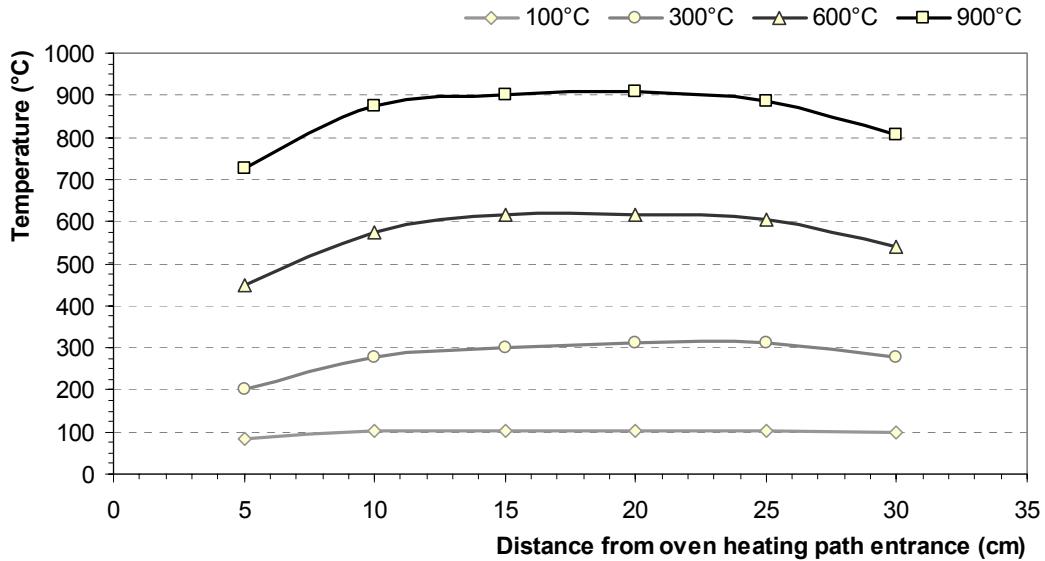

Figure A.2.3: Temperature profile inside the heating path of the oven.

In the operational version of the V-TDMA, the temperature measurement is therefore performed in the maximum temperature section and we are thus confident that the prescribed temperature in the V-TDMA corresponds to the actual aerosol heating temperature.

Under the initial flow conditions described previously and given the real dimensions of the volatilization tube, the mean aerosol velocity on the center-line within the flow tube is 0.3 ms^{-1}, corresponding to a Reynolds number of approximately 200, well within the laminar flow regime. The calculated resulting residence time in the oven heating path (30 cm) is t_R=0.3/0.3=1 s. The air velocity inside the volatilization tube does not change significantly with the oven set temperature Ti between ambient temperature and 1000°C, so we can confirm that the total residence time inside the heating path is not temperature-dependent. The effective residence time (t_E) in the section of maximum and uniform temperature (~10 cm) predicted by FLUENT is 0.33 seconds.

In other V-TDMA systems (e.g. D.A. Orsini et al. 1998, B.J. Brooks et al. 2001), the particle heating system consists of a ¼", 40 cm long stainless steel tube. With an

aerosol sample flow rate of 1 l min^{-1}, the aerosol velocity on the center line is 1.33 ms^{-1}, and the resulting total residence time 0.3 s. The effective residence time is however lower due to the thermal entry length (e.g. t_E=0.23 s, Orsini 1998). A smaller inner tube diameter reduces the time of non-uniform heating across the cross section of the laminar aerosol flow (i.e. lower thermal entry length) but also reduces the effective residence time in the heating path. However, large particles, higher particle concentrations and more particle refractory matter require greater volatilization energies, and in some cases, we believe that aerosol velocities higher than 0.3 ms^{-1} inside the volatilization tube can result in insufficient residence time for complete particle volatilization (Brooks et al. 2001). The residence time of particles in the heated section is a key parameter that controls the effectiveness of the volatilization process. It may explain the differences found between the different types of V-TDMAs used in previous studies.

3. Operating conditions for the V-TDMA

3.1 Thermophoresis aerosol losses in the V-TDMA

Interpretation of the V-TDMA data requires an accurate comparison of the mobility distribution with and without thermal conditioning of the aerosol population. It is important to evaluate the aerosol penetration efficiency through the V-TDMA, in order to be able to correct the measured mobility distributions for the size-dependent losses in the heating flow tube, DMAs and connection tubing. The V-TDMA system therefore requires quantification of particle transport efficiency as a function of size and the description of the response to thermal conditioning of an aerosol of known composition. To measure the total particle losses, the test must include the conditioner and the cooling path up to the DMA2 sample entrance. Ideally, the differences between these two mobility distributions are due to an evaporated mass fraction. The conditioned distribution, however, is additionally transformed by the effects of thermophoresis and diffusion, which are both temperature- and particle size-dependent. Consequently, with the aim of evaluating losses in the V-TDMA (mostly by diffusion and thermophoresis), calibration tests were performed with the experimental set-up described in Figure A.2.1. Sodium chloride (NaCl) aerosol particles were generated in the laboratory with an atomizer (TSI Model 3670) that contained a solution of Ultra Pure Water (ELGA) and NaCl salt. We chose to evaluate

losses in the system by using NaCl particles because they are easily generated and thermally stable up to Ti=500°C and therefore suited to study losses by thermophoresis up to Ti=400°C for a wide range of particle diameters. After dispersion, the polydisperse NaCl aerosol was further mixed with sheath air for drying and dilution in a mixing chamber (100 l) to ensure stable particle concentration. Since both diffusion and thermophoresis are size- and temperature-dependent, the penetration measurements were carried out for a range of particle diameters, Dp (15<Dp<150 nm) and temperature, Ti (25°<Ti<500°C). Comparison of concentration readings from CPC1 and CPC2 gave the transport efficiency η(Ti,Dp).

- The first test was performed to estimate losses at ambient temperature (25°C) of the heating unit. For that purpose, the particle concentration was measured with CPC2 immediately before the aerosol entered DMA2. This accounted for diffusion losses as well as for any possible particle deposition within the laminar flow tube, magnet valves, bones and elbows along the way. The penetration efficiency curve is shown in Figure A.2.4 (labeled "Oven").
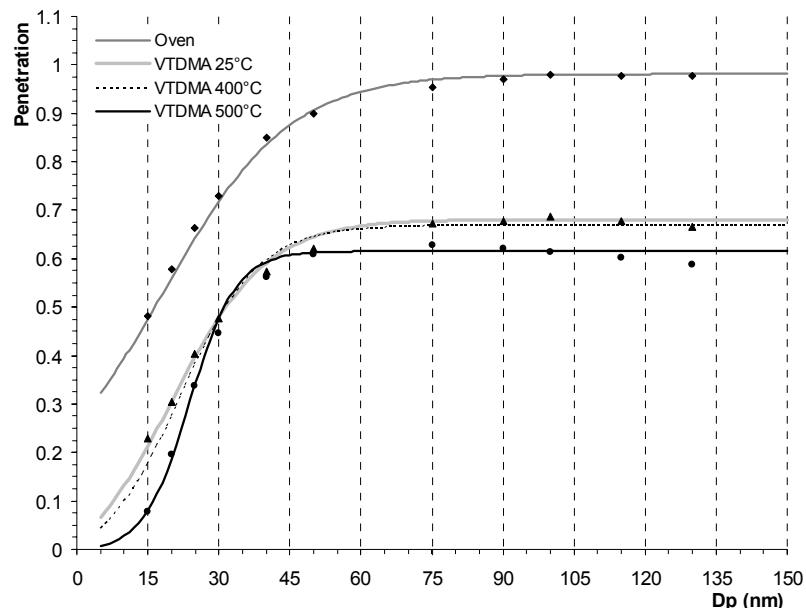

Figure A.2.4: Results of NaCl penetration test showing the efficiency of aerosol transport through the Oven and the V-TDMA depending on the selected particle size and heater temperature (curves are deduced by fitting the measured dot raw data points).

- A second series of tests was performed to estimate losses in the heating unit + DMA2 system for ambient temperature, 400° and 500°C. For that purpose, the particle concentration was measured with CPC2 after DMA2, setting the

same equivalent mobility diameter on each DMA (Figure A.2.4, labeled V-TDMA 25°C, 400°C and 500°C respectively).

The trends in Figure A.2.4 illustrate the combined thermophoretic and diffusional losses. It can be seen that there are no significant differences between ambient temperature and 400°C, but measurements above 500°C deviates significantly. This indicates that thermophoretic losses in the heating unit remain limited for normal operating maximum temperature of 400°C. The deviation at higher temperature for small particles can be due to thermal instability of particles <20 nm at high temperatures.

This can be confirmed using CFD modeling. We studied the effect of heating on the transport of inert particles through the heating unit using the modeled temperature field determined previously. An example of the particle tracks for a wall temperature of Ti=800°C and Dp=100 nm is shown in Figure A.2.5 for the entry, central and exit sections of the unit.
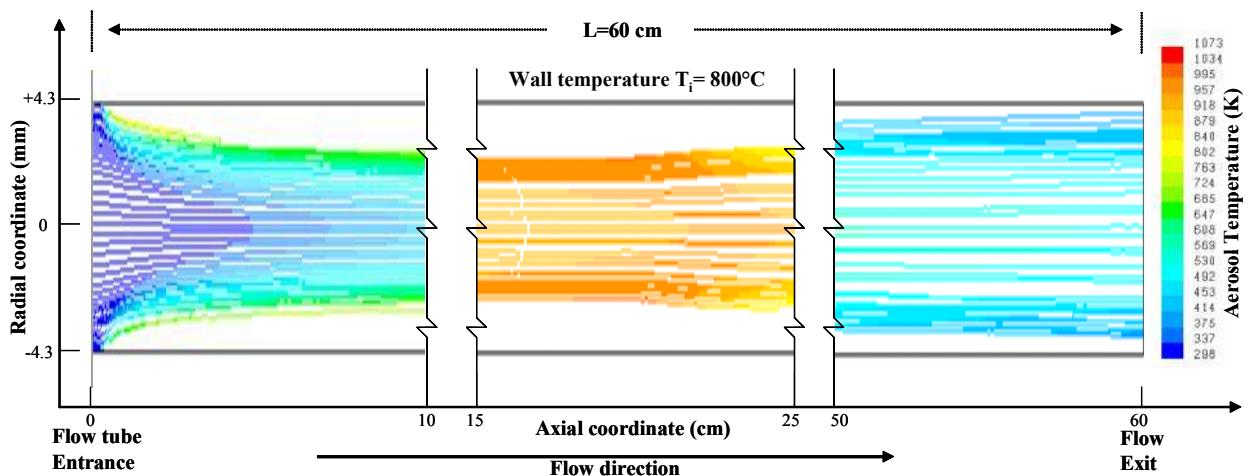

Figure A.2.5: CFD particle tracks and heating prediction for Dp=100 nm and Ti=800°C in the entrance (0 to 10 cm), the center (15 to 25 cm) and the cooling section (50 to 60 cm) of the thermo-desorber unit.

Thermophoresis acts to focus the aerosol on the centerline along the heating path and inversely to the tube walls in the cooling path. For the case of 100 nm particles, the effects of thermophoresis clearly dominate the diffusional effects, as seen by the focused aerosol concentration. A slight re-broadening of the aerosol tracks due to diffusion is observed only after the aerosol has attained the desired temperature of 800°C. The majority of particle losses occur after the aerosol exits the heating path and before entering DMA2. In this path (25 cm), the aerosol cools to room

temperature, and thermophoresis acts in the same direction as diffusion, bringing the particles to the tube walls. In the case of smaller diameter particles (i.e. 5 to 50 nm), the dominant effect is brownian diffusion with higher Cunningham Slip Correction Factor (Cc). Generally, because thermophoretic forces concentrate particles in the center section of the tubes, losses are limited (between the entry and exit section). The aerosol penetration efficiency is between 85-90% for small particles (5-25 nm) and 90-98% in the Aitken/Accumulation particle modes (25-150 nm). The use of large diameter tubing in the heating section seems appropriate to limit losses. These modeling results, thus, confirm the observations.

To account for losses during normal system operation, a parameterized curve fit of the measurement points is calculated, as shown in Figure A.2.4. The fit for each curve is described by the following equation:

$$C_{eff} = b - \frac{a}{1+\exp\left(\frac{D_p - D_1}{D_2}\right)} , \qquad (4)$$

where D_p is the particle diameter and a, b, D_1, D_2 the four constants of best fit . Size distributions measured with the V-TDMA should be corrected with these measured transport efficiency factors. This is accounted for in the inversion procedures.

3.2 Calibration of V-TDMA with standard particles

The thermal response of particles of known size and composition was tested in the V-TDMA system using $(NH_4)_2SO_4$ (Ammonium Sulphate), NaCl (Sodium Chloride), $NaNO_3$ (Sodium Nitrate) and NH_4NO_3 (Ammonium Nitrate). The purpose of these tests was to compare the thermal response as a function of particle size and the composition of this V-TDMA system with other known systems (e.g. Orsini et al. 1998, Brooks et al. 2001.).

For a generated monodisperse 100 nm NaCl aerosol heated stepwise, the normalized concentrations, calculated as the ratio between CPC1 and CPC2 as a function of size, is shown in Figure A.2.6a for different heating temperatures. Upon heating, evaporation of pure NaCl particles shifts the size distribution to smaller sizes, but in a different manner depending on particle size.
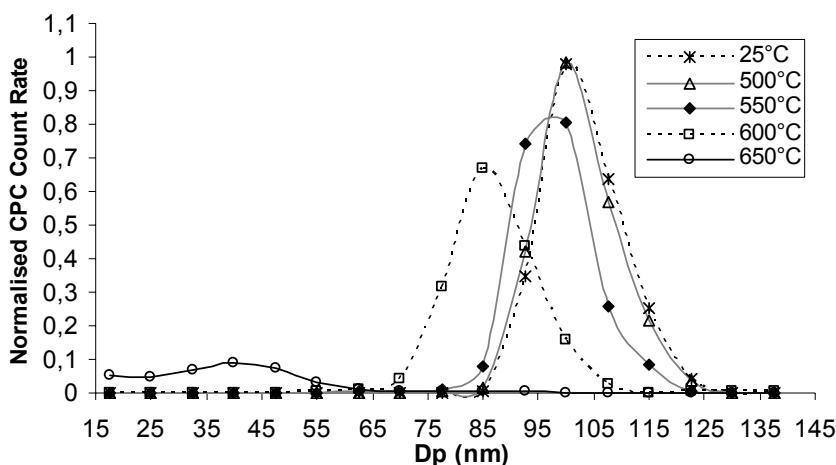
Figure A.2.6a: Volatility scan of 100 nm NaCl laboratory generated aerosol heated stepwise.

The fraction of residual particles at each temperature can be calculated in terms of both number and volume concentrations. These so-called number and volume fractions, RN and RV, can be derived by dividing the total number, N_t and volume, V_t, of the particle measured after heating to T_i (i.e. one of the six oven temperatures), by the N_t and V_t for the unheated reference aerosol (i.e. Ti=25°C), as follows:

$$RN = N_t (T_i°C) / N_t (25°C) \qquad (5)$$

$$RV = V_t (T_i°C) / V_t (25°C) \qquad (6)$$

Nt (T) and Vt(T) are obtained after integration of the size distributions shown on Figure A.2.6a, and comparison for each temperature with the integrated size distribution at 25 °C. The number fraction and volume fraction of volatilized particles obtained as a function of temperature are shown on Figure A.2.6b.
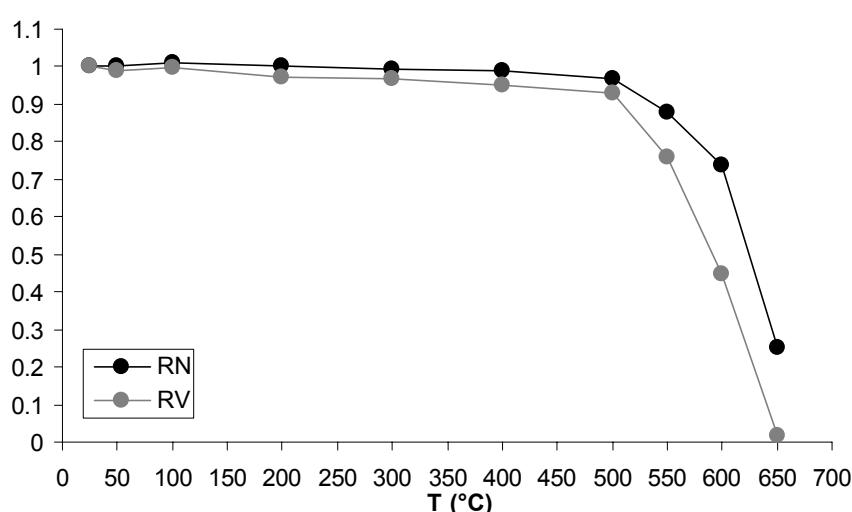

Figure A.2.6b: Fraction of number and volume of particles lost by thermo-desorption as a function of conditioning temperatures. The curves are obtained from volatilization of NaCl particles with 100 nm initial size.

It can be seen that both number and volume of 100 nm NaCl particles start to decrease after about 500 °C, but that they are not completely volatilised (by volume) before 650 °C. At this temperature, about 25 % of the particles have lost most of their volume but are still counted by CPC2.

The ratio between the relative loss in number concentration to the relative loss in volume is represented in Figure A.2.6c. This type of representation reduces the two curves of Figure A.2.6b to one parameter, since the slope accounts for the degree of mixing for particles of a given size.
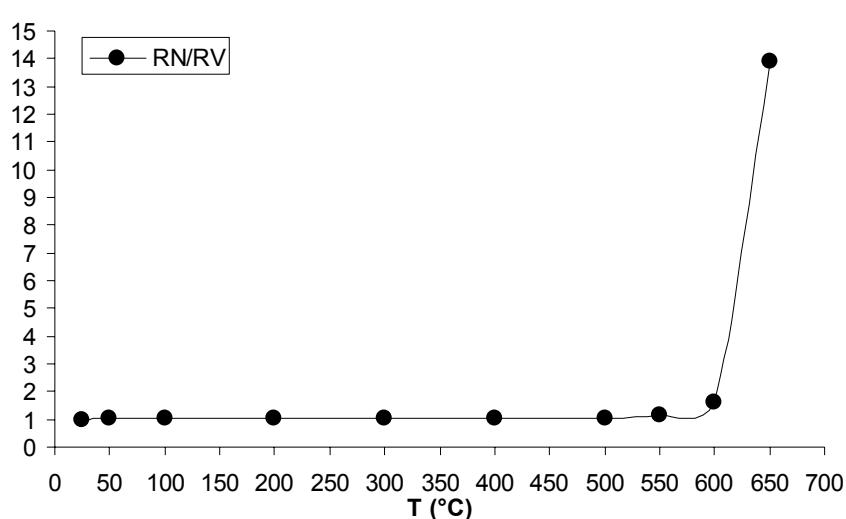

Figure A.2.6c: Number and volume fraction ratio for initial 100 nm NaCl particles.

Externally mixed particles lead to a very rapid increase of RN/RV with temperature once the volatilization temperature of their components is reached contrary internally mixed particles. In the case of externally mixed NaCl particles, the slope is extremely high at temperatures close to 600°C. This representation offers a clearer view of the efficiency of the volatilization process as a function of temperature and should be preferred over the most commonly used thermal response curves as in Figure A.2.6b. This representation is extremely useful for comparing the chemical nature of particles of different size.

Similar data have been retrieved for chemical compounds other than NaCl and for a range of particle diameters between 15 nm and 150 nm. The results are compiled in Table A.2.2 and compared to volatilization temperatures measured in previous V-TDMA systems.

	O'Dowd (1993)	Philippin (1999)	Burtscher (2000)	Brooks (2001)	This work (15 nm)	This work (150 nm)
$(NH_4)_2SO_4$	280°	180°	180°	235°	160°	180°
NaCl	700°	------	-------	650°	500°	650°
$NaNO_3$	------	------	-------	550°	475°	550°
NH_4NO_3	------	------	-------	------	30°	60°

Table A.2.2: Volatilization temperature of different test aerosols in the V-TDMA.

The "*volatility temperature*" is defined as the temperature at which a compound is completely evaporated in the V-TDMA system. The very large range of volatilization temperatures for a single component aerosol indicates that thermal desorption is not only a function of particle composition but also of the particle size. Because smaller particles evaporate faster than large ones, the volatilization efficiency at a given temperature is a function of the residence time of the particle at this temperature. The differences shown in Table A.2.2 for the different studies mostly reflect different oven geometrical factors. Therefore, the residence time of particles in the heated section of the V-TDMA is of primary importance in defining a volatilization temperature.

3.3 Recondensation of evaporating species

Cooling to ambient temperature after thermal conditioning can produce a measurement artefact if the volatilised fraction condenses back onto the residual particles. This artefact was quantified by investigating the thermal properties of NaCl particles coated with a known thickness of DEHS (i.e. Di-Ethyl-Hexyl-Sebacate). The system used is similar to that presented in Figure A.2.1 with liquid DEHS placed in a furnace between DMA1 and DMA2. The temperature of the furnace was varied between 70° and 100°C in order to produce DEHS vapor at different concentrations. The monodispersed aerosol sample from the atomized polydispersed NaCl aerosol was selected in DMA1. The aerosol sample exiting DMA1 was directed either a) through the DEHS furnace or b), through a bypass line depending on the position of the magnet 3-way valves.

a) When the aerosol sample exiting DMA1 was directed through the furnace, the DEHS gas condensed onto NaCl particles thus coating them with a layer of this

compound. The degree of DEHS vapor condensation onto the NaCl aerosol particles is a function of furnace temperature and residence time in the furnace.

b) Directing the NaCl aerosol exiting DMA1 into the bypass gave with the "dry" (uncoated) sample, directly scanned by DMA2.

Then, for different particle sizes and degrees of coating, the test aerosol was thermo-desorbed in the same temperature range by the V-TDMA heating unit to test volatilization efficiency and possible re-condensation.

The result of the DEHS-coated aerosol is shown in Figure A.2.7. The plots represent the original dry NaCl selected particle (labeled "NaCl Dry"), DEHS-coated-NaCl size distribution (labeled "DEHS Coating") and the 100°C DEHS-coated-NaCl heated size distribution (labeled "DEHS Coating at 100°"). The furnace temperature was kept at approximately 100°C. Aerosol growth was seen as the center diameter shift from the selected Dry Dp=35 nm to Dp=58 nm (i.e. Coating Growth Factor =1.65). As seen from these figures, the conditioned sample nearly returned to its original uncoated state. The distribution returned to a median diameter Dp=35 nm (i.e. CGF=1.0).
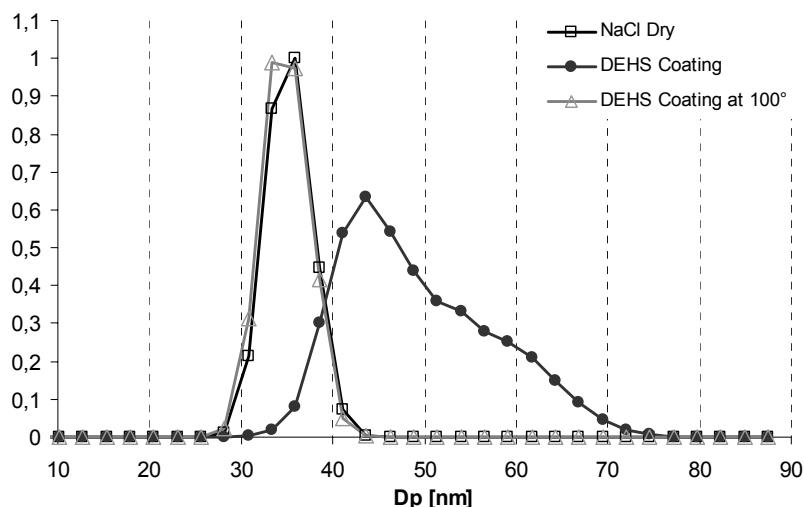

Figure A.2.7: Volatility scan of 35 nm NaCl uncoated and coated size distributions.

The test described above was further extended to a range of aerosol concentrations and heater temperatures. This experiment shows that gentle heating of coated particles can be used to remove a layer of semi-volatile species off the particle surface if the aerosol core is less volatile than the surface layer. This property of the

V-TDMA can be used to investigate mechanisms of particle growth for natural aerosols.

4. Preliminary results for ambient aerosols

The V-TDMA was tested during a field measurement campaign at the Puy de Dôme meteorological station. Five conditioning temperatures were chosen between 25°C and 320°C (i.e. 25°C-100°C-170°C-250°C-320°C). The thermal properties of the two main aerosol modes at 55 nm and 200 nm were investigated. The results defining the residual particle were parameterized in terms of number and volume concentrations as already calculated for Figures A.2.6 b and c. It is clear that when size drops below the detection limit of the second DMA, the particle is considered to have entirely volatilised.

The relative changes in number (RN) and volume (RV) as a function of conditioning temperature for 55 and 200 nm particles are shown in Figure A.2.8a . It is clear that 55nm particles were more sensitive to thermo-desorption than 200 nm particles even at moderate heating (100°C).

From $T_{ambient}$ to 100°C, the particle number concentration decreased by 20% for 55 nm particles and remained unchanged for 200 nm-particles while the volume-fraction loss was 50% and 20%, respectively. This means that the 55 nm particles contained a higher relative fraction of volatile material and a significant fraction of this material was internally mixed with more refractory material.
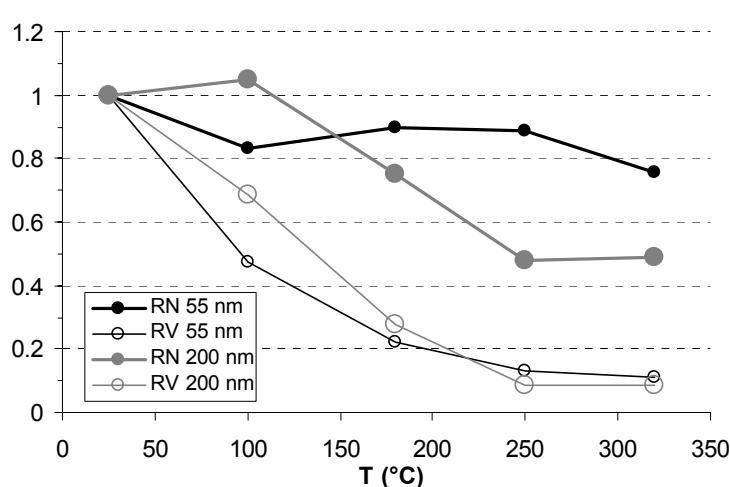

Figure A.2.8a: Number (RN) and volume (RV) fractionation curves derived from volatility size distributions of initial 55 and 200 nm particles at the Puy de Dome Station as a function of conditioning temperatures. The slight increase at 100°C for 200 nm particles is due to instrumental error.

When the temperature increased from 100°C to 250°C, volatile material was evaporated from 55 nm particle surfaces with the number fraction remaining quite stable (within 10 % of the initial concentration). Clearly, Aitken mode particles were formed by a refractory core and subsequent condensation of semi-volatile material.

At 250°, accumulation mode particles had lost 90% of their initial volume and 50% of the initial number concentration. Only a fraction of those particles therefore were formed by condensation onto a core of refractory material, possibly indicating a mixture of at least 2 different sources contributing to 200 nm particles. The residual non-volatile particles showed a mode at 25 nm and 50 nm for initial Dp=55 nm and Dp=200 nm respectively.

Similarities and differences between Aitken and Accumulation mode particles are shown in Figure A.2.8b using the ratio between the residual number fraction and the volume fraction as a function of the conditioning temperature. Clearly, we cannot exclude that the higher sensitivity of 50 nm particles to loss in number results from a higher fraction of particles reduced to diameter lower than 10 nm as respect to 200 nm particles. However, it might also indicate that the smaller particles are not originated from condensation onto a refractory core, i.e. from combustion process, Instead, a significant fraction of the 200 nm particles is formed onto refractory material. The RN/RV representation is a useful way to discriminate particle behavior with respect to temperature.
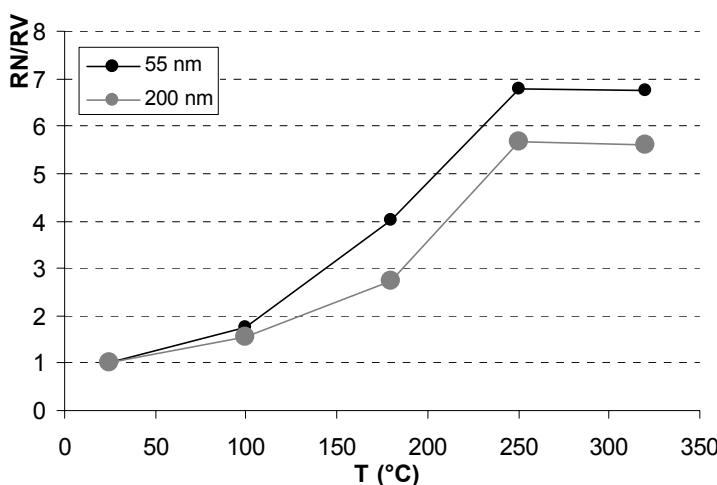

Figure A.2.8b: Number and volume fraction ratio (RN/RV) for initial 55 and 200 nm particles at Puy de Dome Station.

Finally, no changes seemed to occur above 250°C which appeared to be the most appropriate temperature for defining refractory particles. In practice, information

obtained for temperatures lower than 250°C must be interpreted with caution in V-TDMA as they might result from non steady-state size-dependent reaction upon heating, due to limited residence time in the thermo-desorption system.

5. CONCLUSIONS

We have validated measurements of a newly-built volatility TDMA. The instrument is designed with six thermo-desorbers to allow measurement of the volatile fraction of atmospheric aerosol particles with high size resolution (20-550 nm) and improved temporal resolution. Technical information and model results are provided to justify the technical choices and the instrumental design of the V-TDMA. The aerosol heater was constructed with the intention of maximizing aerosol temperature penetration with sufficient residence time for complete volatilization of the various chemical compounds.

Laboratory tests enabled the instrument to be calibrated for different particles of known size and composition. We have confirmed that the volatility temperature for a given chemical species cannot be precisely defined and spans several tens of °C. The size dependency of the volatility temperature shows that the residence time of the particles in the heated section is of primary importance. We recommend that the residence time is increased to more than 0.5 s (0.3 in this version) to limit the size-dependent effect of thermal desorption. In any case, given the increasing use of thermo-desorbing unit in aerosol science, more standardized procedures would be useful for comparing different instrumental set-ups.

The development of this V-TDMA system was completed with a final calibration for diffusion and thermophoretic losses with a NaCl aerosol. Fitted curves to the calibration data provided the back-corrections to be used in normal system operation. We have shown that V-TDMA can be efficiently used to investigate surface properties of atmospheric aerosols. Gentle heating (50°C-100°C) allows for the removal of a surface layer as shown by measurement with DEHS-coated NaCl particles. Our results also showed no re-condensation regardless of the conditioning temperature.

Analyses of thermal responses of natural aerosols sampled at a free-tropospheric station show that a large fraction of Aitken mode particles was formed onto refractory

material while only 50% of the 200 nm particles were still measurable at 250°C. The volume fraction evaporated at this temperature is close to or higher than 90%. Preliminary measurements clearly indicate that V-TDMAs can be used to investigate the formation mechanisms for fine and ultrafine particles, rather than for inferring chemical composition. In our sample, thermo-desorption at 250 to 300°C appeared to be the optimum temperature to avoid size dependent effect due to limited residence time in the thermo-desorption unit. We therefore recommend the use of this standard operation temperature.

References

Brooks, B. J., Smith, M. H., Hill, M. K., O'Dowd, C. D. (2002). Size-differentiated volatility analysis of internally mixed laboratory-generated aerosol. J. Aerosol Sci. 33, 555-579.

Hudson, J.G., and Da X., (1996). volatility and size of cloud condensation nuclei, JGR, 101(2): 4435-4442.

IPCC (Intergovernmental Panel on Climate Change), (1995). Radiative forcing of climate change. In: Houghton, J. T., Meira Filha, L. G., Bruce, J., Hoesung, L., Callander, B. A., Haites, E., Harris, N., Maskell, K. (Eds.), Climate Change 1994. Cambridge University Press, Cambridge, pp. 1-231.

Jennings, S. G., O'Dowd, C. D., Cooke, W. F., Sheridan, P. J. and Cachier, H. (1994). Volatility of elemental carbon. Geophys. Res. Lett. 21 (16), 1719-1722.

Jennings, S. G., Geever, M., McGovern, F. M., Francis, J., Spain, T. G., Donaghy, T. (1997). Microphysical and physico-chemical characterization of atmospheric marine and continental aerosol at Mace Head. Atmos. Env. 31 (17), 2795-2808.

Knutson, E. O. and Whitby, K. T. (1975). Aerosol classification by electric mobility: apparatus, theory, and applications. J. Aerosol Sci. 6, 443-451.

O'Dowd, C. D., Jennings, S. G., Cooke, W. F., Smith, M. H. (1992). A high temperature volatility technique for determination of atmospheric aerosol composition. J. Aerosol Sci., 23(S1): S905-S908.

Orsini, D.A., a. Wiedensohler, and F. Stratmann, 1998. A new tandem differential mobility analyser to measure the volatile sulfuric acid aerosol fraction, Journal of Atmospheric and Oceanic Technology, 16: 760.

Orsini, D. A. (1997). The development of a system to measure the volatile sulfuric acid fraction of marine aerosol particles. Fakultät für Physik und Geowissenschaften. Leipzig, Universität Leipzig, 83.

Philippin, S., Wiedensohler, A., Stratmann, F. (2003). Measurements of non-volatile fractions of pollution aerosols with an eight-tube volatility differential mobility analyzer (VTDMA-8). J. Aerosol Sci. 35, 185-203.

Pinnick, R. G., Jennings, S. G. and Fernandez, G. (1987). Volatility of aerosols in the arid southwestern United States. J. Atmos. Sci. 44, 562-576.

Rader D.J. and P.H. McMurry, 1986: Application of the tandem differential mobility analyser to studies of droplet growth or evaporation. J.Aerosol Sci., 17, 771-787.

Reischl G.P.,Makela J.M., Necid J. (1997). Performance of Vienna type differential mobility analyser at 1,2-20 nanometer. Aerosol Science and technology 27:651-672 (1997)

Sellegri, K., P. Laj, F. Peron, R. Dupuy, M.Legrand, S.Preunkert, J-P.Putaud, H.Cachier, G.Ghermandi, Mass balance of winter time free tropospheric aerosol at the Puy de Dôme (France). J. Geophys. Res., sous presse, 2003

Smith, M. H. and O'Dowd, C. D. (1996). Observations of accumulation mode aerosol composition and soot carbon concentrations by means of a high-temperature volatility technique. J. Geophys. Res. 101 (D14), 19583-19591.

Stolzenburg, M. R. and McMurry, P. H. (1988). TDMAFIT Users' Manual. Minneapolis, Minnesota.

Stratmann F.,Kauffeldt Th., Hummes D., Fissan H. (1997). Differential electrical mobility analysis: a Theoretical study. Aerosol Science and technology 26:368-383 (1997).

Stratmann, F., Orsini, D. and Kauffeldt, T. (1997). Inversion algorithm for TDMA measurements. EAC 1997, Hamburg. J. Aerosol Sci. S701-S702.

Wiedensohler A., (1988): An approximation of the bipolar charge distribution for particles in the submicron size range. J. Aerosol Sci., 19, 387-389.

CHAPITRE I.3

Développement du *Volatility Hygroscopicity Tandem Differential Mobility Analyser (VH-TDMA)*

La mesure du caractère hygroscopique des particules est une information fondamentale dans le cadre des études menées au Laboratoire de Météorologie Physique sur l'interaction aérosol/nuage. Nous ne bénéficiions jusqu'à présent d'aucune mesure directe du caractère hygroscopique d'une particule. Lors de campagnes de mesure précédentes, nous avions bénéficié de mesures de concentration en noyau de condensation de nuage effectuées soit par l'équipe de Jeff Snider (Wyoming), soit par l'équipe de Laurent Gomes (CNRM). Les mesures CCN permettent cependant une mesure en conditions de sursaturation et concernent, compte tenu des sursaturations mises en jeu, les particules de diamètre supérieur à quelques dizaines de nm. De plus, dans leur configuration originale, elles ne permettent pas une sélection préalable de la dimension des particules.

La mesure directe de la croissance hygroscopique d'une particule se fait classiquement par granulométrie tandem à humidité contrôlée (H-TDMA – Hygroscopic Tandem Differential Mobility analyser) (Rader and McMurry, 1986). Suivant leur composition chimique et en fonction de l'humidité relative ambiante, les particules d'aérosol vont absorber une certaine quantité d'eau et ainsi produire une croissance hygroscopique des particules. Cette croissance hygroscopique est décrite en détail par Hanël pour des sels inorganiques. Le système H-TDMA permet la mesure, in situ, de la croissance hygroscopique pour une taille de particule donnée, entre 20 nm et 300 nm. Très schématiquement, il est possible de sélectionner, après séchage (RH<10%), une taille de particules (D_p^{10}) à l'aide d'analyseur de mobilité différentielle (DMA), et d'obtenir un humidographe pour différentes tailles de particules en faisant artificiellement varier le taux d'humidité et en mesurant simultanément la taille de la particule à cette nouvelle humidité (RH=90%, D_p^{90}). C'est le principe de la sonde granulométrie-hygroscopicité. Cette sonde permet de caractériser le *« Hygroscopic Growth Factor »* (D_p^{90}/D_p^{10}), définit comme le rapport entre le diamètre de la particule hydratée à une humidité relative (RH) donnée (par exemple 90%RH) et son diamètre à l'état sec (<10%RH) des particules d'aérosols, avec une résolution temporelle de l'ordre de dix minutes pour une taille de particule donnée.

Toutes les études portant sur l'hygroscopicité des particules mesurée à l'aide de systèmes H-TDMA mettent en évidence l'existence de particules d'hygroscopicité variable. Relier hygroscopicité et composition chimique n'est pas forcement trivial. Par exemple, la condensation de substances organiques à la surface de particules d'aérosols peut modifier ses propriétés hygroscopiques (Facchini et al., 2000 ; Andrews and Larson, 1993 ; Li et al., 1998). Or, la structure surfacique de l'aérosol n'est prise en compte dans l'équation de croissance des aérosols que de manière indirecte via la tension de surface. La compréhension de l'effet de films de surface organiques est encore lacunaire : des études montrent que ces composés peuvent affecter la croissance des gouttelettes aussi bien positivement que négativement (Saxena et al., 1995 ; Raymond and Pandis, 2002 ; Chen et al., 1998 ; Hansson et al., 1998).

Notre objectif était donc de pouvoir disposer d'un système de mesure permettant d'étudier à la fois les propriétés hygroscopiques de particules mais également le rôle de la structure de la particule et en particulier, le rôle des composés déposés par condensation sur la surface des particules sur leur capacité à servir de noyau de condensation. En collaboration avec Laurent Gomes au CNRM, nous avons, au cours d'un certain nombre de campagnes de mesure, procédé à la mesure du nombre de noyaux de condensation d'une population de particules avant et après thermo-désorption < 100°C (Rojas et al., soumis). La température de thermo-désorption était fixée par un système V-SMPS permettant de vérifier que le spectre dimensionnel n'était pas visiblement altéré par ce processus. Les résultats préliminaires de Rojes et al., montrent dans certains cas une modification substantielle de la fraction CCN. L'hypothèse la plus probable pour expliquer ce phénomène est une volatilisation d'une couche de surface soit plus, soit moins hygroscopique que le noyau de la particule.

Suivant la même philosophie et complétant le système V-CCNC, avons développé un système couplant les caractéristiques des H-TDMA et des V-TDMA par la mise au point d'un VH-TDMA. Le VH-TDMA consiste en une mesure de la croissance hygroscopique avec et sans thermo-desorption préalable permettant à la fois la quantification des fractions volatile et non-volatile de l'aérosol, l'analyse de ses propriétés hygroscopiques et la détermination du degré de mélange. Il s'agit donc d'une utilisation différente de la thermo-désorption par rapport à celle présentée dans le chapitre précédent. Il existe à l'heure actuelle un seul exemplaire de VH-TDMA construit par Johnson et al., (2003) à l'International Laboratory for Air Quality and Health, Queensland University of Technology, Brisbane, en Australie. D'autres groupes projettent des systèmes similaires.

Dans ce chapitre I.3, nous présenterons le système VH-TDMA. Ce système est au centre des mesures présentées dans le chapitre II. Un schéma du VH-TDMA est présenté sur la Figure

I.3.1. Le chapitre permettra une brève description du fonctionnement du système et des principaux choix technologiques pour la mesure de l'humidité relative, de l'humidification de l'aérosol, du système de thermo-désorption. Nous présenterons la validation de l'efficacité de transfert du système. En particulier, la validation de la partie H-TDMA du système de mesure a été faite durant un exercice d'intercomparaisons des H-TDMAs disponibles dans les laboratoires Européens. Cette intercomparaison a eu lieu à Leipzig en Février 2006 et fera l'objet d'un article commun en cours de préparation (Kaaden et al, en préparation). Nous ne présentons ici que les mesures de validation relatives à notre système. Le présent chapitre est soumis pour publication à Aerosol Science and Technology.
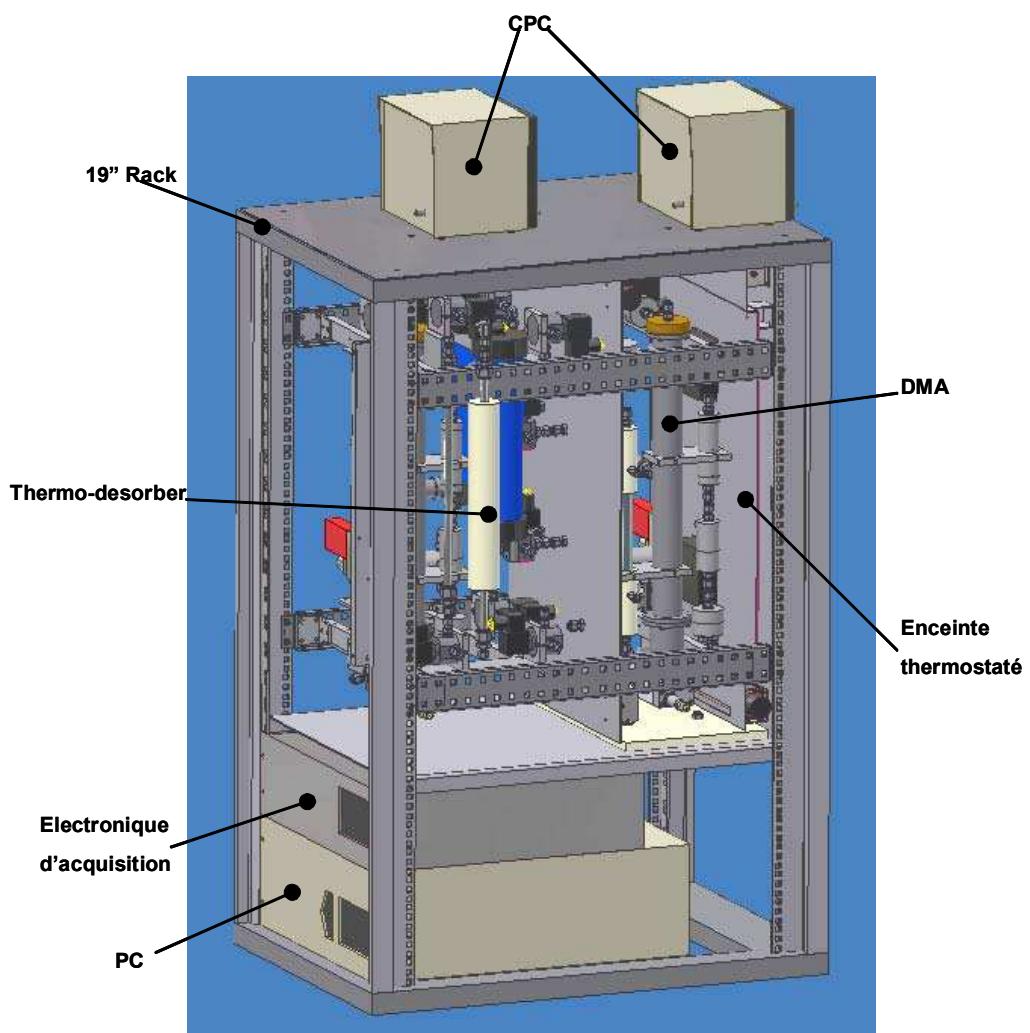

Figure I.3.1: VH-TDMA

A Multi-TDMA to Characterise Relationship Between Thermal and Hygroscopic Properties of Atmospheric Aerosol Particles

P. Villani, D.Picard, P.Laj

ABSTRACT

The nature of atmospheric aerosol is extremely complex and often requires advanced analytical tools for the determination of its physical and chemical properties. In particular, the interaction of particles with the atmospheric water is a complex function of both size and composition. The ability of a particle to grow in humid environment is often controlled by humidity tandem differential mobility analyzing techniques (H-TDMA). In this paper, we present a new development combining thermo-desorption and humidification aerosol conditioning that allows to measure changes in the hygroscopic behavior of aerosol at RH=90% after alteration and/or removal of the particle surface layers. The system subsequently named as Volatility Higroscopic Tandem Differential Mobility Analyser (VH-TDMA, is based on a tandem differential mobility analyser combining volatility and hygroscopicity measurement in series. The main feature of the VH-TDMA is to allow for a rapid (15 minutes) scan of particle response to thermal conditioning, of particle response to RH changes and of both particle response to RH after thermal conditioning.

The aim of the present paper is to describe the instrument design, the calibration process for the determination of the transfer efficiency and the data inversion procedures. We report the first tests with the VH-TDMA system, first for the measurement of hygroscopic behavior of inorganic particles as sodium chloride or ammonium sulfate and, second, for the behavior of organic-coated inorganic particles (i.e., DEHS-coated NaCl) with and without thermo-desorption. We will then describe the innovative sampling methodology for probing the complexity of natural aerosols.

Depending on the thermo-desorption temperature, the Multi-TDMA system is therefore capable of measuring the non-volatile fraction of ambient sub-micrometer aerosols in the range of 15 to 200 nm, and of investigating the influence of volatile fraction of these species on the particle hygroscopic growth. This technique has the potential to distinguish between components such as sea salt or sulfate within submicrometer aerosol particles coated with organic compounds and could be applied in rapid field measurement in the particle size range 15-200 nm. The VH-TDMA system is therefore well-suited to investigate the formation mechanisms of atmospheric particles as well as the effect of particle alteration during transport in the atmosphere.

Keywords: Aerosol particles, Volatility, Hygroscopicity, TDMA

1. INTRODUCTION

The composition and structure of atmospheric particulate matter are not easily characterised by conventional methods although both factors play a major role for determining the role of particles in the atmospheric system. In particular, size and chemical composition and structure are key parameters driving the interaction between aerosol particles and water vapour in the atmosphere. Many techniques for the determination of aerosol complexity are currently used for atmospheric studies. Tandem Differential Mobility Analysers (TDMA) provide information on particle composition and size, in almost real time, and hence offer a powerful advantage over many other chemistry-based methods that require longer time-integration.

The hygroscopic properties of Aitken and accumulation mode particles have been often investigated using the Hygroscopicity Tandem Differential Mobility Analyser (H-TDMA) (Liu et al., 1978; Rader and McMurry, 1986; Stolzenburg, 1988; Svenningsson et al., 1992; Swietlicki et al., 1997; Berg et al., 1998). The basic principle of the H-TDMA technique is to monitor the growth of a particle of known diameter in a high RH environment (typically close to 90 % RH). For a given particle size, the hygroscopic growth is mostly dependent upon particle composition and H-TDMAs are therefore capable of identifying the mixing state of particles as a differential hygroscopic growth factor. An internal mixture exists when all particles consist of the same chemical composition and thus exhibit identical hygroscopic behaviour. In an externally mixed particle population, particle groups exist that contain different chemical constituents. The hygroscopic behaviour of atmospheric particles is typically depending upon the particle origin. The hygroscopic properties of atmospheric particles containing organic and inorganic compounds have been extensively investigated by the Tandem Differential Mobility Analyser (TDMA) technique, in both laboratory and field experiments (Mueller et al., 1982; Saxena et al., 1995; Cruzand Pandis, 1996; Hansson et al., 1998). Elevated hygroscopic growth factors (HGF) are typically found in the marine or coastal atmospheres due to the presence of sea-salt and sulphate aerosols (Berg et al., 1998; Bates et al., 1998; Johnson et al., 2000; Putaud et al., 2000; Raes et al., 2000; Swietlicki et al., 1999; Bower et al., 2000) while reduced HGF are found in the urban areas (Massling et al., 2005; Rissler et al., 2005; Vestin et al., 2005). In most sites however, H-TDMA studies indicate the simultaneous presence of both a less-hygroscopic and a more

hygroscopic particle class, consisting of particles with less and more soluble material, respectively (McMurry and Stolzenbourg, 1989; Svenningsson et al., 1992,1994; Zhang et al., 1993; Covert and Heintzenberg, 1993; Pitchford and McMurry, 1994; Kerminem, 1996; Swietlicki et al., 2000).

The thermal properties of particles are also related to their chemical composition (O'Dowd et al., 1992; Wahlin et al., 2000; Weingartner et al., 2005; Philippin et al., 2003; Rose et al., 2006; Engler et al., 2006). Analyses of particle thermal properties are based on the fact that most components present in aerosols are volatile at a characteristic temperature (Orsini et al., 1998; Burtscher et al., 2000; Brooks et al., 2001). When temperature increases, a fraction of the chemical constituents of an aerosol particle volatilizes resulting in a change in both number concentration (when a particle is totally volatilised) and size. From the temperature at which complete or partial volatilization takes place, the chemical composition and the degree of mixing within the population can be estimated (Clarke, 1993; Jennings et al.1997; Orsini et al., 1998, Philippin et al., 2003). The response of atmospheric aerosols to thermal desorption has been often investigated using Volatility Tandem Differential Mobility Analyser (V-TDMA) (Orsini et al., 1998, Philippin et al., 2003; Villani et al., 2006). Due to difficulties to relate volatilisation temperatures to chemical composition and to the complex nature of atmospheric particles, the use of V-TDMAs for investigating natural aerosols remains problematic.

While V-TDMA techniques can be helpful in quantifying the non-volatile fraction of aerosol particles, they are not able to further distinguish between elemental carbon and low volatile organic species in the non-volatile residue. On the other hand, hygroscopic growth measurement alone cannot be used for investigating the chemical structure of the particles linked, in particular, to their formation process (i.e. condensation onto refractory material or inorganic salt and direct homogeneous nucleation).

The aim of this work was to develop and validate a new TDMA system coupling features of both V- and H-TDMAs. The system, subsequently named as Volatility Hygroscopic Tandem Differential Mobility Analyser (VH-TDMA), is built primarily to investigate the role of semi-volatile species condensed onto the particle surface to limit or increase particle hygroscopic growth. A similar development has been recently presented by Johnson et al. (2004). The differences between the two instruments are also discussed.

2. EXPERIMENTAL SECTION

2.1. Instrument design

As mentioned previously, VH-TDMA features properties of both V-TDMA and H-TDMA. The instrument is capable of rapidly switching to investigate the behaviour of particle under conditioning at constant temperature (i.e. V-TDMA), at constant humidity (i.e. H-TDMA) and at simultaneous constant temperature/humidity (i.e. VH-TDMA). This new system is especially designed to perform automatically measurements with minimal need of maintenance, high reliability and stability of flow rates, as well as precise control of humidity and temperature. The design of the Multi-TDMA system is shown in Figure A.3.1.
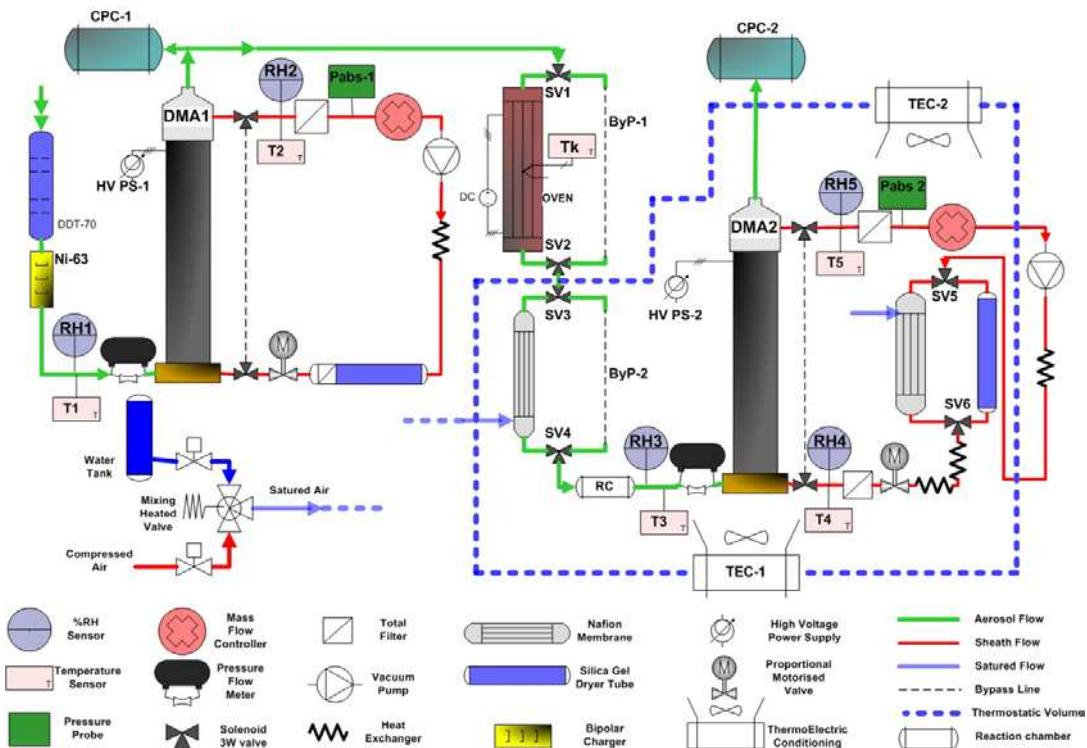
Figure A.3.1: Schematic of the VH-TDMA.

The system is based on a usual TDMA set-up: it consists of a bipolar neutraliser, a fixed voltage long column DMA (custom-made, DMA1) that is used to select a narrow size range of ambient aerosol subsequently counted with a TSI-3010 CPC (CPC1). A second long column DMA (custom-made, DMA2) followed by TSI-3010 CPC (CPC2) operating as a mobility size spectrometer to measure the modified size distribution. Design and performance of the DMA are presented elsewhere (Villani, 2006). Several normally closed electronically-actuated solenoid three way valves are used

in-line throughout the system to allow the DMA2 to alternate dry scan and wet scan simply choosing and bypassing the conditioning units (i.e. humidifier and thermo-desorber). To reduce in-line losses valves with a big inner orifice are used (i.e. orifie diameter = 4mm). The instrument can be broken down into four main TDMA subsystems:

1. *TDMA subsystem*

   Once solenoid valves (SV1 to SV6 in Figure A.3.1) are turned on, both thermo-denuder and aerosol pre-humidifier are steered in bypass line ByP-1 and ByP-2 respectively. DMA2 sheath flow is bypassed into in a silica gel tube dryer to keep RH<10%. By running the second DMA at a low value of RH it is possible to compare the offset of the two DMAs at a range of sizes immediately before and after field or laboratory campaigns to take into account the diameter shift measured by the second DMA. This "Dry scan" is used also to check the DMA transfer function.

2. *H-TDMA subsystem*

   The "wet scan" is actuated when Solenoid valves SV1 and SV2 are turned on while SV3 to SV6 are switched off. Prior entering the pre-humidifier, the aerosol sample flow is bypassed in a stainless-steel line (i.e. ByP-1) which has the same length and dimension of the volatilization tube. This feature permits to have identical losses when the particles pass through all lines. During normal operations, the RH of the second DMA is monitored by sensors RH4 and RH5 placed in the sheath and excess flow lines respectively while the aerosol flow RH is measured by sensor RH3 and sets to %RH5-1%. Up to RH=90%, the relative humidity of the sheath flow (RH4) and excess flow of DMA2 (RH5) agree to within 1.5%. For RH4>90%, RH5 is lower by up to 3% due to small temperature gradients in the system (differences up to 0.5°C). RH5 is considered to be most representative for the effective overall relative humidity in DMA2 was thus used both for regulation of wet DMA RH (i.e. RH=90%) and for all plots and calculations involving RH. Before entering the second DMA, the RH conditioned monodisperse aerosol is introduced into a reaction chamber with a residence time of 7s at a flow rate of 1.0 l min^{-1}. This is much higher than the estimated time of water vapour equilibrium for pure

submicrometer salts at 90% RH and T=25°C (100 milliseconds) (Kerminen, 1997). However, increasing the time exposure of particles at high RH may limit the influence of water inhibiting compounds in the particulate phase (e.g. organic films) that reduce the water uptake across the particle surface and possibly increase the equilibrium time. The mean residence time of the aerosol in the pre-humidifier and in the subsequent line leading to DMA2 is about 6s. In the DMA, the particles stay for another 7 s before being finally separated, leading to an overall conditioning time of 13s.

3. *V-TDMA subsystem*

When solenoid valves SV1 and SV2 are switched off while SV3 to SV6 are on, the sample aerosol flow is conditioned to a well-defined temperature in the volatilization tube and the residual mobility distribution is then measured with DMA2 scanning in dry conditions (i.e. RH<10%). It is important to note that, for the specific conditions of a volatility scan, measuring particle concentration after both DMAs with two CPCs is extremely useful for a relative comparison in terms of volatilised number fraction. Furthermore, comparison of concentration readings from CPC1 and CPC2 gave an absolute evolution of all spectra with time.

4. *VH-TDMA subsystem*

When all solenoid valves (i.e. SV1 to SV6) are switched off, the aerosol sample flow is heated to the same volatility scan temperature as for the V-TDMA subsystem before entering the pre-humidifier. DMA2 is scanning in wet conditions (i.e. the set RH is identical to that of the humidity scan) and measures the hygroscopic behaviour of the aerosol after thermal conditioning.

2.2. Technical specifications of the different elements in the VH-TDMA system

2.2.1. Sheath Airflow System: automatic flow regulation

A re-circulating sheath flow system was used in both DMAs. For the instrument presented in this paper, two membrane pumps were used operating with Teflon membranes, thus avoiding any artefact by outgassing material. DMA1 is operated at flow rates (sample flow/sheath air flow) of 2.0/10 l min^{-1} and the same aerosol/sheath flow ratio (1.0/5 l min^{-1}) is used in DMA2. The sheath air flows are controlled by mass-flow controllers/meters located in the excess air outlet of the DMAs and the sheath flow rate is regulated by motor driven needle valves. Total particle filters are used in both sheath lines and excess-flow lines to ensure that clean, particle-free sheath air is injected at the bottom of the DMAs and protect mass-flow meters and needle valves. The volumetric sheath flow is calculated by measuring the sheath flow absolute pressure and temperature in each DMA loop. These pressures and temperatures are used also to calculate and correct particle mobility in each DMA.

The aerosol sample flow at the outlet of the DMAs is set by the CPC 3010 critical orifice with nominal flow rate of 1.0 l min^{-1}. The aerosol flow at the inlet of the DMAs is also measured and recorded by measuring the pressure drop over calibrated capillaries. It is controlled by adjusting the sheath air flows of the DMA loops using the motorised needle valves in a feed-back regulation system. This feature added to the acquisition program (see Section 2.3) increases system reliability and stability with a flow auto regulation that does not requires assistance. The standard deviation of the aerosol flow rate and the excess air flow rate for both DMAs are less than 1.0% and 0.5% respectively during every measurement scan.

The re-circulating sheath flow loop also contains a Silica Gel Tube Dryer capable of maintaining RH below 10%. DMA1 is continuously operated at low RH (i.e. Dry DMA) to select the monodisperse aerosol while in the sheath circuit for DMA2 the sheath air drier can be switched to the humidifying unit. Technical details concerning the humidifying unit are provided in Section 2.2.3. In both loops, the sheath flow is also introduced into a heat exchanger placed at the pump outlet to ensure sufficient air cooling before injection into the DMA.

2.2.2. RH/T measurements

Five capacitive sensors (Model Rotronic, HygroClip 05) are used in-line throughout the instrument (see Figure A.3.1) to monitor temperature and RH and to allow fast RH regulation.

A first probe is placed at the instrument inlet to monitor the sample flow RH (RH1), a second one is used to measure the dry DMA sheath flow loop RH, placed on the analyser excess flow (RH2).

Three other sensors are employed to check the DMA2 RH: one controls the aerosol sample flow inlet (RH3) and two others control the DMA sheath (RH4) and excess flow (RH5) respectively. These probes are parallel oriented with the flows within a custom-made housing to reduce in-line aerosol particle losses due to turbulent diffusion. The probes have an accuracy of ±1.5% for RHs up to 90%. Above 90% RH, the accuracy deteriorates to ±2%.

Calibration of the humidity probes is performed using saturated salts solutions ($MgCl_2$ salt for 33% RH, NaCl salt for 75% RH and K_2SO_4 for 97% RH). A mercury calibrated thermometer (accuracy ±0.1°C) is used for measuring the temperature during the calibration keeping the probes in a thermostatically stable environment. The reading of the five RH sensors is adjusted according to the relative humidity generates by the saturated salt solution. Figure A.3.2 presents the RH calibration curves. Linear fitting regressions are used to correct the measured value of RH for each humidity probe.
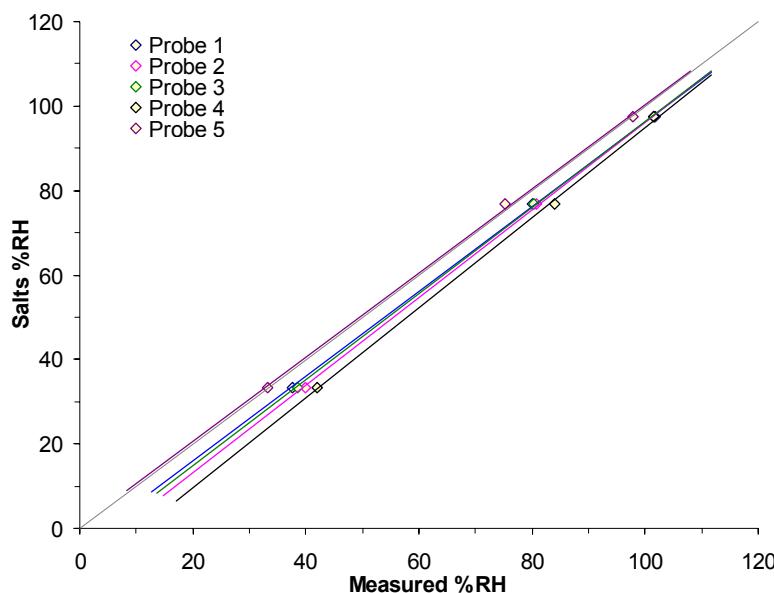

Figure A.3.2: Fit results by linear regression of the humidity measured by the five RH sensors of the VH-TDMA using three saturated salt solutions.

The sensors used for the DMA2 RH regulation are placed in the excess air line and the aerosol inlet line, respectively. During normal humid scan operations, the RH of the aerosol flow is set to 85% (i.e. aerosol pre-humidifier) while RH in the DMA excess flow is maintained at 90%.

2.2.3. RH generation and regulation

In our system, RH of DMA2 sheath flow and the aerosol flow are separately adjusted using independent humidifying circuits. In both case, the flow is humidified by passing through a vertically oriented Nafion membrane (i.e. PermaPure Single Tube MD-110-12S-4 for the aerosol flow and PermaPure Multi Tube PH-60T-12SS for the sheath flow), around which a counter-flow of saturated air was passed. Moisture can diffuse from this secondary flow through the membrane into the flow stream. The secondary saturated airflow is provided by a Controled Evaporation Mixing (i.e. CEM), shown in Figure A.3.3, which mixed two lines of particle-free dry air (up to 16.0 lmin^{-1}) and an Ultra-pure water flow (up to 50 gh^{-1}) that evaporates when injected inside the three-way heating valve. The CEM temperature set point is manually adjusted between 20 - 50°C depending on the atmospheric dew point temperature.
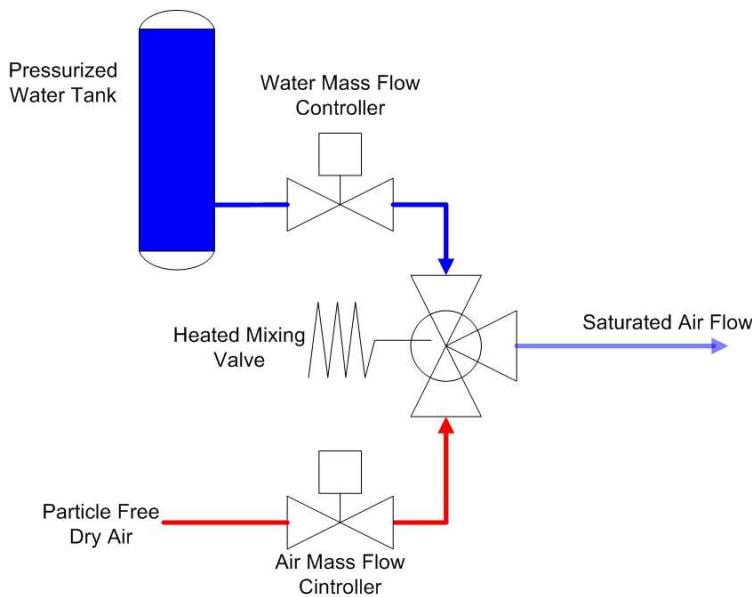
Figure A.3.3: Schematic of the Controled Evaporation Mixing (CEM).

The humidification is regulated by a PID software that controls an "ON/OFF" injection of the secondary flow inside the humidifiers via two three way valves (e.g. one for each humidifier membrane) by comparing a set RH with that measured by capacitive

sensors. The PID control parameters are experimentally determined for each individual humidifier with an adapted tuning procedure.

2.2.4. Temperature control

The determination of RH in DMA2 during field experiments is not trivial due to temperature gradients between inlet and outlet of the DMA. A temperature difference of only 1°C leads to a change in RH up to 6% close to 90% RH. Hence, it is essential that the wet DMA is kept at a constant temperature independent of the ambient temperature fluctuations to minimize RH gradients. This is achieved by isolating DMA2 and the humidity conditioning section into a temperature controlled volume (70 l). Constant temperature in the volume is maintained by two thermoelectric air coolers (TEC, Peltier units 50+50 W) and an improved forced air convection is obtained with four tangential fans placed in the volume wedges (see Appendix A.6). An additional long copper heat exchanger is placed in the sheath line, inside the thermostatic volume, to ensure that the flow temperature is well equilibrated prior entering the DMA. All heat sources, such as pumps, power supplies, thermo-desorber, three-way valves were kept in a separate volume.

2.2.5. Aerosol thermo-desorber conception

The monodisperse aerosol is heated to a predefined temperature in a self-made thermodenuder. The heating column consists of a stainless-steel volatilization tube (i.d.=8.6 mm, o.d.=13.5 mm and length = 45 cm). A heating wire is coiled around the tube over 30 cm to allow fast heating of the aerosol flow. Between the wire and the tube a ceramic non-conductive refractory tape is used to act as an electric insulation and to ensure a stable and homogeneous temperature field along the walls of the heating column. For additional insulation the column heating path is surrounded by ceramic fiber material (outer diameter =6 cm). The aerosol temperature is monitored using a thin thermocouple (1 mm diameter) located at the center of the aerosol tube halfway through the column heating path (i.e. 15cm) (see Appendix A.5). The temperature inside the aerosol heating tube is computer controlled with a self-made PID at ±0.5% of the set-point temperature.

For an aerosol flow rate of 1.0 l min^{-1}, the dimension of the volatilization tube results in a mean aerosol velocity at the center-line of the flow tube of 0.3 ms^{-1}, corresponding to a Reynolds number of approximately 200, well within the laminar

flow regime. The calculated resulting residence time in the oven heating path (30 cm) is t_R=0.3 / 0.3=1 s. The residence time in the heating unit corresponds to that of the V-TDMA apparatus described by Villani et al., submitted. After the heating path (30 cm) the flow is cooled down to ambient temperature over a distance of about 20 cm. The temperature of the heating column, Ti, can be set between ambient temperature and 300°C. Operation for Ti>300°C requires the use of non-oxidative carrier gases, such as nitrogen, to avoid creating artifacts due to charring of organic matter in the particles (Orsini et al., 1998; Burtscher et al., 2000; Brooks et al., 2001).

2.2.6. Measurement control and data acquisition

The Multi-TDMA is controlled by a program written in the National Instruments LabVIEW's graphical programming language. The main program consists of 100 subroutines of which 40 subroutines are created for the Multi-TDMA application and the rest are provided by the LabVIEW standard libraries. The data acquisition is achieved via two National Instruments data acquisition (DAQ) boards (National Instrument Corporation) and a self-designed electronics box that measures the signals attached to the specified board channels. Since them the program has been continuously upgraded to the present version.

2.2.7. Operation procedures

A complete characterization of a particle at specific dry diameter (i.e. "DRY Dp") selected by DMA1 consists of an alternate sequence of three scans: H-TDMA first, VH-TDMA and then V-TDMA. It should be notice that, prior to initial size classification in DMA1, the aerosol is dried to a relative humidity <10% in a diffusion drier tube. It is also important to note that during volatility scans, the humidifying unit remains in operation as for the thermo-desorbing unit during humidity scans. This allows for very rapid switch from one scan type to the other without delays due to equilibrium conditions. DMA2 scanning size range should be, on one side, wide enough, so that the whole hygroscopic growth spectra can be covered, and, on the other side, as narrow as possible to save measurement time. Since a high size resolution decreases the temporal resolution and vice versa, each scan is enhanced for optimum performance. Hygroscopic growth factors (H-GF) are measured as followed:

$$HGF = D_p^{90} / D_p^{10}$$

where D_p^{90} is the particle diameter at RH=90% and D_p^{10} is the particle diameter at RH=10%. HGF are usually measured from 0.8 to 2.5 at all the different dry size leading to a typical duration of the complete procedure (i.e. three scans) for each dry particle diameter of the order of 20 minutes, when 24 different sizes are selected in the DMA2 in stepping-voltage method (i.e. DMPS). To increase temporal resolution during field campaigns, the volatility scan can be repeated once per hour in stable conditions, whereas the system alternates only two wet scans (i.e. Humidity-scan and Volatility-Humidity-scan) every 14 minutes.

Volatility "growth" factors (VGF) are calculated as the ratio between the particle diameter at RH=10%, T>T$_{amb}$ ($D_p^{10,T°}$) and the dry particle diameter at RH=10% and ambient temperature ($D_p^{10,Tamb}$), thus:

$$VGF = D_p^{10,T°} / D_p^{10,Tamb}$$

Therefore the Volatility-Hygroscopic growth factors (VH-GF) are derives as:

$$VHGF = D_p^{90,T°} / D_p^{10,T°}$$

where $D_p^{90,T°}$ is the particle diameter conditioned at T>T$_{amb}$ and subsequently humidified at RH=90%.

3. Validation of VH-TDMA performances

3.1. Aerosol penetration efficiency

The aerosol penetration efficiency through the instrument is determined experimentally in order to correct the measured mobility distributions for the size-dependent losses in DMAs, valves and connection tubings. The Multi-TDMA system therefore requires quantification of particle transport efficiency as a function of size for the four flow pattern (i.e. TDMA, H-TDMA, V-TDMA and VH-TDMA).

The evaluation of particle losses is performed using Sodium chloride (NaCl) aerosol particles generated in the laboratory with an atomizer (TSI Model 3670) filled with a solution of Ultra Pure Water (ELGA) and NaCl salt. NaCl is well suited for calibrating because it is thermally stable for a wide range of particle diameters. After dispersion, polydisperse NaCl aerosol particles were further mixed with sheath air for drying and dilution in a mixing chamber (100 l) to ensure stable particle concentration. Particle diffusion is size dependent, and, therefore, the penetration measurements are carried

out for a range of particle diameters, Dp (10 < Dp< 120 nm) at ambient temperature and RH<10%. Comparison of concentration readings from CPC1 and CPC2 gave the transport efficiency η(Ti,Dp) for dry flow patterns (i.e. TDMA and V-TDMA) and wet flow patterns (i.e. H-TDMA and VH-TDMA). The Figure A.3.4 illustrate the results of the penetration efficiency measurements. Particle losses are quite similar for each of the four flow patterns of the Multi-TDMA.
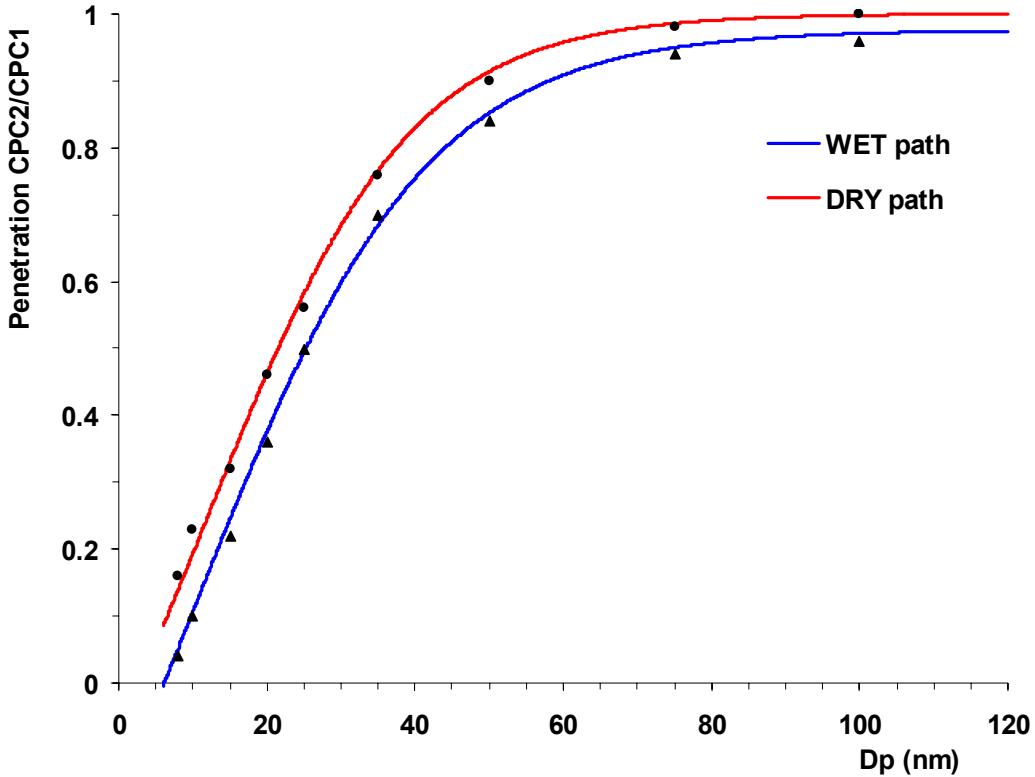

Figure A.3.4: Transport efficiency η as a function of particle diameter Dp and flow patterns of the Multi-TDMA.

For the dry patterns η=100% for Dp=100 nm and $Dp^{50\%}$=21 nm; for the wet patterns η=97% for Dp=100 nm and $Dp^{50\%}$=25 nm. The fit for each curve is described by the following equation:

$$C_{eff} = b - \frac{a}{1+\exp\left(\frac{D_p-D_1}{D_2}\right)}, \qquad (1)$$

where D_p is the particle diameter and a,b,D_1,D_2 the four constants of best fit . Size distributions measured with the VH-TDMA should be corrected with these measured transport efficiency factors. This is accounted for in the inversion procedures.

3.2. H-TDMA calibration

The H-TDMA performances have been evaluated in February 2006 during the first European H-TDMA workshop intercalibration at the Institute for Tropospheric Research (IfT) in Leipzig (Germany) under the ACCENT NoE program. Six different TDMA- based systems (2 from IFT-Leipzig, 1 from UMIST-Manchester, 1 from U. Helsinki, 1 from U. Lund and 1 from U. Clermont-Ferrand) for different experiments participated to the workshop to compare performances and hygroscopic results for laboratory generated particles and for atmospheric aerosol particles. A specific paper is in preparation relating the intercomparison (Kaaden et al., in preparation). Here, we will restrict the discussion to the features related to the performances of the H-TDMA subsystem of VH-TDMA.

The H-TDMA intercomparison has been organized with several experiments aimed at evaluating instrumental performances, including calibration. The different experiments performed during the intercomparison procedures are summarized in Table A.3.1. For all experiments particles are generated using 1 or 2 aerosol generator(s) type TSI 3760.

Exp. #	Particle type	Particle size	Humidity
1	Ammonium Sulphate	Dp=15,30,50,70,100 nm	DMA 1: 10% RH DMA 2: 10% RH
2	Ammonium Sulphate	for Dp=50 nm	DMA 1: 10% RH DMA 2: 90% RH
3	Ammonium Sulphate	Dp=70 nm	DMA 1: 10% RH DMA 2: scan 73-80% RH
4	Soot + Ammonium Sulphate	Dp=50 nm	DMA 1: 10% RH DMA 2: 75 and 85% RH
5	Soot + Ammonium Sulphate	Dp=30,50,70,100 nm	DMA 1: 10% RH DMA 2: 90% RH

Table A.3.1: List of experiments for the IfT-HTDMA intercalibration.

The calculation of hygroscopic growth requires a relative calibration of DMA2 with respect to DMA. This is performed as a standard calibration procedure for TDMA measurements. Ammonium sulphate particles are produced into a 1 m^3 mixing chamber. Five specific particle sizes are selected by DMA1 in the range of 15 to 100 nm. The selected size is then measured by DMA2 after the humidity regulation is switched off. Results are presented in Table A.3.2 and show that DMA2 underestimates the selected diameter of DMA1 by 1 to 5 %.

Selected diameter DMA1	15	30	50	70	100
Selected diameter DMA2	14.2	29.3	49.3	69.0	99.0
Deviation in percent	5.4	2.4	1.5	1.3	1.0

Table A.3.2: Results of the DMA2 shift calibration using Ammonium Sulphate particles.

The DMA2 shift is relatively higher for small diameters possibly due to an offset or an error in the lower voltage range of the DMA power supplies, which may be different for both devices. The relationship between DMA1 and DMA2 diameters is fitted by linear regression:

$$D_p^{DMA2} = 0.9959 * D_p^{DMA1} - 0.6264$$

All growth factors measured with the H-TDMA and presented in this work have been corrected for this size shift.

A second experiment has been performed to control the humidity regulation in DMA2. This is clearly a pre-requisite to guarantee high data quality for hygroscopic growth measurements. The humidity regulation is clearly dependent on the proper calibration of the RH sensors (see Section 2.2.2). In turn, the stability of the humidity regulation is checked monitoring the variations of the growth factor of 50 nm ammonium sulphate particles at 90% RH.
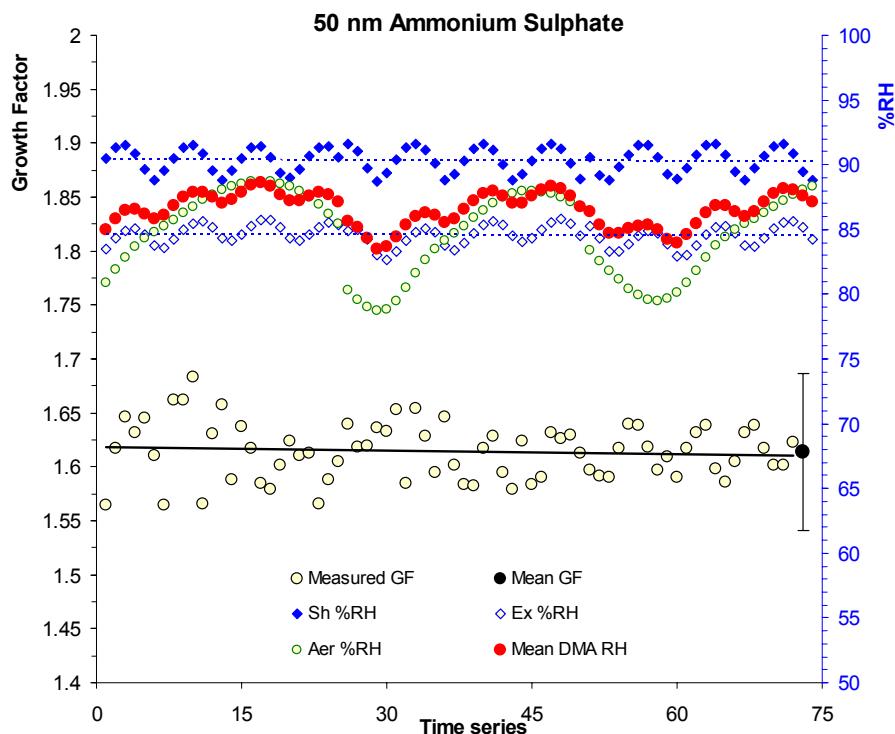
Figure A.3.5: Hygroscopic growth for pure ammonium sulphate 50 nm particles measured during the H-TDMA workshop for 90 %RH DMA2 sheath flow set point.

The measured growth factors during a 9 hours run (75 scans) are presented in Figure A.3.5. The theoretical growth factor for 50 nm ammonium sulphate particles is 1.66 (Tang et al., 1994). As shown in Figure A.3.5, the mean hygroscopic growth factor (1.61 ±0.8) is lower than the theoretical value (1.66).

A possible explanation for lower growth factors than the theoretical value is that the effective RH in DMA2 is lower than 90%. It can be seen from Figure A.3.5 that the sheath flow RH oscillates around 90% (±2%) and the aerosol flow around 85% (±3%). Simultaneously, RH at the DMA outlet (Figure A.3.5, "blue circle") oscillates around 85% (±2%). This means that the DMA effective relative humidity is lower than the set point value as is visible in Figure A.3.5 (red dot Mean DMA RH= 87.5% ±2% for a setpoint of 90%), so a lower growth factor than predicted by the theory. In fact, the DMA humidity-PID regulates the RH by the measurement of the humidity sensor placed on the DMA sheath flow with a set point value of 90%. To ensure a better mean RH inside the DMA (i.e. average of sheath and excess flow RH close to 90% RH) we chose PID regulation with the RH measurement of the excess flow RH sensor. The theoretical growth factor for Ammonium sulphate 50 nm particles at 87.5% RH is 1.59 (Tang et al, 1994; Hameri et al, 2000) so we can conclude that the hygroscopic growth factor accuracy measurements of the VH-TDMA is ±2.5%.

Another important result is that the RH oscillations inside the DMA imply a growth factor measurement oscillation. In Figure A.3.5 is clearly shown that the measured growth factor variability (i.e. ±3.5%) is due to a sinusoidal mean DMA humidity instability (e.g. ±2%) during time. An improve PID regulation is being developed for a new version of the H-TDMA. Overall, the hygroscopic growth factor for pure ammonium salts can be measured with a precision of less than 5% as compared to theoretical values. The variability of the HGF, as measured by the standard deviation of the mean is lower than 0.03.

The ability of the instrument to properly measure the relative humidity of deliquescence (DRH) of pure ammonium sulphate 70 nm diameter particles is tested (experiment #3). The deliquescence behaviour of inorganic salts have been extensively studied (Junge, 1952; Tang, 1980; Richardson, 1984; Cohen, 1987). Hygroscopic growth spectra were taken at defined levels of relative humidity in the range of the theoretically expected deliquescence relative humidity (i.e. 73% to 80% RH). The DRH value calculated at ambient temperature (i.e. 25°C) found in the literature for ammonium sulphate is 79.9%. The RH step is set to 1% given the

precision of the humidity PID regulation. The results of this calibration are shown in Figure A.3.6.
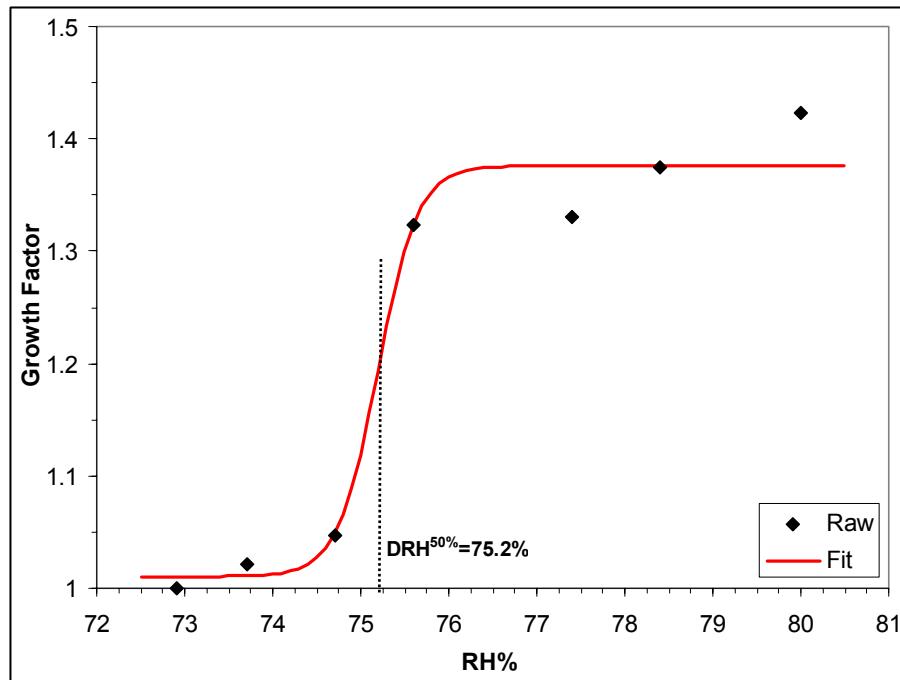
Figure A.3.6: Deliquescence relative humidity (DRH) measured with the VH-TDMA of 70 nm ammonium sulphate particles.

The HGF versus RH measurements are fitted with a 4 parameters-curve give the adequacy of the fitting.

$$S = b - \frac{a}{1 + \exp\left(\dfrac{x - c}{d}\right)}, \qquad (2)$$

with   a= 0.36555, b= 1.37607, c= 75.19718, d= 0.22767 and a MSE= 1.13E-3 (i.e. Mean Square Error).

The experimental deliquescent point is calculated as the inflexion point of the fitting curve (i.e. $S^{50\%}$). The measured DRH is 75.2 ±5% in the range of the theoretically expected deliquescence relative humidity (i.e. 73% to 80% RH). Due to the humidity and temperature uncertainties it is difficult to assign a corrected value of the deliquescent relative humidity.

An externally mixed aerosol is generated into a mixing chamber using two atomizers with electrolyte solutions of pure ammonium sulphate salt and soot respectively. Selecting just one diameter particle (i.e. 50 nm) from the external mixed aerosol, a comparison of hygroscopic growth has been performed at RH both lower and higher than DRH of pure ammonium sulphate (i.e. 75% and 85% RH) to check the

sensitivity of growth factors matching for all systems (experiment #4)., The averaged hygroscopic spectrum found for this experience is shown in Figure A.3.7.
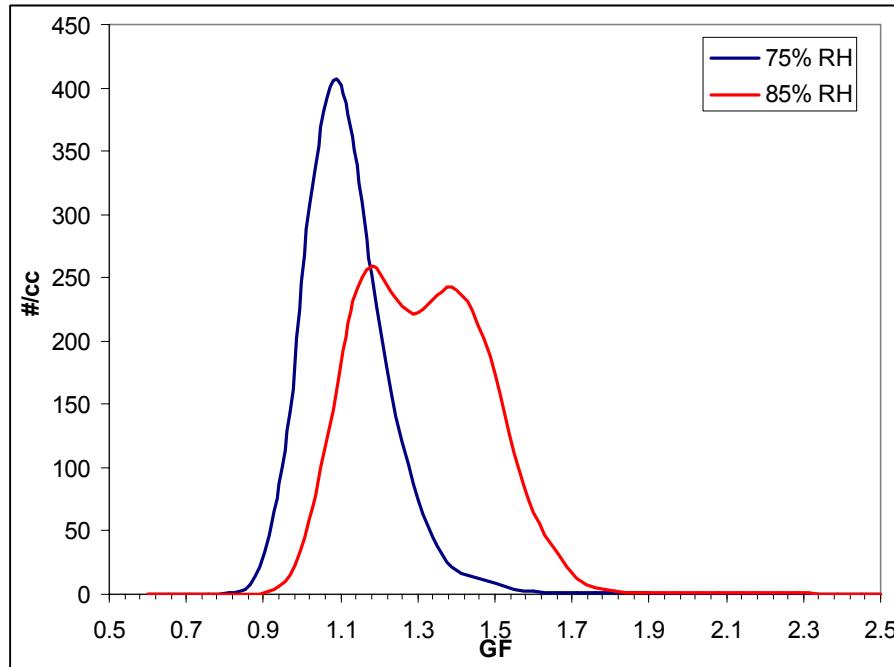
Figure A.3.7: Hygroscopicity averaged spectra of an external mixture of soot and ammonium sulphate particles measured at 75% RH (blue curve) and 85% RH (red curve).

Two distinct hygroscopic modes appear at RH higher than the DRH of pure ammonium sulphate (i.e. 80.0% RH) : the first one with GF=1.2 correspond to the hydrophobic class and the second one with GF=1.51 hygroscopic class. The reason why the pure soot mode have not a GF=1.0 is unclear but may be related to the presence of trace levels of ammonium sulphate on the hydrophobic particles. .

Using the same particles generation set up of "Experiment #4" the ability of the H-TDMA to resolve two hygroscopicity classes is tested in experiment #5. Hygroscopic growth spectra were taken at 90% RH for 30, 50, 70, 100 nm diameter particles. Examples of retrieved averaged H-TDMA spectra are given in Figure A.3.8a, b, c, d for various particle sizes. As expected, at least 2 modes are retrieved corresponding to soot particles (nearly hydrophobic mode with HGF = 1.1 ± 0.1) and to ammonium sulphate particles (more hygroscopic mode with HGF = 1.7 ± 0.1). A third mode is often measured with HGF = 1.4 ± 0.1. This last mode may be resulting from mixing through coagulation between the two particle types inside the chamber and long inlet tubing (7 m). We propose that the intermediate HGF results from increased hygroscopicity of soot particles containing traces of ammonium sulphate.
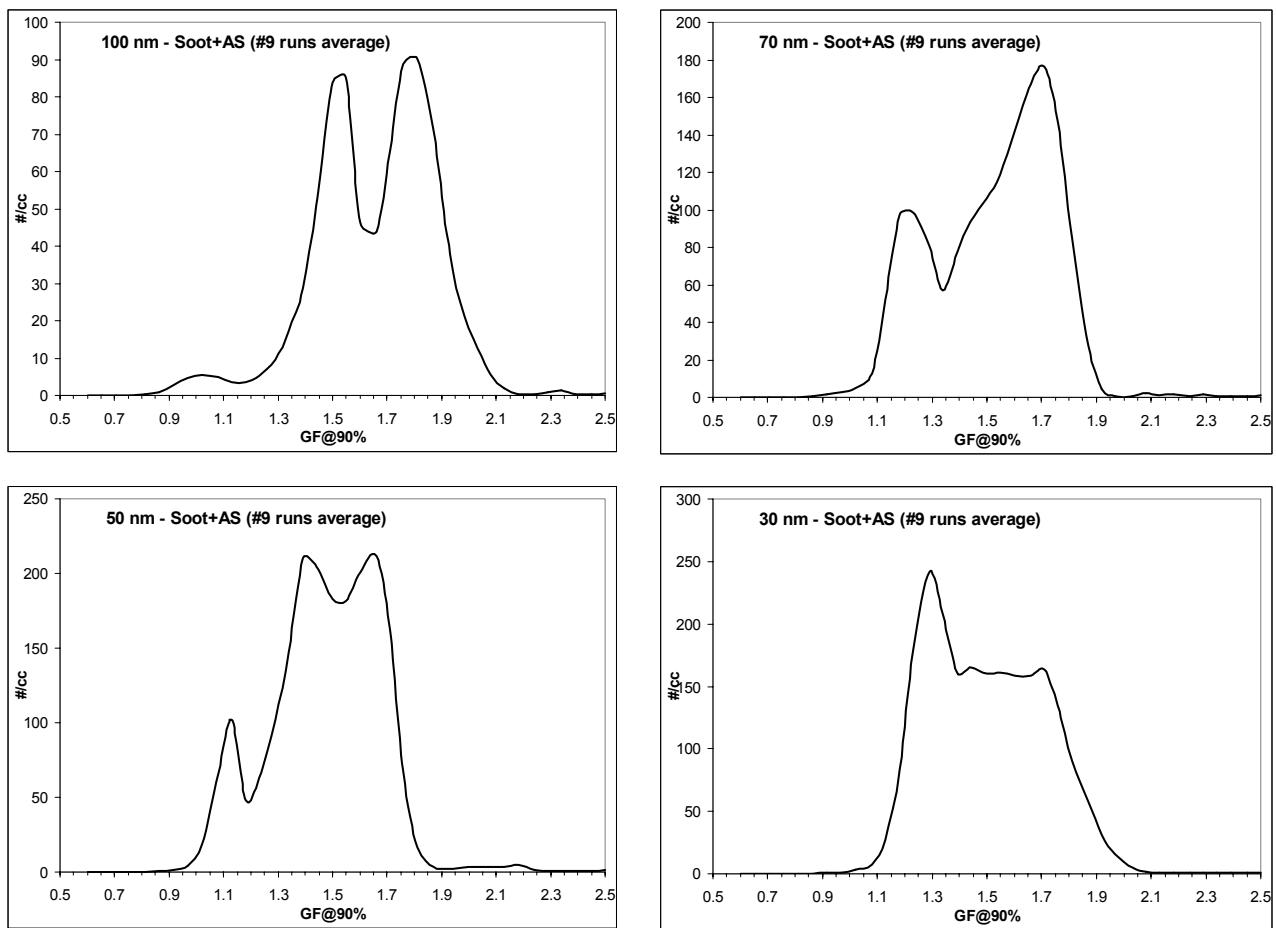
Figure A.3.8a,b,c,d: Hygroscopicity spectra measured with the VH-TDMA for an external mixing of soot and ammonium sulphate particles.

It can be notice from the figures that only for 100 nm particles the hydrophobic mode is clearly seen (i.e. GF=1.0). For the others sizes the hydrophobic class growth factor is about 1.1-1.25 but is not an effect of averaging the data. A possible explanations is that this growth factor is resulting from a mixture of soot and a very few quantity of hygroscopic material.

We have tested the H-TDMA for a variety of compounds. Table A.3.3 summarises the results for each single species aerosols tested. In general, there is good agreement between the observed hygroscopic growth factors and those found in literature except for sodium chloride for which the measured hygroscopic growth is slightly lower than theoretically expected (i.e. GF=2.35). This might be due to a time limitation in the H-TDMA system to reach equilibrium between H_2O and NaCl.

Species	BP (°C)	$T_{vol} \pm 2$ (°C)	GF@90% ±0.05
DEHS	252°	115°	1.02
NaCl	1413°	650°	2.20
$(NH_4)_2SO_4$	205°	180°	1.69
H_2SO_4	330°	115°	1.65
NH_4NO_3	210°	60°	1.50
Table A.3.3: Physical data, volatilization temperatures and diameter growth factors at 90% RH for 100 nm particles of different compounds tested in this work.			

Finally, we have compared the measured hygroscopic growth of $(NH_4)_2SO_4$ particles with theoretical model calculations using the Tang et al., (1994) modelling approach. The hygroscopic growth of 100nm particles as a function of relative humidity in the H-TDMA system derived both experimentally and theoretically is shown in Figure A.3.9.
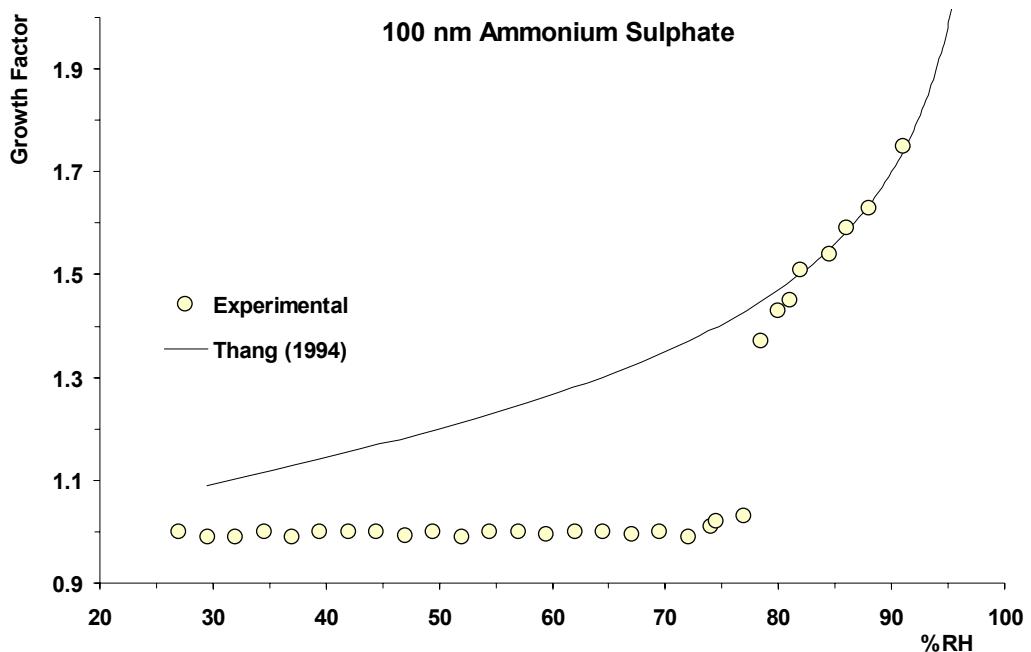
Figure A.3.9: Particle diameter change (growth factor) as a function of relative humidity for ammonium sulphate 100 nm particles. The H-TDMA data with increasing RH are indicated with open symbols, the theoretical calculation is shown as line.

Results show a good agreement between theoretical values and experimental results is good for RH>80%. The H-TDMA sub-system of the VH-TDMA is therefore well controlled to provide accurate (± 4%) measurements of hygroscopic growth.

3.3. VH-TDMA calibration

We have tested the response of the VH-TDMA using an internally mixed aerosol composed of sodium chloride and DEHS (Di-2-Ethylhexyl-Sebacat). The thermal and hygroscopic properties of pure NaCl and DEHS are summarized in Table A.3.3 above. We produced 100 nm pure NaCl particles coated with DEHS with a PALAS MAG-2010 Monodisperse Aerosol Generator, using NaCl as the seeding aerosol. The size distributions of pure NaCl seeding particles and of DEHS-coated NaCl particles are measured by DMA1 and CPC1 (Figure A.3.10).
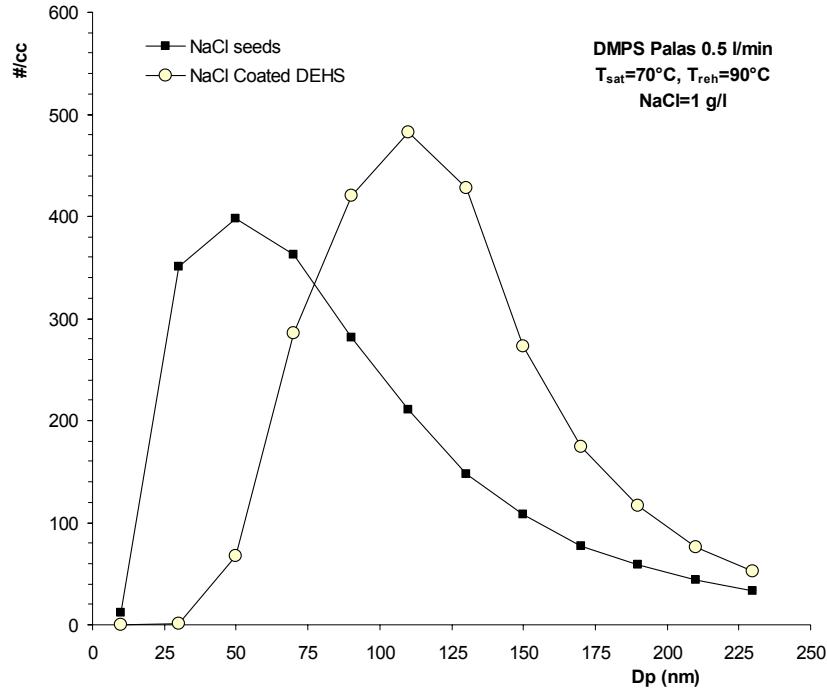
Figure A.3.10: Size distribution of pure NaCl seeding aerosol (1 g/l) and DEHS coated NaCl using Palas generator at 70°C saturator temperature.

In this case the DEHS liquid evaporates in the generator at 70°C (i.e. saturator temperature) and the particle size at the peak concentration shifted from 50 nm fore pure NaCl to 115 nm for NaCl with DEHS exposure, indicating an increase in the particle size due to DEHS coating. The large increase in size and the absence of small particles after DEHS exposure indicate that external mixture of NaCl and DEHS is limited and that DEHS homogeneous nucleation does not take place. The low temperature gradient between saturator and reheater of the MAG generator prevents the formation of pure DEHS particles.

We performed a complete VH-TDMA scan of the NaCl internally mixed particles. The temperature dependence of the humid and dry sizes as well as the corresponding VHGF for 100 nm particles is shown in Figure A.3.11.
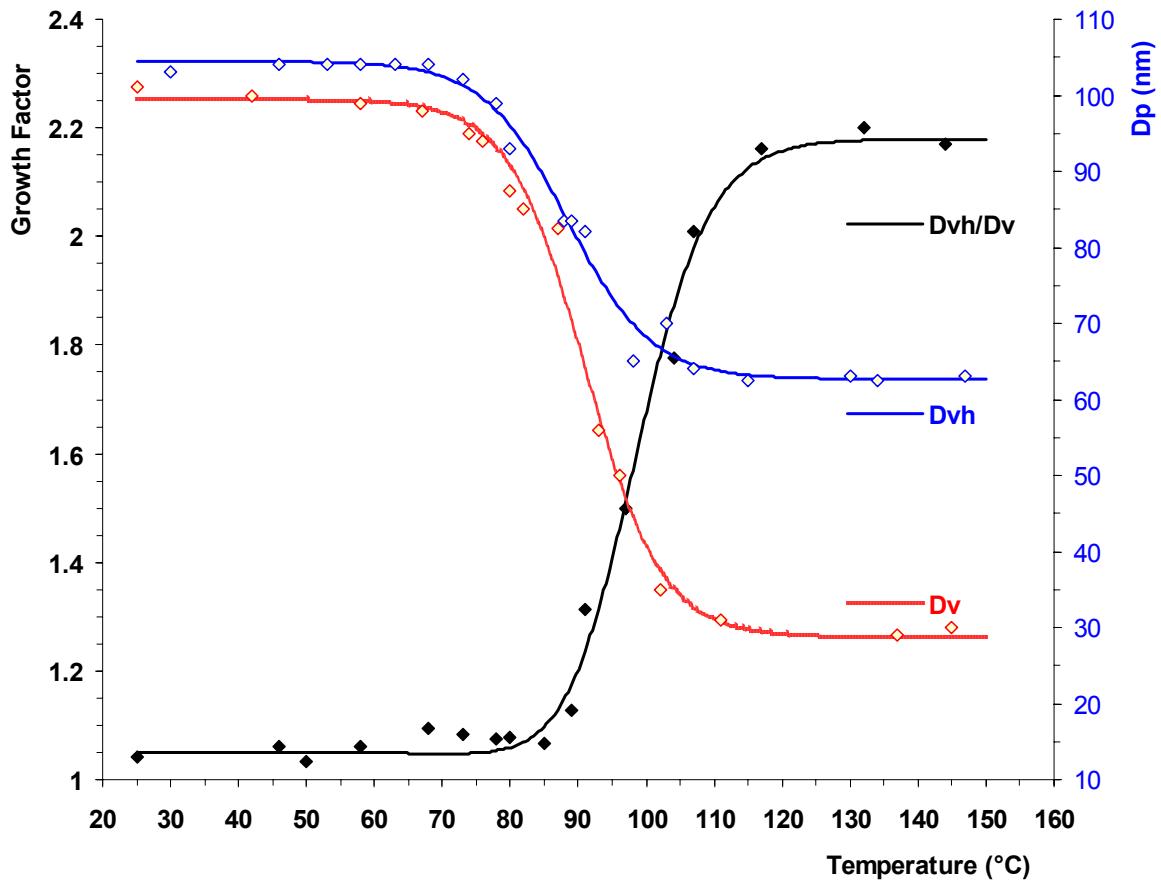
Figure A.3.11: Particle diameter after volatilization (Dv), diameter after subsequent hygroscopic growth at 90% RH (Dvh) and diameter hygroscopic growth factor (VHGF=Dvh/Dv, black line) vs. thermodenuder temperature for NaCl-seeded DEHS aerosol.

The raw measurements points are fitted using equation (2) (i.e. with a 4 parameters-curve). The DEHS component begins to evaporate at 70°C and is completely removed at 120°C. The diameter hygroscopic growth factor begins to increase as the DEHS component evaporates and reaches a value of 2.18 (±4%) when all of the DEHS has been removed. The NaCl seeding particles diameter is about 30 nm. This growth factor value well agree with the theoretical value of 2.23 calculated using the model by Hameri et al. (2001) for 30 nm NaCl particles at 90% RH. The DEHS coating has been removed by thermo-desorption and the measured HGF is now that of the original NaCl particle.

4. Summary and conclusions

We presented the original design of Multi-TDMA with the capability of measuring the hygroscopic behaviour of in internally mixed particles and their non-volatile residues. All components of the VH-TDMA have been separately validated. In particular, we have shown that the H-TDMA sub-system properly retrieves measurements of HGF close to theoretical expectations. The instrument has been compared to other similar apparatus available in 6 different European laboratories showing satisfactory agreements with both theoretical expectations and other instruments. In addition, specific features of the VH-TDMA have been tested. In particular, we have measured the change in hygroscopic growth of internally mixed particles during thermal removal of its more volatile components. Our results show that the thermo-desorption process is very efficient to remove adsorbed semi volatile material from the particle surface. We showed that, once the volatilization temperature of the semi-volatile component is reached, the measured HGF is that of the core-forming component of the internally mixed particle.

This technique is therefore useful for investigating particle formation process and differentiating seeded heterogeneous nucleation and homogenous nucleation through its capacity to distinguish between components of similar volatility but differing hygroscopic behaviour within particles consisting of several species. The choice of the thermo-desorbing temperature permits to investigate the role of different types of chemical compounds on the hygroscopic growth. The VH-TDMA can be used to investigate the volume fraction of the semi-volatile particle constituents of a submicrometer aerosol and the hygroscopic behaviour of the particulate residues for different temperatures.

References

Andrews, E. and Larson, S. M. (1993). Effect of surfactant layers on the size changes of aerosol particles as a function of relative humidity. Environ. Sci. Technol. 27, 857-865.

Burtscher, H., Baltensperger, U., Bukowiecki, N., Cohn, P., Huglin, C., Mohr, M., Matter, U., Nyeki, S., Scmatloch, V., Streit, N., Weingartner, E. (2001). Separation of volatile and non-volatile aerosol fractions by thermodesorption: instrumental development and applications. J. Aerosol Sci. 32, 427-442.

Chen, Y. Y., Lee W. M. G. (1999). Hygroscopic properties of inorganic-salt aerosol with surface-active organic compounds. Chemosphere 38 (10), 2431-2448.

Cruz, C. N., Pandis, S. N. (1998). The effect of organic coatings on the cloud condensation nuclei activation of inorganic atmospheric aerosol. J. Geophysical Res. 103, D13, 111-123.

.Cruz, C. N., Pandis, S. N. (2000). Deliquescence and hygroscopic growth of mixed inorganic-organic atmospheric aerosol. Environ. Sci. Technol. 34, 4313-4319.

Dua, S. K., Hopke, P. K., Raunemaa, T. (1998). Hygroscopicity of diesel aerosols. Water Air and Soil Pollution. 112: 247-257.

Gysel, M., Weingartner, E. and Baltensperger, U. (2002). Hygroscopic of aerosol particles at low temperature. 2. Theoretical and experimental hygroscopic properties of laboratory generated aerosols. Environ. Sci. Technol. 36, 63-68.

Hameri, K., Rood, M. J., Hansson, H. C. (1992). Hygroscopic properties of a NaCl aerosol coated with organic compounds. J. Aerosol Sci. 23, S437-S440.

Hameri, K., Charlson, R. J., Hansson, H. C., Jacobson, M. (1997). Hygroscopic properties of ammonium sulphate aerosols mixed with slightly soluble organic compound. J. Aerosol Sci. 28 (S1), S153-S154.

Hanssson, H. C., Rood, M. J., Koloutsou-Vakakis, S., Hameri, K., Orsini, D., Wiedensohler, A., (1998). NaCl aerosol particle hygroscopicity dependence on mixing with organic compounds. J. Atmos. Chemistry 31:321-346.

Hennig, T., Massling, A., Brechtel, F. J., Wiedensohler, A. (2005). A tandem DMA for highly temperature-stabilized hygroscopic particle growth measurement between 90% nd 95% relative humidity, Aerosol Sci. 36, 1210-1223.

Johnson, G. R., Ristovski, Z. and Morawska, L. (2004). Method for measuringthe hygroscopic behaviour of lower volatility fractions in an internally mixed aerosol. J. Aerosol Sci. 35, 443-455.

Kohler, H. (1936). The nucleus and growth of hygroscopic droplets. Trans. Faraday Soc. 32, 1152-1161.

Kramer, L., Poschl, U., Niessner, R. (2000). Microstructural rearrangement of sodium chloride condensation aerosol particles on interaction with vapor. J. Aerosol Sci. 6, 673-685.

Kreidenweis, S. M., Koehler, K., DeMott, P., Prenni, A. J., Carrico, C., Ervens, B. (2005). Water activity and activation diameters from hygroscopicity data-Part I: Theory and application to inorganic salts. Atmos. Chem. Phys. Discuss. 5, 287-323.

Lehmann, K., Massling, A., Tilgner, A., Mertes, S., Galgon, D.,Wiedensohler, A. (2005). Size-rsolved soluble volume fractions of submicrometer particles in air masses of different character. Atmos. Environment 39, 4257-4266.

Massling, A., Wiedensohler, A., Bush, B. (1999). Concept of an advanced hygroscopic tandem differential mobility analyser with a great operation stability. J. Aerosol Sci. 30 (S1) S395-S396.

Mikhailov, E., Vlasenko, S., Niessner, R., Poschl, U. (2003). Interaction of aerosol particles composed of protein and salts with water vapor: hygroscopic growth and microstructural rearrangement. Atmos. Chem. Phys. Discuss. 3, 4755-4832.

Svenningsson, B., Rissler, J., Swietlicki, E., Mircea, M., Bilde, M., Facchini, M. C., Decesari, S., Fuzzi, S., Zhou, J., Monster, J., Rosenorn, T. (2005). Hygroscopic growth and critical supersaturations for mixed aerosol particles of inorganic and organic compounds of atmospheric relevance. Atmos. Chem. Phys. Discuss. 5, 2833-2877.

Weingartner, E., Gysel, M. and Baltensperger, U. (2002). Hygroscopic of aerosol particles at low temperature. 1. New low-temperature H-TDMA instrument: setup and first applications. Environ. Sci. Technol. 36, 55-62.

Chapitre II

La croissance hygroscopique de l'aérosol atmosphérique et l'impact des propriétés de surface des particules

La seconde partie de ce travail s'intéresse plus particulièrement aux résultats obtenus par l'utilisation du VH-TDMA lors de plusieurs campagnes de mesure sur différents sites Européens et en laboratoire.

La première utilisation du VH-TDMA a eu lieu dans le cadre de la campagne Européenne QUEST-BACCI à Hyytiala en zone boréale de la Finlande. D'autres campagnes ont suivi, à Mace Head, zone cotière de l'Irlande dans le cadre de la campagne Européenne MAP, au puy de Dôme, dans la zone sub-urbaine de Clermont-Ferrand sur le site des Cézeaux (campagne spécifique PRIMEQUAL) et enfin, à Leipzig, dans le cadre d'une campagne européenne d'intercomparaison des H-TDMA organisée dans le cadre d'ACCENT.

Nous avons choisi ici de présenter les résultats sous forme de 3 articles qui décrivent 1- les mesures H-TDMA uniquement sur les différents sites (chapitre II-1 : « Hygroscopic behaviour of aerosol particles in diverse environnements ») et qui montre les variations de la croissance hygroscopique en fonction des sources d'aérosols et 2- les mesures de VH-TDMA sous la forme de 2 articles distincts. Le premier article décrit les premiers résultats du VH-TDMA obtenus après la campagne de Hyytiala où, pour la première fois, nous mettions en évidence des modifications du caractère hygroscopique des particules d'aérosols après thermo-désorption. Cet article, soumis au Geophysical Research Letters, a été refusé malgré son intérêt scientifique reconnu par les évaluateurs, car nous ne fournissions pas l'ensemble des données de la campagne. Nous avons néanmoins tenu à l'intégrer dans ce travail de thèse puisque l'ensemble des données est analysé dans la section suivante qui traite des mesures VH-TDMA effectuées durant les différentes campagnes.

Hygroscopic behaviour of aerosol particles in diverse environments

Villani, P., Sellegri, S. and Laj, P.

1. Introduction

Anthropogenic aerosols create a significant perturbation in the Earth's radiative balance on regional scales (Charlson et al., 1992; NRC, 1996, IPCC, 2001) by absorbing and scattering solar radiation. The direct climate effect of aerosol particles is based on their interaction with the incoming sunlight. Aerosol particles scatter and absorb sunlight depending on their size and their chemical composition, which causes warming or cooling in the atmosphere. For quantification of the direct climate effect, it is necessary to determine the physical and chemical properties of the particles such as humidity dependent aerosol particle number size distribution, the chemical composition, the refractive index, and the state of mixture. Aerosol particles also act as cloud condensation nuclei for the formation of fog and cloud droplets. The influence of aerosol particles on cloud formation and cloud lifetime is called the indirect climate effect. Hygroscopic properties of atmospheric particles mainly influence cloud formation processes, and thus influence the resulting droplet size distribution, which affects cloud albedo (Swietlicki et al., 1999). Depending on their chemical composition, the particles can take up water at relative humidities below 100% and thus grow to larger sizes, which leads to an increase of scattering coefficients.

Information on the hygroscopic properties of aerosols is important for determining aerosol size distributions, and thus determine scattering and absorption coefficients at ambient conditions (Ogren and Charlson,1992). Moreover, measuring the hygroscopic properties allows an estimate of the amount of soluble material contained in the particle, which is an important input parameter in cloud models.

Aerosol particles also affect human health (Peters et al., 1997a, b; Cooney, 1998; Pope and Dockery, 1999). Particles deposit in the respiratory tract, thus possibly causing diseases such as asthma and respiratory cancer (Pope and Dockery, 1999),

though the exact mechanisms are not well understood. The number concentration, particle size, and chemical composition of these particles are important parameters in this context. Hygroscopic growth of aerosol particles determines the location and rate of particle deposition in the respiratory tract because of size-dependent deposition mechanisms. The relative humidity in the deep lung is estimated to be approximately 99 to 99.5% (Ferron et al., 1998). When the aerosol is exposed to these high values of RH, an increase in diameter by a factor of three to six is realistic for hygroscopic particles depending on their chemical compounds.

Aerosol emissions also influence the air quality in urban areas by decreasing the visibility. Studies show that a decrease in visibility is correlated with an increase in aerosol number concentration or aerosol mass (Noll et al., 1968; Charlson, 1969). Horvath (1993) reported that the visibility in unpolluted areas of North and South America ranges from 150 to 250 km over extended periods, whereas that in rural locations in Europe ranges from 40 to 50 km due to the high density of sources for anthropogenic aerosols.

The degradation of visibility is probably the most readily perceived impact of air pollution. One of the original reasons to study hygroscopic properties of aerosol particles was the dependence of visibility on the relative humidity. It has been shown, that the visibility continuously decreases with increasing relative humidity.

Urban aerosols consist of a complex mixture of locally produced particles (from traffic, domestic heating, and industrial facilities) and particles that are transported in polluted regional air masses. Investigation of the hygroscopic properties of urban aerosol particles is crucial for resolving health related and global climate problems.

The Hygroscopicity-Tandem Differential Mobility Analyser (H-TDMA) system was introduced in the late 1970s by Liu et al. (1978) to determine the hygroscopic properties of atmospheric particles in the submicrometer size range.

Numerous measurements in continental air masses have shown that tropospheric aerosol particles exhibit a modal external mixture with respect to their hygroscopic behaviour, implying an external mixture also from a chemical point of view. This is clearly manifested in measurements with H-TDMA instruments (Hygroscopic Tandem Differential Mobility Analyser; see Chapter I.3 for a description) by a handful of groups around the world (McMurry and Stolzenburg, 1989; Zhang et al., 1993; Covert and Heintzenberg, 1993; Svenningsson et al., 1997; Berg et al., 1998a,b; Swietlicki

et al., 1997b,c, Massling et al., 2003,2004). However, the particles cannot be described simply as being either hydrophobic or hygroscopic.

When taken from a dry state to a fixed humidified state e.g., from 10% to 90% RH, a group of sub-micrometer particles exhibits significant diameter growth. These particles are denoted more-hygroscopic particles. On the other hand, a large number of particles show even less diameter growth when analysed in the same way with the H-TDMA instrument. These particles are denoted less-hygroscopic and nearly hydrophobic particles. Typically 10% of the volume of the individual particles in this group can be accounted for by inorganic salts. Only a small number fraction of the particles are truly hydrophobic (Massling et al., 2004, Lehmann, 2005). In continental air masses, the submicrometer aerosol particles thus exhibit a multi-modal hygroscopic behaviour. Instead of displaying a continuum of hygroscopic growth factors, the particles separate into the less- and the more-hygroscopic groups discussed above, thus implying an external mixture also in chemical composition (Swietlicki et al., 1999; Rissler et al, 2005).

A fourth sub-micrometer hygroscopic group of particles can occasionally be observed in marine environments influenced by production of sea spray particles through bubble bursting (Blanchard, 1983; Swietlicki et al., 1997). In marine air masses, a fourth mode can sometimes be observed, that contains particles exhibiting GFs close to that of pure sea salt (Berg et al., 1998; Massling et al., 2003; Svenningsson et al., 1992; Swietlicki et al., 1997b). This modal growth behaviour implies that particles of one size are externally mixed with respect to their chemical composition. Over the Pacific and Southern Oceans, externally mixed sea spray particles were observed with a TDMA as far down in size as 50 nm (Berg et al., 1998b).

The objective of the present study is to contribute a better knowledge of hygroscopic behaviour of aerosol particles in diverse environments. This was done in 2005 and 2006 by using the H-TDMA to determine hygroscopic growth factors of different aerosol types in diverse European locations.

2. Sampling and technique

2.1. Experimental

The hygroscopic properties of sub-micrometer tropospheric aerosol particles were measured with a H-TDMA (Hygroscopic Tandem Differential Mobility Analyser) instrument. The H-TDMA (Rader and McMurry, 1986; Stolzenburg and McMurry, 1988) measures the hygroscopic diameter growth of individual aerosol particles when taken from a dry state 10% RH to a controlled humidified state RH ranging between 15 and 95%. The H-TDMA consists mainly of three parts; (1) a Differential Mobility Analyser (DMA) which selects a narrow size range of the atmospheric aerosol, (2) humidifiers which condition the air to a well-defined RH and (3) a second DMA which determines the change in diameter caused by the humidification (see Chapter I.3). During normal operation, the humidity in the second DMA is kept constant (e.g., 90% RH), but it can also be varied so that atmospheric aerosol particles showing RH-hysteresis behaviour deliquescence and crystallisation can be studied. The sheath air and the aerosol entering DMA2 were humidified separately. During normal operation, the sheath air humidification was set to control at 90% RH while the aerosol was set to 88% RH. The performance of the H-TDMA instrument was checked in Leipzig during the H-TDMA calibration workshop (see Chapter I.3). This included tests of the TDMA transfer function using dry sheath air in both DMA's, and tests using pure Ammonium Sulfate particles at relative humidities around the deliquescence point 75% RH and the growth of these salt particles at 90% RH.

2.2. Sites characteristics

Hygroscopic properties of aerosol particles were measured using a Hygroscopicity-Tandem Differential Mobility Analyser (H-TDMA) system at five locations in Europe in the years 2005 and 2006. Figure A.4.1 shows the sites location on the Europe map and Table A.4.1 summarizes the sampling sites location and characteristics.

Figure A.4.1: Map showing the sampling sites location.

Site #	Sampling site	Site position	Sampling period	Site type
1	SMEAR II - Hyytiala (Finland)	61°51'N,24°17'E	April 2005	Background
2	Puy de Dome (France)	45°75'N,3°E	October 2005	Background
3	LaMP - Cezeaux (France)	45°45'N,3°06'E	Decembre 2005	Urban
4	Mace Head (Ireland)	53°20'N,9°54'W	January 2006	Background
5	IfT - Leipzig (Germany)	51°21'N,12°27'E	February 2006	Urban
Table A.4.1 : Sampling periods and sampling sites characteristics.				

Site #1

The H-TDMA has been operated for the first time during the BACCI/QUEST campaign that took place in April 2005 at the SMEAR II field station in Hyytiälä, Finland. SMEAR II is located in a rather homogenous Scotch pine stand on a flat

terrain at Hyytiälä Forestry Field Station, University of Helsinki (181 m above sea level), 220 km northwest of Helsinki. Besides Scotch pine, the stand consists of only 1% other species. The region's annual average mean temperature is 3.0°C and the annual mean precipitation is 690 mm. The air quality at the site represents typical background conditions with a large influence of biogenic organic compounds emissions.

At SMEAR II, continuous measurements of submicron aerosol number size distribution have been carried out since January 1996 (every 10 min). They show approximately 40 days per year with clearly detectable aerosol particle formation events. The most typical time for these events is March-April. Subsequent to the new particle formation, significant particle growth is usually observed. Data presented in this paper are based on samplings achieved during 14 days: from April 13-27, 2005.

Site #2

From October 19-26, 2005 aerosol particles were sampled in the experimental station located at the summit of Puy de Dome (1465 m above sea level). Meteorological parameters including wind speed and direction, temperature, pressure, relative humidity, and radiation (global, UV and diffuse), gases (O3, Nox, SO2, CO2, CO), black carbon (BC) and particle size distribution are monitored throughout the year. From October to April, acces to the site is restricted to authorized persons, cars being stopped 5 km before the summit at 850 (a.s.l.) elevation. Winter temperature typically vary from -10°C to +10°C and westerly and northerly winds are frequent although periods of southern winds can occasionally take place. Long-term records of gases and meteorological parameters indicate than in winter the site is mainly located in free troposphere.

Site #3

From December 1-15, 2005 aerosol particles were sampled in the city of Aubiere Cedex, France. A field campaign were performed at the LaMP (Laboratoire de Meteorologie Physique), a few kilometers south-est of the Clermont-Ferrand city center, at the Ceseaux Campus (394 m a.s.l.). The choice of the site is justified by the fact that shows both an urban character because of an intense circulation at peak hours of working days and a perish-urban character during the night and the public holidays, being located at a few kilometers of the centre town of Clermont-Ferrand.

Site #4

Located on the western coast of Ireland, the research station in Mace Head (88 km of Galway) offers an exposure to the Northern Atlantic Ocean, hence the possibility to study the atmospheric composition of background of the northern hemisphere during western wind sectors and continental emissions of Europe during eastern conditions sector. Hygroscopic properties of 20 nm and 85 nm particles were determined from Jan 12 to Jan 27 2006.

Site #5

Urban aerosol particles were sampled in the city of Leipzig, Germany, during the H-TDMA calibration workshop (see Chapter I.3). The H-TDMA atmospheric measurements were performed on February 10, 2006 at the Institute for Tropospheric Research (IfT), a few kilometers northwest of the city center. The IfT is surrounded by residential housing and is located near considerably frequented roads, particularly relevant during early morning and late afternoon rush hours. Thus, sources for primary and secondary aerosols are available, comprising sulfate, nitrate, and carbonaceous compounds.

Hygroscopic properties of particles with dry diameter of 30, 50, 70 and 100 nm were determined at 90% relative humidity (RH) for a period of 12 hours.

3. Results and discussion

3.1. Data evaluation

Parameters needed to maintain the quality of a hygroscopic growth distribution (e.g., aerosol number concentration, flowrates, temperatures and RH stability) were stored along with the H-TDMA scan (1 data point/10 s, one scan lasting 10 min). The first step in the basic data analysis was to exclude lower quality data. Scans showing one data point deviating more than 3% from the sheath air default humidity, or flowrate deviating more than 1% from the default flowrate, or inlet concentration deviating more than 20% from the average inlet concentration of the scan, did not pass the quality criteria.

The result of an H-TDMA scan is a hygroscopic growth distribution. The calculation of hygroscopic growth requires a relative calibration of DMA2 with respect to DMA1 (see Chapter I.1.1). Thus, in a second step, all atmospheric data have been corrected for the DMA2 size shift.

When an external particle mixture is present, different hygroscopic groups appear in this hygroscopic growth distribution. In a third step, a parameterization of the hygroscopic growth distribution was performed by fitting a sum of Gaussian functions to identify the so-called hygroscopic growth modes.

The hygroscopic growth distribution has then been reduced to one parameter: the hygroscopic growth factor GF(RH) of each particle class found in the hygroscopic growth distribution. GF(RH) is determined by the ratio of the particle diameter D_p measured at that specific RH (in our study, this RH was always 90%) and the dry D_p measured at RH=10%.

Often, the humidified distributions measured in the second DMA show a modal behaviour. **In this study** the observed groups of particles are denoted as the "*I class*" (i.e. hydrophobic mode) with GF in the range 1.0-1.3 (±0.1), the "*II class*" (i.e. moderately-hygroscopic mode) with GF in the range 1.3-1.6 (±0.1) and the "*III class*" (i.e. hygroscopic mode) with GF in the range 1.6-2.3 (±0.1).

3.2. Observations of hygroscopic growth

The H-TDMA was set to operate more or less continuously during the measurements at the five locations. Table A.4.2 summarises the TDMA experiments for each location divided by air mass type/origin back trajectories analysis (NOAA HYSPLIT MODEL, http://www.arl.noaa.gov). Not all data taken were evaluated. The data chosen to be presented here are mostly in the accumulation mode (i.e dry size ca. 100 nm).

Site	Period	Dates	Dry size	Air Mass Type/Origin
#1-Hyytiala Finland				
	1	13 to 18 April, 2005	20, 30, 50,100 nm	Marine Air Mass/West
	2	20 to 22 April, 2005		Marine Air Mass/North-Est
	3	23 to 29 April, 2005		Continental Air Mass/North (Finland)
#2- Puy de Dome France				
	1	22 to 24 October, 2005	100 nm	Marine Air Mass/West
	2	25 to 26 October, 2005	100 nm	Continental Air Mass/Sud-West (Spain)
#3- Cezeaux France				
	1	1 to 4 December, 2005	100 nm	Continental Air Mass/ Sud-West (Spain)
	2	5 to 9 December, 2005	100 nm	Marine Air Mass/North-West
	3	10 to 16 December, 2005	100 nm	Continental Air Mass/North-Est (Germany)
#4-Mace Head Ireland				
	1	16 to 22 January, 2006	85 nm	Marine Air Mass/West
	2	23 to 26 January, 2006	85 nm	Continental Air Mass/South-Est (France)
#5-Leipzig Germany				
		10 February, 2006	30-50 70-100 nm	Continental Air Mass

Table A.4.2: Air mass type categorized with NOAA HYSPLIT MODEL back trajectories analysis calculated on three days for the five sampling sites.

3.2.1 Hyytiala campaign

The VH-TDMA was used in the field for the first time during the Hyytiala campaign. As a first test, a direct comparison of the VH-TDMA in its H-TDMA settings and the H-TDMA operated by the University of Helsinki was performed. Results are presented in Figure A.4.2 for particle of size 50 nm. The Figure shows that both H-TDMA measure similar growth factors 1.4 decreasing down to 1.1 later in the day for internally mixed particles.
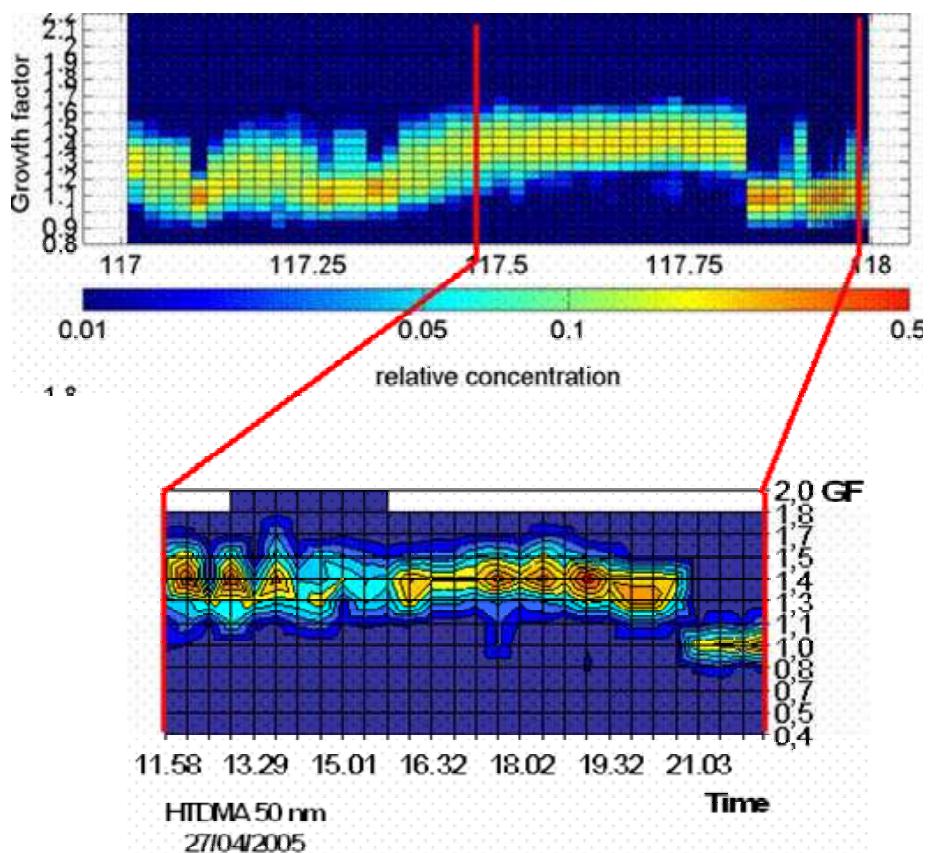
Figure A.4.2 : Comparaison between the Finnish H-TDMA and the French H-TDMA for temporal variation of hygroscopic growth factor for 50 nm measured the 27th of April .

Representative variations of the particle size distribution measured by SMPS during the three sampling periods are shown in Figure A.4.3a,b,c.
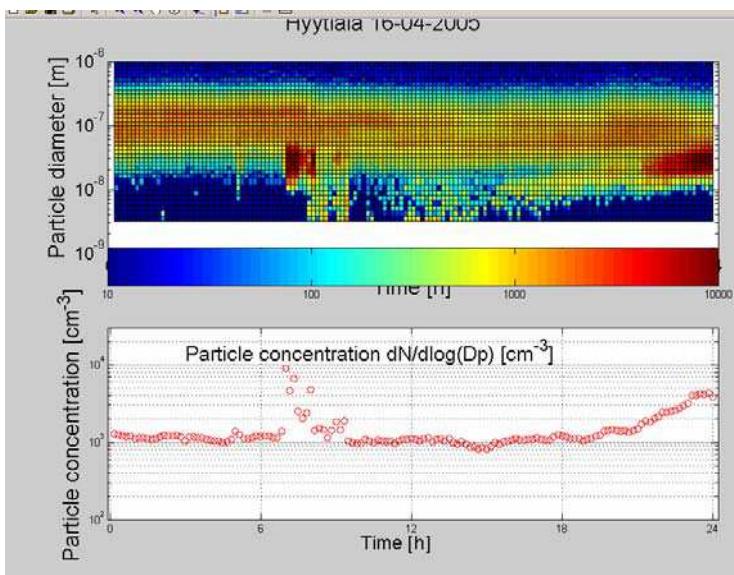
Figure A.4.3a: Period 1 (Marine air mass) is characterised by low concentrations of particles mostly found in the accumulation mode (100 nm). A second mode at 20-30 nm is sometimes observed when nucleated particles grow into the Aitken mode during the night.
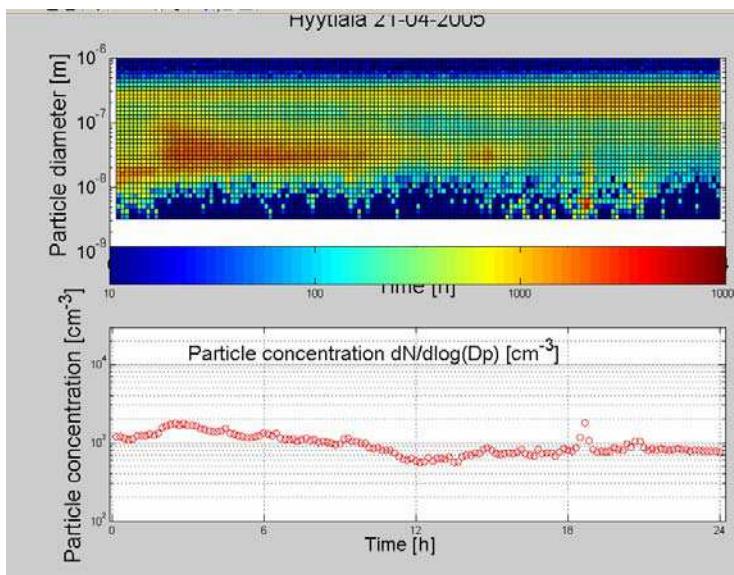
Figure A.4.3b: During period 2 marine air masses coming from North-Est are less concentrated in the accumulation mode. Particles in the Aitken range (20-30 nm) are still influencing the number concentration of the days following nucleation events.
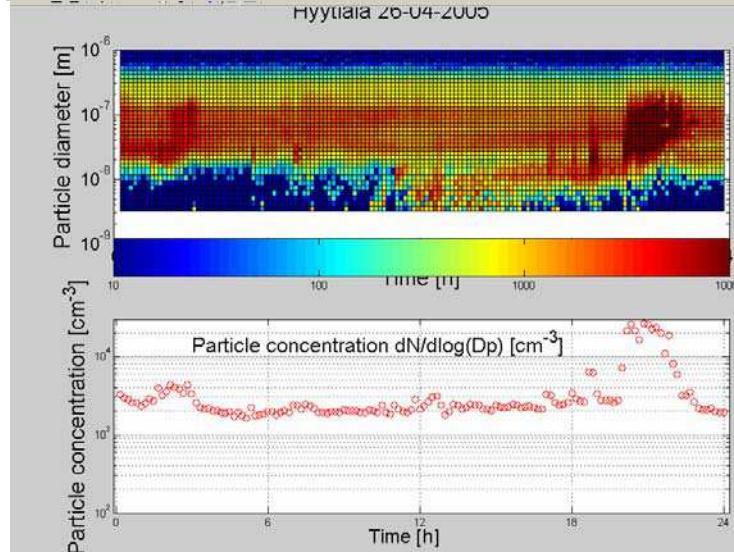
Figure A.4.3c: Sampling period 3 is characterised by average total 20-100 nm particle concentration of 2000 #/cc. Bursts of polluted air masses occur during the day and night, presumably arriving from local (5-100 km) contamination.

Figure A.4.3a,b,c: Representative variations of the particle size distribution during the three sampling periods.

Period 3 is clearly different from period 1 and 2, regarding the particle size and concentrations. Period 1 and 2 are both representatives of marine air masses, with period 1 containing higher concentrations in the accumulation mode than period 2 representative of more arctic marine air. However, period 2 is more often locally contaminated, as the air mass is sometimes passing over inhabited areas of Finland. The VH-TDMA was then used at the forest site in Finland (SMEAR II field station, Hyytiala) to scan hygroscopic growth over a range of particle during these different periods. The GFs are averaged and sorted according to the hygroscopic growth classification presented previously (Table A.4.3).

Growth factor at 90% RH	Period	Dry particle diameter			
		20 nm	30 nm	50 nm	100 nm
Total number of observation		91	72	106	20
"**Hydrophobic**" particles groups					
growth factor (averaged±s.d.) number fraction (averaged)	1	1.15(±0.12) (1.0)	1.18(±0.10) (1.0)	1.21(±0.05) (1.0)	-
	2	1.25(±0.10) (1.0)	1.17(±0.06) (0.68)	-	1.10(±0.04) (0.10)
	3	-	-	1.23(±0.07) (1.0)	1.29(±0.10) (1.0)
Moderately-hygroscopic particles groups					
growth factor (averaged±s.d.) number fraction (averaged)	1	-	-	-	1.53(±0.04) (1.0)
	2	-	1.44(±0.06) (0.32)	1.5(±0.06) (1.0)	1.50(±0.05) (0.90)
	3	1.33(±0.08) (1.0)	1.42(±0.10) (1.0)	-	-

Table A.4.3: Summary of the H-TDMA observation of hygroscopic growth at 90% RH during measurements in Hyytiala.

Both periods 1 and 2 show a hydrophobic mode for 20 and 30 nm particles. During period 1, these hydrophobic particles reach 50 nm, but 50 nm particles are found moderately hygroscopic during period 2, which could be the signature of more aged particles. In fact, already at 30 nm, period 2 starts to show a significant contribution of moderately hygroscopic particles as an external mixing. The 100 nm mode of both periods is almost completely to "moderately hygroscopic", as expected for more aged particles. Pure marine aerosol that will be shown later in this chapter, will show higher hygroscopic characteristics, hence we can suppose that marine aerosol when arriving to Hyytiälä, have been relatively modified with organic condensing species.

Analysis of daily variations of the hygroscopic growth revealed a diurnal behaviour of the hygroscopic growth, with higher growth factors at day time (typically GF=1.4) and lower during night (GF=1.1), as shown during previous observations in the forest (Vakeva et al., 2001, Hameri et al., 2001b). This general observation could be due to the frequent occurrence of nucleation events on the site. The occurrence of nucleation bursts at the Hyytiala site has been documented in previous publications (Kulmala et al., 2004; Dal Maso et al., 2005; Makela et al., 1997). During the 2005 campaign, very few of theses events were detected, possibly due to non adequate meteorological conditions (very inhomogeneous). Only one significant event was clearly detected on the 14th of April, but indication of nucleated particles already grown arriving on site have also been observed (Figure 16th and 26th of April). The increase in particle number and the evolution of size distribution during the event can be seen in Figure A.4.4.
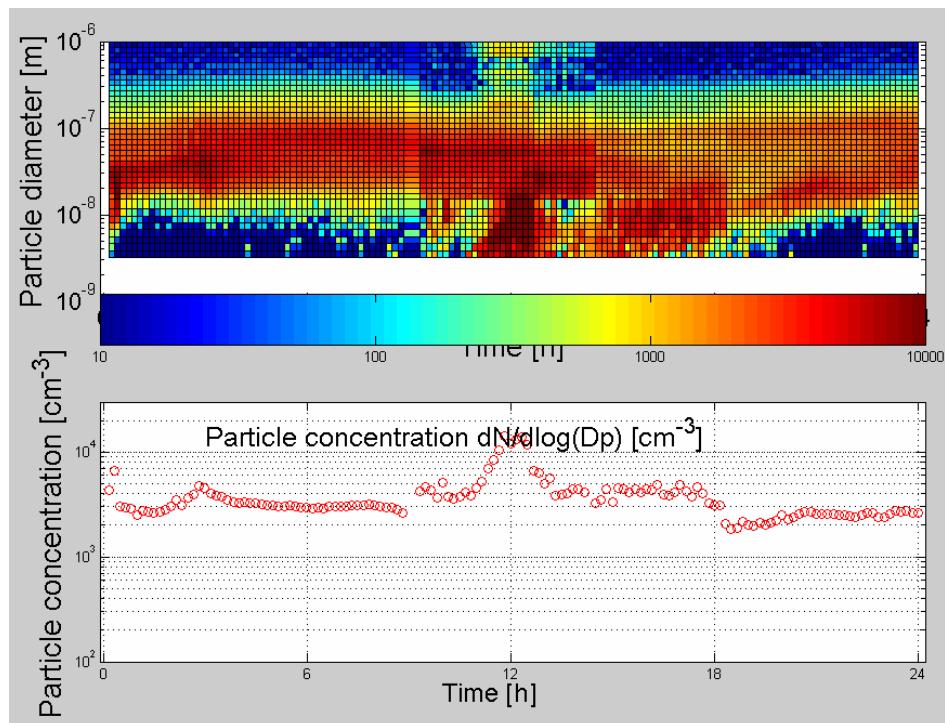
Figure A.4.4: Temporal variation of the DMPS particle size distribution and total number concentration during the nucleation event of April 14th.

In the boreal forest, organic compounds emitted during the day are different from the ones emitted during the night. Because the growth of the particles produced in the morning is mainly observed during the day time, it is believed that condensable organic species are produced photochemically. After daily fresh condensation, aerosol particles would "age" during the night. Until now, however, very few

explanations for this diurnal variation have been proposed in the literature. Other parameters such as the diurnal variation of organic species in the gas phase are needed in order to interpret this observation.

3.2.2. Puy de Dôme Campaign

The hygroscopic growth of particle at puy de Dôme has never been documented previously. However, a certain number of studies on aerosol/cloud interactions performed during the CIME project (Schwarzenboeck et al., 2001, Geremyet al., 2000 , Mertes et al., 2001) and PDD2001 campaign (Sellegri et al., 2003) clearly indicated that a large fraction of the aerosol population is externally mixed with at least 2 hygroscopic modes leading to chemical differences between CCN and interstitial particles. The use of the VH-TDMA at this site therefore provides a good opportunity to test whether results observed for saturation above 100% can be confirmed for lower RH.

During the observation period, the total particle concentration at puy de Dôme varied substantially from less than 1000 particles/cm3 (night of 23-24 October) to more than 15000 particle at midday/afternoon of 24, 25 and 26 October. In particular, October 25th is characterised by elevated concentrations of both particles (up to 17000 particle/cm3) and BC (400 ng/m3), as measured by aethalometer. Analysis of the size distribution of particles measured by SMPS during the sampling period is shown in Figure A.4.5 and A.4.6 and shows different features:

Period 1:

- October 22nd: that day is characterised by very stable concentrations of particles in the accumulation mode (mode at 100 nm). In the afternoon hours, an additional source, possibly from exchanges with boundary layer air, or grown nucleated particles.

- October 23rd: this day is characterised by low concentrations of particles mostly found in the Aitken mode (40 nm). These particles seem to have been formed on the previous nucleation event of day 22nd.

- October 24th: Similar conditions as for October 23rd is still prevalent on that day ow particle concentration of the previous day. At mid-day, increase in particles over the entire size spectrum certainly due to mixing with boundary layer air.

Period 2:

- October 25th: strong nucleation event around mid-day together with a significant increase of the accumulation mode particle concentration, probably representative of a boundary layer input into the free troposphere.
- October 26th: Particles in the Aitken range formed during the previous nucleation event are still influencing the number concentration in the free troposphere. At mid-day, boundary layer air replaces free tropospheric conditions installed in the previous night.

Figures A.4.5 and A.4.6 shows the variation of size distribution measured by SMPS and hygroscopic growth data obtained with the H-TDMA over the time period 1 and 2 (given in Table A.4.2) for 100 nm particles sampled at the Puy de Dome field station.
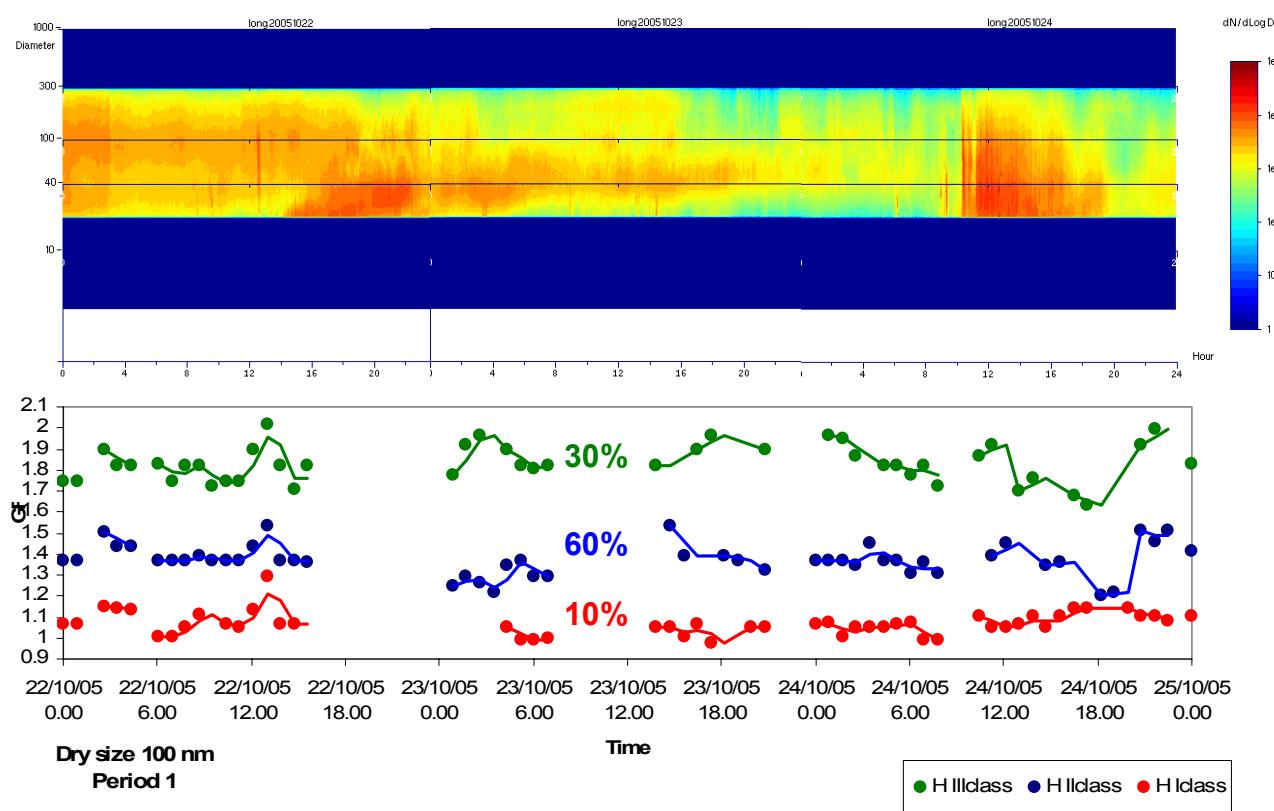
Figure A.4.5 : Variations of the size distribution and hygroscopic growth factor for 100 nm particle in the cases when two or more hygroscopic classes were present at PDD during the measurement campaign Period 1 (Marine Air mass/West).
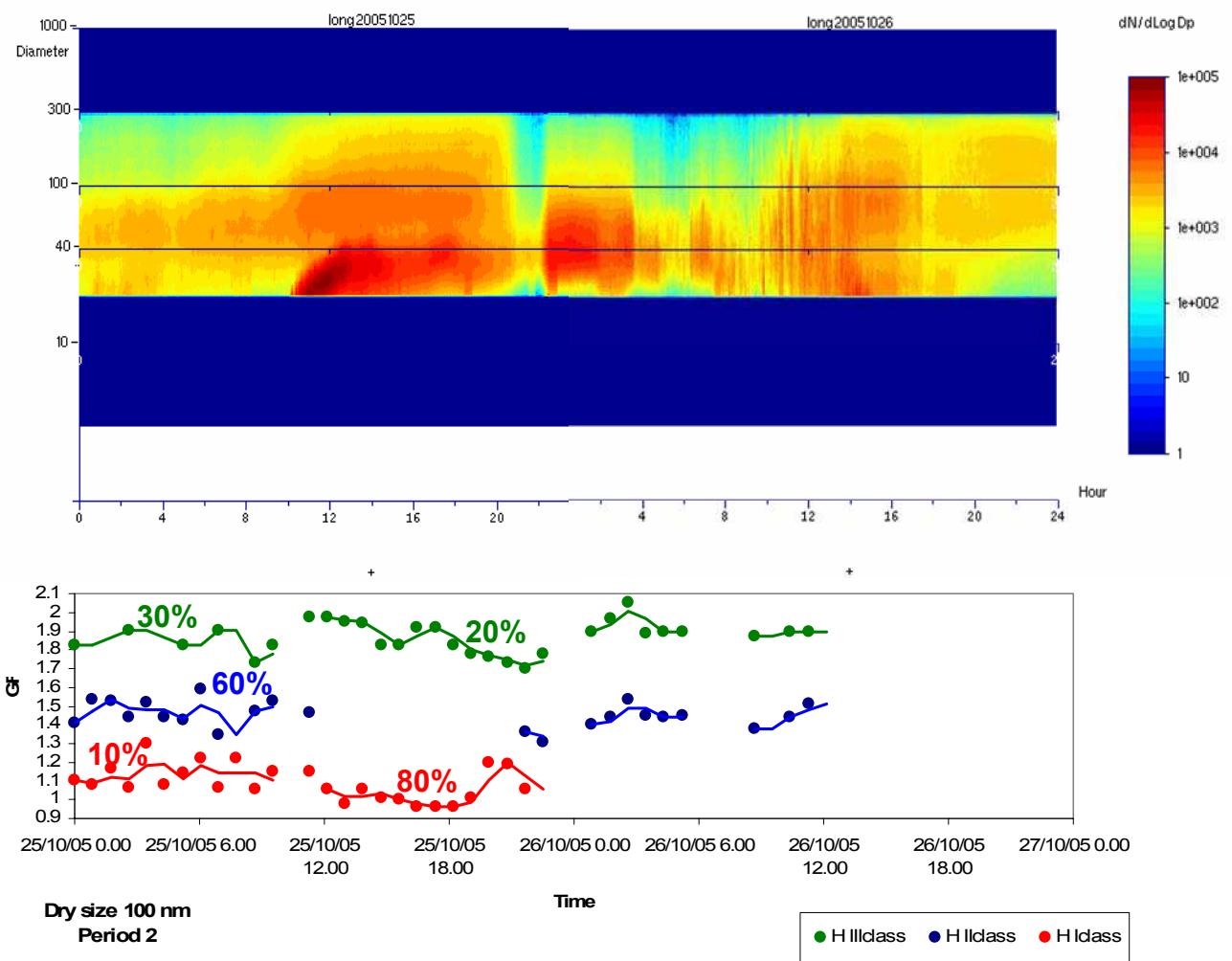
Figure A.4.6 : Variations of the size distribution and hygroscopic growth factor for 100 nm particle in the cases when two or more hygroscopic classes were present at PDD during the measurment campaign Period 2 (Continental Air mass/Sud West-Spain)

Both periods of measurements introduce the same feature of a trimodal hygroscopic behaviour of the accumulation mode particles and a nearly constant growth factor for almost 3 days (from 22 to 25 October, 2005). Several indications can be retrieved from these graphs:

1- An hygroscopic class of aerosol particles (i.e. III class, average GF=1.85, standard deviation=0.09) is found for all time periods during the measurements (from 22 to 26 October, 2005). Because the air mass back trajectory indicates a western origin, such a high GF typically would probably correspond to sea salt particles internally mixed with other inorganic salts reducing the hygroscopic growth.

2- A moderately-hygroscopic particles class (i.e. II class, average GF=1.40, standard deviation=0.08) is generally present except during the afternoon period of October 25th. The growth factor corresponds to a mixture of organic and inorganic salts.

3- An hydrophobic particles fractions (i.e. I class, average GF=1.08, standard deviation=0.07) is found all the time periods except during last period of measurement (i.e. 26 October 2005).

The number fraction of particles in each class (i.e. nf) is not trivial to estimate. On a first approximation, based on the analysis of a few hygroscopic spectra, we found the following apportionment amongst the 3 classes (Table A.4.4):

Site	Dry Size (nm)	Period	Averaged H-GF groups		
			I class	II class	III class
Puy de Dome	100	2	1.07±0.06 (nf 0.12)	1.37±0.08 (nf 0.62)	1.83±0.09 (nf 0.26)
		3-25/10/05	1.09±0.09 (nf 0.80)	-	1.87±0.08 (nf 0.20)
		3-26/10/05	-	1.45±0.07 (nf 0.57)	1.87±0.08 (nf 0.43)

Table A.4.4: Summary of the H-TDMA observation of hygroscopic growth at 90% RH during measurements at the Puy de Dome.

A large majority of particles during background period belongs therefore to the moderately-hygroscopic group (57% to 62%). Chemical analysis of particles performed during the campaign, as well as information from previous studies, clearly show that carbon species (mostly organics) are the main components of the aerosol mass (Sellegri et al., 2003a). Previous studies also show that the aerosol sampled at the puy de Dôme is usually found as an external mixture of 1) an "organic mode" (mode 1) centred on 200 nm and 2) an "inorganic mode" (mode 2) located between 300 and 500 nm. At 100 nm, both modes have a significant contribution (Sellegri et al., 2003a). Furthermore, each mode (mode 1 and mode 2) show a CCN behaviour of an internal mixture rather than pure organic or pure inorganic particles. The moderately hygroscopic group (i.e. II class) is certainly resulting from a mixture of organics and a few quantity of salts (sulphate and ammonium) driving the growth of mode 1 to these fairly high values, while the hygroscopic group, always present with at number fraction ranging from 20% to 43%, could typically be mode 2, hence aged free tropospheric aerosols composed of inorganic salts (sulphate, nitrate and ammonium) mixed with a few organics.

The 100 nm particles sampled there are representative of the accumulation mode transported from the boundary layer (BL). However, the transport from the BL is observed at the same time than a nucleation event (20 nm mode). Because the nucleated particles usually show hydrophobic characteristics in other environments (i.e. Boreal or Marine) there is a possibility than organic condensable species, responsible of the nucleation of new particles, are also contributing to a change of hygroscopic properties of larger size particles. During 10 hours of October 25th, from 10:00 am to 20 pm the fraction of hydrophobic particles increases at the expense of the moderately- and hygroscopic group, reaching more than 80% of the particles against 10% approximately of the previous days (see Figure A.4.6).

3.2.3. Cézeaux Campaign

The Cezeaux Campus is located a few kilometers south-est of the Clermont-Ferrand city center. The choice of the site of Cézeaux is justified by the fact that it presents an urban character because of an intense circulation during the working days and at the same time a perish-urban character the night and the public holidays being then located at a few kilometers of the centre town of Clermont-Ferrand. The urban character of the site moreover was more particularly accentuated during by the presence of machines of building site carrying out of work in proximity of the site of taking away. We thus have very schematically a source of particles of combustion in proximity being superimposed on an urban/perish-urban background noise.

Measurements of particulate mass during the period of November 17 to December 15, 2005 show an important variability of the concentrations being able to reach hourly values higher than 100 µg/m^3 (Figure A.4.7). It should nevertheless be noted that the concentrations average day labourers over the duration of the field campaign reach only 10 µg/m^3 on average and that, other than certain episodes, we are thus in a situation of reduced particulate pollution.
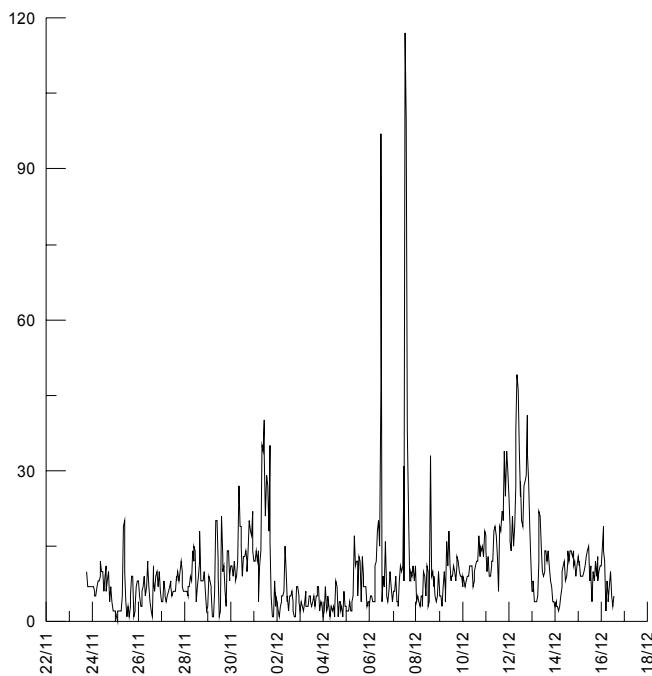
Figure A.4.7 : PM2.5 variability during the field campaign.

The daily PM2.5 variation generally shows two maximum between 6h and 10h of the morning and 17h and 19h the evening, corresponding to the maximum of intensity of the local emissions. This daily variability can also be detected on the level of the particles number concentrations. This is illustrated on Figure A.4.7, on which it is also possible to distinguish the schedules of work of the workmen on the building site (06: 30 UTC-11: 00 UTC and 12:30 UTC-16: 00 UTC).

The size distribution of particles shows (Figure A.4.8a,b) that the diurnal increase can be seen for all particle sizes from 30 to 100 nm while measurements at night are characterised by the presence of larger particles in the Aitken – Accumulation mode.
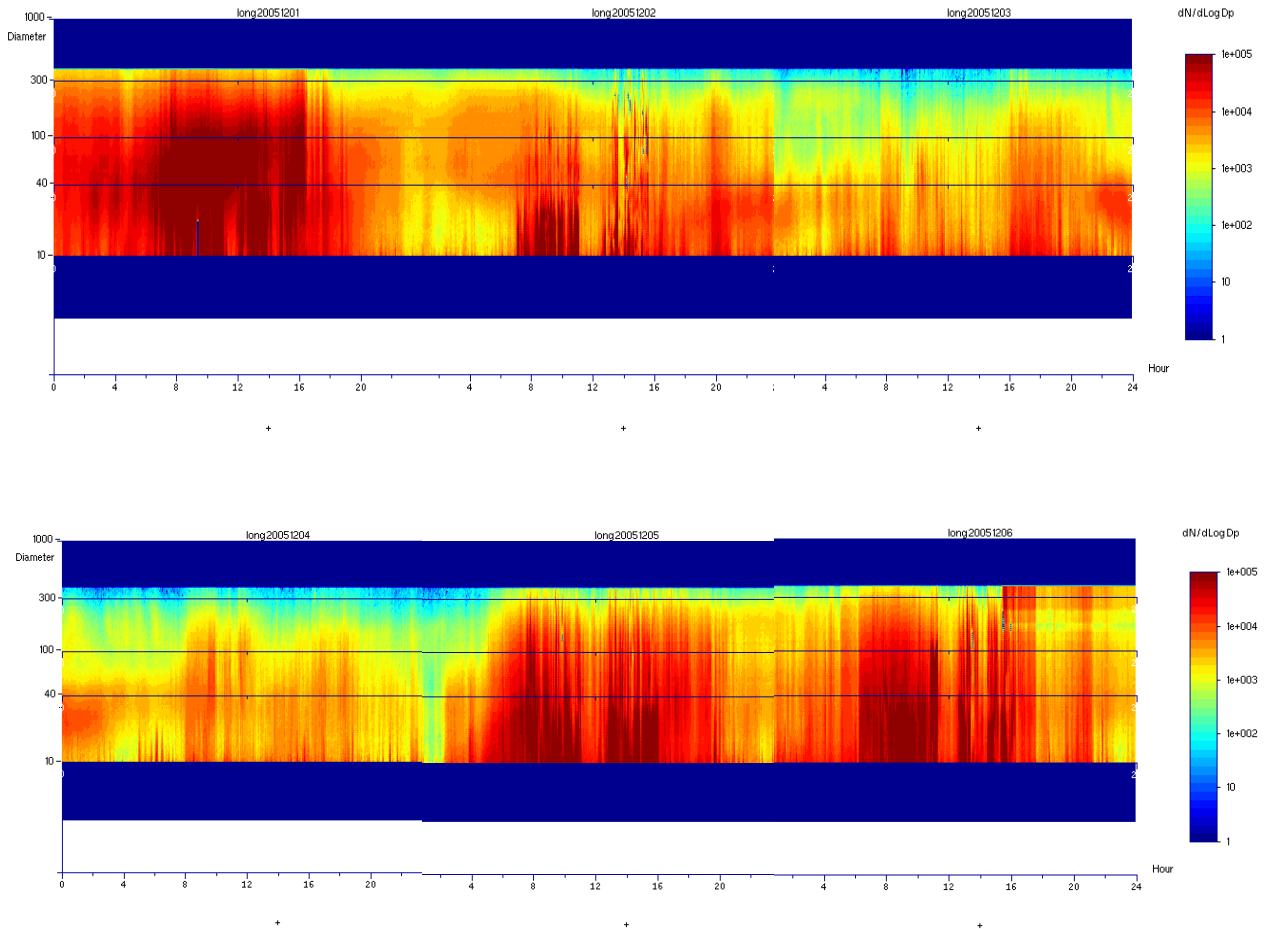
Figure A.4.8a,b : Variation of th size distribution at the Cezeaux Campus measured by SMPS from 1st to 6th of December during period 1.

Measurements of hygroscopic growth of 100 nm particles have been performed during the campaign. There is a periodicity in the diurnal evolution of aerosol particles sampled at the Cezeaux, that we attempted to further investigate. The evolution of the size distribution for the same time period is indicated in Figure A.4.9.
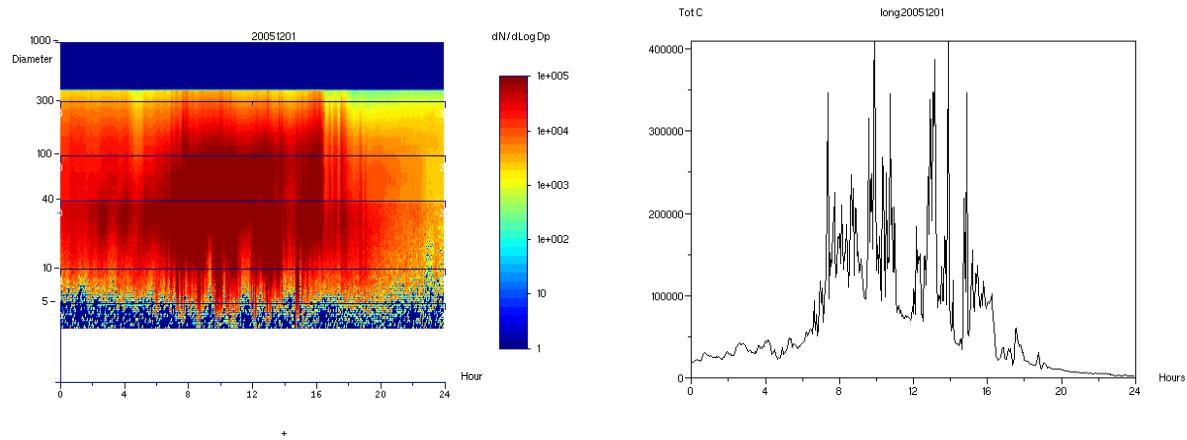
Figure A.4.9: Evolution of the size distribution and total particle concentration for day 01/12/2006.

An example of hygroscopic growth spectrum is given in Figure A.4.10 averaged over several periods for a typical working day 01/12/05. These distributions were averaged for the first part of the night corresponding to 00:00-07:00, then for the morning and afternoon, by excluding the pause from 12h, then finally for the period of 19h with 23:30.
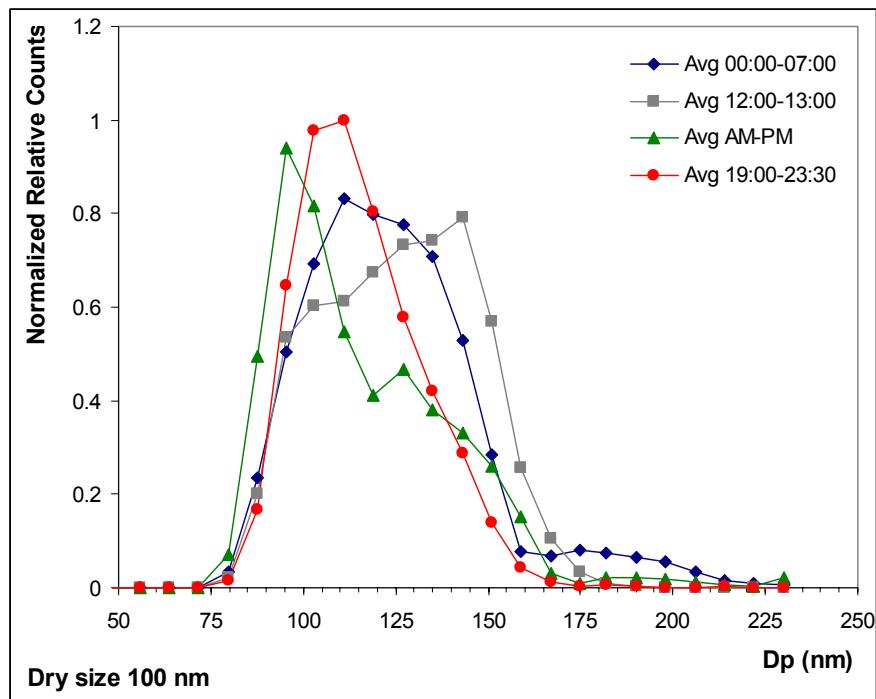
Figure A.4.10: Averaged 100 nm hygroscopic growth spectrum for day 01/12/2006.

The temporal evolution of the hygroscopic growth clearly shows a diurnal evolution with almost hydrophobic particles (GF=1.1) during daytime and moderately hygroscopic particles (GF=1.3-1.4) during nighttimes. The increase in hygroscopic

growth between 12:00 and 13:00 corresponds to lunch break of the construction work. Clearly, freshly emitted particles from diesel engines are hydrophobic. Instead, a significant urban background is composed of moderately hygroscopic particles either photochemically evolved from traffic emissions or of extra-urban origin or internally mixed particles with BC. An indication of different origin of the two classes arises from comparison of SMPS and V-SMPS (T=280°C) measurements. The remaining fraction after thermo-desorption at 280°C is considered the no-organic carbon core of the particles.

Figure A.4.11a,b shows the variations of the particle size distribution between ambient temperature and 280°C for a strongly polluted day (1/12/05) and during week-end (3/12/05, no local sources). These Figures show, in red the disappearance of particles between 40 and 100 nm made up of volatile species, for the benefit of the appearance, in blue, of "cores" refractory of elementary carbon, about 10 nm (and smaller, not detected), for the two days of the 01 and the 03/12/2005.
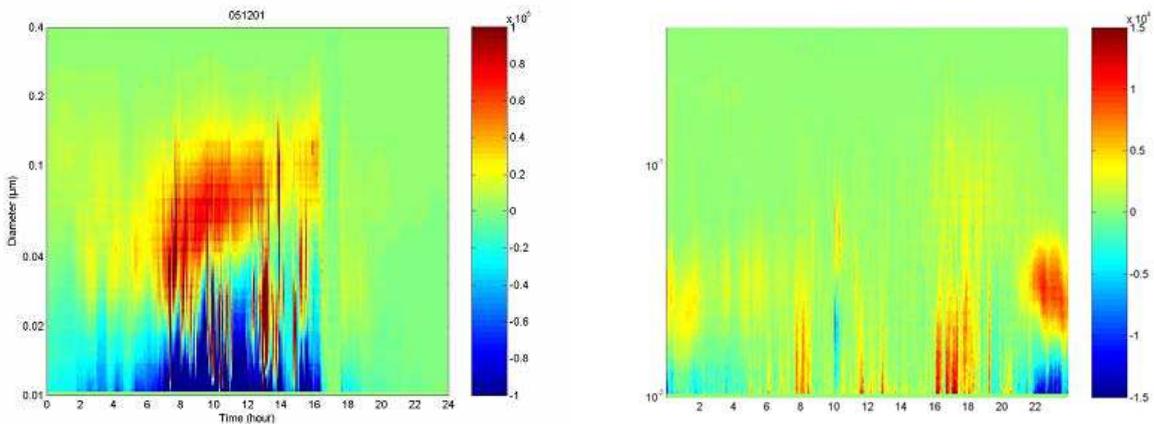
Figure A.4.11a : Difference SMPS – VSMPS for the day 1/12/05

Figure A.4.11b : Difference SMPS – VSMPS for the day 3/12/05

In the very locally polluted case of the 01/12/2005, one can note that the peaks of particles ranging between 200.000 and 400.000 particles per cm^3 are eliminated by the heating with 280 °C, and appear have carbon core in the 10-20 nm range. On the contrary, during weekend (3/12/05), the fraction of non-volatile particles is reduced, showing rather the presence of particles not originating from combustion processes.

On the contrary, during week-end (3/12/05), the fraction of non-volatile particles is reduced, showing rather the presence of particles not originating from combustion processes.

Figure A.4.12 shows the hygroscopic growth factors measured for 5 days in December 2005 (period 2 and 3). For all the sampling periods a bimodal hygroscopic distribution was found with an averaged growth factor of 1.06 in the first class (standard deviation=0.05), 1.40 in the second class (standard deviation=0.11). The particle growth factors measured at the Cezeaux Campus are characteristic of an urban aerosol, as already evidences in previous studies (Massling et al., 2004). While GF in the first class remains low most of the day, GF in the second class appears higher at night (1.4) than during the day (1.25).
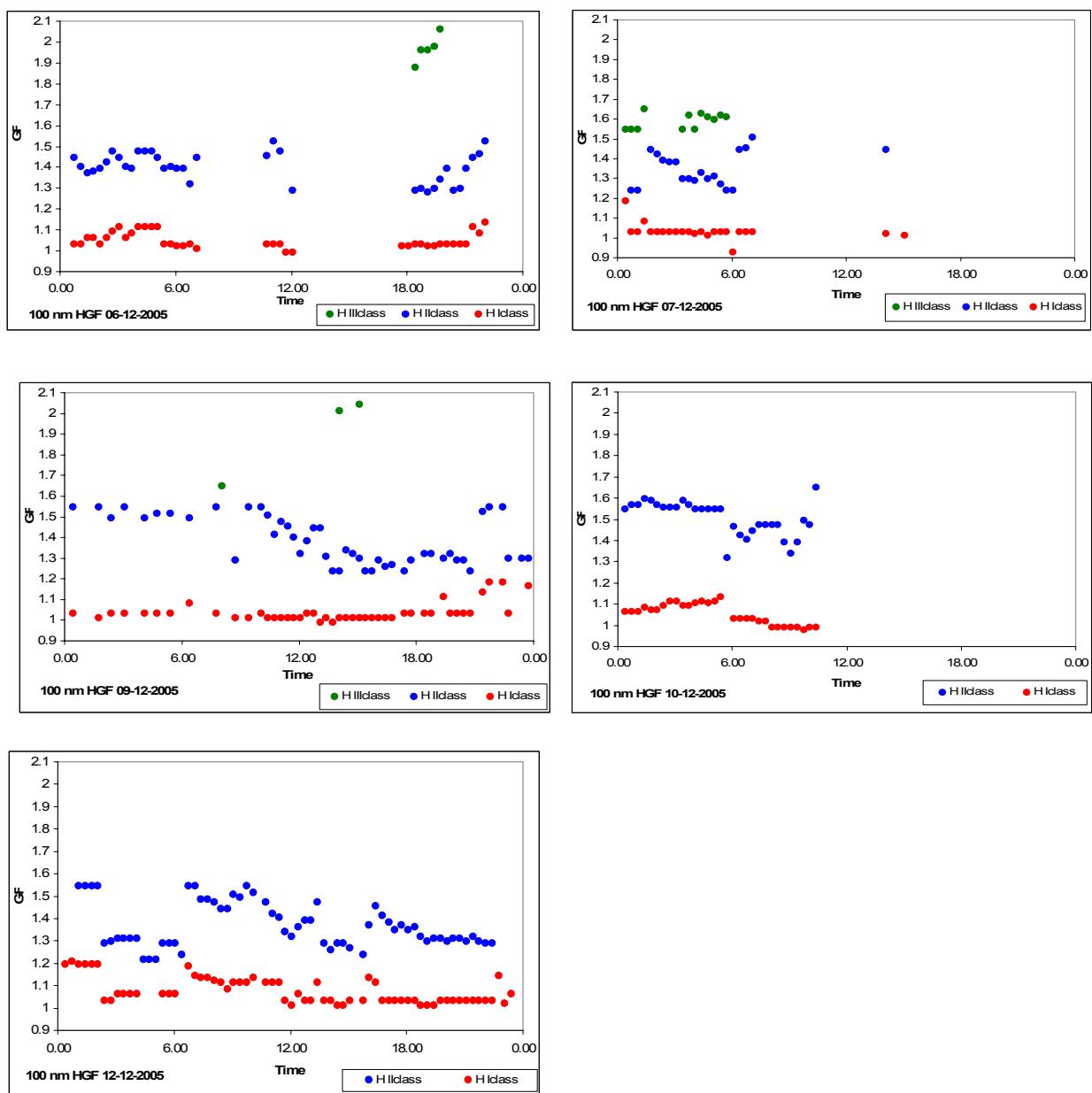

Figure A.4.12: The hygroscopic diameter growth factor for 100 nm particle in the cases when two or more hygroscopic classes were present at the Cezeaux during the campaign.

This confirms the observations made on 1/12/05 (see Figure A.4.11a) and Figure A.4.10. It should be noticed that more-hygroscopic particles (GF= 1.7) are regularly observed throughout the campaign. These are similar GF to those observed at Puy de Dôme for the background aerosol (see previous section). At this point, we cannot exclude a contribution of background aerosols to the urban particle loading.

The number fraction in each mode is described in Table A.4.5. As expected in urban areas, Class I particles contribute to the majority of 100 nm particles (60-70%). The moderately hygroscopic group (II class) accounts for the remaining fraction (30-40%). The contribution of the hygroscopic group (III class), when present, is negligible.

Site	Dry Size (nm)	Period	Averaged H-GF groups		
			I class	II class	III class
Cezeaux	100	2	1.04±0.04 (nf 0.68)	1.38±0.10 (nf 0.32)	1.74±0.19 (when present)
		3	1.08±0.06 (nf 0.61)	1.41±0.12 (nf 0.39)	-

Table A.4.5: Summary of the H-TDMA observation of hygroscopic growth at 90% RH during measurements at the Cezeaux Campus.

While the origin of the hydrophobic fraction is clearly from automobile sources, the processes leading to the presence of a moderately hygroscopic group are still uncertain.

3.2.4. Mace Head Campaign

The chemical composition and hygroscopicity of marine aerosols have been widely studied during ship measurement campaigns over a large variety of oceans and seas. However, we have only a limited knowledge of the variability over time of these properties. The chemical composition and concentration of marine aerosols is depending on parameters such as wind speed and white cap coverage, but also depending on the sea water composition. Recent findings have shown that sub-micron marine aerosols not only contain sea salt and sulfate, but also contain substantial levels of organic carbon. This organic content has a seasonal variability with maximum concentrations during the spring and autumn seasons, corresponding to the blooming periods of phytoplankton (O'Dowd et al., Nature, 2004).

Yet we do not know how these organic species are integrated into the particulate phase. Two possible processes are:

1) Primarily, during the mechanical process of bubble bursting: the sea surface layer is known to be enriched with organic matter and film/jet drops are likely to be enriched as well.

2) Secondarily, through condensation of low volatile organic gases released in the marine atmosphere by microorganisms.

It is possible to partly investigate whether the organic particulate matter is primarily or secondarily produced by observing the mixing state of particles. The MAP campaign's main goal is to understand what the origin of the large organic fraction of submicron aerosol. The use of the H-TDMA measurements should give new insight into this question.

During wintertime clean marine air conditions, it was necessary to study the properties of both aitken and accumulation modes. The investigated particle diameters were 20 nm (the smallest sizes of particles detectable) and 85 nm: 100 nm particles could not be studied there, because of elevated GF that shifted the selected mode to the limit of the instrument scanning capacities.

Clean marine air conditions were observed during several consecutive days at the beginning of the campaign (period 1).

Clean sectors are determined according to several criteria:

- ❖ Wind direction from 190° to 300°
- ❖ Total particles concentration <700 #/cc
- ❖ BC (Black Carbon) <50 ngm^{-3}

During this period, the size distribution of aerosol particles sampled with a SMPS, showed low concentrations in the accumulation mode, typical for Atlantic air masses (see Figure A.413).
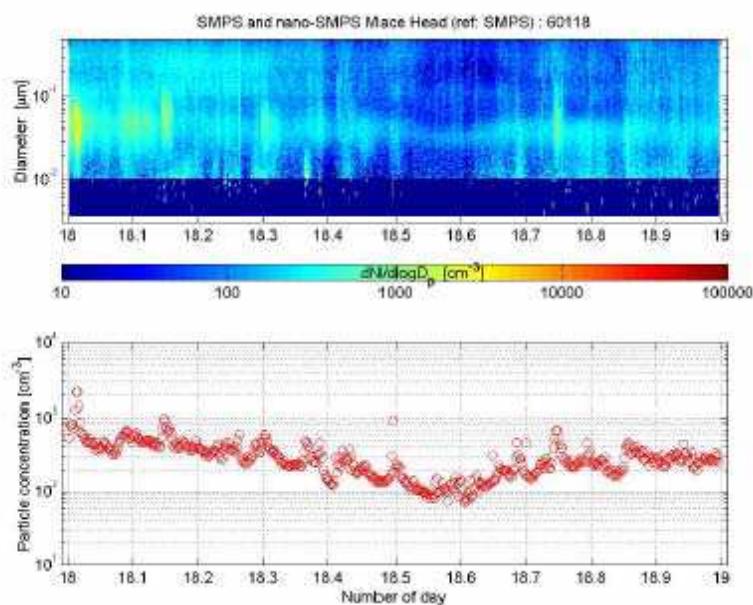
Figure A.4.13: Typical size distribution measured by SMPS during Period 1 (clean marine sector).

On some occasions, measurements performed with a nano-SMPS showed nucleation events were observed around mid-day. During the clean marine sectors, relatively stable GF were observed between night and day conditions, indicating that secondary processes resulting from photooxidation were not significant regarding the hygroscopic properties of the marine aerosol. In fact, West/South West marine air masses (see Figure A.4.14) are characterised by both a moderately-hygroscopic and a hygroscopic particle fraction with averaged growth factor of 1.59 and 1.88 respectively (both standard deviations of 0.18).
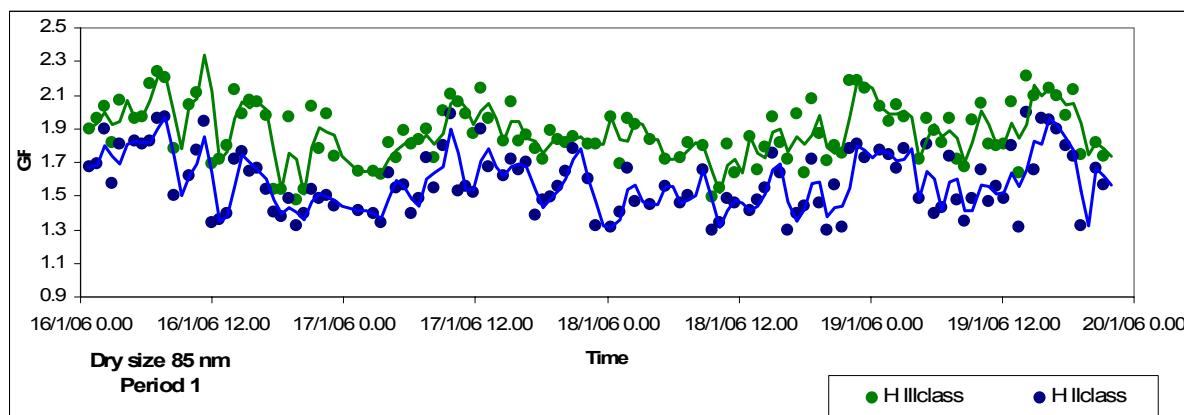
Figure A.4.14: The hygroscopic diameter growth factor for 85 nm particle in the cases when two or more hygroscopic classes were present at Mace Head during period 1.

Little differences were observed between the 20 nm and the 85 nm particles regarding their hygroscopic properties. It was possible to experimentally bubble synthetic air through either natural sea water, or synthetic sea water, or river water coming from various sources in the coastal area. These river waters are very rich with organic material, because they run through thick layers of tuff. The comparison between the GF distribution of a 85 nm particle produced by bubble bursting in the laboratory experiment (Figure A.4.15) and the clean marine sector 85 nm aerosol GF distribution shows a larger dispersion and variability in the *in situ* measurement. The bimodal characteristic of the *in situ* GF distribution could be explained by a combination between sea water and river water bubbling. These results should be confirmed with longer periods of laboratory tests, though.
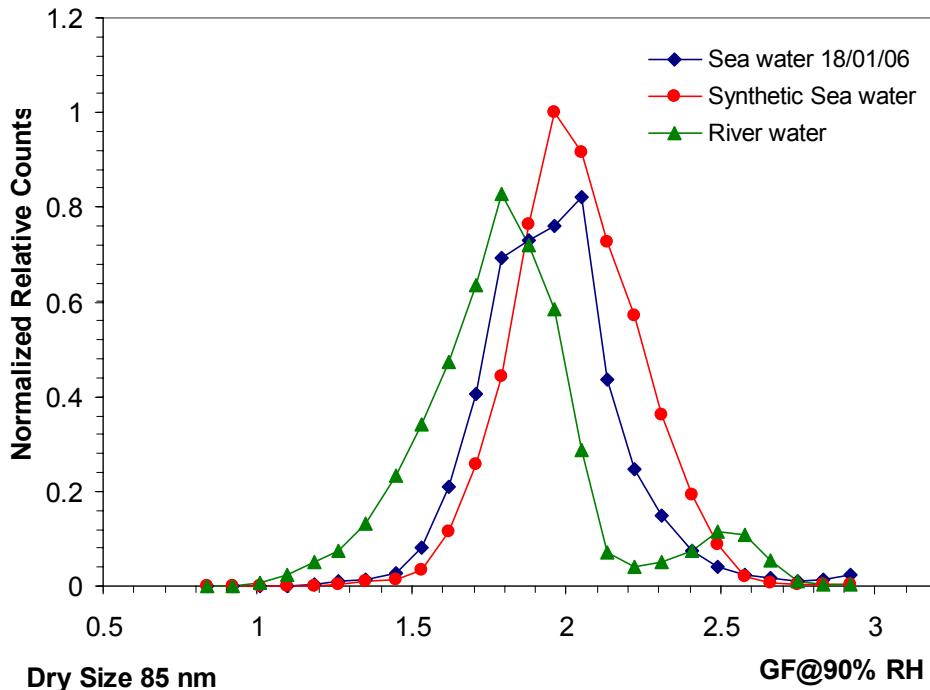
Figure A.4.15: The hygroscopic diameter growth factor for 85 nm particles produced in laboratory experiment by bubble bursting.

GF close to 1.8 is lower than expected for pure sea-salt and might be reflecting a mixture of seasalt with less hygroscopic material (organics). Such a hypothesis would be supported either by recent evidence of a strong carbon contribution to the marine aerosols in the submicron range (O'Dowd et al., 2005).

A hydrophobic mode is also observed occasionally in the in-situ measurements. This mode is usually less than 10% of the total number of aerosol selected. However, it becomes significant when a nucleation event occurs (for example on the 14/01/06 around noon) on both 20 nm and 85 nm particles (i.e. around 70%). Hence, as already mentioned for the Hyytiala and Puy de Dome sites, we can hypothesis that when secondary condensing (and nucleating) processes occur, they seem to do so on the whole size distribution and give a typical hydrophobic property also to large particles. This aspect will be discussed in the next section dealing with VH-TDMA measurements.

At Mace Head, the change in air masses from period 1 (South-West/West, from Atlantic Ocean) to period 2 (South-Est, from France) offers a very straightforward way of evidencing the various hygroscopic characters of aerosol particles. Figure A.4.16 shows a representative example of the size distribution measured by SMPS during period 2.
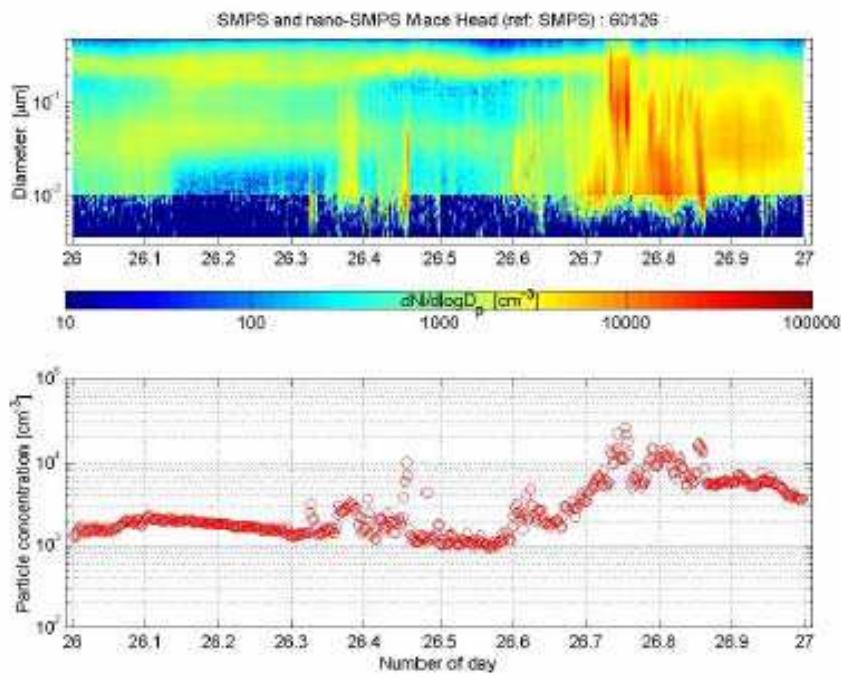
Figure A.4.16: Typical size distribution measured by SMPS during Period 2 (continental air mass).

During sampling period 2, when continental polluted air masses came from France, hydrophobic particle fraction were found accompanied from a moderately-hygroscopic particle fraction (see Figure A.4.17) with averaged growth factor of 1.11 and 1.45 respectively (standard deviation of 0.14 and 0.13).
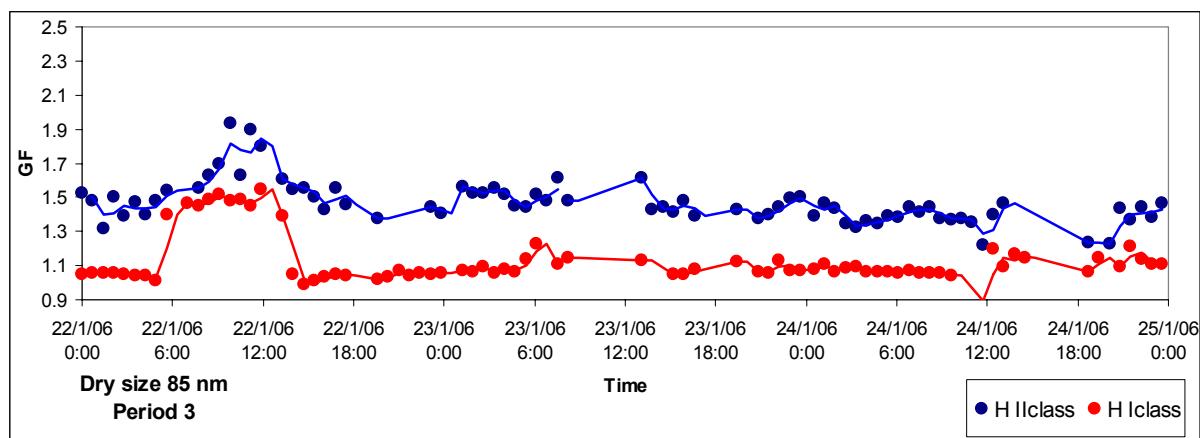
Figure A.4.17: The hygroscopic diameter growth factor for 85 nm particle in the cases when two or more hygroscopic classes were present at Mace Head during period 2.

In that case, the moderately-hygroscopic class evidences GF close to those measured at Puy de Dôme. This is the signature of evolved continental aerosols containing a mixture of inorganic salts and organic material.

Contrarily to clean marine aerosols, a strong and regular diurnal variation is observed in polluted air masses transported to Mace Head (Figure A.4.18).
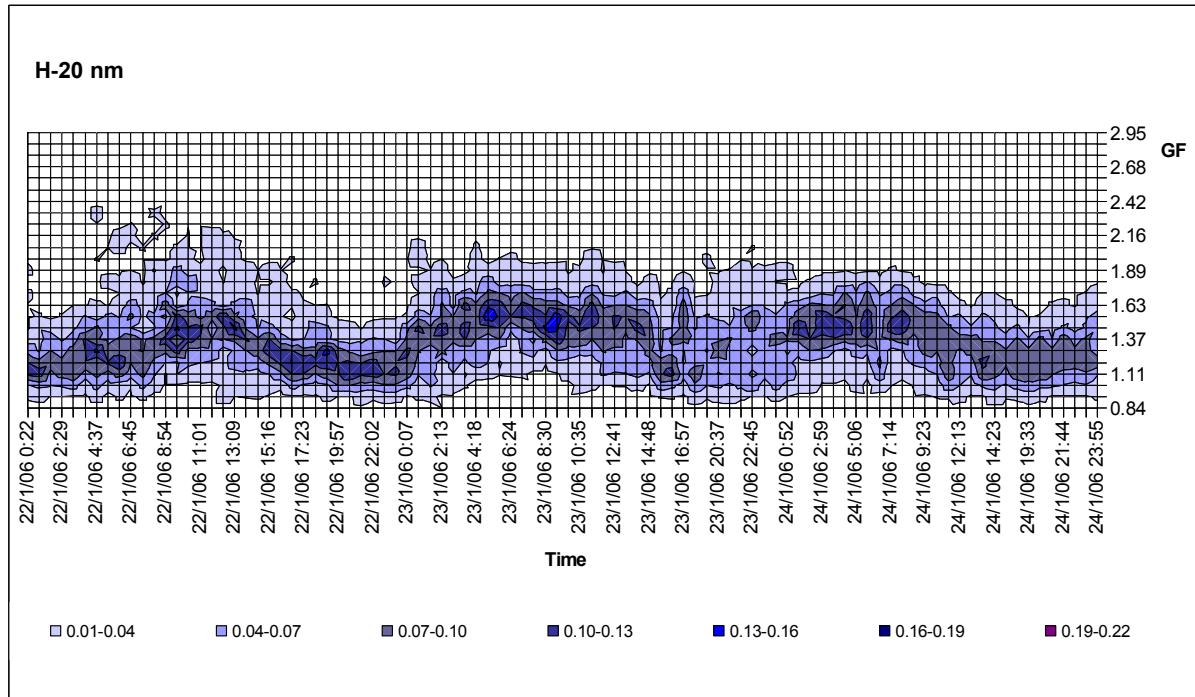
Figure A.4.18: Diurnal variation of hygroscopic growth factor for 20 nm particles during period 2 at Mace Head (z-axis represents Relative counts).

Because the air mass origin is relatively stable during this period, this could be indicative of different local sources between night and day. In the area, heating is mainly ensured by tuff burning that could contribute to the hydrophobic mode of the particles sampled during the night.

The fraction of particles in the various classes for the different periods is given in Table A.4.6 and shows a slight prevalence of more hygroscopic particles (53-63 %) for marine air masses.

Site	Dry Size (nm)	Period	Averaged H-GF groups		
			I class	II class	III class
Mace Head	85	Nucleation event on 14th Jan	1.09±0.05 (nf 0.70)	1.58±0.17 (nf 0.30)	-
		1	-	1.60±0.18 (nf 0.47)	1.87±0.16 (nf 0.53)
		2	1.11±0.14 (nf 0.54)	1.45±0.12 (nf 0.46)	-

Table A.4.6 : Summary of the H-TDMA observation of hygroscopic growth at 90% RH during measurements in Mace Head.

However, this ratio shows that the aerosol is clearly found as an external mixture also for pure marine conditions, which would indicate two separate origins or production processes of 85 nm particles.

3.2.5. Leipzig Campaign

Measurements in the sub-urban area of Leipzig took place in the framework of the ACCENT H-TDMA intercomparison experiment. Hygroscopic properties of particles with dry diameter of 30, 50, 70 and 100 nm were determined at 90% relative humidity (RH) for a period of 8 hours. Results for 100 nm particles are shown in Figure A.4.19.
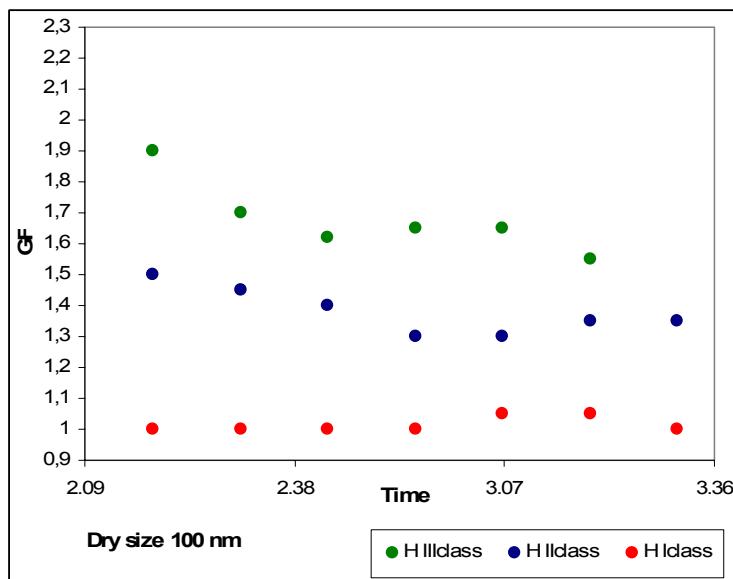
Figure A.4.19: The hygroscopic diameter growth factor for 100 nm particle measured in Leipzig.

For all sizes, the size distributions revealed an external aerosol particles mixture with three hygroscopic particles fractions. In Table A.4.7 are summarized the averaged growth factors and standard deviations for the sampled dry sizes.

Dry size	Averaged GF I class (Std Dev.)	Averaged GF II class (Std Dev.)	Averaged GF III class (Std Dev.)
100 nm	1.02 (±0.02)	1.39 (±0.08)	1.70 (±0.12)
70 nm	1.04 (±0.03)	1.37 (±0.10)	1.66 (±0.12)
50 nm	1.03 (±0.04)	1.40 (±0.06)	1.65 (±0.12)
30 nm	1.04 (±0.04)	1.39 (±0.06)	1.64 (±0.08)
Table A.4.7: Averaged hygroscopic growth factor for 30,50,70 and 100 nm during a 4 hours sampling in Leipzig.			

The fraction of particles in the different classes is summarized in Table A.4.8 for 100nm and 30 nm particles.

Site	Dry Size (nm)	Period	Averaged H-GF groups		
			I class	II class	III class
Leipzig	100		1.01 (nf 0.20)	1.47 (nf 0.35)	1.81 (nf 0.45)
	30		1.0 (nf 0.55)	1.35 (nf 0.30)	1.66 (nf 0.15)
Table A.4.8 : Averaged hygroscopic growth factor and number fraction (nf) for 30 and 100 nm particles.					

As expected, the fraction of Class I particles is increasing with decreasing diameter while the Class II contribution remains more or less constant, around 35-40%. Only the hygroscopic Class III shows a dependence of GF with size. However, the hygroscopic group is found in significant fraction only for the 100 nm aerosols.

Again, measurements in a urban sub-urban area shows a mixture of Class I particles most likely freshly emitted particles from automobile sources and of Class II particles most likely composed of a mixture of inorganic salts and organic material formed from aging of Class I particles. The lifetime required for aging from Class I to Class II particles cannot be derived from our measurements but is certainly of the order of 1 day.

4. Conclusion

Measurements of the hygroscopic properties of 100 nm aerosols at five different sites representative of background air masses in marine, forest area or free tropospheric areas, or more polluted sites in sub-urban locations, have shown features that could be characteristic of a specific site, or common between all sites. The first information that these measurements have provided is the degree of mixing (external and internal). We found on all sites that the natural aerosol particles of the accumulation mode are never pure, even on sites representative of a very strong unique source (Mace Head with clean sector). In fact, most sites show at 100 nm an external mixture of moderately-hygroscopic particles with either hydrophobic particles in polluted air masses (Cezeaux, Leipzig and polluted air masses encountered at the Puy de Dôme and Mace Head) or hygroscopic particles in clean air masses originating from marine sectors at Mace Head and the Puy de Dôme. In these external mixtures of two hygroscopic modes, each hygroscopic mode itself was

mostly composed of an internal mixture of several compounds, as the measured hygroscopicity was never the one of pure NH_4SO_4 salt or pure sea salt. Only in Hyytiälä the 100 nm mode was one single internally mixed aerosol, either moderately hygroscopic or hydrophobic. We suspect that at Hyytiälä, the hydrophobic properties of particles were acquired when a new particle formation event took place and fresh organic substances would condense on nucleated clusters, as well as on larger particles such as the 100 nm particles that we studied. This phenomenon was also observed at other environments were new particle formation event took place, such as the Puy de Dôme and Mace Head: for several hours, hydrophobic properties were acquired by 85 nm and 100 nm particles.

Lastly, as a common feature between sites, we have been able to observe that "aged" aerosols were tending to acquire moderately-hygroscopic properties. This was clearly observed at night on sites were a local source of secondary aerosol was present only during the day (at Hyytiälä, Puy de Dôme, Cezeaux, Mace Head/European continental wind sector) and all the time on remote sites. As a result, the moderately hygroscopic mode is almost always present for 100 nm, except for exceptional conditions such as nucleation events or local sources of secondary aerosol production.

This study has the advantage of presenting the hygroscopic growth factor of varied aerosol types sampled at different locations with the same instrument, hence that can be directly compared, which is hardly the case in a literature review of hygroscopic growth factors, because of significant operational differences between instruments. The results show general trends that can be used in an exercise prediction of the hygroscopic properties of a given aerosol type, even if one must be careful in the diurnal variations of the growth factors, as well as a probable seasonal variation. This work will be continued, not only on the process point of view by studying the influence of the surface properties of the aerosol in its global hygroscopic behaviour, but also on a descriptive point of view of different air masses at different time of the year, by the automatisation of standard H-TDMAs on atmospheric research stations in Europe.

THE ROLE OF SURFACE LAYERS ON PARTICLE HYGROSCOPIC PROPERTIES

[1]_Paolo Villani,_ [1]_David Picard,_ [1]_Karine Sellegri ,_ [1]_Paolo Laj,_ [2]_Markku Kulmala_

[1]Laboratoire de Météorologie Physique ,CNRS, Université Blaise Pascal, Aubière, France

[2]University of Helsinki, Department of Physical Sciences

Paolo Villani
Laboratoire de Météorologie Physique (LaMP/CNRS)
Observatoire de Physique du Globe de Clermont-Ferrand
Université Blaise Pascal, Clermont-Ferrand, France
Tel :+33 4 73 40 52 78
Fax :+33 4 73 40 51 36
P.Villani@opgc.univ-bpclermont.fr

Prof. Markku Kulmala
University of Helsinki, Department of Physical Sciences
P.O. Box 64 FIN-00014 University of Helsinki
Tel: 358-9-19150756
Fax: 358-9-19150717

Abstract

The hygroscopic properties of aerosol particles are often related to their content of soluble material, on the basis of the Kohler theory. Recent studies, however, seem to indicate that the role of aerosol particle surface properties has been underestimated. In this study, we used a novel method based on a Tandem Differential Mobility Analyser (TDMA) system combining particle volatilisation and humidification conditioning (VH-TDMA) to test the effect of surface properties on particle hygroscopic growth. The VH-TDMA measurements were performed during the BACCI/QUEST campaign that took place in April 2005 at Hyytiälä, Finland. Preliminary results show that the particle hygroscopic properties can either be enhanced or decreased after thermal conditioning of the surface layer at moderate temperatures (50 to 90°C). These results indicate that surface properties are not sufficiently accounted for by the Kohler theory.

Keywords: Hygroscopicity, DMA, Kohler theory, Cloud Condensation Nuclei.

1. Introduction

Atmospheric aerosol particles play an important, but still poorly-understood role in cloud formation. The Kohler theory (Pruppacher and Klett, 1997) is often used to describe the critical supersaturation at which a Cloud Condensation Nuclei (CCN) of known size is activated, i.e. grows into a cloud droplet. The reliability of the model calculation strongly depends on the input parameters of the model, e.g. the surface tension, the molality of the solution formed on the aerosol particle, fraction of soluble material, protonation constants, Van't Hoff factor, etc... Most of these properties are often not measurable in the field and input parameters are often simplified to a reduced number of compounds.

Due to these limitations, the Kölher theory appears well-suited to describe the activation of pure inorganic particulate matter (e.g., Ammonium Sulphate, Sodium Chloride etc.), but not the behaviour of more complex mixtures including organic material. Organic compounds tend to have limited water solubility, which implies that they are less CCN active. However, some studies (Saxena et al., 1995; Raymond and Pandis, 2002) have shown that organic material can affect the hygroscopic behaviour of aerosol particles and activate particles more easily than the Kohler theory predicts. In other cases, however, the Kohler theory tends to overestimate droplet number concentration (Snider and Brenguier, 2000).

One of the reasons for the limitations of the theory may be linked to inadequate representation of surface properties. Theoretical calculations of sub-saturation growth mainly involve the solubility of the particle bulk, with the role of the particle surface being taken into account through the surface tension of the solute, and through the accommodation coefficient of water on the hydrated surface.

However, it is not yet known how the surface of the particles influences their growth rate when they are exposed to a humid environment. Surface tensions and accommodation coefficients are poorly documented and it is still an open question whether this theoretical approach is accurate or not. Laboratory studies of hygroscopic growth of inorganic salts coated with condensable organic material show that the absorption of water vapour can be inhibited significantly by a surface organic film (Chen et al., 1998, Hansson et al., 1998). However, synthetic particles do not properly simulate the chemical complexity of natural aerosols. The objective of the

present study was, therefore, to investigate to what extent a modification of particle surface properties affects its ability to grow in a humid environment.

2. Methods

The need to gain some insight into the chemical nature of sub micrometer aerosols has previously lead to the development of hygroscopic growth and volatility methods for aerosol research. Because the extent of hygroscopic growth depends on the chemical properties of the aerosol, sized particles of different composition can be distinguished through their differing growth response to humidification. Frequently, these properties are investigated using tandem differential mobility analyser (TDMA) systems (Rader and McMurry, 1986). Furthermore, volatile compounds can often be distinguished by the differences in their volatilisation temperatures (i.e. with a V-TDMA system, Orsini et al., 1998, Philippin et al., 2003).

In this study, the method is based on a TDMA system combining volatilisation and humidification conditioning of the particles (Volatility Hygroscopicity Tandem Differential Mobility Analyser, VH-TDMA). The instrument is composed of two DMAs in series (i.e., Differential Mobility Analyser) and CPCs (i.e., Condensation Particle Counter), separated by a thermo-desorption and a hydration device in series (Figure A.5.1).
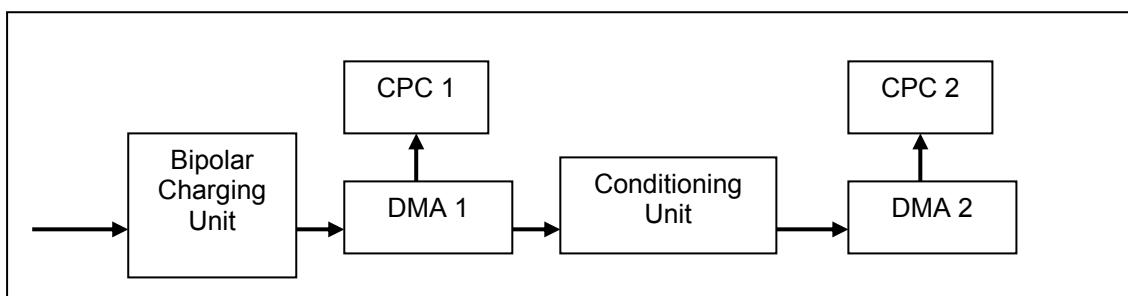
Figure A.5.1: Block diagram showing the working principle of the VH-TDMA analysing method

Complete characterization of a particle of a specific diameter (Dp) consists in measuring the size change obtained after slight heating (close to T=100°C) (Volatility-Scan), then the size change due to exposure to a humid flow (RH=90%) (Humidity-Scan), and finally the size change due to heating followed by humidifying (Volatility-Humidity-Scan). The duration of the complete scan for each particle diameter is of the order of 15 minutes. The heating temperature for the volatility and

Volatility-Humidity scans is identical and set between 70°C and 100°C. Such conditioning leads to a reduction of the particle diameter of less than 5%, corresponding to a change in mass of less than 15%. At these temperatures, our working hypothesis based on previous V-TDMA studies was that semi-volatile compounds condensed onto the particle surface can be volatilised back to the gas-phase. Each number concentration downstream from DMA2 is normalised in relation to the total number concentration of the initial selected particle diameter (i.e., "DRY" Dp). Measuring particle concentration at both DMAs with two CPCs is useful for an absolute comparison of the evolution of the four spectra with time. A complete description of the VH-TDMA system is presented elsewhere (Villani et al., in preparation).

The system was tested for the first time during the BACCI/QUEST campaign that took place in April 2005 in Hyytiälä, Finland, where frequent new particle formation events have been observed these last years. The SMEAR II experimental station (Station for Measuring Forest Ecosystem-Atmosphere Relations) located in Hyytiälä, southern Finland (61°51°N, 24°17E, 181m asl) is representative of the boreal coniferous forest. Meteorological parameters including wind speed and direction, temperature, pressure, relative humidity, and global radiation are measured at different levels above the ground, using a 72-m-high mast on a permanent basis (Kulmala et al., 2001). Data presented in this paper are based on samples taken during 3 weeks: from April 14 to May 3rd, 2003.

3. Results

The VH-TDMA was operated on a continuous basis over a wide range of aerosol particle size, including Aitken and accumulation mode particles (Dp ranging from 20 to 150 nm). The hygroscopic growth of aerosol particles varied from 1.1 to 1.8 during the course of the campaign with larger particles being generally more hygroscopic. Comparisons with other H-TDMA instruments used during the campaign show good agreement. A complete analysis of hygroscopic and volatility scans performed during the campaign will be presented elsewhere (Villani et al., in preparation).

The focus of this paper is to describe and discuss specific VH-TDMA scans that took place on several occasions during the campaign. Results show that, under some

conditions that might be linked to nucleation events, the hygroscopic properties of aerosol particles significantly changed when the particle surface layer was removed or decomposed by heating. Figure A.5.2a shows a complete suite of TDMA, V-TDMA, H-TDMA and VH-TDMA scans performed on 14/04/2005 at 17:00 UTC+2 and Figure A.5.2b on 21/04/2005 at 12:00 UTC+2. The total particle number concentration did not change significantly during the duration of either scan.
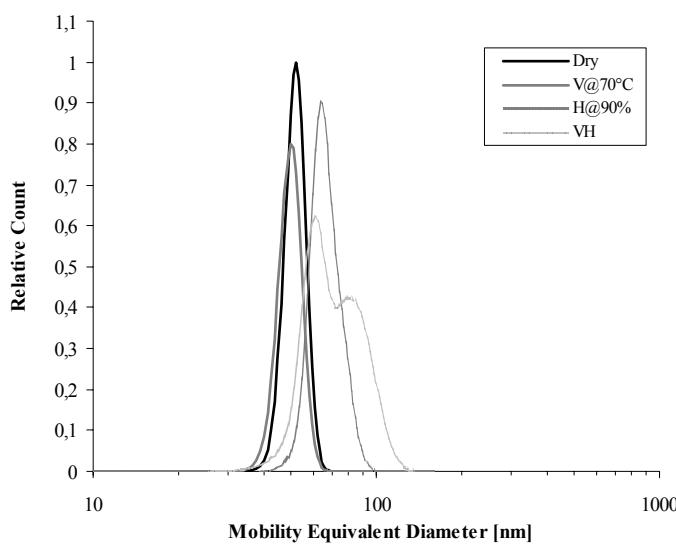
Figure A.5.2a: Normalised and fitted size distributions of selected 52 nm particles ("DRY" curve), after volatilisation at 70°C ("V70°C" curve), hydration at RH=90% ("H" curve), and volatilisation followed by hydration ("VH" curve).
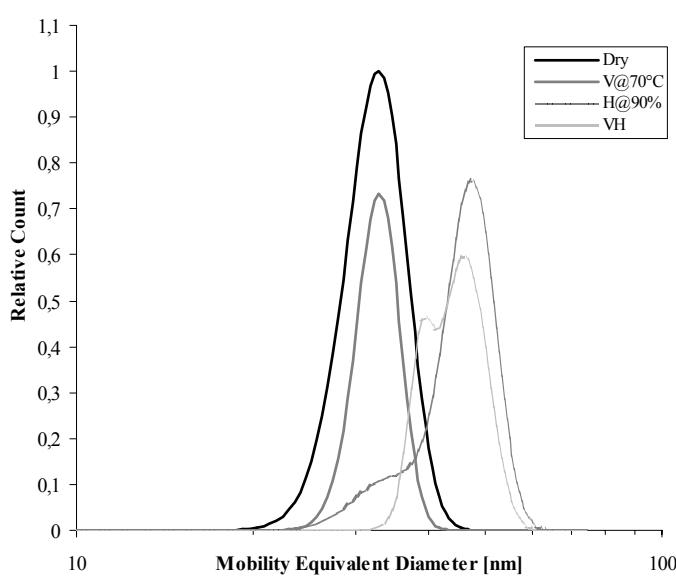
Figure A.5.2b: Normalised and fitted size distributions of selected 33 nm particles ("DRY" curve), after volatilisation at 70°C ("V70°C" curve), hydration at RH=90% ("H" curve), and volatilisation followed by hydration ("VH" curve).

The modes were determined by fitting the distribution after an inversion procedure that accounts for the instrumental broadening of the modes caused by the finite width of the DMA transfer functions, and for the system transmission efficiency. For simplicity, it is often assumed that the growth factors within each group of particles

are normally distributed. The Hygroscopic Growth Factor (i.e., HGF) is a diameter ratio defined as the particle diameter of a growth mode at the elevated, DMA2 *RH* (e.g. 90%) divided by the particle diameter at the lower, DMA1 RH (e.g. < 15%). For completely hydrophobic particles this growth factor is obviously unity (1). The Volatility Growth Factor (i.e., VGF) is the ratio between the particle diameter of volatilisation mode at oven temperature (e.g., 70°C) and the particle diameter at ambient temperature. The Volatility-Hygroscopicity Growth Factor (i.e., VHGF) is defined in a similar manner to HGF where the reference particle diameter at the lower RH is the volatility modal diameter exiting the heating path.

In both examples, while the size of the volatilised particles did not change appreciably, their HGFs differed after heating. As summarized in Table A.5.1, the change in HGFs after thermal conditioning is significant.

Table A.5.1: Results of two TDMA observations made in Hyytiälä, Finland during the BACCI/QUEST campaign that took place in April 2005

Date	Dp [nm]	V-Dp [nm]	VGF	HGF Mode 1	HGF Mode 2	VHGF Mode 1	VHGF Mode 2	VHGF / HGF Mode 1	VHGF / HGF Mode 2
21/04/2005	33	33	1	1,03	1,44	1,17	1,39	1,14	0,96
14/04/2005	50	48	0.96	1,20		1,19	1,60	1	1,33

A very interesting feature of our results is that the change in HGF after heating can be towards a gain or a loss of hygroscopicity:

- On the 14th of April (Figure A.5.2a), particles of 52 nm were studied. In this case, the "VH" curve showed the existence of two hygroscopic classes after aerosol conditioning (i.e. hydration after heating) even though the hydration (i.e. "H" curve) exhibited a mono modal size distribution. While some of the particles did not seem to be significantly modified by the heating treatment, (HGF=1.20 for both H and VH curves), a significant fraction of the particles were more hygroscopic after heating (H-GF=1.60), with an increase in HGF of over 30%.

- On the 21st of April 33 nm particles already showed a bi-modal less- and more-hygroscopic behaviour before heating, thus implying an external mixture in chemical composition (Figure A.5.2b). Subsequent to aerosol volatilisation

and hydration the bi-modal size distribution was preserved with a sensitive hygroscopic growth gain (14%) for the first mode.

Relative increases or decreases in HGF following thermal conditioning were measurable on several occasions during the campaign for a wide range of particle diameters. It is interesting to note that no hygroscopic change was measured for temperatures below 50°C. We cannot exclude, however, the hypothesis that thermal conditioning modifies the chemical properties of the species present on the particle surface or that the kinetics of aerosol hygroscopic growth in the VH-TDMA is reduced or increased, resulting in an apparent modification of the HGF. Clearly, with the first assumption (evaporation of semi-volatile compounds), the nature of the volatilised chemical species remains unknown at this point. Because measurements were performed in the boreal forest during spring, species deposited on particle surfaces are likely to be linked to the emission of biogenic organic compounds.

The removal of this surface coating had very little effect on either the size or the mass of the particle but led to a significant change in its HGF. Depending on the nature of the particle coating, or the nature of the non-volatile material remaining on the particle, the HGF was either increased or decreased. The presence of specific material on the surface therefore appears to partially control the hygroscopic behaviour of the particle. The conditions leading to higher or lower hygroscopic growth are still under investigation. This demonstrates, however, that prediction of hygroscopic growth based on bulk aerosol composition may lead to erroneous results. Additional studies on particle surface properties are required to better predict CCN concentrations.

4. Conclusions

In order to study these surface effects of particles on their hygroscopic properties, a TDMA system combining volatilisation and humidification conditioning (VH-TDMA) was developed and first used during the BACCI-QUEST campaign. After modifying their surface by gentle heating (50°C-100°C), the hygroscopic properties of particles were measured. It was demonstrated that the particle hygroscopic growth was governed not only by the fraction of hygroscopic material in the dry particle, but also by the presence of semi-volatile compounds on the particle surface. The particles hygroscopic properties significantly changed after volatilisation of a fraction of their

mass that did not change their size. The change could be either towards an increase, or a decrease of their hygroscopic potential, or a separate effect resulting in a bimodal behaviour that did not exist before the heating treatment. One explanation for this could be that the core of the particles heated had an external mixture which was hidden by the subsequent deposition of a surface layer. These results demonstrate that the Kohler theory, that is mostly sensitive to the particle chemical composition and its soluble fraction, can lead to erroneous estimation of CCN concentration for internally mixed particles.

Acknowledgments

References

Mikhailov E. et al. (2003), Interaction of aerosol particles composed of protein and salts with water vapor, *Atmos. Chem. Phys. Discuss*., 3, 4755-4832.

Kreidenweis et al. (2005), Water activity and activation diameters from hygroscopicity data-Part I, *Atmos. Chem. Phys. Discuss*., 5, 278-323.

Mäkelä, J.M et al. (1997), Observations of ultrafine aerosol particle formation and growth in boreal forest, *Geophys. Res. Letts*., 24, 1219-1222, 1997.

Pruppacher R. and Klett J.D.(1997), Microphysics of clouds and precipitation

Rader D.J. and P.H. McMurry (1986), Application of the tandem differential mobility analyser to studies of droplet growth or evaporation. *J.Aerosol Sci*., 17, 771-787.

Villani et al., Hygroscopic and surface properties of boreal forest sub-micrometer particles during BACCI/QUEST field campaign (in preparation).

Svenningsson B. et al. (2005), Hygroscopic growth and critical supersaturations for mixed aerosol particles of inorganic and organic compounds of atmospheric relevance. *Atmos. Chem. Phys. Discuss*., 5, 2833-2877.

Mircea, M. et al. (2005), Importance of the organic aerosol fraction for modeling aerosol hygroscopic growth and activation: a case study in the Amazon Basin., *Atmos. Chem. Phys. Discuss*., 5, 5253-5298, 25-7.

Effect of surface modification on the hygroscopic properties of natural aerosol particles

Villani, P., Sellegri, S., Monier M.and Laj, P.

1. Introduction

The hygroscopic behaviour of atmospheric aerosol particles is often assumed to be adequately described by the inorganic material, more specifically by major inorganic ions present in the particles. Organic substances have until recently often been considered insoluble (hydrophobic) and were thus neglected when considering the hygroscopic growth of particles.

Some recent studies have raised the question whether it is necessary to take into account also the organic volume fraction when describing the hygroscopic properties of aerosol particles.

The role of organic material on aerosol activation has been the focus of considerable attention in the recent literature (Novakov et al., 1993; Cruz et al., 1997; Laaksonen et al., 1998; Facchini et al., 2000; Charson et al., 2001; Nenes et al., 2002; Lohmann et al., 2004). However, there has been considerable debates over the exact role of organic compounds. In fact, these species can affect hygroscopic growth in three main ways:

- by adding soluble and insoluble material to the droplet solution (Raoult effect).
- by lowering or increasing the surface tension of the liquid phase (Kelvin effect).
- by affecting the wettability of particle surface, and the growth kinetics.

Numerous studies have investigated the role of organic matter in the control of the hygroscopic properties of particles. However, results of such studies, especially the few of those performed in the natural atmosphere, are sometimes contradictory due to the different organic compounds considered, and the differences in the treatment of chemical and physical properties, such as surface tension, solubility and degree of dissociation. Despite this disagreement, a conclusion which can be drawn from the

currently available evidence is that the relative contribution of organics to water uptake should be most significant under lower relative humidity conditions (Saxena et al., 1997; Ansari et al., 2000), that is below the deliquescence points of inorganic hygroscopic species.

Organics can span the full range from highly nonpolar (hydrophobic) to highly polar, and they are expected to exist in the atmosphere mainly (i) as coating on insoluble/soluble inorganics core, and (ii) as solution mixtures with inorganics compounds. Several laboratory research efforts have attempted to examine whether organic coatings can alter the hygroscopic behaviour of the core. Again, laboratory studies lead to contradictory results. Under some conditions, no changes in the behaviour of a hygroscopic core are measured after coating with hydrophobic substances (Hansson et al., 1990; Hameri et al., 1992; Cruz et al., 1998). There, the presence of inorganic salts appears to lead hygroscopic growth regardless of the presence of a hydrophobic organic fraction. On the contrary, other studies have seen retardation or suppression of water uptake (Andrews et al., 1993; Xiong, 1998).

Saxena et al. (1995) used H-TDMA and cascade impactor to indicate that organic material can affect the hygroscopic behaviour of aerosol particles at water vapour sub-saturation. From their data evaluation, they drew the conclusion that the organic fraction of freshly produced aerosol particles hinders the hygroscopic growth, while organic species in particles found in aged air masses seemed to increase the growth. These organic species should be both water-soluble and liable to condense on existing aerosol particles under atmospheric conditions. Clearly, additional studies are needed to better identify how condensation processes of anthropogenic and biogenic species may influence the rate and amount of water uptake by particles. Most of the process-oriented studies were however performed in idealized laboratory conditions and very few studies have actually attempted to identify to role of organic species in the natural atmosphere.

The purpose of this study is to investigate to which extent the hygroscopic growth of nm-size natural particles is controlled by chemical species condensed onto their surface. For that purpose, we have used a newly developed Volatility-Humidity Tandem Differential Mobility Analyser (VH-TDMA). Operating conditions of the VH-TDMA are described in details by Villani et al., (2006b). The technique allows the investigation of the hygroscopic growth of particles after a thermal processing. As shown by laboratory experiment, thermal processing is very effective to remove a

layer of semi-volatile species from the particle surface (Villani et al., 2006b). We have applied the VH-TDMA technique to investigate the hygroscopic behaviour of natural and thermo-desorbed particles in different environments: near emission sources in the urban area of Clermont-Ferrand (France), in the coastal environment at Mace Head (Ireland) and in the Boreal Forest at the Hyytiala station (Finland) , and far from emission sources at the free tropospheric site of puy de Puy de Dôme (France) and in anthropogenic air masses sampled at Mace Head (Ireland). The hygroscopic behaviour of particles is the focus of a companion paper (Villani et al., 2006c). Here, we will focus on the hygroscopic growth changes before and after thermal treatment.

2. Fields campaigns and operating conditions

2.1 Description of Field campaigns

Measurements used in this study are performed over a number of sites representing different environments and different air masses. At each site, we have sampled one or more air mass types during the duration of the field campaign which lasted from one week (Puy de Dôme campaign) to one month (Hyytiala and Clermont-Ferrand campaigns).

Air mass characteristics are described in more details in a companion paper but, in order to ease the comprehension of the present paper, they are briefly summarized in Table A.6.1.

Site	Period	Dates	Dry size	Air Mass Type/Origin
#1-Hyytiala Finland				
	1	13 to 18 April, 2005	20, 30,	Marine Air Mass/West
	2	20 to 22 April, 2005	50,100	Marine Air Mass/North-Est
	3	23 to 29 April, 2005	nm	Continental Air Mass/North (Finland)
#2- Puy de Dome France				
	1	22 to 24 October, 2005	100 nm	Marine Air Mass/West
	2	25 to 26 October, 2005	100 nm	Continental Air Mass/Sud-West (Spain)
#3- Cezeaux France				
	1	1 to 4 December, 2005	100 nm	Continental Air Mass/ Sud-West (Spain)
	2	5 to 9 December, 2005	100 nm	Marine Air Mass/North-West
	3	10 to 16 December, 2005	100 nm	Continental Air Mass/North-Est (Germany)
#4-Mace Head Ireland				
	1	16 to 22 January, 2006	85 nm	Marine Air Mass/West
	2	23 to 26 January, 2006	85 nm	Continental Air Mass/South-Est (France)
#5-Leipzig Germany				
		10 February, 2006	30-50 70-100 nm	Continental Air Mass

Table A.6.1: Air mass type categorized with NOAA HYSPLIT MODEL back trajectories analysis calculated on three days for the five sampling sites.

2.2 VH-TDMA operating procedures

If H-TDMAs have been extensively used to study the atmospheric aerosol, very few VH-TDMAs are currently being used despite strong evidences of a close link between thermal and hygroscopic properties of particles. Johnson et al. (2004) have developed a VH-TDMA that is operating in slightly different conditions from the one used in this study. The operating conditions of our VH-TDMA are described in Villani et al., (2006b). Here, we will only provide a brief description of the main features of this newly developed instrument. As mentioned previously, VH-TDMA features properties of both V-TDMA and H-TDMA. The instrument is capable of rapidly switching to investigate the behaviour of particle after conditioning at constant temperature (i.e. V-TDMA), at constant humidity (i.e. H-TDMA) and at simultaneous constant temperature/humidity (i.e. VH-TDMA). It consists of a first differential Mobility Analyser (custom made DMA1) selecting particle in a given size range counted by a condensation particle counter (CPC1-TSI 3010). It should be noticed that, prior to initial size classification in DMA1, the aerosol is dried to a relative humidity <10% in a diffusion drier tube. Monodispersed particles (sample flow) are processed either by a thermo-desorbing unit (V-scan -Villani et al., 2006a), or by a humidity unit (H-scan Villani et al., 2006b) or by both units (VH scans). The effect of thermal and humid processing on aerosol size and concentration is controlled by a second DMA (custom made DMA2) and CPC (CPC2-TSI 3010).

At all sites, we followed an identical operation procedure for the VH-TDMA. A complete characterization of a particle at specific dry diameter (i.e. "DRY Dp") selected by DMA1 consists of an alternate sequence of three scans: H-TDMA first, VH-TDMA and then V-TDMA. HGF are usually measured from 0.8 to 2.5 at all the different dry sizes leading to a typical duration of the complete procedure (i.e. three scans) for each dry particle diameter of the order of 18 minutes, when 24 different sizes are selected in the DMA2 in stepping-voltage method (i.e. DMPS). The sample aerosol flow is conditioned to a well-defined temperature in the volatilization tube, chosen between 90°C and 110°C for these experiences. To increase temporal resolution, the volatility scan can be repeated once per hour in stable conditions, whereas the system alternates only two wet scans (i.e. Humidity-scan and Volatility-Humidity-scan) every 10 minutes.

The calibration of the instrument consists of independent calibration of the V-TDMA (Villani et al., 2006a) and H-TDMA (Kaaden et al., in preparation) sub-systems. Laboratory studies confirmed that thermo-desorption is very efficient to remove species condensed onto the particle surface as long as the prescribed volatilisation temperature of the thermo-desorbing unit exceeds the volatilisation temperature of the volatilised gas. Laboratory studies showed that, under these conditions, re-condensation during cooling does not primarily take place onto the particles and therefore does not need to be considered in this study.

As mentioned in Villani et al., (2006c), the VH-TDMA is operated side by side with a scanning mobility particle sizer.

2.3. VH-TDMA Data reduction

The Hygroscopic growth factor (HGF) at 90%RH is measured as followed:

$$HGF = D_p^{90} / D_p^{10}$$

where D_p^{90} is the particle diameter at RH=90% and D_p^{10} is the particle diameter at RH=10%., the Volatility "growth" factor (VGF) can be derived from the Volatility scan. It is the relative size change of a particle due to thermal conditioning. For a given thermo-desorbing temperature T°, it is calculated as the ratio between the particle diameter at RH=10% ($D_p^{10,T°}$) and the dry particle diameter at RH=10% and ambient temperature ($D_p^{10,Tamb}$), thus:

$$VGF = D_p^{10,T°} / D_p^{10,Tamb}$$

Logically, the Volatility-Hygroscopic growth factors (VHGF), that is the hygroscopic growth of a thermally processed particle is derived as:

$$VHGF = D_p^{90,T°} / D_p^{10,T°}$$

where $D_p^{90,T°}$ is the particle diameter at RH=90% and T>T$_{amb}$. The VHGF is therefore calculated considering the "new" diameter resulting from thermo-desorption.

The uncertainty on the VHGF measurements propagates from the uncertainty on the HGF measurements. It was pointed out in a recent H-TDMA intercomparison workshop (Kaaden et al., 2006), that most variability in HGF measurements results from the RH control of DMA2. Because the VH-TDMA scans are performed under the same conditions of RH and because no RH drift in DMA2 has been detected,

uncertainty on the VH-GF measurements are similar to that on the H-GF measurement, that is close to ±2.5% (see Villani et al., 2006b).

3. Measurements

Averaged measurement of HGF and VHGF (and their respective standard deviations) for the time periods corresponding to the air masses described in Table A.6.1 are summarized in Table A.6.2 for the different field campaigns.

As for Villani et al. (2006), HGF are sorted into 3 hygroscopic classes: Class 1- hydrophobic particles (HGF< 1.3), Class 2- moderately hygroscopic particles (1.3<HGF<1.6) and Class 3, more hygroscopic particles (HGF>1.6). VHGF are sorted in a similar manner. Clearly, the aerosol population for a given diameter is composed of several hygroscopic classes, an indication of externally mixed particles (see Villani et al. 2006c).

Table A.6.2: Averaged measurement of HGF and VHGF (with standard deviation) corresponding to air masses described in Table A.6.1 and different field campaigns.

Site	Dry Size (nm)	Period	Averaged H-GF groups			T_{vol} (°C)	Averaged VH-GF groups			VGF
			I class	II class	III class		I class	II class	III class	
Hyytiala	20	1	1.15±0.12	-	-	70°	1.13±0.12	-	-	0.99
		2	1.25±0.10	-	-	70°	1.23±0.11	-	-	0.95
		3	-	1.33±0.08	-	110°	-	1.51±0.11	-	0.72
Puy de Dome	100	1	1.07±0.06	1.37±0.08	1.83±0.09	70°	1.15±0.06	1.43±0.11	x	0.94
		2-25/10	1.09±0.09	1.37±0.08	1.86±0.08		1.11±0.07	1.51±0.09	x	0.97
		2-26/10	-	1.45±0.07	1.89±0.08		-	1.48±0.07	1.71±0.08	
Clermont-Ferrand	100	2	1.04±0.04	1.38±0.10	1.74±0.19	70°	1.06±0.04	1.39±0.08	1.71±0.07	0.95
		3	1.08±0.06	1.41±0.12	-		1.12±0.07	1.34±0.07	-	0.92
Mace Head	85	1	-	1.58±0.18	1.87±0.16	90°	-	1.71±0.19	2.02±0.17	0.95
		2	1.11±0.14	1.45±0.12	-		1.18±0.19	1.53±0.15	-	0.89
Leipzig	100		1.01	1.47	1.81	50°	1.0	1.45	x	0.99
	30		1.0	1.30	-		1.07	1.41	-	0.9

The VHGF measured are usually of the same order of magnitude as the HGF. However, even considering the uncertainty on the VHGF measurements, the difference between VHGF and HGF is sometime significant and can result in either significantly >1 (thermo-desorbed particles grow more than the original one, or significantly <1 (thermo-desorbed particle grow less that the original one). Table A.6.3 provides the averaged as well as the minimum and maximum values of the VHGF/HGF ratio for the different hygroscopic classes and the different air masses.

Table A.6.3: Averaged VH/H GF ratio for different hygroscopic classes and air masses (maximum ratio value in red, minimum in blue)

Site	Dry Size (nm)	T_{vol} (°C)	I class		II class		III class	
Hyytiala	20	70°	0.98	1.12 / 0.85	-		-	
		70°	0.99	1.10 / 0.87	-		-	
		110°	-		1.14	1.23 / 1.04	-	
Puy de Dome	100	70°	1.08	1.16 / 0.99	1.05	1.14 / 0.96	x	
			1.02	1.11 / 0.93	1.10	1.17 / 1.03	x	
			-		1.03	1.10 / 0.96	0.91	0.97 / 0.86
Clermont-Ferrand	100	70°	1.02	1.07 / 0.97	1.00	1.09 / 0.92	0.98	1.03 / 0.93
			1.04	1.13 / 0.95	0.95	1.04 / 0.86	-	
			-		1.08	1.19 / 0.91	1.08	1.18 / 0.96
			1.06	1.16 / 0.96	1.06	1.20 / 0.94	-	
Leipzig	100	50°	0.99		0.98		-	
	30		1.07		1.08		-	

The decrease and increase in hygroscopic growth can be as high as 14% on average for class 2 particles at Hyytiala (Finland). This is significantly higher than the uncertainty on the VHGF/HGF ratio. For single cases, changes as high as + 20 % and as low as –15% can be measured after thermo-desorption.

Examples of HGF changes after thermo-desorption are given below. On some occasions, thermally processed particles result in a higher growth factor than the original ones. At Hyytiala (Finland), thermo-desorption of 20 nm particles at 110°C leads to the formation of 15 nm particles. However, the HGF does not change drastically between ambient and thermo-desorbed particles resulting in a VHGF/HGF of 1.14 (Figure A.6.1a). At Clermont Ferrand, the resulting change in size after thermo-desorption of 100 nm particles is limited (Figure A.6.1b) but the hygroscopic growth factor of class 2 particles is slightly increased. At Puy de Dôme, thermo-desorption of class 3 particles at 70°C leads to a drastic decrease of the hygroscopic mode (Figure A.6.1c). A similar feature (suppression of the hygroscopic mode) is seen already at 50°C for the Leipzig particles (Figure A.6.1d) and Mace Head (Figure A.6.1e) with thermally processed particles of the hygroscopic group undergo a significant decrease in HGF. On some occasions, no change can be detected: either the thermally processed particles are not modified in size and grow to similar

sizes such as 20 nm particles in Hyytiala (Figure A.6.1f) or the thermally processed particles are slightly modified in size but the resulting VHGF is also decreased as respect to the HGF by the same amount (Figure A.6.1g). Another example is given by measurements at Mace Head with similar shift of both ambient and thermo-desorbed sizes and HGF and VHGF growth factors (Figure A.6.1h).

Figure A.6.1a: Thermo-desorption of 20 nm particles at 110°C sampled at SMEAR II field station, Hyytiala, Finland

Figure A.6.1b: Thermo-desorption of 100 nm particles at 70°C sampled at Clermont Ferrand, France.

Figure A.6.1c: Thermo-desorption of 100 nm particles at 70°C sampled at Puy de Dome station, France.

Figure A.6.1d: Thermo-desorption of 100 nm particles at 50°C sampled at IfT, Leipzig, Germany.

Figure A.6.1e: Thermo-desorption of 85 nm particles at 90°C sampled at Mace Head, Ireland.

Figure A.6.1f: Thermo-desorption of 20 nm particles at 70°C sampled at SMEAR II field station, Hyytiala, Finland.

Figure A.6.1g: Thermo-desorption of 100 nm particles at 70°C sampled at Clermont Ferrand, France.

Figure A.6.1h: Thermo-desorption of 85 nm particles at 90°C sampled at Mace Head, Ireland.

Results are summarized in Figure A.6.2. In this Figure, the relative change in the growth factor is plotted against the original HGF for the different air masses and the different locations. It should be noted that we have subsequently sorted air masses according to other characteristics as for example Free Troposphere / Boundary Layer air for the Puy de Dôme site or night/day for the Clermont-Ferrand site. In this figure, we can consider than any change > +3.5% or <-3.5% is significant.
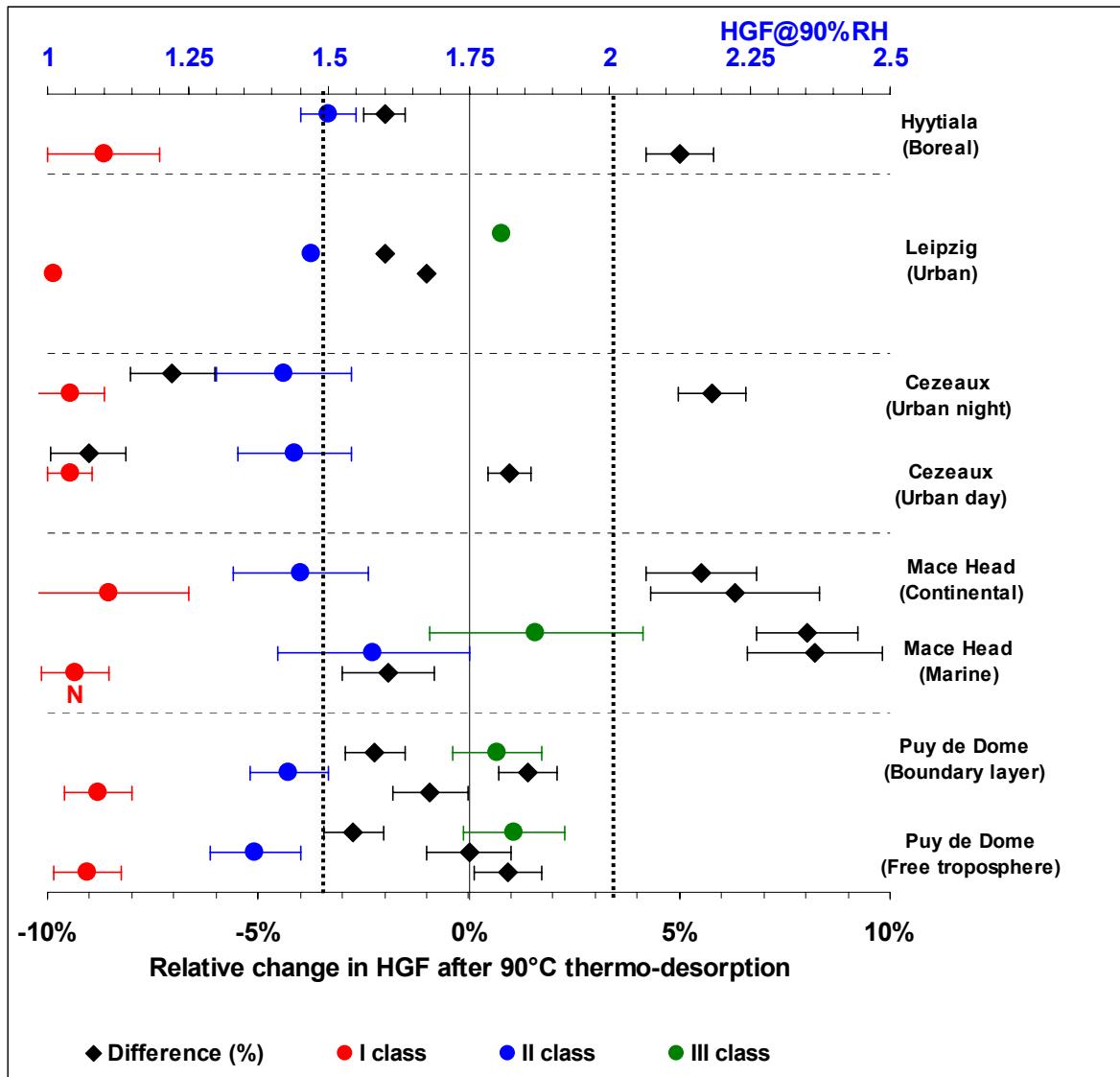
Figure A.6.2 : Relative change in the hygroscopic growth factor of particles sampled for different locations and air masses.

It is clear that thermo-desorption of particles can have a significant effect on particle growth that cannot be explained by a change in size only (Kelvin effect). Careful analysis of Figure A.6.2 shows that:

- ❖ The HGF of hydrophobic particles (class I) can be increased by thermo-desorption of the particles. This is clearly the case at Mace Head for continental air masses (+6±1.5%), Clermont-Ferrand Cézeaux during night-time conditions (+6±1%) and Hyytiala (+5±0.5%). It is likely that the volatilised compounds present on the surface layer of the particles are more hydrophobic than the particle itself.

- ❖ On other occasions, the HGF of class I particles is not modified by thermal processing of particles as for puy de Dôme, Leipzig and day time at Clermont-Ferrand Cézeaux.

- ❖ The HGF of the hygroscopic particles (Class III) is usually decreased after thermal processing except at Mace Head. It should be noted that in the case of Puy de Dôme, thermal processing often leads to disappearance of the hygroscopic group.

- ❖ Finally, thermal processing of moderately hygroscopic particles (Class II) either leads to increased HGF as in the case of Mace Head (+ 6±1.5%) or decreased HGF as in the case of Clermont-Ferrand Cézeaux (-8±1%).

We can conclude that thermal processing can significantly affect hygroscopic growth of some particles. The change can be either positive or negative. In some cases, no change is detected. It should be kept in mind that the thermo-desorption temperature is chosen to avoid visible changes of the particle size as seen from the size distribution. On average, thermal processing at 100°C only leads to a 5 nm change in particle diameter for original particles of 100 nm. This is a 5% change in size resulting in a 15% change in volume. In the following, we have used a numerical model of hygroscopic growth to simulate the effect of composition change on HGF.

4. Theoretical model calculations

The numerical model of hygroscopic growth is based on the Kohler theory that describes the interaction between water vapor and aerosol particles by combining the Kelvin curvature effect and Raoult's law (Kohler, 1936). This theory, with some improvements, is still widely in use when describing the water uptake of particles. By combining the Kelvin curvature effect and Raoult's law (the salt effect), the new equilibrium saturation ratio over a water droplet containing soluble material can be written:

$$e_{ssa} \big/ e_{sw} = a_w C_k . \quad (1)$$

where e_{ssa} is the saturation water vapor pressure over a droplet solution and e_{sw} the saturation vapor pressure.

At subsaturation, the behaviour of most solutions deviates from ideal solutions. Therefore, the water activity has to be determined empirically. This can be done using various methods, such as osmometry (Kiss et al., 2003) or electrodynamic balances (Tang et al., 1994). The water equilibrium between an aqueous solution droplet and an air parcel at a certain relative humidity (RH), can be expressed with the following equation:

$$RH\big/100 = a_w C_k. \quad (2)$$

Using this equation one assumption is made: the particle (solution droplet) and the surrounding moist air are in thermodynamic equilibrium. On the right-hand of this equation, a_w is the activity of water in a salt solution and is expressed as a function of the salt concentration. The water activity describes the reduction of water vapour pressure due to dissolved material. The second term, C_k, the Kelvin correction factor, accounts for the vapour pressure increase due to the curvature of a droplet and become important as particle sizes that are smaller than 100 nm are investigated. The Kelvin correction factor is given by:

$$C_k = \exp\left(4\sigma v_w\big/RTd\right). \quad (3)$$

Here σ is the surface tension, v_w is the partial molar volume of water in the solution, R is the gas constant, T is temperature and d is the diameter of the particle. Since v_w and σ depend on the solute concentration of the droplet, we used polynomial fits to experimental data on liquid densities and surface tensions to calculate their values.

Table A.6.4 resumes the functional forms of the fits for pure ammonium sulphate (AS) and pure NaCl of water activity (a_w), surface tension (σ) and density (ρ).

	Parameter	Value	Reference
(NH$_4$)$_2$SO$_4$			
Water Activity	$a_w = 1 - 2.715 \cdot 10^{-3} \cdot w_f + 3.113 \cdot 10^{-5} \cdot w_f{}^2 - $ $2.336 \cdot 10^{-6} \cdot w_f{}^3 + 1.412 \cdot 10^{-8} \cdot w_f{}^4$		Tang and Munkelwitz (1994)
Density	$\rho_{sol} = (0.9971 + 5.92 \times 10^{-3} \cdot w_f - 5.036 \times 10^{-6} \cdot w_f{}^2 + $ $1.0242 \times 10^{-8} \cdot w_f{}^3) \times 1000$		Hameri et al.(2001)
Surface Tension	$\sigma = 0.072 + 0.00234 \cdot m$		Pruppacher and Klett (1997)
NaCl			
Water Activity	$a_w = \exp(-0.03604 \cdot m$ $+ 0.01649\left[\left((1 + 1.37 \cdot m^{1/2}) - 4.60517 \cdot \log(1 + 1.37 \cdot m^{1/2}) - \dfrac{1}{(1 + 1.37 \cdot m^{1/2})}\right)\right]$ $- 1.1601 \cdot 10^{-3} \cdot m^2 - 2.6572 \cdot 10^{-4} \cdot m^3 + 1.7029 \cdot 10^{-5} \cdot m^4)$		Tang et al., (1996)
Density	$\rho_{sol} = 0.99845 + 6.9599 \times 10^{-3} \cdot w_f + 2.58586 \times 10^{-5} \cdot w_f{}^2$		Hameri et al.(2001)
Surface Tension	$\sigma = 0.072 + 0.0017 \cdot m$		Pruppacher and Klett (1997)

* here w is the mass fraction of the salt, w_f salt mass fraction expressed in percent, and m is molality. The molality has unit of mol/kg (moles of solute per kilogram of water) and surface tension is expressed in N/m.

Table A.6.4: Polynomial fits used in the model for pure ammonium sulphate (AS) and pure NaCl of water activity (a_w), surface tension (σ) and density (ρ).

Using these values, we can simulate the effect of a change in size without change in chemical composition of particles for inorganic salts. We can see that, in order to produce significant changes in the HGF, a thermo-desorption process that would remove all particle component regardless of their chemical composition would need to produce more than a 5% change in size. For pure AS particles, noticeable effects of thermo-desorption are detected only after a diameter decrease of the particle of more than 40% of its original value (see Figure A.6.3). The growth factor change at 90% RH is about 2% (i.e. from 1.70 to 1.67): the Kelvin effect alone cannot explain our results. But our results can originate from preferential volatilization of one or more of the aerosol components.
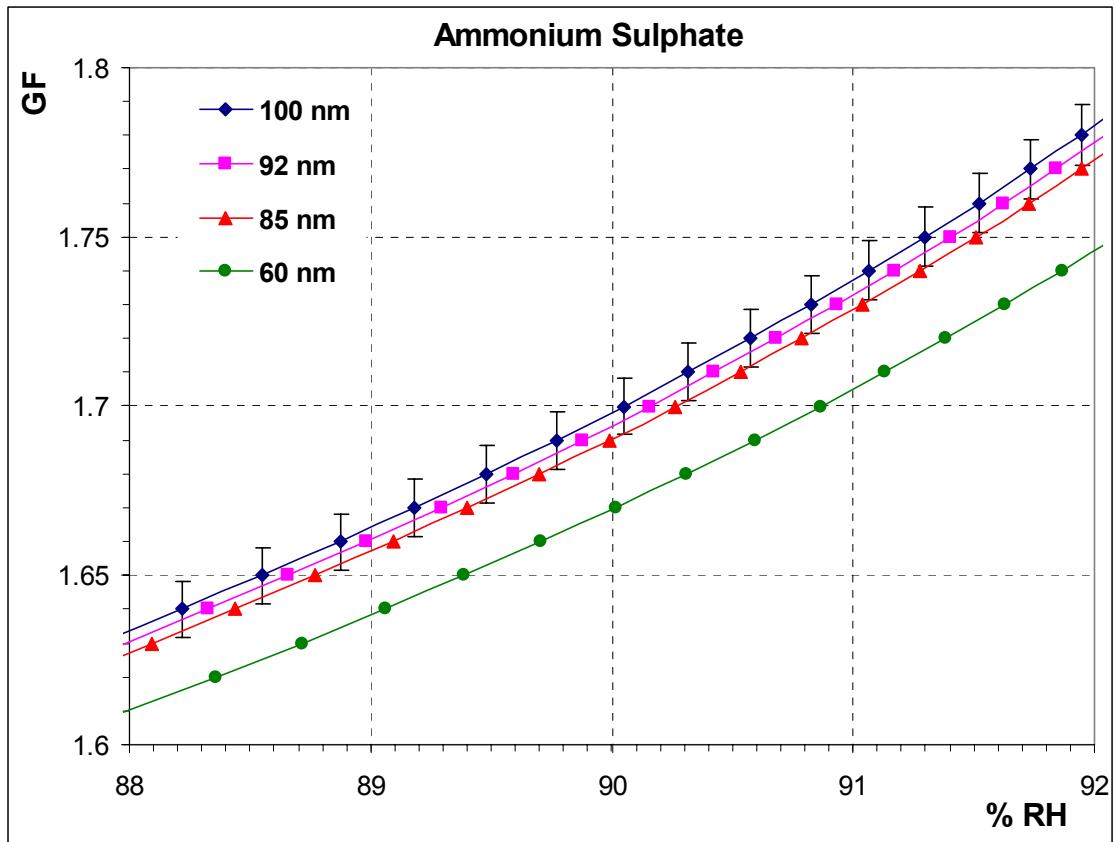
Figure A.6.3: Theoretical hygroscopic growth of 60, 85, 92 and 100 nm pure AS particles.

To check for the effect of preferential volatilization of one aerosol component, we have chosen an extreme case of a particle composed of fully hygroscopic compound (sulphuric acid) with a fully hydrophobic compound (fulvic acid).

In that case, the inorganic particle fraction is considered hygroscopically active, while the organic fraction is assumed to be inactive and does not interact either with the water condensed on the particles nor the surrounding water vapour. The particles are considered to be originally composed of 40% Fulvic acid and 60% Sulphuric acid (by mass).

The choice of this simplified composition for these sensitivity tests is based on the fact that a few inorganic ions make up a large mass fraction of tropospheric aerosol particles (Heintzenberg, 1989) and that thermodynamic data exist for the inorganic compounds. On the contrary, we have chosen fulvic acid as a proxy for the organic fraction because thermodynamic data is largely lacking for the majority of relevant organic species (Saxena and Hildemann, 1996) in particular for the relevant organic species which might be of importance for the hygroscopic behaviour. Water activity

(a_w), surface tension (σ) and density (ρ) for the fulvic-sulphuric Acids composition tests are calculated by a physic-chemical model (Topping et al., 2005).

Figure A.6.4 shows the modelled parameters (water activity (a_w), density (ρ) and surface tension (σ)) with polynomial fits for an initial particle composition of 40:60 fulvic-sulphuric Acid.
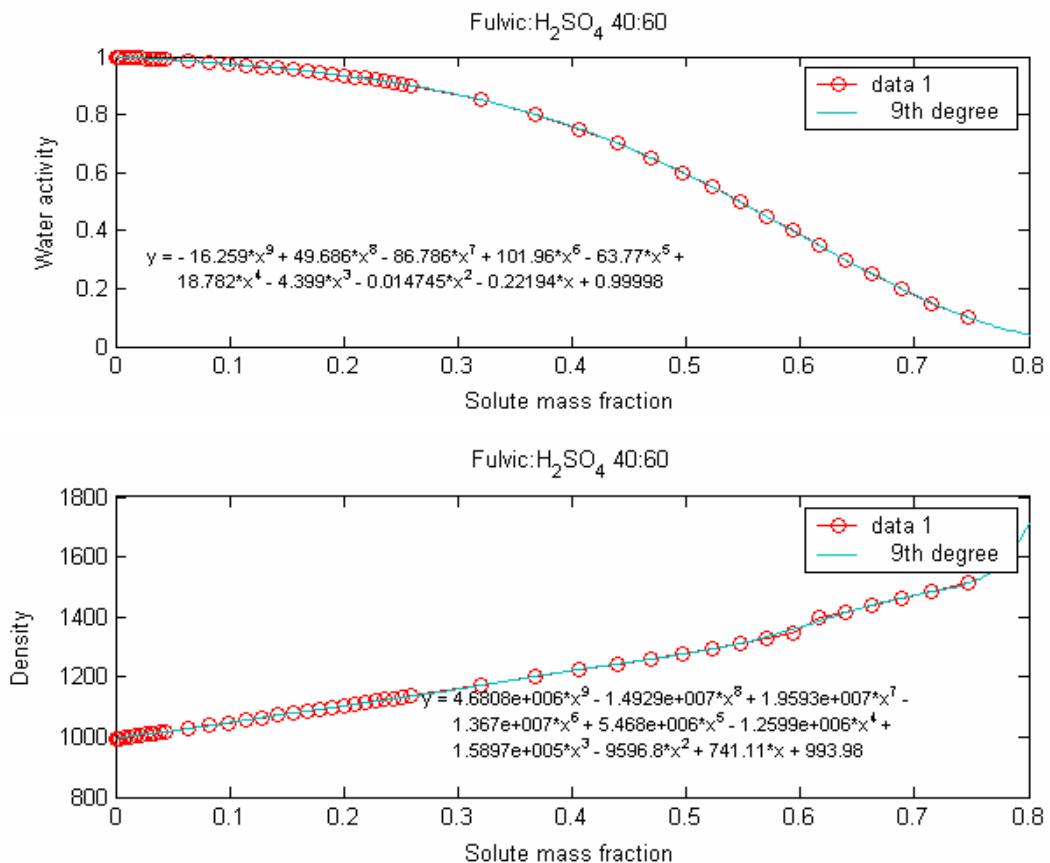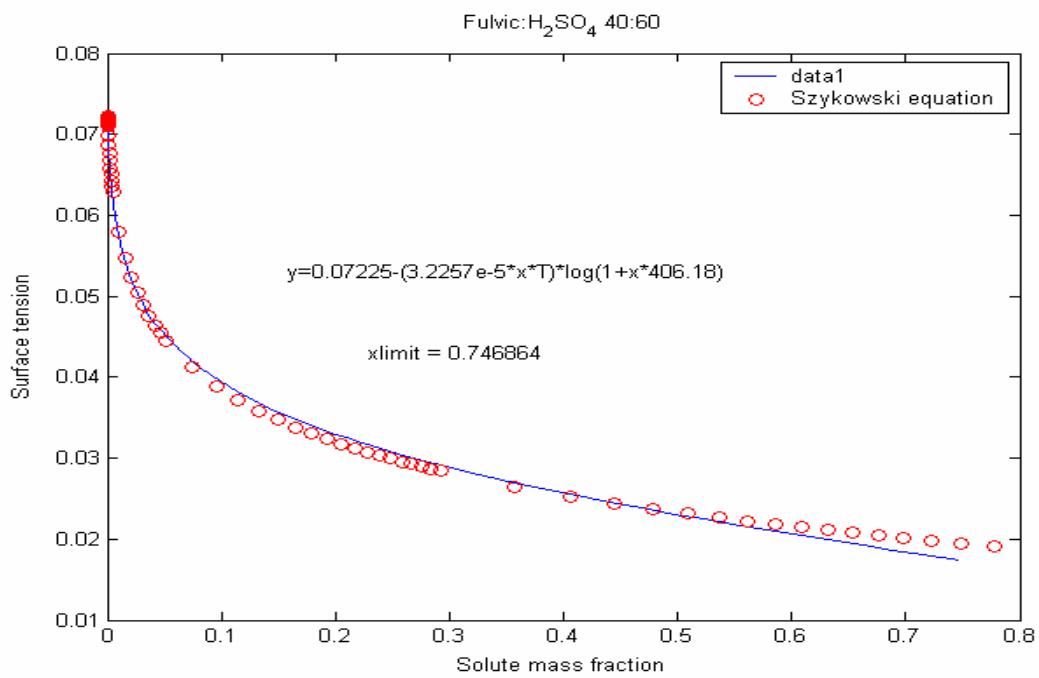
Figure A.6.4: Modeled functional fits of water activity, density and surface tension for Fulvic-Sulphuric Acid particle composition (40:60 in mass) used in the sensitivity test.

In a first sensitivity test, we have considered that 1/3 of the sulphuric acid mass is lost during thermo-desorption, resulting in a thermally processed particle composed of equal mass of both fulvic and sulphuric acids (i.e. composition 50:50). Figure A.6.5 shows the calculated parameters (water activity (a_w), density (ρ) and surface tension (σ)) with polinomial fits for particle composition of 50:50 Fulvic-Sulphuric Acid.
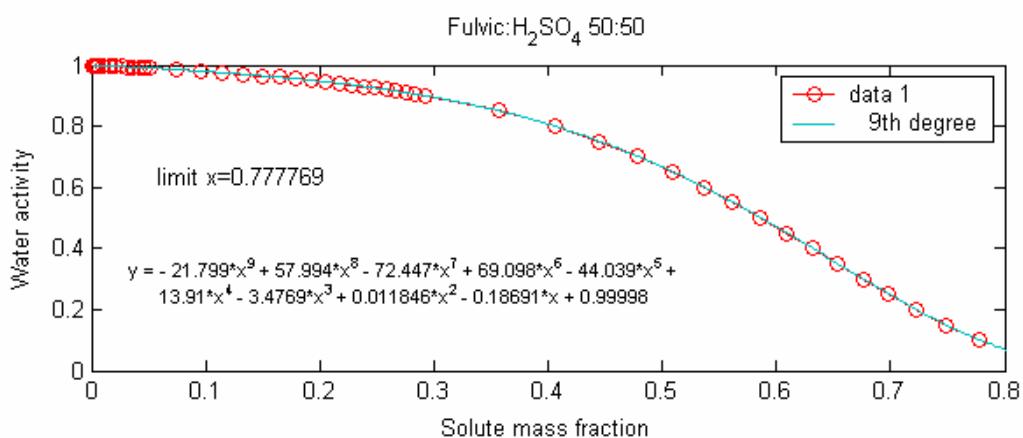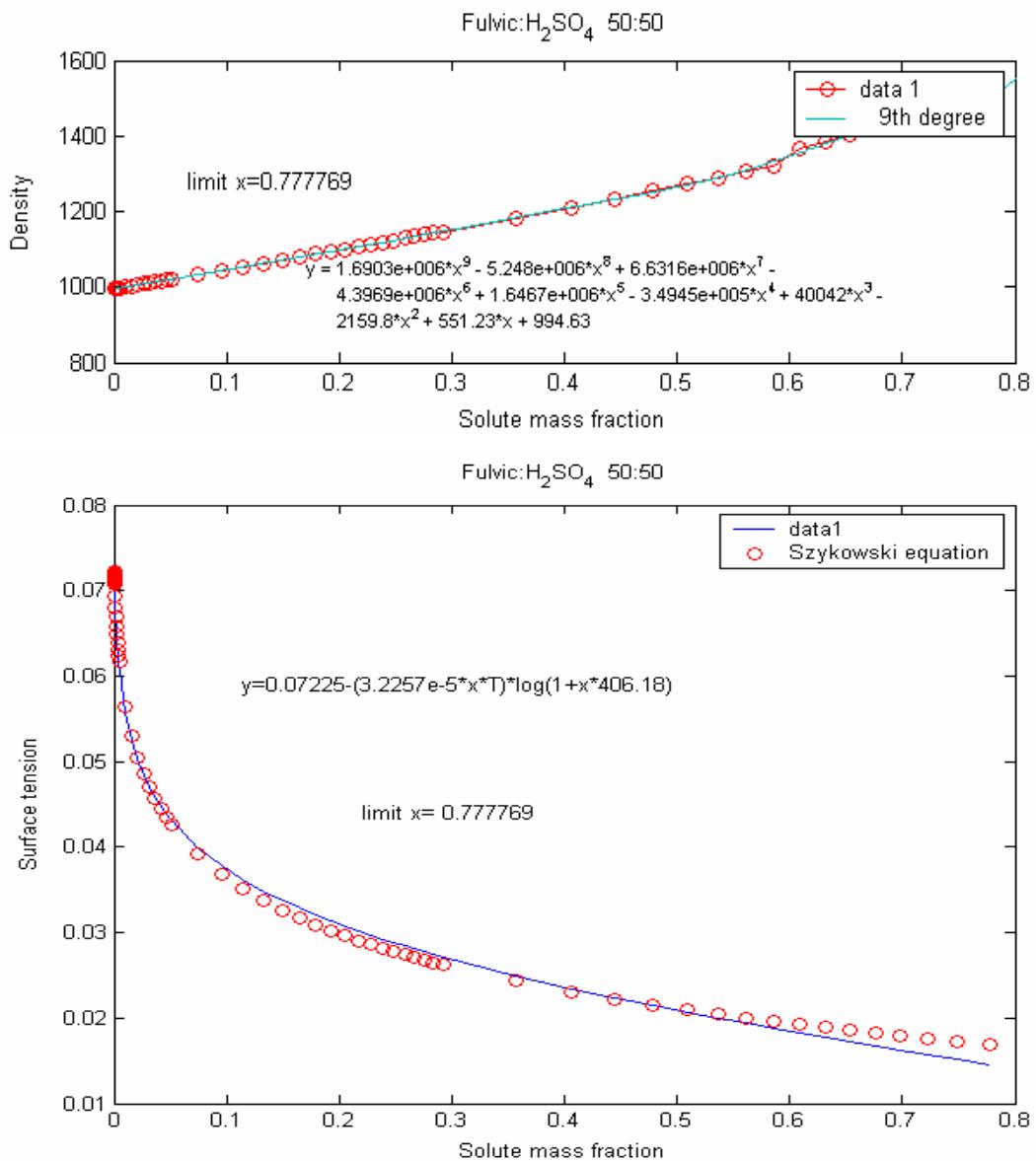
Figure A.6.5: Modeled functional fits of water activity, density and surface tension for fulvic-sulphuric Acid particle composition (50:50 in mass) used in the sensitivity test.

This leads to a diameter reduction of 7% of the original particle diameter (93 nm as respect to 100 nm) and of 20% of the particle volume. Results of this sensitivity test are shown in Figure A.6.6.
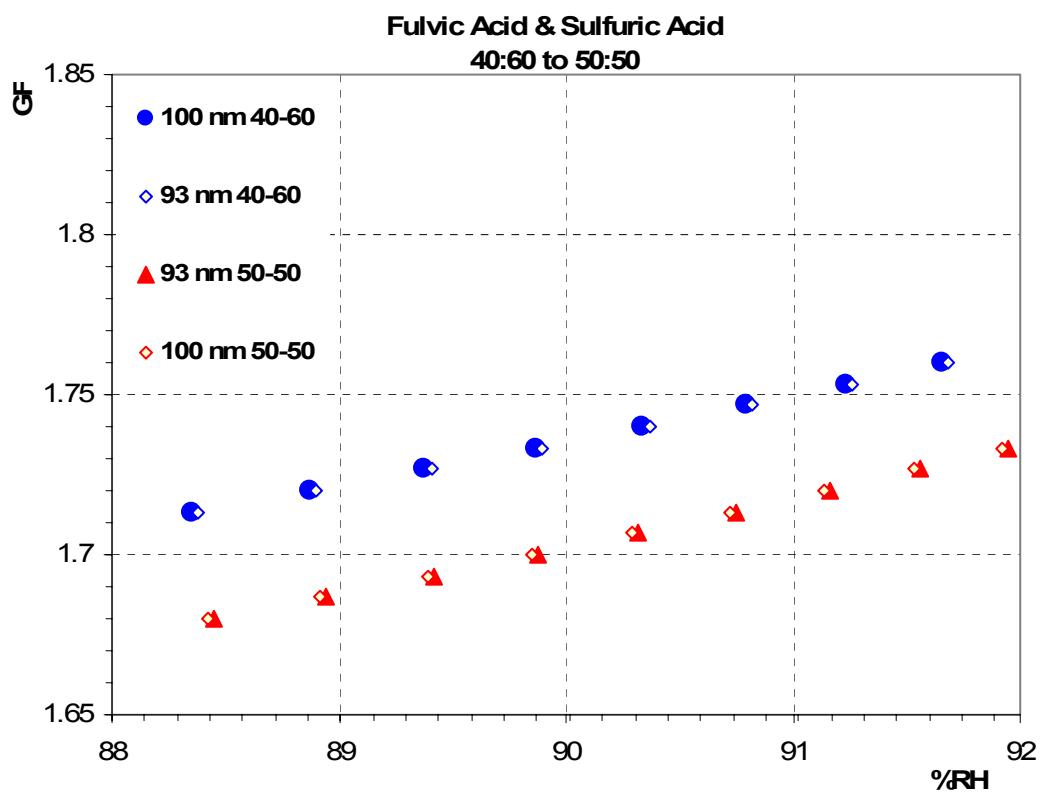
Figure A.6.6: Modeled hygroscopic particle growth with initial composition of 40:60 (mass ratio) fulvic acid-sulphuric acid and preferential desorption of sulphuric Acid.

Not surprisingly, this test confirms that the ratio between soluble and insoluble material in a particle highly influences the hygroscopic growth (Kulmala et al.,1996; Swietlicki et al., 1999). The thermally processed particle is in that case less hygroscopic than the original particle. The change in HGF is of the order of 3%, regardless of the particle size. The Raoult effect is there much more efficient than the Kelvin effect to modify hygroscopic growth as shown by results of other sensitivity tests with 93 nm particle with identical composition of the original particle and for 100 nm particle with modified chemical composition. It should be noticed that the modelled growth factor at 90%RH of pure sulphuric acid 100 nm particles is about 1.80 (Topping et al., 2005).

We can obviously perform the opposite test to increase particle HGF. The original particle is this time originally composed of 40% sulphuric acid and 60% fulvic acid (calculated parameters are shown in Figure A.6.7).
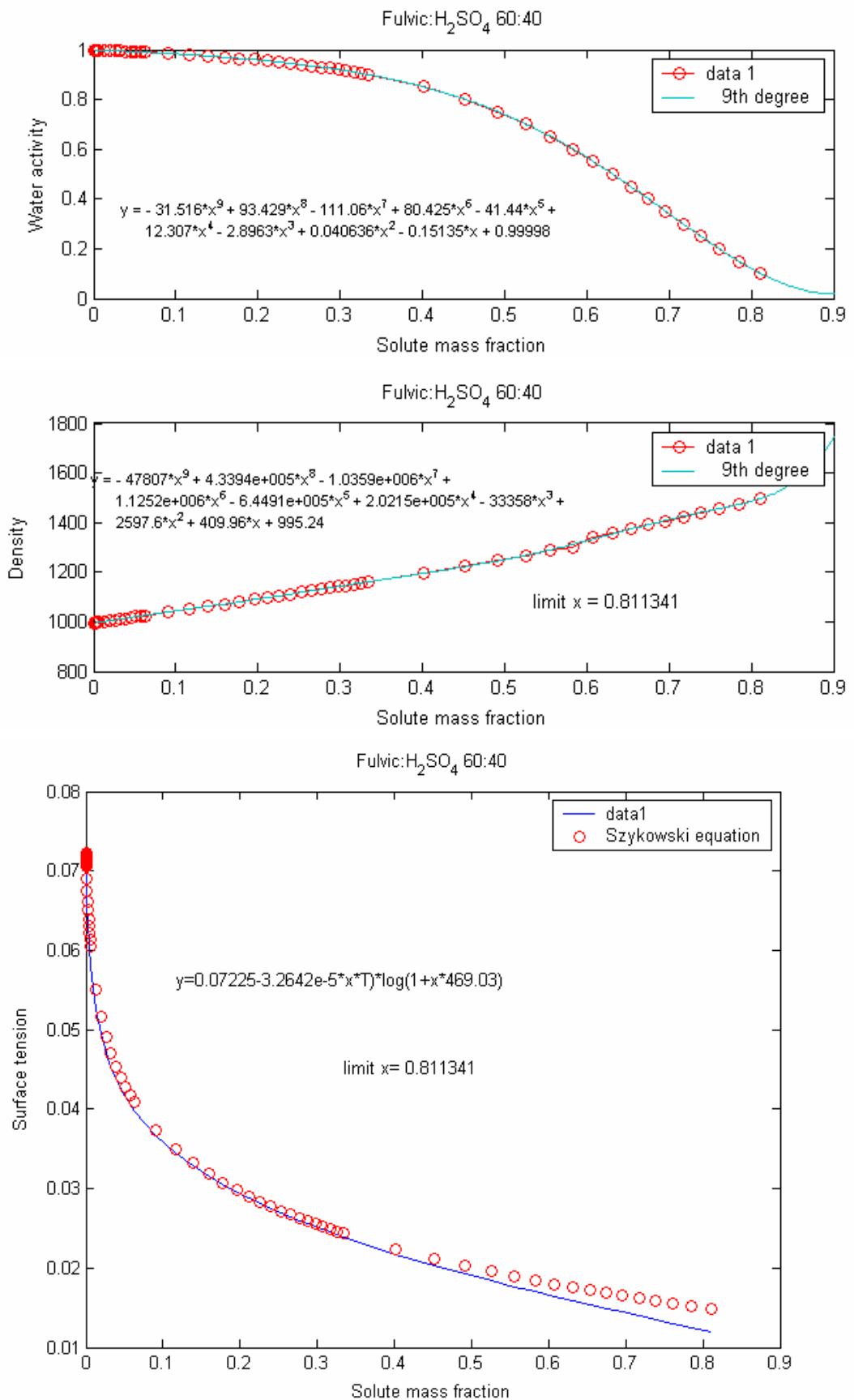
Figure A.6.7: Modeled functional fits of water activity, density and surface tension for Fulvic-Sulphuric Acid particle composition (60:40 in mass) used in the sensitivity test.

Preferential desorption of 1/3 fulvic acid during the thermal processing leads to a particle composed of equal quantities of fulvic and sulphuric acids and to an increase in hygroscopic growth (Figure A.6.8).
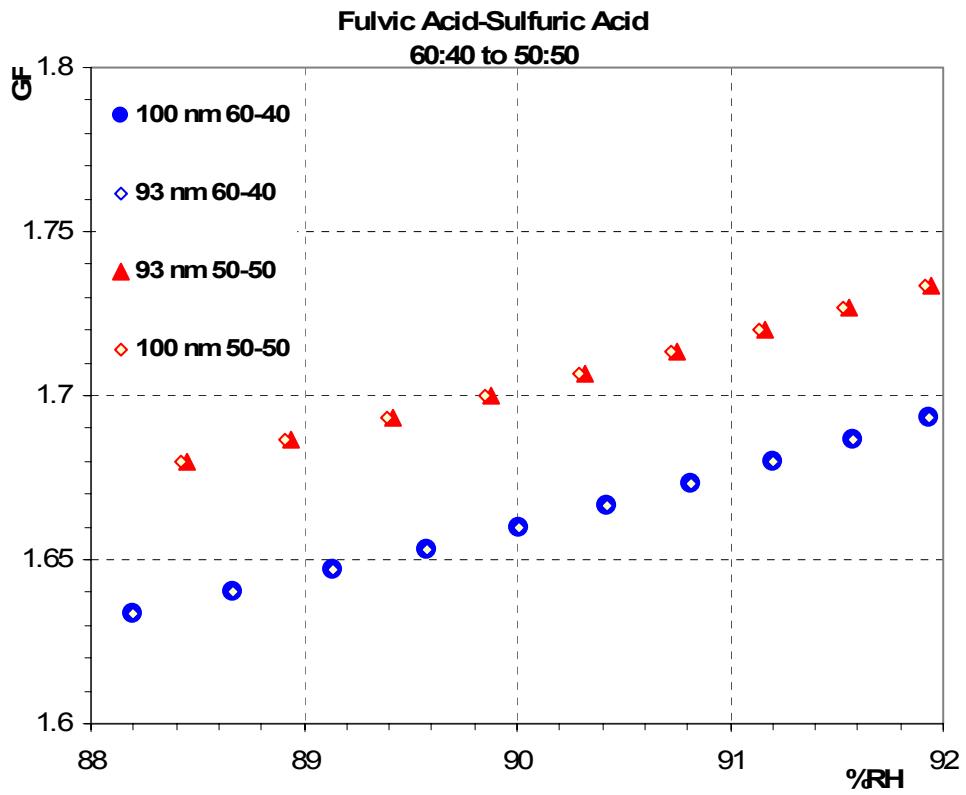
Figure A.6.8: Modeled hygroscopic particle growth with initial composition of 60:40 (mass ratio) fulvic acid-sulphuric acid and preferential desorption of fulvic Acid.

For a diameter reduction of 7% as respect to the original diameter (20% by volume), the new HGF is 1.7 at 90% RH as respect to the original value of 1.66. Note that this change in HGF is again, independent of particle size.

In conclusion, we can see that, change in HGF of a few % (both positive and negative) can be obtained by changes in the particle composition. Obviously, because the numerical simulations are performed with a mixture of completely hydrophobic and completely hygroscopic compounds, the resulting HGF is maximized. Yet, it is of the same order of magnitude (and sometime even lower) than measured values for natural aerosol.

5. Discussion

This numerical simulation has to be considered as the maximum change of HGF due to the Raoult effect. In fact, we considered a mixture of totally soluble and totally hydrophobic substances which is not representing natural aerosols. We therefore believe that, in addition to the Raoult effect due to preferential desorption of the most volatile components of the particles, an additional surface effect is taking place. Other hypotheses, such as changes in the chemical structure of particles (i.e. polymerization) induced by heating cannot be excluded at this point, but appear less straightforward to account for both positive and negative changes.

This surface effect is due to thermo-desorption of semi-volatile compounds present on the particle surface. As shown by laboratory experiments (Villani et al., 2006b), the VH-TDMA has been used to measure significantly different growth factors for a hygroscopic core (GF=2) and for the same coated core with a hydrophobic coating (GF=1). The VH-TDMA is then capable of removing the surface coating of the hydrophobic material without altering the HGF of the inner core material. This implies that chemical properties of the particle coating material influences hygroscopic growth. The specific properties of surface material are not resolved in most hygroscopic growth models.

The behaviour of particles in a humid environment is therefore both dependent upon both the bulk chemical composition and the composition of the particle surface layer. For the specific cases studied in this work, we can formulate the following hypotheses:

1- Disappearance of the more hygroscopic mode of Free Tropospheric aerosol at PDD might be linked to volatilization of HNO_3 present on the particle surface. Chemical analyses of particles sampled simultaneously at PDD with both ambient and heated inlets indicate a clear loss of NO_3^- after thermo-desorption at 70°C. Presence of HNO_3 on the particle surface, even at low concentration, is likely to increase hygroscopic growth. After removal of HNO_3, the more hygroscopic particles have HGF similar to the moderately hygroscopic particles.

2- Increase in HGF after thermo-desorption of the moderately hygroscopic particles at Cezeaux/Clermont-Ferrand, Hyytiala and for both moderately hygroscopic and hygroscopic particles at Mace Head may be resulting from

volatilization of hydrophobic organic substances from the particle surface. The nature of the thermo-desorbing material is unknown in that case but can certainly be of both biogenic (Mace Head and Hyytiala) and anthropogenic (Clermont-Ferrand) origins. Investigation of the chemical nature of the thermo-desorbing material would be of great interest.

6. Conclusions

We have shown in our study that, under some air mass conditions, gentle thermal processing of aerosol particles can lead to significant changes of the hygroscopic growth factor. These changes are either positive (thermally processed particles are more hygroscopic than the original ones) or negative (thermally processed particles are less hygroscopic than the original ones). These changes are, in some cases, significant.

Using numerical modelling of hygroscopic growth, we have shown that the Kelvin effect alone cannot explain our findings. We have simulated hygroscopic growth for internally mixed particles composed of fulvic and sulphuric acids, one totally hydrophobic and the other totally soluble. Results showed that preferential removal of one component leads to increased of decreased HGF values in the range of those measured in the field.

Because numerical modelling considers a mixture of totally soluble and totally hydrophobic substances, results of the simulation provide maximum estimates for the Raoult's effect. We therefore believe that an additional surface effect is taking place due to preferential desorption of the volatile fraction present on the particle surface. Other hypotheses, such as changes in the chemical structure of particles (i.e. polymerization) induced by heating cannot be excluded at this point, but appear less straightforward to account for both positive and negative changes. At puy de Dôme, we have evidences that disappearance of the hygroscopic mode is linked to volatilization of HNO_3. At Hyytiala, Mace Head and Clermont-Ferrand, volatilization of hydrophobic substances lead to higher HGF only for the Class I mode.

The surface effect on particle growth is therefore of potential significant effect on hygroscopic growth. Because the link between hygroscopic growth and CCN activity is not linear, it is difficult at this point to predict the surface affect on CCN activation.

Acknowledgments

References

Andrews, E. and Larson, S. M. (1993). Effect of surfactant layers on the size changes of aerosol particles as a function of relative humidity. Environ. Sci. Technol. 27, 857-865.

Ansari, A. S., Pandis, S. N. (2000). Water absorption by secondary organic aerosol and its effect on inorganic aerosol behavior. Env. Sci. and Technology 34, 71-77.

Brooks, S. D., Garland, R. M., Wise, M. E., Prenny, A. J., Cushing, M., Hewitt, E., Tolbert, M. A. (2003). Phase changes in internally mixed maleic acid/ammonium sulfate aerosols. J. Geophys. Res. 108, D15, 4487.

Cantrell, W., Shaw, G., Benner, R. and Veazey, D. (1997). Evidence for sulfuric acid coated particles in the arctic air mass. Geophys. Res. Lett. 24 (23), 3005-3008.

Chen, Y. Y., Lee W. M. G. (1999). Hygroscopic properties of inorganic-salt aerosol with surface-active organic compounds. Chemosphere 38 (10), 2431-2448.

Corrigan, C. E. and Novakov, T. (1999). Cound condensation nucleus activity of organic compounds: a laboratory study. Atmos. Environ. 33, 2661-2668.

Cruz, C. N., Pandis, S. N. (1998). The effect of organic coatings on the cloud condensation nuclei activation of inorganic atmospheric aerosol. J. Geophysical Res. 103, D13, 111-123.

Cruz, C. N., Pandis, S. N. (2000). Deliquescence and hygroscopic growth of mixed inorganic-organic atmospheric aerosol. Environ. Sci. Technol. 34, 4313-4319.

Decesari, S., Facchini, M. C., Mircea, M., Cavalli, F., Fuzzi, S. (2003). Solubility properties of surfactants in atmospheric aerosol and cloud/fog water samples. J. Geophysical Res. 108, D21, 4685.

Dua, S. K., Hopke, P. K., Raunemaa, T. (1998). Hygroscopicity of diesel aerosols. Water Air and Soil Pollution. 112: 247-257.

Gysel, M., Weingartner, E. and Baltensperger, U. (2002). Hygroscopic of aerosol particles at low temperature. 2. Theoretical and experimental hygroscopic properties of laboratory generated aerosols. Environ. Sci. Technol. 36, 63-68.

Hameri, K., Rood, M. J., Hansson, H. C. (1992). Hygroscopic properties of a NaCl aerosol coated with organic compounds. J. Aerosol Sci. 23, S437-S440.

Hameri, K., Charlson, R. J., Hansson, H. C., Jacobson, M. (1997). Hygroscopic properties of ammonium sulphate aerosols mixed with slightly soluble organic compound. J. Aerosol Sci. 28 (S1), S153-S154.

Hänel, G. (1976) The properties of atmospheric aerosol as function of the relative humidity at the thermodynamic equilibrium with the surrounding moist air. *Adv. in Geophys.* **19**, 74–183.

Hanssson, H. C., Rood, M. J., Koloutsou-Vakakis, S., Hameri, K., Orsini, D., Wiedensohler, A., (1998). NaCl aerosol particle hygroscopicity dependence on mixing with organic compounds. J. Atmos. Chemistry 31:321-346.

Hennig, T., Massling, A., Brechtel, F. J., Wiedensohler, A. (2005). A tandem DMA for highly temperature-stabilized hygroscopic particle growth measurement between 90% nd 95% relative humidity, Aerosol Sci. 36, 1210-1223.

Huff Hartz, K. E., Tischuk, J. E., Chan, M. N., Chan, C. K., Donahue, N. M., Pandis, S. N. (2006). Cloud condensation nuclei activation of limited solubility organic aerosol. Atmos. Environ. 40,605-617.

Johnson, G. R., Ristovski, Z. and Morawska, L. (2004). Method for measuringthe hygroscopic behaviour of lower volatility fractions in an internally mixed aerosol. J. Aerosol Sci. 35, 443-455.

Joutsensaari, J., Vaattovaara, P., Vesterinen, M., Hameri, K., Laaksonen, A. (2001). A novel tandem differential mobility analyser with organic vapor treatment of aerosol particles. Atmos. Chem. Phys., 1, 51-60.

Kerminem, V. M. (1997). The effects of particle chemical character and atmospheric processes on particle hygroscopic properties. J. Aerosol Sci. 28, 121-132.

Kohler, H. (1936). The nucleus and growth of hygroscopic droplets. Trans. Faraday Soc. 32, 1152-1161.

Kotzick, R., Niessner, R. (1999). The effects of aging processes on critical supersaturation ratios of ultrafine carbon aerosols. Atmos. Environ. 33, 2669-2677.

Kramer, L., Poschl, U., Niessner, R. (2000). Microstructural rearrangement of sodium chloride condensation aerosol particles on interaction with vapor. J. Aerosol Sci. 6, 673-685.

Kreidenweis, S. M., Koehler, K., DeMott, P., Prenni, A. J., Carrico, C., Ervens, B. (2005). Water activity and activation diameters from hygroscopicity data-Part I: Theory and application to inorganic salts. Atmos. Chem. Phys. Discuss. 5, 287-323.

Lehmann, K., Massling, A., Tilgner, A., Mertes, S., Galgon, D.,Wiedensohler, A. (2005). Size-rsolved soluble volume fractions of submicrometer particles in air masses of different character. Atmos. Environment 39, 4257-4266.

Massling, A., Wiedensohler, A., Bush, B. (1999). Concept of an advanced hygroscopic tandem differential mobility analyser with a great operation stability. J. Aerosol Sci. 30 (S1) S395-S396.

Massling, A., Stock, M., Wiedensohler, A. (2005). Diurnal, weekly and seasonal variation of hygroscopic properties of submicrometer urban aerosol particles. Atmos. Environment 39, 3911-3922.

McMurry, P. H., Litchy, M., Huang, P. F., Cai, X., Turpin, B. J., Dick, W. D., Hanson, A. (1996). Elemental composition and morphology of individual particles separated by size and hygroscopicity with the TDMA. Atmos. Environment 30, 101-108.

Mircea, M., Facchini, M. C., Decesari, S., Cavalli, F., Emblico, L., Fuzzi, S., Vestin, A., Rissler, J., Swietlicki, E., Frank, G., Andreae, M. O., Maenhaut, W., Rudich, Y., Artaxo, P. (2005). Importance of the organic aerosol fraction for modeling aerosol hygroscopic growth and activation: a case study in the Amazon Basin. Atmos. Chem. Phys. Discuss. 5, 5253-5298.

Mikhailov, E., Vlasenko, S., Niessner, R., Poschl, U. (2003). Interaction of aerosol particles composed of protein and salts with water vapor: hygroscopic growth and microstructural rearrangement. Atmos. Chem. Phys. Discuss. 3, 4755-4832.

Prenny, A. J., DeMott, P. J., Kreidenweis, S. M. (2003). Water uptake of internally mixed particles containing ammonium sulfate and dicarboxylic acids. Atmos. Environment 37, 4243-4251.

Sellegri, K., Laj, P., Peron, F., Dupuy, R., Legrand, M., Preunkert, S., Putaud, J.-P., Cachier, H. and Ghermandi, G. (2003). Mass balance of free tropospheric aerosol at the Puy de Dome (France) in winter. J. Geophys. Res. Lett. 108 (D11), 4333.

Svenningsson, B., Rissler, J., Swietlicki, E., Mircea, M., Bilde, M., Facchini, M. C., Decesari, S., Fuzzi, S., Zhou, J., Monster, J., Rosenorn, T. (2005). Hygroscopic growth and critical supersaturations for mixed aerosol particles of inorganic and organic compounds of atmospheric relevance. Atmos. Chem. Phys. Discuss. 5, 2833-2877.

Swietlicki, E., Zhou, J., Berg, O. H., Martinsson, B. G., Frank, G., Cederfelt, S. I., Dusek, U., Berner, A., Birmili, W., Wiedensohler, A., Yuskiewicz, B., Bower, K. N. (1999). A closure study of sub-micrometer aerosol particle hygroscopic behaviour. Atmos. Research 50, 205-240.

Topping, D. O., G. B. McFiggans and H. Coe (2005), A curved multi-component aerosol hygroscopicity model framework: Part 1 - Inorganic compounds, Atmos. Chem. Phys., 5, 1205-1222

Topping, D. O., G. B. McFiggans and H. Coe (2005), A curved multi-component aerosol hygroscopicity model framework: Part 2 - Including organic compounds, Atmos. Chem. Phys., 5, 1223-1242.

Weingartner, E., Gysel, M. and Baltensperger, U. (2002). Hygroscopic of aerosol particles at low temperature. 1. New low-temperature H-TDMA instrument: setup and first applications. Environ. Sci. Technol. 36, 55-62.

Weingartner, E., Burtscher, H. and Baltensperger, U. (1996). Hygroscopic properties of carbon and diesel soot particles. Atmos. Environment 31 (15) 2311-2327.

Conclusions et perspectives

Ce travail se concentre sur le développement et l'application de la technique du « Tandem Differential Mobility Analyser » (TDMA) pour étudier, par classe de taille, l'aérosol submicronique et ses propriétés physico-chimiques. En principe, un TDMA est constitué d'un premier DMA (Differential Mobility Analyser) qui sélectionne une fraction monodispersée en taille de l'aérosol, d'une unité de conditionnement pour modifier l'aérosol et d'un analyseur, constitué d'un second DMA et d'un CPC (Condensation Particle Counter), pour mesurer les changements de la fraction d'aérosol sélectionnée.

Jusqu'ici, un certain nombre d'études ont employé soit la technique de volatilité pour déterminer avec une courte échelle de temps la fraction non volatile de l'aérosol submicronique en fonction de la taille et de la température (ie. V-TDMA), soit la technique d'hygroscopicité pour étudier la croissance hygroscopique de l'aérosol en fonction de l'humidité relative (ie. H-TDMA). L'objectif de ce travail a été de combiner les techniques de volatilité et d'hygroscopicité de l'aérosol dans le but de mieux comprendre sa structure et ses propriétés. Différentes étapes ont été nécessaires pour arriver à la réalisation d'un appareil de mesures avancé : un « Volatility-Hygroscopicity-TDMA » (VH-TDMA).

Une grande partie de ce travail a été basée sur la conception, le dessin et la réalisation de chaque élément du système (sauf les CPCs). Concernant le dessin de chaque élément, nous avions pour contraintes de pouvoir utiliser le système avec un minimum de maintenance, une stabilité élevée pour les mesures des différents paramètres ainsi qu'une facilité de transport et d'utilisation durant les campagnes intensives. Une attention particulière a été portée sur les éléments de sélection de la taille et de conditionnement de l'aérosol dans l'appareil pour une évaluation précise de la qualité de la mesure.

En premier lieu, nous avons procédé à l'optimisation et à la réalisation d'un DMA au LaMP. Les résultats issus des expériences en laboratoire montrent que le dispositif redessiné augmente les performances du DMA. En plus de la géométrie et du dessin du DMA utilisé, les débits de l'air propre, de l'air en excès et de l'échantillon définissent la précision de la mobilité électrique appliquée et donc le diamètre de la particule sélectionnée. Pour cette raison, un système compact de flux et un mécanisme de régulation ont été développés pour contrôler et ajuster les flux à l'intérieur du TDMA. Finalement, la stabilité des flux garantit la haute qualité des données obtenues.

Le nouveau dessin du Volatility-TDMA (6-VTDMA) (Dupuy, 2003) et l'expérience acquise nous a permis de développer et de construire un nouvel instrument pour mesurer les

changements dans le comportement hygroscopique des particules comme les composés volatiles qui sont enlevés par processus thermique. Le nouveau système, combinant le conditionnement de la température et de l'humidité, a été appelé VH-TDMA.

Les deux instruments ont été testés et calibrés au laboratoire pour tenir compte de la perte de particules dans les lignes d'échantillonnage due à la diffusion et la thermophorèse. L'efficacité de transport diminue avec une diminution de la taille de la particule et une augmentation de la température. De façon schématique, dans le V-TDMA à température ambiante (25°C), 100% des particules avec un diamètre de 100 nm traversent le système alors qu'à 500°C, cette valeur passe à 88%. Suivant la température, l'efficacité de transport dans les deux systèmes diminue à 50% pour les particules dont le diamètre est compris entre 20 et 25 nm. Cela suggère de grandes incertitudes pour les mesures TDMA des particules ayant un diamètre inférieur à 20 nm.

De plus, des mesures en laboratoire ont été réalisées pour tester la volatilité d'aérosols artificiels, ayant une composition connue, dans le V-TDMA. Nous avons trouvé des températures de volatilisation caractéristiques pour des particules de diamètre supérieur à 150nm. En commençant à 30°C, le nitrate d'ammonium est volatile (aussi bien à 60°C pour les plus grosses particules). A 180°C, tout les composés sulfatés dont le sulfate d'ammonium sont complètement évaporés.

Ces résultats sur la volatilité des particules quasi-monodispersées sont nouveaux car les températures de volatilité sont considérablement plus basses que celles trouvées dans les études précédentes sur le chauffage d'une population entière d'aérosols, nous proposons d'ailleurs de mieux standardiser les mesures de volatilité des particules. A 280°C, les composés volatiles additionnels (dans les aérosols atmosphériques), eg. Les carbones organiques les plus volatiles, sont évaporés dans le système V-TDMA (Novakov et al., 1997). Les composés réfractaires restants sont considérés non-volatiles, comprenant du carbone non-volatile et peut être des composés organiques moins volatiles. Il a été trouvé que les matériaux non-volatiles, comme les sels marins ou le nitrate de sodium, sont évaporés dans le V-TDMA à 650°C et 550°C respectivement. Nous avons également démontré que chauffer doucement les particules couvertes de DEHS (ie. Di-Ethyl-Hexyl-Sebacate) peut être utilisé pour retirer la couche d'espèces semi volatiles de la surface de la particule si le noyau de l'aérosol est moins volatile que la couche de surface. De plus, ces expériences avec le V-TDMA montrent qu'il n'y a pas de recondensation de la fraction volatilisée après le conditionnement thermique.

Finalement, le système VH-TDMA a été testé pour ses incertitudes sur l'humidité relative et ses performances pendant le premier workshop européen sur l'intercalibration des H-TDMA à l'Institut pour la recherche Troposphérique (IfT) à Leipzig (Allemagne) sous le programme ACCENT NoE.

Nous avons ensuite testé et démontré, pendant les expériences en laboratoire, la capacité du VH-TDMA à mesurer le facteur de grossissement hygroscopique du diamètre des aérosols constitués d'un noyau de NaCl recouvert de DEHS. Ces expériences en laboratoire ont montré que :

1) l'hygroscopicité des aérosols recouverts de DEHS est significativement différente de celle avec juste un noyau de NaCl.

2) le processus thermique est très efficace pour retirer la couche d'espèces semi volatiles de la surface des particules.

Basé sur les résultats des particules d'aérosols synthétiques, la prochaine étape de notre travail a été d'appliquer la technique VH-TDMA pour étudier le comportement hygroscopique des particules naturelles et thermo-désorbées dans différents environnements : proche des sources d'émission (en zone urbaine à Clermont Ferrand (France), dans l'environnement côtier de Mace Head (Irlande) et dans la forêt boréale de la station d'Hyytiälä (Finlande)) et loin des sources d'émission (sur le site en troposphère libre du puy de Dôme (France) et dans les masses d'air anthropiques échantillonnées à Mace Head (Irlande)). Ces études ont l'avantage de présenter des facteurs de grossissement hygroscopique de différents types d'aérosols échantillonnés à différents endroits avec le même instrument. Par conséquent, ces différents facteurs peuvent être comparés directement, ce qui est difficilement le cas dans la littérature sur les facteurs de grossissement hygroscopique à cause des différences opérationnelles significatives entre les instruments.

Dans l'atmosphère, la distribution des matériaux inorganiques et organiques au sein des particules d'aérosols varie considérablement dans l'espace et le temps et dépend en premier de ses sources (eg. Processus de combustion dans le cas du carbone non volatile). Cependant, dû au mélange des populations d'aérosols issues des différentes sources et des processus de transformation (eg. Condensation, nucléation, coagulation et photo-oxydation), la composition et la structure de l'aérosol est altérée substantiellement, de façon dépendante du nombre de sources et de la distance depuis les sources. Nos principaux résultats mettent en évidence la complexité de l'aérosol naturel, lequel est rarement composé d'un unique mélange d'aérosols inorganique/organique pour une taille donnée. Cependant, des caractéristiques principales des aérosols ont été mesurées, qui sont communes à tous les environnements :

❖ Sur tous les sites, les particules d'aérosols naturels du mode d'accumulation ne sont jamais pures, même sur les sites représentatifs d'une source unique (Mace Head avec un secteur propre). En fait, la plupart des sites montrent à 100 nm soit un mélange externe de particules modérément hygroscopique avec quelques particules hydrophobes dans les masses d'air polluées (Cézeaux, Leipzig et masses d'air polluées rencontrées au puy de Dôme et à Mace Head) soit des particules hygroscopiques dans les masses d'air propres originaires de secteurs marins à Mace Head et au puy de Dôme. Il n'y a qu'à Hyytiälä que le mode à 100 nm est constitué d'un unique mélange interne d'aérosol soit modérément hygroscopique soit hydrophobique.

❖ A Hyytiälä, les propriétés hydrophobes des particules sont acquises lorsqu'un évènement de formation de nouvelles particules se déroule et les nouvelles substances organiques se condensent sur les clusters crées, aussi bien que sur les plus grosses particules comme celles de 100 nm que nous avons étudiées. Ce phénomène a été également observé dans d'autres environnements où la formation de nouvelles particules se fait, comme le puy de Dôme ou Mace Head.

❖ Comme résultat commun entre les sites, nous avons été capable d'observer que l'aérosol âgé avait tendance à acquérir des propriétés modérément hygroscopiques. Cela a clairement été observé soit la nuit sur les sites où les sources locales d'aérosols secondaires étaient présentes seulement la journée (Hyytiälä, puy de Dôme, Cézeaux, Mace Head/secteur de vent européen continental) soit tout le temps sur les sites éloigné des sources.

❖ La présence de deux modes hygroscopique constamment observés dans les zones urbaines conduit à des questions concernant la formation de particules. L'origine du mode le plus hygroscopique est toujours incertaine et peut être liée au transport longue distance ou le résultat d'un processus d'oxydation rapide de l'aérosol le moins hygroscopique. Ce constat est d'une grande importance pour la définition de la meilleure stratégie pour limiter les niveaux PM en zones urbaines.

Nous avons montré dans notre étude que, sous certaines conditions de masses d'air, un faible chauffage des particules d'aérosols atmosphériques peut conduire à des changements

significatifs du facteur de grossissement hygroscopique. Ces changements peuvent être positifs (les particules chauffées sont plus hygroscopiques que celles d'origine) ou négatifs (les particules chauffées sont moins hygroscopiques que celles d'origine). Le HGF des particules hydrophobes (classe I) est augmenté par la thermo-désorption à Mace Head pour les masses d'air continentales, au Cézeaux la nuit et à Hyytiälä. Il est probable que les composés volatilisés présents dans la couche de surface de la particule sont plus hydrophobes que la particule elle-même. Le chauffage des particules modérément hygroscopiques (classe II) conduit soit à une augmentation du HGF à Mace Head soit à une diminution du HGF aux Cézeaux. Le HGF des particules hygroscopiques (classe III) est généralement diminué après le chauffage excepté à Mace Head. Au puy de Dôme, nous avons mis en évidence que la disparition du mode hygroscopique est liée à la volatilisation du HNO_3. Il est clair que le nouveau VH-TDMA est un outil très utile pour mieux comprendre la structure des particules et son rôle dans la croissance hygroscopique.

Finalement, en utilisant un modèle numérique de croissance hygroscopique, nous avons montré que l'effet Kelvin seul ne pouvait pas expliquer nos observations. Nous avons simulé le croissance hygroscopique pour des particules en mélange interne, des aérosols totalement hydrophobes et d'autre complètement solubles. Les résultats montrent que le retrait préférentiel de ces composés conduit à une augmentation ou une diminution de la valeur du HGF dans la gamme de celles mesurées en campagne. Dû au fait que le modèle numérique considère un mélange de substances totalement soluble et hydrophobe, les résultats de la simulation apportent des estimations de l'impact maximal de l'effet Raoult. Il est clair que, si notre étude apporte des réponses sur l'importance des propriétés de surface des particules par rapport à leur capacité CCN, quelques points restent encore à être compris.

D'abord, l'hygroscopicité d'un mélange complexe d'espèces chimiques ne force pas la somme équilibrée de hygroscopicités des divers composants du mélange. Nous croyons donc qu'un effet de surface additionnel a lieu dû à l'effet préférentiel de la fraction volatile présente sur la surface de particules. Des mesures avancées, dans des conditions plus contrôlées, sur des particules synthétiques en mélange interne seraient extrêmement utiles.

Puisque le lien entre la croissance hygroscopique et l'activité CCN n'est pas linéaire, il est difficile actuellement de prévoir de quelle façon la surface affecte sur l'activation des CCNs. Il aurait été intéressant, dans cette étude, d'effectuer une mesure indépendante de l'activité CCN des particules d'aérosol comparées aux particules thermo-désorbées (ie. DMA-V-CCN).

A l'avenir, il sera nécessaire de s'orienter sur des mesures parallèles d'activité CCN et des propriétés hygroscopiques des particules en fonction de la quantité de composants volatiles et non-volatiles de l'aérosol.

De façon générale, il s'avère que notre étude souligne le besoin d'une approche plus complète de la matière particulaire dans l'atmosphère. Ceci inclut la nécessité d'une information avec d'avantage de critères et donc pas limitée aux paramètres mesurés et réglés pour les PM10. L'utilisation de la volatilité à 280°C, dans des conditions calibrées, doit être poursuivie car elle permet, d'une manière très simple, d'accéder à la fraction réfractaire (à lier à l'EC) des particules. Les mesures hygroscopiques et V-Hygroscopiques peuvent également fournir une information très valide sur les sources de particules et leur évolution dans l'atmosphère. Nous préconisons donc fortement une utilisation plus étendue de ces paramètres même pour des activités de surveillance de la qualité de l'air. Les développements exigés pour l'usage de TDMAs dans les activités de surveillance peuvent sembler trop complexes actuellement mais le développement d'une nouvelle génération de TDMAs, plus simples et rentables, dans le cadre du programme d'EUSAAR peut être une première étape vers une utilisation plus large de ces techniques très utiles.

Références bibliographiques

Adachi M., Kousaka Y. and Okuyama K. (1985). Unipolar and bipolar diffusion charging of ultrafine aerosol particles. *J. Aerosol Science*. 16-2, 109-123.

Andrews, E. and Larson, S. M. (1993). Effect of surfactant layers on the size changes of aerosol particles as a function of relative humidity. Environ. Sci. Technol. 27, 857-865.

Ankilov, A., Baklanov, A., Colhoun, M., Enderle, K. H., Gras, J., Julanov, Y., Kaller, D., Lindner, A., Lushnikov, A. A., Mavliev, R., McGovern, F., O'Connor, T. C., Podzimek, J., Preining, O., Reischl, R., Rudolf, R., Sem, G. J., Szymanski, W. W., Vrtala, A. E., Wagner, P. E., Winklmayr, W., Zagaynov, V. (2002). Particle size dependent response of aerosol counters. J. Atmos. Research. 62, 209-237.

Ankilov, A., Baklanov, A., Colhoun, M., Enderle, K. H., Gras, J., Julanov, Y., Kaller, D., Lindner, A., Lushnikov, A. A., Mavliev, R., McGovern, F., O'Connor, T. C., Podzimek, J., Preining, O., Reischl, R., Rudolf, R., Sem, G. J., Szymanski, W. W., Vrtala, A. E., Wagner, P. E., Winklmayr, W., Zagaynov, V. (2002). Intercomparison of number concentration measurements by various aerosol particle counters. J. Atmos. Research. 62, 177-207.

Ansari, A. S., Pandis, S. N. (2000). Water absorption by secondary organic aerosol and its effect on inorganic aerosol behavior. Env. Sci. and Technology 34, 71-77.

Banse, D. F., Esfeld, K., Hermann, M., Sierau, B., Wiedensohler, A. (2000). Particle counting efficiency of the TSI CPC 3762 for different operating parameters. J. Aerosol Sci. 32, 157-161.

Birmili, W., Stratmann, F. and Wiedensohler, A. (1999). Design of a DMA-based spectrometer for a large particle size range and stable operation. J. Aerosol Sci. 30 (4), 549-553.

Birmili, W., Stratmann, F., Wiedensohler, A., covert, D., Russell, L. M. (1997). Determination of Differential Mobility Analyser Transfer Functions using identical instruments in series. Aerosol Sci. and Techno. 27:215-223.

Brooks, S. D., Garland, R. M., Wise, M. E., Prenny, A. J., Cushing, M., Hewitt, E., Tolbert, M. A. (2003). Phase changes in internally mixed maleic acid/ammonium sulfate aerosols. J. Geophys. Res. 108, D15, 4487.

Brooks, B. J., Smith, M. H., Hill, M. K., O'Dowd, C. D. (2002). Size-differentiated volatility analysis of internally mixed laboratory-generated aerosol. J. Aerosol Sci. 33, 555-579.

Burtscher, H., Baltensperger, U., Bukowiecki, N., Cohn, P., Huglin, C., Mohr, M., Matter, U., Nyeki, S., Scmatloch, V., Streit, N., Weingartner, E. (2001). Separation of volatile and non-volatile aerosol fractions by thermodesorption: instrumental development and applications. J. Aerosol Sci. 32, 427-442.

Cantrell, W., Shaw, G., Benner, R. and Veazey, D. (1997). Evidence for sulfuric acid coated particles in the arctic air mass. Geophys. Res. Lett. 24 (23), 3005-3008.

Chen, D. R., Pui, Y. H., Mulholland, W. and Fernandez, M. (1999). Design and testing of an aerosol/sheath inlet for high resolution measurements with a DMA. J. Aerosol Sci. 30 (8), 983-999.

Chen, Y. Y., Lee W. M. G. (1999). Hygroscopic properties of inorganic-salt aerosol with surface-active organic compounds. Chemosphere 38 (10), 2431-2448.

Chen, D. R., Pui, Y. H., Hummes, D., Fissan, H., Quant, F. R. and Sem, G. J. (1998). Design and evaluation of a nanometer aerosol differential mobility analyzer (Nano-DMA). J. Aerosol Sci. 29 (5/6), 497-509.

Collins, D. R., Nenes, A., Flagan, R. C. and Seinfeld, J. H. (2000). The scanning flow DMA. J. Aerosol Sci. 31 (10), 1129-1144.

Corrigan, C. E. and Novakov, T. (1999). Cound condensation nucleus activity of organic compounds: a laboratory study. Atmos. Environ. 33, 2661-2668.

Cruz, C. N., Pandis, S. N. (1998). The effect of organic coatings on the cloud condensation nuclei activation of inorganic atmospheric aerosol. J. Geophysical Res. 103, D13, 111-123.

Cruz, C. N., Pandis, S. N. (2000). Deliquescence and hygroscopic growth of mixed inorganic-organic atmospheric aerosol. Environ. Sci. Technol. 34, 4313-4319.

Cubison, M. J., Coe, H., Gysel, M. (2005). A modified hygroscopic tandem DMA and a data retrieval method based on optimal estimation. Aerosol Sci. 36, 846-865.

Decesari, S., Facchini, M. C., Mircea, M., Cavalli, F., Fuzzi, S. (2003). Solubility properties of surfactants in atmospheric aerosol and cloud/fog water samples. J. Geophysical Res. 108, D21, 4685.

Dua, S. K., Hopke, P. K., Raunemaa, T. (1998). Hygroscopicity of diesel aerosols. Water Air and Soil Pollution. 112: 247-257.

Flagan, R. C. (1999). On differential mobility analyszer resolution. Aerosol Sci. and Technol. 30:556-570.

Flagan, R. C. (2004). Opposed migration aerosol classifier (OMAC). Aerosol Sci. and Technol. 38:890-899.

Gysel, M., Weingartner, E. and Baltensperger, U. (2002). Hygroscopic of aerosol particles at low temperature. 2. Theoretical and experimental hygroscopic properties of laboratory generated aerosols. Environ. Sci. Technol. 36, 63-68.

Hameri, K., Rood, M. J., Hansson, H. C. (1992). Hygroscopic properties of a NaCl aerosol coated with organic compounds. J. Aerosol Sci. 23, S437-S440.

Hameri, K., Koponen, I. K., Aalto, P. P., Kulmala, M. (2002). The particle detection efficiency of the TSI-3007 condensation particle counter. J. Aerosol Sci. 33, 1463-1469.

Hameri, K., Charlson, R. J., Hansson, H. C., Jacobson, M. (1997). Hygroscopic properties of ammonium sulphate aerosols mixed with slightly soluble organic compound. J. Aerosol Sci. 28 (S1), S153-S154.

Hänel, G. (1976) The properties of atmospheric aerosol as function of the relative humidity at the thermodynamic equilibrium with the surrounding moist air. *Adv. in Geophys.* **19**, 74–183.

Hanssson, H. C., Rood, M. J., Koloutsou-Vakakis, S., Hameri, K., Orsini, D., Wiedensohler, A., (1998). NaCl aerosol particle hygroscopicity dependence on mixing with organic compounds. J. Atmos. Chemistry 31:321-346.

Hennig, T., Massling, A., Brechtel, F. J., Wiedensohler, A. (2005). A tandem DMA for highly temperature-stabilized hygroscopic particle growth measurement between 90% nd 95% relative humidity, Aerosol Sci. 36, 1210-1223.

Hermann, M. and Wiedensohler, A. (1996). Modification and calibration of a TSI 7610 condensation particle counter for high altitude airborne measurements. J. Aerosol Sci. 27 (S1), S303-S304.

Hermann, M. and Wiedensohler, A. (1998). Dependence of the TSI 7610 condensation particle counter on pressure and temperature difference. J. Aerosol Sci. 29 (S1), S343-S344.

Hermann, M. and Wiedensohler, A. (2001). Counting efficiency of condensation particle counters at low-pressure with illustrative data from the upper troposphere. J. Aerosol Sci. 32, 957-991.

Huff Hartz, K. E., Tischuk, J. E., Chan, M. N., Chan, C. K., Donahue, N. M., Pandis, S. N., (2006). Cloud condensation nuclei activation of limited solubility organic aerosol. Atmos. Environ. 40,605-617.

Hudson, J. G. and Da, X. (1996). Volatility and size of cloud condensation nuclei. J. Geophys. Res. 101 (D2), 4435-4442.

IPCC (Intergovernmental Panel on Climate Change), (1995). Radiative forcing of climate change. In: Houghton, J. T., Meira Filha, L. G., Bruce, J., Hoesung, L., Callander, B. A., Haites, E., Harris, N., Maskell, K. (Eds.), Climate Change 1994. Cambridge University Press, Cambridge, pp. 1-231.

Jennings, S. G., O'Dowd, C. D., Cooke, W. F., Sheridan, P. J. and Cachier, H. (1994). Volatility of elemental carbon. Geophys. Res. Lett. 21 (16), 1719-1722.

Jokinen, V. and Makela, M. (1997). Closed-loop arrangement with critical orifice for DMA sheath/excess flow system. J. Aerosol Sci. 28 (4), 643-648.

Johnson, G. R., Ristovski, Z. and Morawska, L. (2004). Method for measuringthe hygroscopic behaviour of lower volatility fractions in an internally mixed aerosol. J. Aerosol Sci. 35, 443-455.

Joutsensaari, J., Vaattovaara, P., Vesterinen, M., Hameri, K., Laaksonen, A. (2001). A novel tandem differential mobility analyzer with organic vapor treatment of aerosol particles. Atmos. Chem. Phys., 1, 51-60.

Karlsson, M. N. A., Frank, G. and Martinsson, B. G. (2000). Measurement of the differential mobility analyser transfer function. J. Aerosol Sci. 31 (S1), S23-S24.

Karlsson, M. N. A. and Martinsson, B. G. (2003). Method to measure and predict the transfer function size dependence of individual DMAs. J. Aerosol Sci. 34, 603-625.

Kerminem, V. M. (1997). The effects of particle chemical character and atmospheric processes on particle hygroscopic properties. J. Aerosol Sci. 28, 121-132.

Kohler, H. (1936). The nucleus and growth of hygroscopic droplets. Trans. Faraday Soc. 32,1152-1161.

Kotzick, R., Niessner, R. (1999). The effects of aging processes on critical supersaturation ratios of ultrafine carbon aerosols. Atmos. Environ. 33, 2669-2677.

Knutson, E. O. and Whitby, K. T. (1975). Aerosol classification by electric mobility: apparatus, theory, and applications. J. Aerosol Sci. 6, 443-451.

Kramer, L., Poschl, U., Niessner, R. (2000). Microstructural rearrangement of sodium chloride condensation aerosol particles on interaction with vapor. J. Aerosol Sci. 6, 673-685.

Kreidenweis, S. M., Koehler, K., DeMott, P., Prenni, A. J., Carrico, C., Ervens, B. (2005). Water activity and activation diameters from hygroscopicity data-Part I: Theory and application to inorganic salts. Atmos. Chem. Phys. Discuss. 5, 287-323.

Kreidenweis, S. M., McInnes, L. M. and Brechtel, F. J. (1998). Observations of aerosol volatility and elemental composition at Maquarie Island during the First Aerosol Characterization Experiment (ACE 1). J. Geophys. Res. 103 (D13), 16511-16524.

LaFranchi, B. W., Knight, M., Petrucci, G. A. (2003). Leaching as a source of residual particles from nebulization of deionized water. J. Aerosol Sci. 34, 1589-1594.

Le Bronec, E., Renoux, A., Boulaud, D. and Pourprix, M. (1998). Use of a radial flow mobility analyser to determine the mass and density of aerosol particles. J. Aerosol Sci. 29 (S1), S409-S410.

Le Bronec, E., Renoux, A., Boulaud, D. and Pourprix, M. (1999). Effect of gravity in differential mobility analysers. A new method to determine the density and mass of aerosol particles. J. Aerosol Sci. 30 (1), 89-103.

Lehmann, K., Massling, A., Tilgner, A., Mertes, S., Galgon, D.,Wiedensohler, A. (2005). Size-rsolved soluble volume fractions of submicrometer particles in air masses of different character. Atmos. Environment 39, 4257-4266.

Londahl, J., Pagels, J., Swietlicki, E., Zhou, J., Ketzel, M., Massling, A., Bohgard, M. (2005). A set-up for field studies of respiratory tract deposition of fine and ultrafine particles in humans. J. Aerosol Sci.

Maisels, A., Kruis, F. E., Fissan, H. (2004). Coagulation in bipolar chargers. J. Aerosol Sci. 35, 1333-1345.

Massling, A., Wiedensohler, A., Bush, B. (1999). Concept of an advanced hygroscopic tandem differential mobility analyzer with a great operation stability. J. Aerosol Sci. 30 (S1) S395-S396.

Massling, A., Stock, M., Wiedensohler, A. (2005). Diurnal, weekly and seasonal variation of hygroscopic properties of submicrometer urban aerosol particles. Atmos. Environment 39, 3911-3922.

McMurry, P. H., Litchy, M., Huang, P. F., Cai, X., Turpin, B. J., Dick, W. D., Hanson, A. (1996). Elemental composition and morphology of individual particles separated by size and hygroscopicity with the TDMA. Atmos. Environment 30, 101-108.

Mertes, S., Schroder, F. and Wiedensohler, A. (1995). The particle detection efficiency curve of the TSI-3010 CPC as a function of the temperature difference between saturator and condenser. Aerosol Sci. and Technol. 23:257-261.

Mircea, M., Facchini, M. C., Decesari, S., Cavalli, F., Emblico, L., Fuzzi, S., Vestin, A., Rissler, J., Swietlicki, E., Frank, G., Andreae, M. O., Maenhaut, W., Rudich, Y., Artaxo, P. (2005). Importance of the organic aerosol fraction for modeling aerosol hygroscopic growth and activation: a case study in the Amazon Basin. Atmos. Chem. Phys. Discuss. 5, 5253-5298.

Mikhailov, E., Vlasenko, S., Niessner, R., Poschl, U. (2003). Interaction of aerosol particles composed of protein and salts with water vapor: hygroscopic growth and microstructural rearrangement. Atmos. Chem. Phys. Discuss. 3, 4755-4832.

O'Dowd, C. D. and al. (1992). A high temperature volatility technique for determination of atmospheric aerosol composition. J. Aerosol Sci. 23 (S1), S905-S908.

O'Dowd, C. D., Aalto, P. P., Yoon, Y. J., Hameri, K. (2004). The use of the pulse height analyser ultrafine condensation particle counter (PHA-UCPC) technique applied to sizing of nucleation mode particles of differing chemical composition. J. Aerosol Sci. 35, 205-216.

Orsini, D. A., Wiedensohler, A., Stratmann, F. and Covert, D. S. (1999). A new volatility tandem differential mobility analyzer to measure the volatile sulfuric acid fraction. J. Atmos. Oceanic Technol. 16, 760-772.

Orsini, D. A., Wiedensohler, A., Stratmann, F. (1996). Performance of a tandem differential mobility analyzer to study volatile chemical compounds in the particle size range 10-150 nm. J. Aerosol Sci. 27 (S1), S141-S142.

Philippin, S., Wiedensohler, A., Stratmann, F. (2003). Measurements of non-volatile fractions of pollution aerosols with an eight-tube volatility differential mobility analyzer (VTDMA-8). J. Aerosol Sci. 35, 185-203.

Pinnick, R. G., Jennings, S. G. and Fernandez, G. (1987). Volatility of aerosols in the arid southwestern United States. J. Atmos. Sci. 44, 562-576.

Prenny, A. J., DeMott, P. J., Kreidenweis, S. M. (2003). Water uptake of internally mixed particles containing ammonium sulfate and dicarboxylic acids. Atmos. Environment 37, 4243-4251.

Rader, D. J. and McMurry, P. H. (1986). Application of the tandem differential mobility analyzer to studies of droplet growth or evaporation. J. Aerosol Sci. 17, 771-787.

Reischl, G. P., Makela, J. M., Necid, J. (1997). Performance of Vienna type differential mobility analyser at 1.2-20 nanometer. Aerosol Sci. and Technol. 27:651-672.

Rood, M. J., Covert, D. S. and Larson, T. V. (1987). Temperature and humidity controlled nephelometry: improvements and calibration. Aerosol Sci. & Technol. 7, 57-656.

Sellegri, K., Laj, P., Peron, F., Dupuy, R., Legrand, M., Preunkert, S., Putaud, J.-P., Cachier, H. and Ghermandi, G. (2003). Mass balance of free tropospheric aerosol at the Puy de Dome (France) in winter. J. Geophys. Res. Lett. 108 (D11), 4333.

Sem, G. J. (2002). Design and performance characteristics of three continuous-flow condensation particle counters: a summary. J. Atmos. Research 62, 267-294.

Scheibel, H. G. and Porstendörfer, J. (1983). Generation of monodisperse Ag- and NaCl-aerosols with particle diameters between 2 and 300 nm. J. Aerosol Sci. 14, 113-126.

Smith, M. H. and O'Dowd, C. D. (1996). Observations of accumulation mode aerosol composition and soot carbon concentrations by means of a high-temperature volatility technique. J. Geophys. Res. 101 (D14), 19583-19591.

Stolzenburg, M. R. and McMurry, P. H. (1988). TDMAFIT Users' Manual. Minneapolis, Minnesota.

Stratmann, F., Orsini, D. and Kauffeldt, T. (1997). Inversion algorithm for TDMA measurements. EAC 1997, Hamburg. J. Aerosol Sci. S701-S702.

Stratmann, F.,Kauffeldt, T., Hummes, D. and Fissan, H. (1997). Differential electrical mobility analysis: a theoretical study. J. Aerosol Sci. and technol. 26,368-383.

Svenningsson, B., Rissler, J., Swietlicki, E., Mircea, M., Bilde, M., Facchini, M. C., Decesari, S., Fuzzi, S., Zhou, J., Monster, J., Rosenorn, T. (2005). Hygroscopic growth and critical supersaturations for mixed aerosol particles of inorganic and organic compounds of atmospheric relevance. Atmos. Chem. Phys. Discuss. 5, 2833-2877.

Swietlicki, E., Zhou, J., Berg, O. H., Martinsson, B. G., Frank, G., Cederfelt, S. I., Dusek, U., Berner, A., Birmili, W., Wiedensohler, A., Yuskiewicz, B., Bower, K. N. (1999). A closure study of sub-micrometer aerosol particle hygroscopic behaviour. Atmos. Research 50, 205-240.

Topping, D. O., G. B. McFiggans and H. Coe (2005), A curved multi-component aerosol hygroscopicity model framework: Part 1 - Inorganic compounds, Atmos. Chem. Phys., 5, 1205-1222

Topping, D. O., G. B. McFiggans and H. Coe (2005), A curved multi-component aerosol hygroscopicity model framework: Part 2 - Including organic compounds, Atmos. Chem. Phys., 5, 1223-1242.

Ulrich, E., Beckmann, C. and Israel, G. (1990). The chrarcterization of carbon species in particulate matter by successive thermal desoprtion. J. Aerosol Sci. 21 (Suppl. 1), 609-612.

Weingartner, E., Gysel, M. and Baltensperger, U. (2002). Hygroscopic of aerosol particles at low temperature. 1. New low-temperature H-TDMA instrument: setup and first applications. Environ. Sci. Technol. 36, 55-62.

Weingartner, E., Burtscher, H. and Baltensperger, U. (1996). Hydration properties of diesel soot particles. J. Aersol Sci. 27 (S1) S695-S696.

Weingartner, E., Burtscher, H. and Baltensperger, U. (1996). Hygroscopic properties of carbon and diesel soot particles. Atmos. Environment 31 (15) 2311-2327.

Wang, S. C. and Flagan, R. C. (1990). Scanning electrical mobility spectrometer. Aerosol Sci. and Technol. 13:230-240.

Wehner, B., Philippin, S., Wiedensohler, A. (2002). Design and calibration of a thermodenuder with an improved heating unit to measure the size-dependent volatile fraction of aerosol particles. J. Aerosol Sci. 33, 1087-1093.

Wiedensohler, A. (1988). An approximation of the bipolar charge distribution for particles in the submicron size range. J. Aerosol Sci. 3, 387-389.

Wiedensohler, A., Orsini, D., Covert, D. S., Coffmann, D., Cantrell, W., Havlicek, M., Brechtel, F., Russel, L., Weber, R. J., Gras, J., Hudson, J. G., Litchy, M. (1996). Performance of the counting efficiency of the TSI-3025 UCPC, the TSI-3010 CPC and the TSI-3760/7610 CPC for different operating conditions. J. Aerosol Sci. 27 (S1), S337-S338.

Annexes

A.1. Bipolar Diffusion Charger

Le neutraliser est utilisé pour charger les particules d'aérosols avant qu'elles ne rentrent dans les DMAs (cf. Appendix A.2). A l'intérieur du chargeur, il y a une faible source radioactive (Nickel 63, 10mCi 555MBq) qui produit des ions positifs et négatifs qui vont charger les particules à travers la diffusion bipolaire.
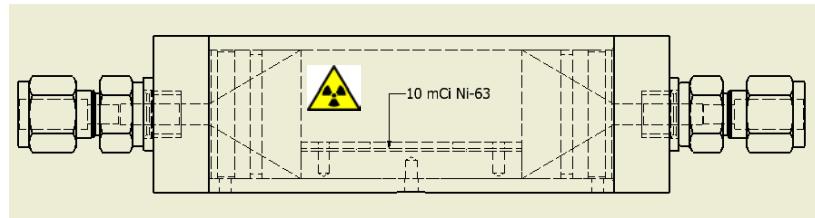
Figure A-1 : Schéma du chargeur bipolaire.

Un schéma du chargeur est montré sur la Figure A-1. Grâce à l'utilisation de cette source, la distribution de charge des particules est connue : elle est déterminée à partir de la théorie de Fuchs (1963) et calculée par Wiedensohler (1988). La formule permettant d'approximer la distribution de la charge (i.e. fraction de particules portant une charge de -2, -1, 0, +1, +2) est la suivante :

$$F(N) = 10^{\left(\sum_{i=0}^{5} a_i(N) \left(\log \frac{Dp}{nm} \right)^i \right)} \qquad (\text{ I })$$

a0	a1	a2	a3	a4	a5	Charge
-26,3328	35,9044	-21,4608	7,0867	-1,3088	0,1051	-2
-2,3197	0,6175	0,6201	-0,1105	-0,1260	0,0297	-1
-0,0003	-0,1014	0,3073	-0,3372	0,1023	-0,0105	0
-2,3484	0,6044	0,4800	0,0013	-0,1553	0,0320	1
-44,4756	79,3772	-62,8900	26,4492	-5,7480	0,5049	2

Tableau A-1 : Coefficients pour la distribution des charges utilisés dans l'equation (I).
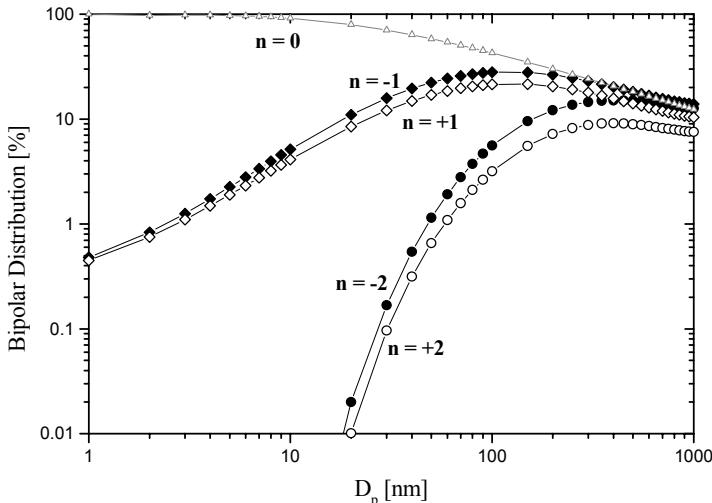
Figure A-2 : Distribution de la charge par diffusion bipolaire correspondant à l'equation (I).

On peut remarquer que la fraction des particules chargées avec une ou deux charges augmente avec la taille de la particule et, comment, à partir de 80-100 nm le nombre de particules ayant une charge multiple commence à devenir important. La distribution des ions positifs et négatifs n'est pas symétrique : les ions négatifs sont en effet plus nombreux à cause de leur plus grande mobilité électrique. La mobilité électrique dépend à la fois du nombre de charge en surface d'une particule et de son diamètre aérodynamique (voir équation II). A partir de la connaissance de la relation Taille / Charge, il est donc possible de sélectionner les particules possédant une certaine charge dans un analyseur différentiel de mobilité.

A.2. Differential Mobility Analyser (DMA)

Les analyseurs de mobilité électrique sont des appareils couramment utilisés en métrologie des aérosols. Ces dispositifs sont constitués par des condensateurs plans ou cylindriques à l'intérieur desquels l'aérosol circule en écoulement laminaire (voir Figure A-3). Ils combinent les effets aérauliques et électriques afin de sélectionner les particules en fonction de leur mobilité électrique. En effet, dans un tel analyseur, les particules chargées sont soumises d'une part, à une force de traînée qui entraîne les particules (si la pesanteur et la diffusion sont négligeables) le long des lignes de courant du fluide porteur, d'autre part, à une force électrostatique qui permet aux particules de changer de ligne de courant.
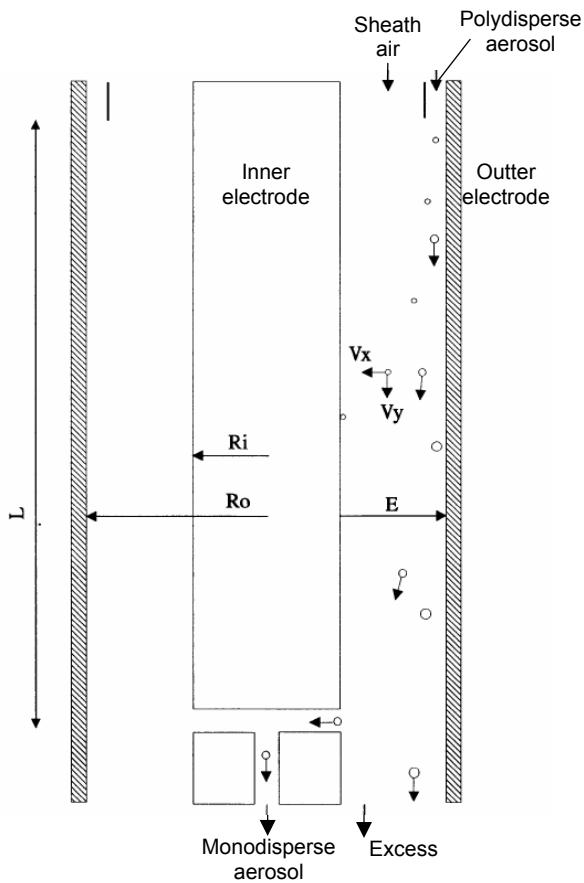
La relation entre la mobilité électrique d'une particule et son diamètre est donnée par l'équation de Millikan-Fuchs :

$$Z_p = \frac{i \cdot e_0 \cdot C_c(D_p)}{3\pi \cdot \mu \cdot D_p} \; ; \qquad \text{(II)}$$

D_p="Diamètre équivalent de mobilité" de la particule

i = nombre des charges élémentaires (e_0) transportées de la particule

$\mu(T)$ = viscosité dynamique du fluide

$C_c(D_p,\lambda)$ = Coefficient de correction de Cunningham (Slip Correction Factor)

Figure A-3 : Principe d'une colonne DMA.

Les analyseurs différentiels de mobilité électrique permettent donc de mesurer avec une grande précision la distribution en mobilité d'un aérosol (Knutson et Whitby, 1975b) dans un domaine de dimensions compris entre quelques nanomètres (Hussin *et al.*, 1983) et environ 2 micromètres (Le Bronec, 1998). Ces analyseurs ont de nombreuses applications en métrologie des aérosols. Citons par exemple, la génération d'aérosols monodispersés submicroniques (Liu et Pui, 1974b), la mesure de la distribution granulométrique d'un aérosol (Knutson, 1976) ou bien la possibilité d'étudier les variations de dimension des particules (Rader et McMurry, 1986) lorsqu'on associe deux analyseurs différentiels en serie.

A.3. Condensation Particle Counter (CPC)

La concentration des particules à la sortie du DMA est déterminée par un compteur de particules à condensation (CPC,TSI Model 3010). Le débit d'aérosol à l'intérieur du compteur est fixé à 1 lmin^{-1}. Le schéma de principe du CPC est présenté sur la Figure A-4.
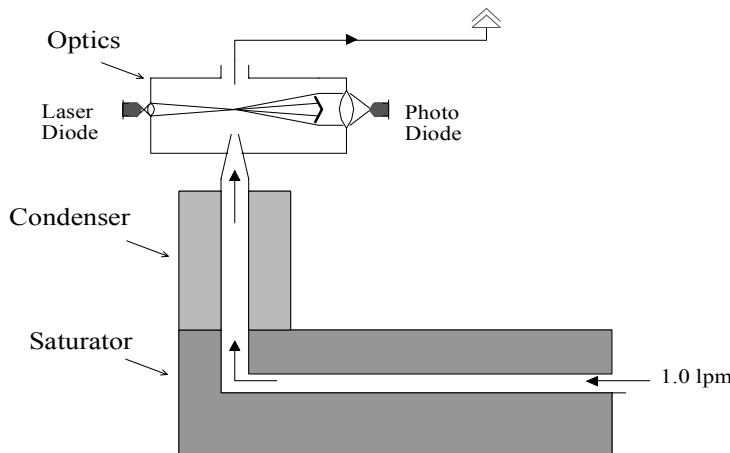
Les aérosols rentrent dans une chambre chauffée et saturée en vapeur de butanol (saturateur) et refroidissent ensuite dans une chambre de condensation. Le refroidissement provoque la condensation de vapeur d'alcool sur les particules d'aérosols qui grossissent jusqu'à une taille permettant leur détection par des instruments optiques (Laser + Photodiode).

Figure A-4. Schéma du compteur de particules à condensation TSI-3010.

Les particules, qui sont maintenant dans le spectre du visible, passent à travers un rayon laser et la lumière diffusée par chaque particule est mesurée par une photodiode. Le signal enregistré est donc un indice du nombre total des particules et, rapporté au débit, il permet d'en mesurer directement la concentration (Ncm^{-3}).

Les concentrations obtenues par le CPC peuvent être lues soit par le port série, soit par la sortie analogique du compteur. Toutefois, le plus intéressant, et le plus juste, est de récupérer directement le signal en « digital pulse ». En effet, pour chaque gouttelette qui passe à travers le rayon laser, le CPC envoie un pulse de 5 volts. Cette méthode, en plus de l'exacte connaissance du debit effectif du compteur (voir Appendix A.4), permet d'améliorer la statistique du comptage pour les faibles concentrations (i.e. <100 par cm^3) normalement mesurées avec la deuxième section d'un Tandem-DMA.

L'utilisation des CPCs est simple mais demande quelques précautions en particulier concernant la détermination de l'efficacité de comptage en fonction de la taille des particules. En effet, malgré les courbes d'efficacité données par le constructeur, les CPCs ne comptent

pas le même nombre de particules alors qu'ils sont censés tous les deux compter 100 % des particules. Plutôt qu'étalonner les compteurs de manière absolue, on a retenu plus important de connaître l'efficacité relative des deux CPCs utilisés dans le Tandem-DMA.

L'expérience consiste à étalonner en relatif les deux CPCs qui sont utilisés dans le même tandem. Le montage utilisé pour la calibration est obtenue en plaçant les deux compteurs (CPC-1 et CPC-2) connectés en parallèle apres un DMA qui sélectionne les particules.
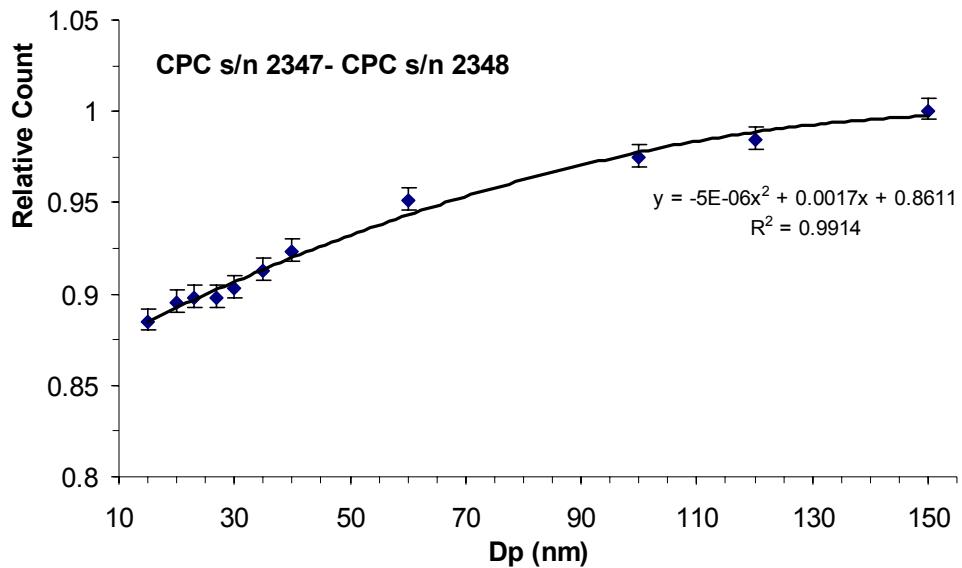
Figure A-5 : Efficacité des deux CPCs TSI 3010 en parallèle.

Pour chaque diamètre de particules entre 10-150 nm, 20 secondes de mesures nous permettent d'obtenir une courbe de calibration, réitérée 12 fois. La moyenne de ces courbes de calibration est donnée en Figure A-5. Un des deux CPCs (i.e. CPC s/n 2347) a une efficacité plus faible pour des particules inferieures à 150 nm lorsqu'on le compare à l'autre (i.e. CPC s/n 2348). Par la suite, cette correction sera donc appliquée aux données du CPC 3010 s/n 2347.

A.4. Mesure et régulations des débits du DMA

Un des points fondamentaux de la mesure avec les DMAs est la régulation des débits, en particulier les flux d'aérosols (Qa) et d'air propre (Qsh). Un contrôle très précis des débits est donc requit pour la mesure DMA qui posera des problèmes supplémentaires lorsque 2 DMAs seront utilisés en série parce que les débits des deux analyseurs sont « connectés ».

Le contrôle de ces débits doit d'une part être effectué avant la mesure mais également pouvoir être contrôlé au cours de la mesure. Pour chacun des DMAs, il est nécessaire de régler 4 débits différents: le "*Sheath Flow*" Qsh d'air sec et propre, le flux d'aspiration (*Excess Flow*,Qex) en sortie, le debit d'aérosol à la rentrée du DMA (*Sample Flow*,Qs) et celui en sortie (*Aerosol Flow*,Qa). Dans la pratique, on assume que les débits qui rentrent et ceux qui sortent du DMA sont équilibrés (i.e. Qsh=Qex, Qs=Qa) mais c'est la méthode de réglage qui permet d'assurer des conditions idéales pour une mesure correcte de la mobilité des particules. En effet, une faible différence entre les conditions d'entrée et de sortie du DMA peut perturber à la fois l'analyse de la mobilité électrique et la détermination de la concentration des particules (Knutson and Whitby, 1975 ; Stonzelbourg, 1988).

Ils existent plusieurs techniques qui permettent ce réglage d'une manière plus ou moins précise et stable. Un choix soigneux a été porté pour la mise au point de la méthode de mesure et de régulation des debits pour pouvoir disposer d'un appareil de mesure qui était :

1. Stable et précis dans le temps
2. Simple pour l'utilisateur
3. Simple à transporter dans les sites de mesures

Tout d'abord, nous avons choisi d'éliminer l'air comprimé comme gaz porteur dans les DMAs. On utilise donc une pompe qui recircule le flux (i.e. « closed loop ») entre la rentrée et la sortie du DMA et un débitmètre / controleur pour régler le débit. La Figure A-6 montre le schéma de cet arrangement utilisé pour chaque DMA. Des filtres à particules sont utilisés pour pouvoir disposer d'un flux propre, du silicagel pour assécher l'air (i.e. RH<10%) et un échangeur de chaleur à la sortie de la pompe pour équilibrer la température. Cette méthode assure un équilibre des débits stable dans le temps. Un avantage non négligeable de ce système est de ne pas utiliser un compresseur qui, dans certain cas, peut poser des problèmes dû au transport ou à l'accessibilité du site de mesure.
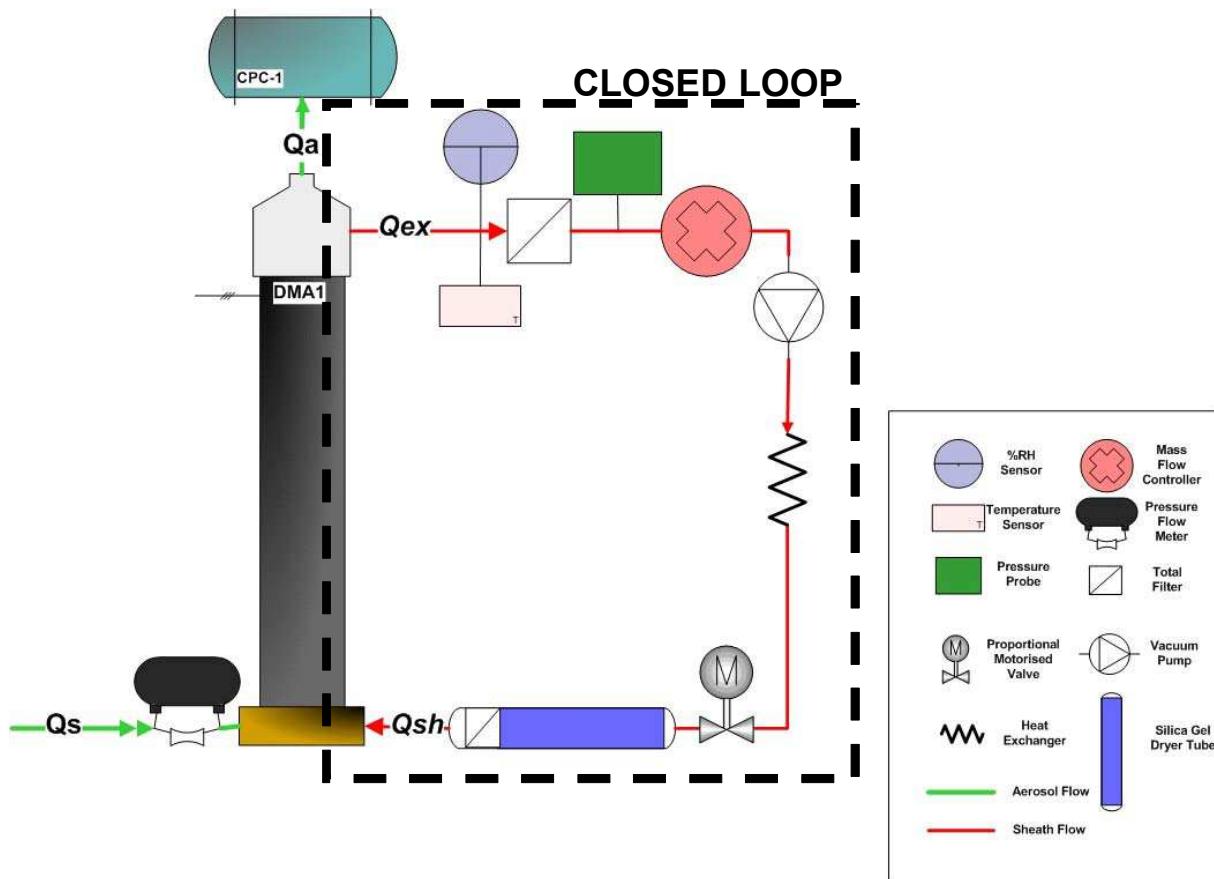
Figure A-6 : Schéma de l'arrangement en closed-loop pour un DMA.

Ensuite, nous avons decidé d'utiliser un dispositif de mesure de débit pour l'aérosol (i.e. Qs) à la rentrée de chaque DMA (i.e. PFM, Pressure Flow Meter, voir Section A.4.1) dans le but de contrôler et de corriger automatiquement des variations durant le fonctionnement de l'analyseur. Une variation eventuelle du débit d'aérosol (Qs) est corrigée à l'aide de la vanne proportionelle placée à la rentrée du sheath flow (Qsh) du DMA, alors que les débits en sortie Qa et Qex sont reglés par l'orifice critique du CPC et par le débitmètre régulateur, respectivement.

Le débit d'aérosol (Qs) à l'entrée du premier DMA est de 2 lmin⁻¹ du fait de l'utilisation de deux CPCs 3010 en série et de 1 lmin⁻¹ sur le deuxième. Ce débit est influencé par les pressions en entrée et sortie des DMAs, ce qui justifie une régulation à partir de la mesure des pressions différentielles.

A.4.1. Réalisation du Pressure Flow Meter (PFM)

Le dessin du dispositif qui a été construit pour ce but est présenté sur la Figure A-7 :
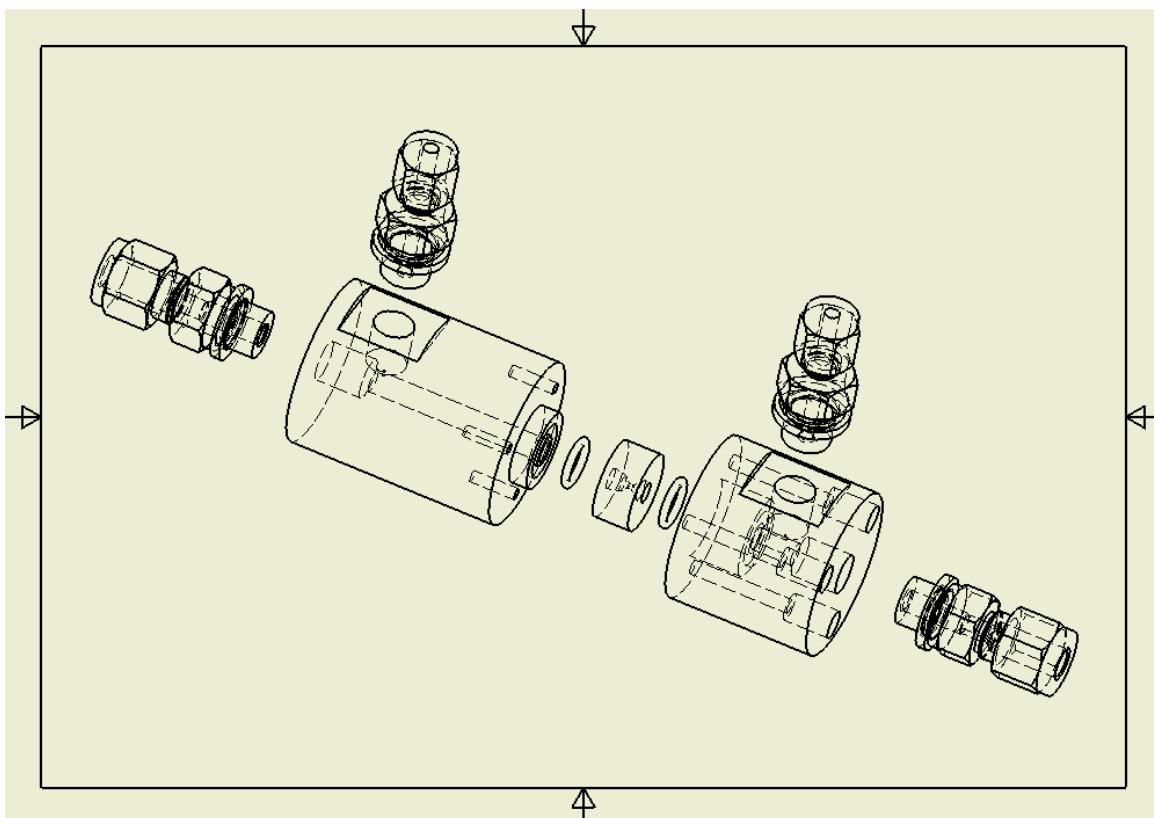
Figure A-7 : Schema du dispositif PFM pour la mesure du debit d'aerosol.

La relation qui existe entre le débit et la différence de pression due à l'orifice est évaluée à travers un bilan de l'énergie mécanique en négligeant les pertes et les dissipations (cas idéal) :

$$Q_{th} = \rho \cdot w \cdot S_d = S_d \cdot \sqrt{2 \cdot \rho \cdot \Delta p} \qquad (\text{ III })$$

où Q_{th} est le débit théorique en Kgs^{-1}, ρ la Densité de l'air en Kgm^{-3}, w la vitesse en ms^{-1}, S_d la section de l'orifice en m^2, Δp la différence de pression en Pa et d le diamètre de l'orifice en m. Par suite,

$$\Delta p_{th} = \frac{Q^2 \cdot 16}{2 \cdot \rho \cdot \pi^2 \cdot d^2} \qquad (\text{IV})$$

Naturellement ces pertes de charges calculées sont théoriques et sous-estiment les valeurs réelles puisqu'il est nécessaire de considérer que le flux n'est pas idéal au travers de l'orifice. En effet, la différence de pression peut subir une augmentation due aux pertes de charge turbulentes dans le jet qui seront d'autant plus fortes que le trou est petit et que le débit est

important. Ces pertes sont quantifiées par l'introduction dans la formule théorique d'un coefficient d'afflux ε. Ce coefficient est un nombre adimensionnel compris entre 0 et 1, qui dépend seulement de l'orifice. Quand sa géométrie devient semblable à celle d'un tube de Venturi qui correspond à la suite de tube convergent, parallèle et divergent, ce coefficient peut atteindre des valeurs maximales comprises entre 0,6 et 0,7 (selon les Normatives UNI).

Par suite, l'équation (IV) devient :

$$\Delta p_{norm} = \frac{Q^2 \cdot 16}{2 \cdot \rho \cdot \pi^2 \cdot d^2 \cdot \varepsilon} \qquad (V)$$

Pour mieux dimensionner l'orifice en fonction du débit et pour mieux choisir sa géométrie une étude couplant une modélisation avec le logiciel FLUENT (5.5-6.0) et des calibrages expérimentaux a été réalisée (voir Section A.4.2.).

Cette opération avait pour but non seulement d'évaluer la perte de charge en fonction du débit et du diamètre du trou mais également d'évaluer la meilleure géométrie du dispositif (i.e. PFM) avec les deux prises de pression. En effet, afin que la mesure de débit soit la plus précise possible, il est nécessaire de bien positionner la prise de pression en aval de l'orifice, car il faut que le profil de vitesse et donc de pression soit complètement développé. La Figure A-8 montre les géométries du diaphragme examinées.
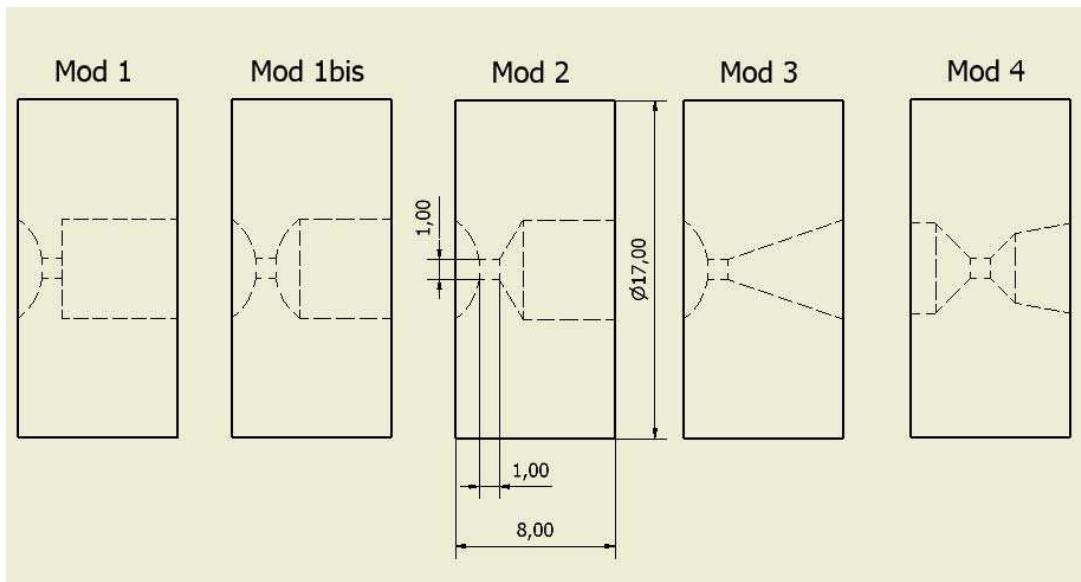
Figure A-8 : Les différentes géométries des orifices.

A.4.2. Modélisation et calibrage du PFM

Les Figures A-9.a,b,c montrent le résultat des simulations faites en utilisant un diamètre du trou de 1 mm et un débit de 1 lmin^{-1} pour trois géométries différentes du diaphragme (i.e. Mod1, Mod2 et Mod3) . Il est évident (cf. Figure A-9.c) que l'utilisation d'un profil divergent suffisamment long après le trou du diaphragme évite la formation de recirculation.
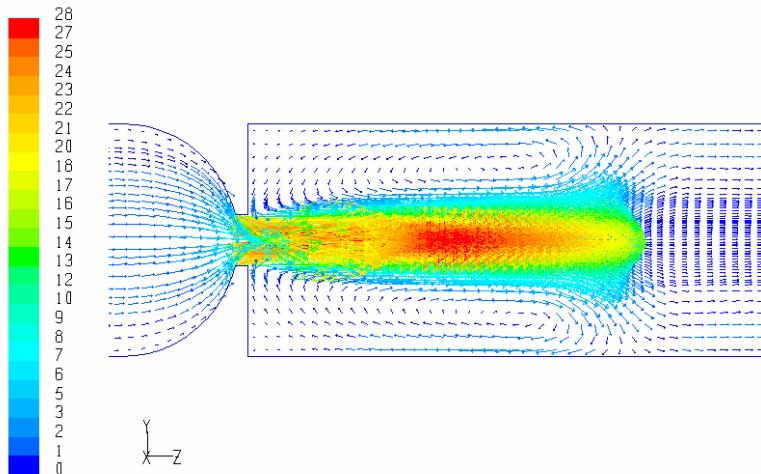
Figure A-9.a: Vecteurs de vitesse en ms^{-1} pour la première géométrie (Mod1) de l'orifice.
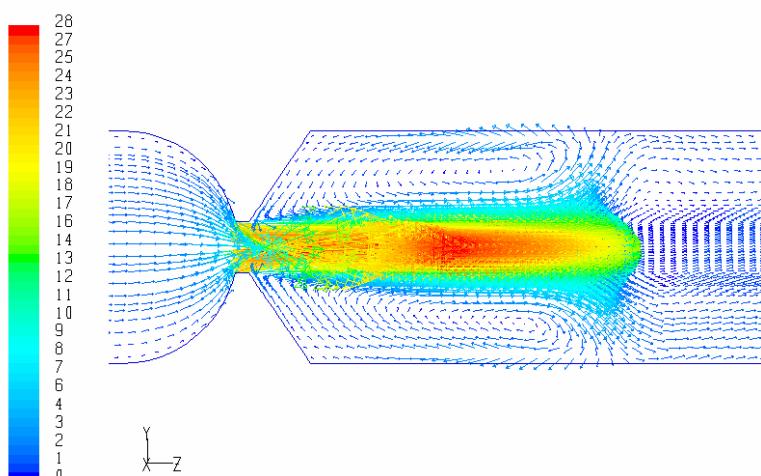
Figure A-9.b : Vecteurs de vitesse en ms^{-1} pour la deuxième géométrie (Mod2) de l'orifice.
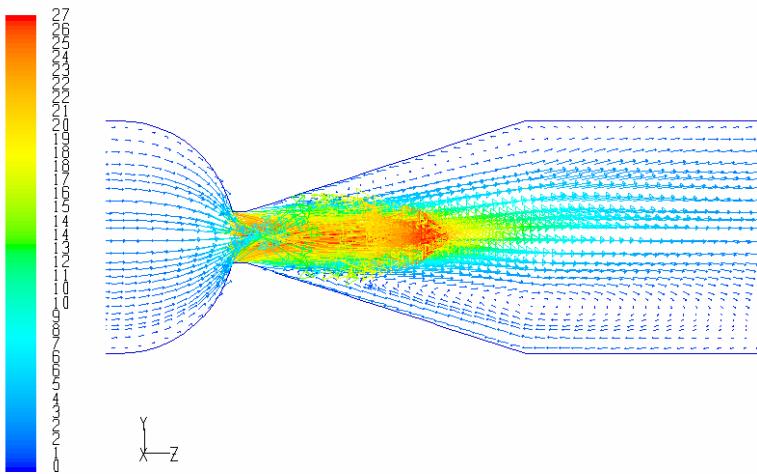
Figure A-9.c : Vecteurs de vitesse en ms^{-1} pour la troisième géométrie (Mod3) de l'orifice.

La longueur du diaphragme (i.e. la largeur du disque) est la même dans les trois cas (i.e. 8 mm) mais le profil de vitesse à l'intérieur du tuyau est sensiblement mieux développé pour la troisième géométrie. Entre autres, étant la géométrie plus proche au tube de Venturi, les pertes et les dissipations mécaniques seront mineures avec une pression différentielle (P_1-P_2) plus faibles (i.e. 450 Pa au lieu de 600 Pa), comme le montre la Figure A-10.
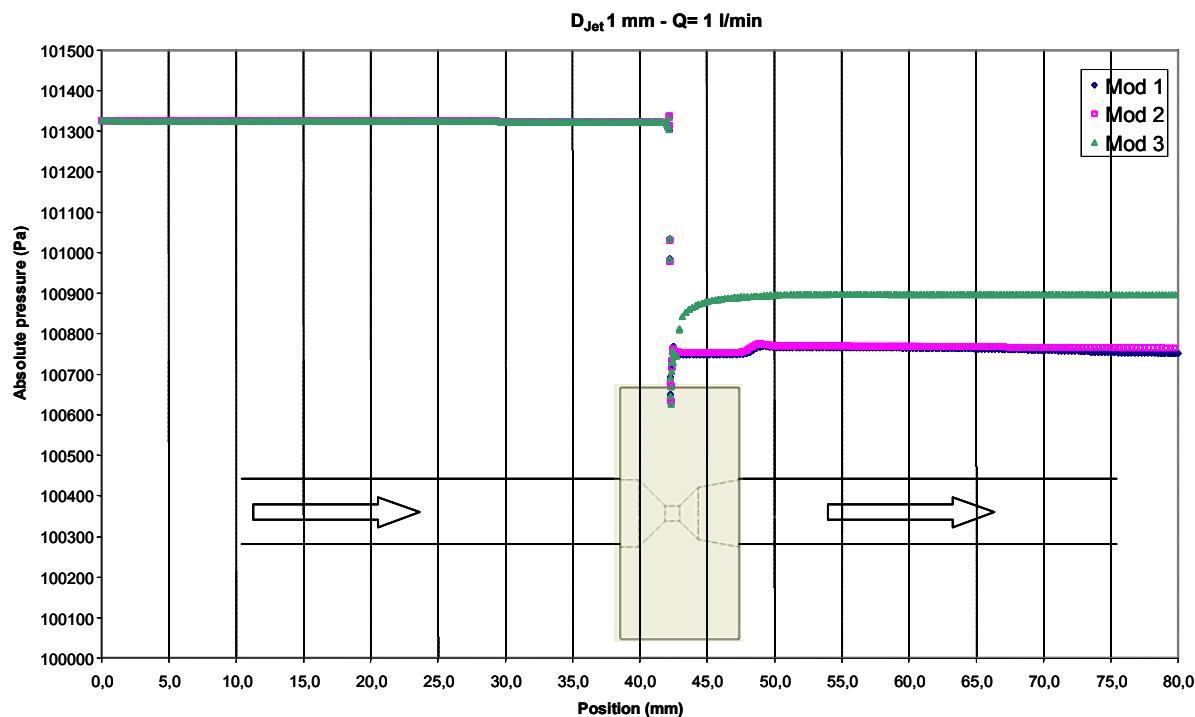
Figure A-10 : Pressions en amont et en aval de l'orifice calculées par FLUENT pour les trois géométries considérées.

La modélisation nous a permis de visualiser les différences d'écoulement de l'air à l'intérieur de plusieurs géométries de l'orifice. De l'inox à été utilisé pour construire les disques pour réduire l'interaction avec les particules d'aérosols échantillonnées et un dimensionnement

respectant « *la règle d'or* : D/W=1 » a été choisi (D=diamètre du trou, W=profondeur du trou) pour limiter les pertes de charge turbulentes et les pertes en particules.

Comme expliqué précédemment et indiqué dans la Figure A-7, les mesures de pression sont faites en 2 points avant et après l'orifice par une sonde de pression différentielle (0-20 mbar). Afin de vérifier la validité de ces mesures par rapport aux calculs theoriques et le correct positionnement de la prise de pression en aval, nous avons effectué une série de mesures pour plusieurs diamètres du trou, géométries de l'orifice et débit.

Le montage instrumental mis en oeuvre pour l'étalonnage des orifices est le suivant (Figure A-11) :
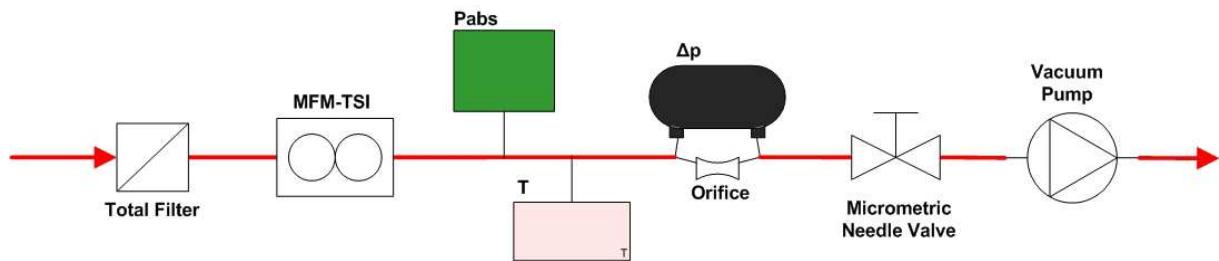
Figure A-11 : Montage instrumental pour l'étalonnage des orifices.

Ces mesures ont été effectuées en utilisant un débitmètre supplémentaire (i.e. MFM TSI-4140, 0.01-10 lmin^{-1}, précision 0.005 std lmin^{-1}) qui a servi de référence. Une vanne micromètrique a permis de règler le débit avec une très grande précision entre 0.1 et 3.0 lmin^{-1}. La Figure A-12 montre un résultat de ces mesures pour un orifice, dont la géométrie correspond au « Mod4 » de la Figure A-8, pour un diamètre du trou de 0.7 mm.
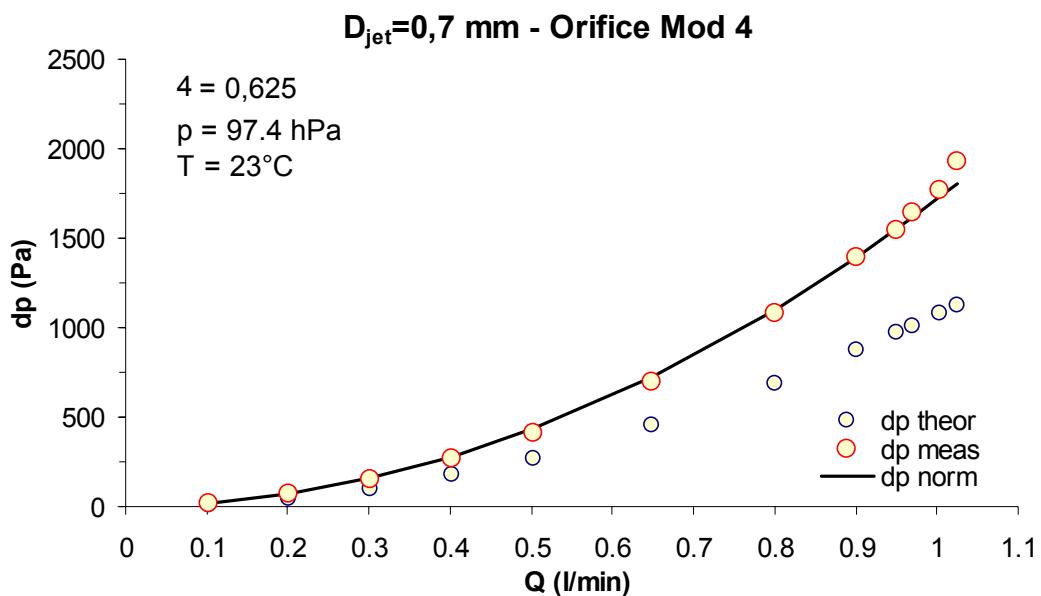
Figure A-12 : Etalonnage d'un orifice Mod4.

La courbe « *dP theor* » a été calculée en utilisant l'équation (IV) et la courbe « *dP meas* »
correspond à l'étalonnage en faisant varier le débit entre 0-1 lmin[-1]. La courbe « *dP norm* »
est obtenue de la courbe théorique en utilisant un coefficient d'afflux ε =0.625 : même si la
méthode de calcul n'est pas si rigoureuse, la valeur du coefficient est bien en accord avec la
littérature. La précision de la mesure de ce dispositif est inférieure à ±1% de la lecture.

Cette géométrie « de Venturi » s'est demontrée efficace aussi pour contenir les pertes en
particules comme le montre la Figure A-13. Le principe de cette expérience est de placer un
premier CPC TSI-3010 avec le dispositif contenant l'orifice et un deuxième CPC TSI-3010 en
aval d'un DMA qui sélectionnera un aérosol monodispersé autour d'un diamètre de particule,
puis de faire varier le diamètre échantillonné par le DMA. Pour cette expérience, on a generé
au laboratoire un aérosol monodispersé de NaCl et on a fait varier les diamètres dans la
gamme 15-300 nm. Le résultat de cet étalonnage montre que l'orifice ne modifie presque pas
la distribution granulomètrique à l'entrée de chaque DMA surtout pour les petites particules.
Une baisse de la pénétration des particules d'environ 10%, observée à partir de 150 nm de
diamètre et qui semble constant pour des plus gros diamètres, est probablement du aux
impacts inertiaux sur l'orifice.
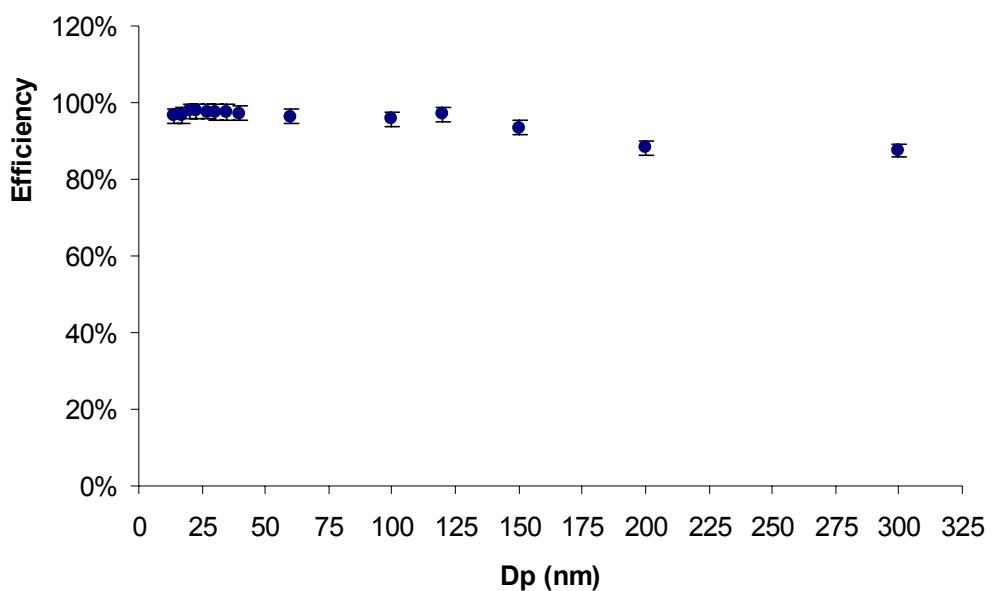
Figure A-13 : Pénétration de particules dans le dispositif PFM avec un orifice Mod4, d=0.7 mm
et Q=1 lmin[-1]. Les barres d'erreur correspondent à 12 mesures (3%).

Suite à l'étalonnage des orifices, on a choisi l'orifice de 1.0 mm de diamètre pour le premier
DMA (i.e. Qs=2.0 lmin[-1]) et 0.7 mm de diamètre pour le deuxième DMA (i.e. Qs=1.0 lmin[-1]).

A.5. Le système de thermo-désorption

Le système de chauffage de l'aérosol retenu (Figure A-14) utilisé dans le V-TDMA et VH-TDMA, est constitué d'un tube en acier inoxydable (d.i. = 8.6 mm ; d.e. = 13.5 mm ; longueur = 42.5 cm) autour duquel est placé un ruban papier céramique (épaisseur = 1 mm). La résistance chauffante est enroulée autour du ruban en céramique pour une longueur totale de 30 cm. Cela assure à la fois, une bonne diffusion de la chaleur et donc une température uniforme en surface de la colonne de chauffage de l'aérosol pour 30 cm et l'isolation électrique entre le tube métallique et le fil chauffant.
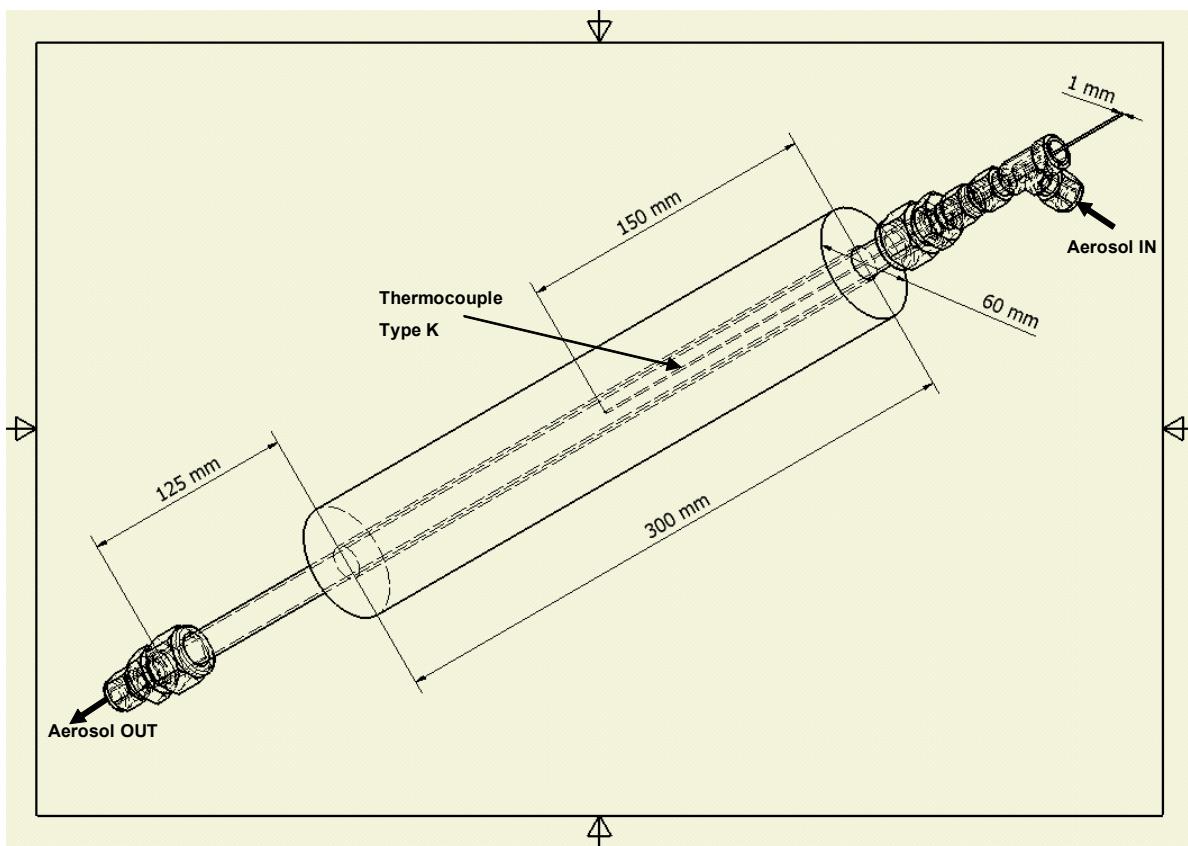
Figure A-14 : Schema du thermo-desorbeur.

A la sortie de la zone de réchauffement, le flux gazeux se refroidit jusqu'à la température ambiante (25°C) sur 13 cm environ.

L'isolation est assurée par un matériau réfractaire en laine céramique qui permet de réduire la température de 1200°C à 150° pour une épaisseur de 50 mm. L'épaisseur choisie de l'isolant est de 30 mm environ (d.e. = 60 mm), ce qui permet des températures d'utilisation maximales bien plus élevées que 300°C avec des températures maximales de surface acceptables (60°C) tout en conservant un poids du four minimal (environ 1 kg).

Dans le Tableau A-2 sont resumés les caractéristiques des matériaux utilisés pour la réalisation du four.

	Matière	Conductivité thermique, l[W/m°C]	Température Max. d'utilisation [°C]
Tube acier	316L – ASTM A269	100	540
Ruban céramique	Fibre d'Alumine-75 % de Al$_2$O$_3$ + Silice	0.054 à 300°C 0.19 à 1370°C	1400
Laine céramique	Fibre d'Alumine-75 % de Al$_2$O$_3$	0.2	1260
Tableau A-2 : Caractéristiques des matériaux du thermo–désorbeur.			

Une série de modélisations des profils thermiques et de la dynamique des particules réalisées à l'aide du logiciel FLUENT 6.1 ont montré (Villani et al., 2006a) que le chauffage radial du flux gazeux atteint une température maximale d'équilibre uniforme sur la largeur du tube environ 15 cm après l'entrée dans le système de thermo-désorption. Des mesures de température faites au travers du tube de thermo-désorption à 5 cm d'intervalle ont à la fois validé les modélisations et confirmé que le maximum de température est atteint approximativement au centre de la zone de réchauffement pour chaque température de four.

La mesure de la température se fait dans la section correspondant au maximum et directement à l'intérieur du tube inox via un thermocouple blindé (Type K, Inconel, d.e. = 1 mm) assurant un très bon niveau de confiance sur la température effectivement appliquée à l'aérosol.

A.6. Les humidificateurs PermaPure
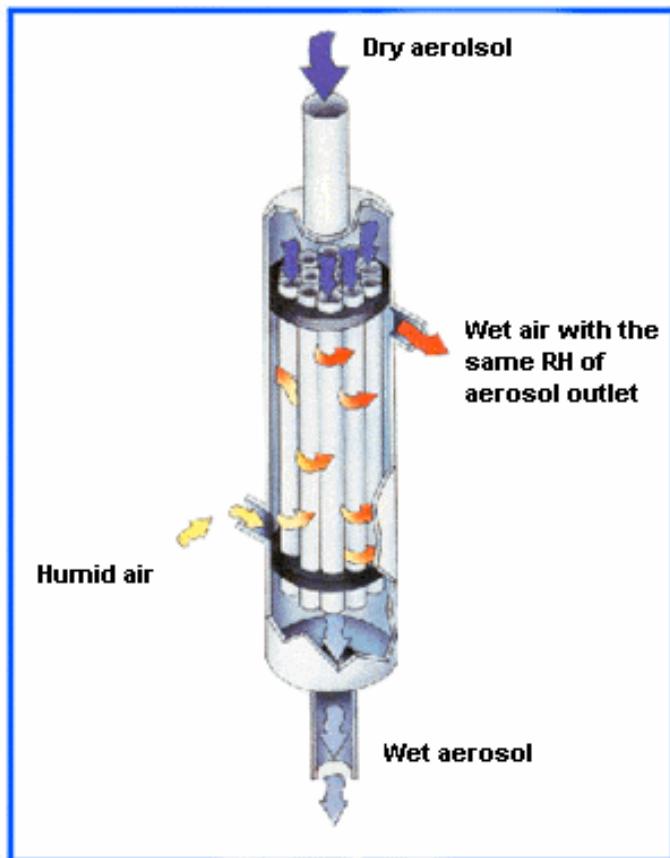
Figure A-15 : Schéma de l'humidificateur à membrane Nafion.

Les tubes Nafion PermaPure (Figure A-15) sont des membranes en Teflon parsemées de groupes sulfonates qui absorbent la vapeur d'eau. Le flux d'aérosol (ou d'air) passe à travers les tubes autours desquels s'écoule un débit d'air humide (ou d'eau) en contre-flux. Suite à un gradient de pression de la vapeur d'eau, l'aérosol atteint la même humidité relative que l'air humide. Deux tubes PermaPure différents sont utilisés dans le VH-TDMA : un multi-tubes (PH-110-12S) pour humidifier le débit de sheath flow du DMA2 et un single-tube (MD-110-12S-4) pour l'humidification de l'aérosol.

La Figure A-16 montre le système de montage des deux membranes PermaPure et le schéma qui permet de réguler individuellement l'humidité relative. Un débit d'air saturé (15 lmin^{-1}) est produit dans le CEM (Controled Evapotation Mixing) et il est envoyé d'abord dans la membrane qui humidifie le sheath flow du DMA2 (i.e. PPure Multi Tube) et ensuite, dans la membrane qui humidifie l'aérosol (i.e. PPure Single Tube). Deux mesures de %RH (i.e. RH Probe) en aval des deux membranes permettent de connaître l'humidité des deux débits à chaque instant. A travers deux régulateur PID (Progressive-Integral-Differential, custom-made), le PC et la carte d'acquisition electronique (i.e. Daq Board), deux électrovannes, placées à l'entrée des deux tubes PermaPure, permettent de dévier l'air saturé lorsque la valeur de %RH lue par les sondes d'humidité dépasse la valeur de la consigne (i.e. 90% pour le sheath flow et 88% pour l'aérosol).
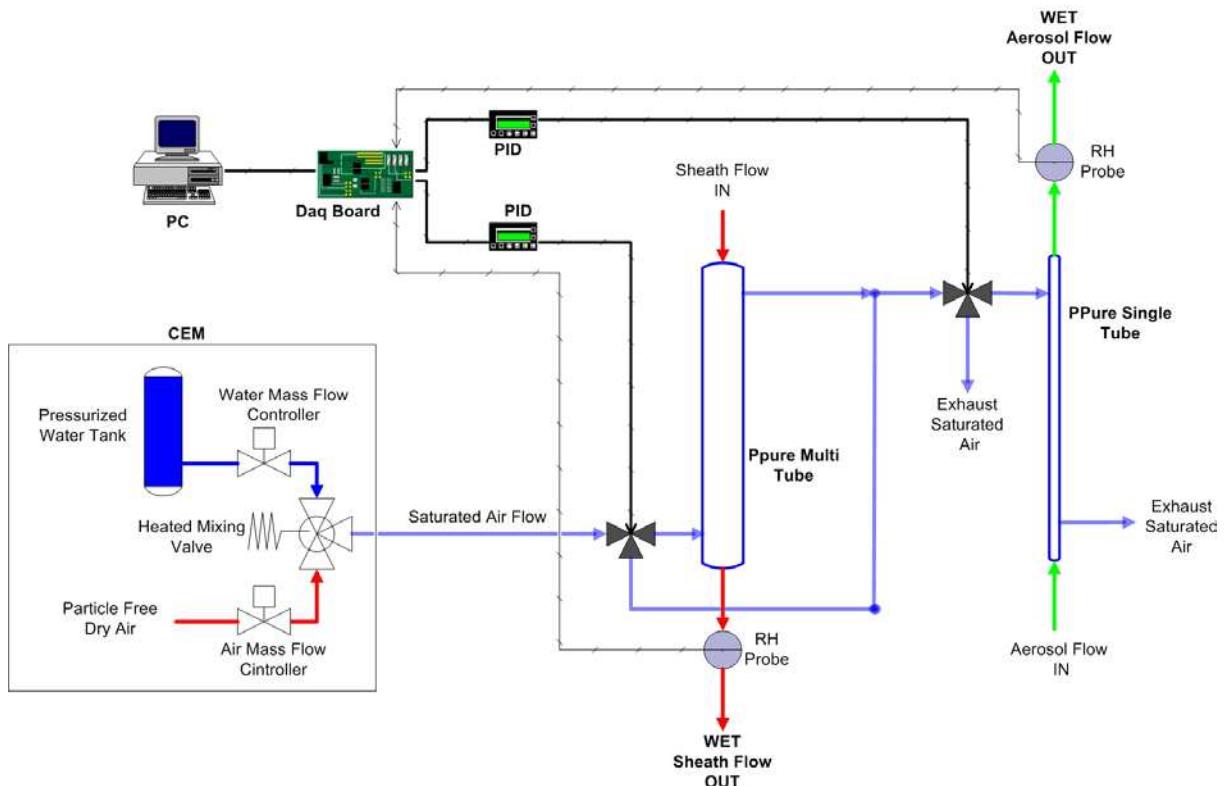
Figure A-16 : Schéma de montage et de régulation de l'humidité du VH-TDMA.

A.7. L'enceinte thermo-controlée

Etant donné que l'humidité de l'air est fortement dépendante de la température, il a été nécessaire d'isoler et contrôler thermiquement le deuxième DMA pour éviter des variations importantes et instantanées des conditions climatiques. Pour cela, un système de thermo-régulation (Figure A-17) a été conçu en minimisant le volume et en optimisant les échanges thermiques.
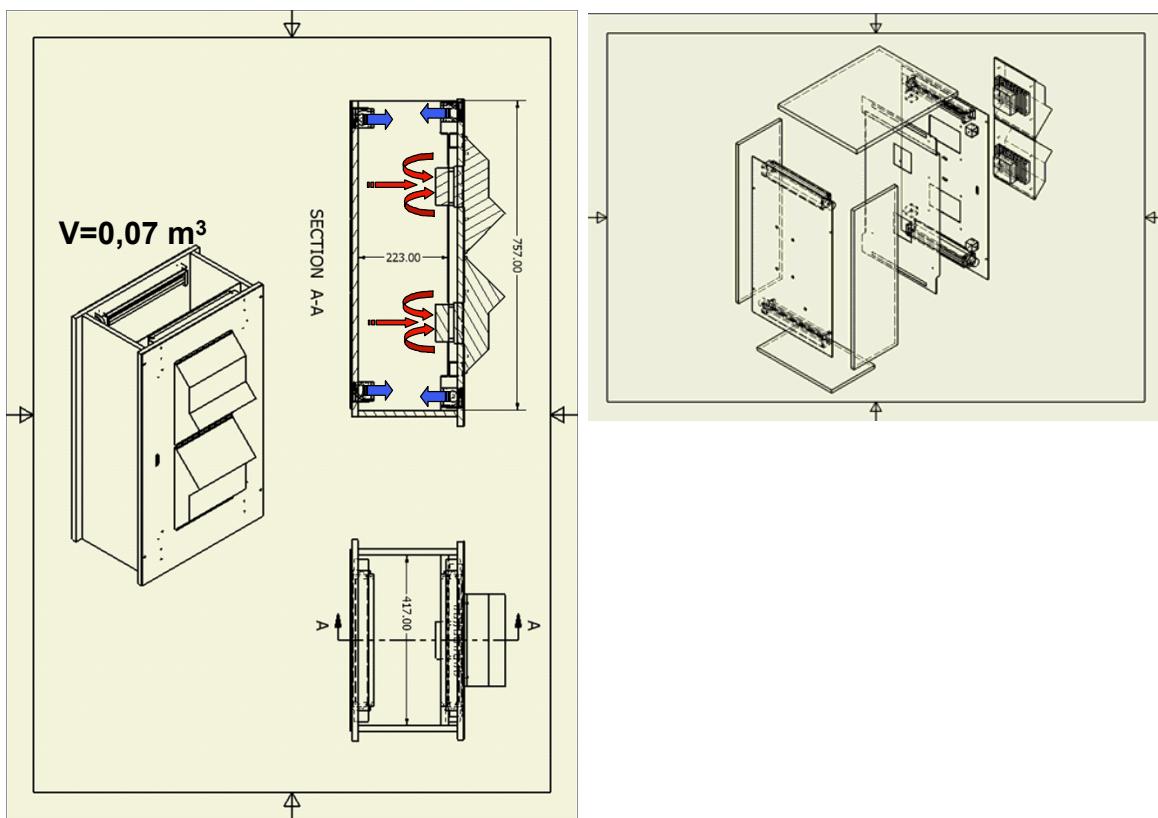
Figure A-17 : Schéma et principe de fonctionnement du volume thermostaté.

Deux éléments thermo-électriques permettent de dissiper la puissance thermique à l'intérieur du volume qui est isolé depuis l'extérieur grâce à des panneaux de mousse de polystyrène appliqués sur les six cotés de l'enceinte. L'homogénéité de la température de l'air et les échanges thermiques sont optimisés via la convection forcée de l'air en utilisant six ventilateurs (2 de type axial et 4 de type tangentiel, voir Figure A-17). Ce type de climatisation de l'air autour du DMA humide permet de minimiser les gradients verticales de température (<0.1°C) et de stabiliser la température interne à 20°C environ si la température ambiante est de 25°C.

A.8. Inversion des données

La concentration mesurée en aval du DMA2 n'est pas la concentration réelle de particules resultant du processus de conditionnement, mais représente la convolution de la distribution réelle avec la fonction de transfert du DMA (i.e. TF, voir Chapitre I.1.1) comme representé sur la Figure A-18. Par suite, le spectre dimensionnel des particules résiduelles mesuré par le deuxième DMA a besoin d'être recalculé à l'aide d'un algoritme d'inversion assez complexe.
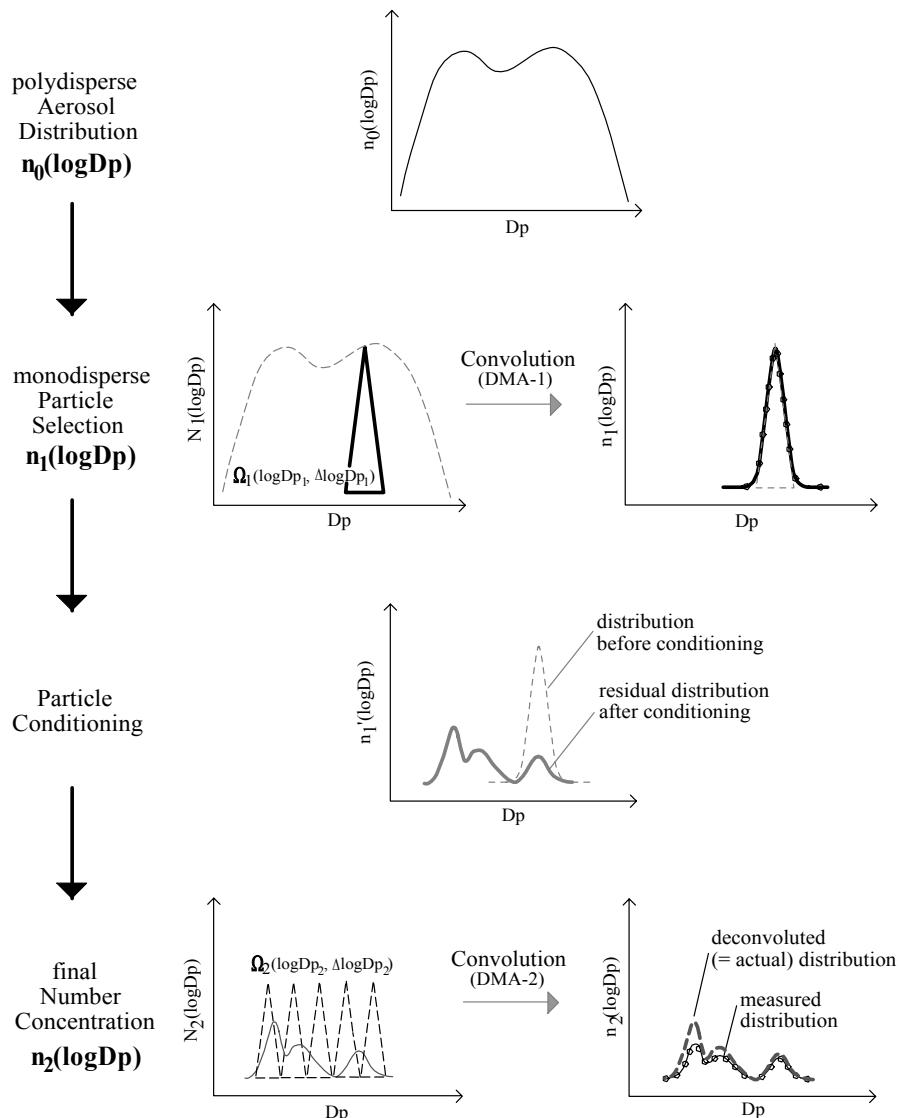
Figure A-18 : Description schématique de la méthode d'échantillonnage TDMA et de son traitement.

Les mesures Tandem-DMA (i.e. basées en général sur un DMA) sont basées sur la classification des particules suivant leur mobilité electrique (voir Chapitre I.1.1). Ainsi, pour en déduire le diamètre correspondant, il est nécessaire de connaître le nombre de charges

qu'elles possèdent. Or, à partir d'un diamètre d'environ 80 nm, la possibilité d'avoir des particules avec plusieurs charges devient significative (voir Appendix A.1). Par suite, des particules avec une seule charge et un diamètre de 150 nm ont la même mobilité électrique qu'une avec deux charges de 235 nm ou de trois charges de 313 nm de diamètre. En accord avec l'équilibre de charge bipolaire calculé (Wiedensohler, 1989 ; Keady et al., 1983) leurs existence correspond environ à 28% (singlets), 13% (doublets) and 5% (triplets).

Corriger la présence de particules ayant plusieurs charges pour des mesures TDMA ne peut être fait que si on connaît, à chaque instant, la concentration et l'évolution dans le temps de la granulométrie de l'aérosol. Pour cela, il serait nécessaire d'utiliser, en parallèle d'un Tandem-DMA, un granulomeètre (i.e. DMPS ou SMPS) qui permettrait de connaître la concentration des particules avec plusieurs charges. En deuxième lieu, le déplacement du diamètre d'une particule chargée plusieurs fois suite au conditionnement ne peut pas être distingué de celui d'une particule chargée une fois.

Etant donné que la fraction de particules chargées plusieurs fois échantillonnée par un Tandem-DMA dans la gamme 15-200 nm est faible et à cause de l'indisponibilité d'un granulomètre, nous avons preferé ne pas inverser la concentration mesurée en aval du DMA2 par rapport à la présence de charges multiples.

La méthode utilisée pour traiter les données des TDMAs dans ce travail est donc basée sur l'algorithme d'inversion « TDMA FIT », developpé par Stolzenbourg and McMurry, 1988. Ce programme utilise une régression aux moindres carrés afin d'ajuster la fonction de transfert théorique du TDMA à la distribution d'aérosols mesurée, en supposant que les spectres de mobilité en aval du DMA2 soient distribués normalement avec un ou deux modes. La fonction de transfert du DMA considérée dans l'algorithme est idéale (i.e. triangulaire, voire Chapitre I.1.1), en négligeant l'effet de diffusion. D'autres corrections sont effectuées suivant l'efficacité de transmission du système (voir Chapitre I.2.1 et Chapitre I.3.1), et pour tenir compte de l'efficacité de mesure des CPC (voir Appendix A.3).

En tous cas, l'inversion des données d'un Tandem-DMA reste un problème ouvert. Plusieurs inconvénients restent à éliminer et plusieurs points à améliorer. En effet, en l'état actuel, le logiciel ne peut pas traiter les données d'une facon automatique car souvent, il n'arrive pas à converger vers une solution. Ce sera dans ce cas l'utilisateur qui doit diriger la convergence à l'aide de plusieurs paramètres avec une perte importante de temps.

Liste des figures

Introduction

Chapitre I

Article 1

Article 2

Article 3

Article 4

period 2 at Mace Head (z-axis represents Relative counts).

Article 5

Figure A.5.1: Block diagram showing the working principle of the VH-TDMA analysing method

Figure A.5.2a: Normalised and fitted size distributions of selected 52 nm particles ("DRY" curve), after volatilisation at 70°C ("V70°C" curve), hydration at RH=90% ("H" curve), and volatilisation followed by hydration ("VH" curve).

Figure A.5.2b: Normalised and fitted size distributions of selected 33 nm particles ("DRY" curve), after volatilisation at 70°C ("V70°C" curve), hydration at RH=90% ("H" curve), and volatilisation followed by hydration ("VH" curve).

Article 6

Figure A.6.1a: Thermo-desorption of 20 nm particles at 110°C sampled at SMEAR II field station, Hyytiala, Finland

Figure A.6.1b: Thermo-desorption of 100 nm particles at 70°C sampled at Clermont Ferrand, France.

Figure A.6.1c: Thermo-desorption of 100 nm particles at 70°C sampled at Puy de Dome station, France.

Figure A.6.1d: Thermo-desorption of 100 nm particles at 50°C sampled at IfT, Leipzig, Germany.

Figure A.6.1d: Thermo-desorption of 100 nm particles at 50°C sampled at IfT, Leipzig, Germany.

Figure A.6.1e: Thermo-desorption of 85 nm particles at 90°C sampled at Mace Head, Ireland.

Figure A.6.1f: Thermo-desorption of 20 nm particles at 70°C sampled at SMEAR II field station, Hyytiala, Finland

Figure A.6.1g: Thermo-desorption of 100 nm particles at 70°C sampled at Clermont Ferrand, France.

Figure A.6.1h: Thermo-desorption of 85 nm particles at 90°C sampled at Mace Head, Ireland.

Figure A.6.2 : Relative change in the hygroscopic growth factor of particles sampled for different locations and air masses.

Figure A.6.3: Theoretical hygroscopic growth of 60, 85, 92 and 100 nm pure AS particles.

Figure A.6.4: Modeled functional fits of water activity, density and surface tension for Fulvic-Sulphuric Acid particle composition (40:60 in mass) used in the sensitivity test.

Figure A.6.5: Modeled functional fits of water activity, density and surface tension for fulvic-sulphuric Acid particle composition (50:50 in mass) used in the sensitivity test.

Figure A.6.6: Modeled hygroscopic particle growth with initial composition of 40:60 (mass ratio) fulvic acid-sulphuric acid and preferential desorption of sulphuric Acid.

Figure A.6.7: Modeled functional fits of water activity, density and surface tension for Fulvic-Sulphuric Acid particle composition (60:40 in mass) used in the sensitivity test.

Figure A.6.8: Modeled hygroscopic particle growth with initial composition of 60:40 (mass ratio) fulvic acid-sulphuric acid and preferential desorption of fulvic Acid.

Annexes

Figure A-1 : Schéma du chargeur bipolaire.
Figure A-2 : Distribution de la charge par diffusion bipolaire correspondant à l'equation (I).
Figure A-3 : Principe d'une colonne DMA.
Figure A-4. Schéma du compteur de particules à condensation TSI-3010.
Figure A-5 : Efficacité des deux CPCs TSI 3010 en parallèle.
Figure A-6 : Schéma de l'arrangement en « closed-loop » pour un DMA.
Figure A-7 : Schéma du dispositif PFM pour la mesure du débit d'aérosol.
Figure A-8 : Les différentes géométries des orifices.
Figure A-9.a: Vecteurs de vitesse en ms^{-1} pour la première géométrie (Mod1) de l'orifice.
Figure A-9.b : Vecteurs de vitesse en ms^{-1} pour la deuxième géométrie (Mod2) de l'orifice.
Figure A-9.c : Vecteurs de vitesse en ms^{-1} pour la troisième géométrie (Mod3) de l'orifice.
Figure A-10 : Pressions en amont et en aval de l'orifice calculées par FLUENT pour les trois géométries considerées.
Figure A-11 : Montage instrumental pour l'étalonnage des orifices.
Figure A-12 : Etalonnage d'un orifice Mod4.
Figure A-13 : Pénétration de particules dans le dispositif PFM avec un orifice Mod4, d=0.7 mm et Q=1 $lmin^{-1}$. Les barres d'erreur correspondent à 12 mesures (3%).
Figure A-14 : Schéma du thermo-désorbeur.
Figure A-15 : Schéma de l'humidificateur à membrane Nafion.
Figure A-16 : Schéma de montage et de régulation de l'humidité du VHTDMA.
Figure A-17 : Schéma et principe de fonctionnement du volume thermostaté.
Figure A-18 : Description schématique de la méthode d'échantillonnage TDMA et de son traitement.

Liste des tableaux

Article 5

Table A.5.1: Results of two TDMA observations made in Hyytiälä, Finland during the BACCI/QUEST campaign that took place in April 2005

Article 6

Table A.6.1: Air mass type categorized with NOAA HYSPLIT MODEL back trajectories analysis calculated on three days for the five sampling sites.
Table A.6.2: Averaged measurement of HGF and VHGF (with standard deviation) corresponding to air masses described in Table A.6.1 and different field campaingns.
Table A.6.3: Averaged VH/H GF ratio for different hygroscopic classes and air masses (maximum ratio value in red, minimum in blue)
Table A.6.4: Polynomial fits used in the model for pure ammonium sulphate (AS) and pure NaCl of water activity (a_w), surface tension (σ) and density (ρ).

Annexes

Tableau A-1 : Coefficients pour la distribution des charges utilisées dans l'équation (I)
Tableau A-2 : Caractéristiques des matériaux du thermo–désorbeur.